Low-Temperature & Transfer-Free Graphene Growth: Process and Underlying Mechanisms

Chang Seok Lee

THÈSE

Présentée pour obtenir le grade de

DOCTEUR DE L' ÉCOLE POLYTECHNIQUE

Spécialité: Physique

Par

Chang Seok LEE

Low-Temperature & Transfer-Free Graphene Growth:

Process and Underlying Mechanisms

Soutenue le 10 / 10 / 2012 devant le jury constitué de :

Mme. Annick Loiseau	Directeur de recherche à l'ONERA	Rapporteur
M. Tiberiu Minea	Professeur à l'Université Paris Sud 11	Rapporteur
M. Young Hee Lee	Professeur à Sungkyunkwan University	Examinateur
M. Pierre Legagneux	Ingénieur Thales Research&Technology	Examinateur
M. Costel Sorin Cojocaru	Chargé de recherche au CNRS	Examinateur
	Enseignant à l'École polytechnique	
M. Jean-Luc Maurice	Directeur de recherche au CNRS	Directeur de Thèse

LABORATOIRE DE PHYSIQUE DES INTERFACES ET COUCHES MINCES (LPICM)

CNRS, UMR7647, ÉCOLE POLYTECHNIQUE

THÈSE

Présentée pour obtenir le grade de

DOCTEUR DE L' ÉCOLE POLYTECHNIQUE

Spécialité: Physique

Par

Chang Seok LEE

Low-Temperature & Transfer-Free Graphene Growth:

Process and Underlying Mechanisms

Soutenue le 10 / 10 / 2012 devant le jury constitué de :

Mme. Annick Loiseau	Directeur de recherche à l'ONERA	Rapporteur
M. Tiberiu Minea	Professeur à l'Université Paris Sud 11	Rapporteur
M. Young Hee Lee	Professeur à Sungkyunkwan University	Examinateur
M. Pierre Legagneux	Ingénieur Thales Research&Technology	Examinateur
M. Costel Sorin Cojocaru	Chargé de recherche au CNRS	Examinateur
	Enseignant à l'École polytechnique	
M. Jean-Luc Maurice	Directeur de recherche au CNRS	Directeur de Thèse

Acknowledgments

Up to this very moment that putting my hands to type acknowledgements for thesis, I can't believe how fast time goes by. In this short page, I want to recall all surrounding me. This dissertation would not have been possible without the help of many people.

I would first like to thank Bernard Drévillon, Director of LPICM (Laboratoire de Physique des Interfaces et des Couches Minces) for giving me the chance to work in his laboratory. I also want to thank Yvan Bonnassieux, Pere Roca i Cabarrocas, Bernard Geffroy, Denis Tondelier, Linwei Yu, Jean Eric Bourée, Erik Johnson, Pavel Bulkin, Tatiana Novikova, Marc Chaigneau, Romain Cariou, Benedict O'Donnell, Rosa Ruggeri, Igor Sobkowicz, Alfonso Torres Rios, and whole group of the LPICM for a very enjoyable, generous, and collaborative environment.

Thank you Garry Rose Kitchner, Éléonor Caristan (Leo), Eric Paillassa, Frédéric Liege, Jacqueline Tran, Frédéric Farci, Cyril Jadaud, and Jean-Luc Moncel for technological, security problems. Thanks Laurence Corbel, Chantal Geneste, and Carine Roger-Roulling for the administrative help.

I thank Korean friends who are studying abroad in France for doctor/master degree, Ka-hyun Kim, Jong woo Jin, Taewoo Jeon, Changhyun Kim, Jinwoo Choi, Tae-ha Hwang, Kihwan Seok, Hojoong Kwon, Heechul Woo, and Sungyup Jung, and I hope they can achieve what they want. And I'm missing those guys who already left France, Munho Song, Youngbin Jung, Myung Jin Lim, Jinyoun Cho, and Youn-ho Heo.

Our NanoMaDe group, is strongly supported by Marc Châtelet,F atima Zahra Bouanis, Bérengère Lebental, Emmanuel Lefeuvre, Kihwan Kim, Evgeny Norman, Lucie Leveau, and Waleed Moujahid. And François Le Normand in Strasbourg is our close collaborator.

My appreciation also goes to my formal colleagues in NanoMaDe, Amaël Caillard, Bernd Marquardt, Arnaud-Julien Guilley, Heejin Jung, Sunghoon Lim, Gowtham Manoharan, Joonwon Lim, Laurent Eude, Aurélien Gohier, and Anirban Dhar.

I am grateful to Zhanbing He for his advice on paper work. He is certainly a hard worker and a passionate scientist. Laurent Baraton is my mentor in France, and he is really smart guy to organize/conduct the experiments. I greatly enjoyed my time as a member of the group, and miss you all.

One day, when our precious PECVD was out of order, Costel Sorin Cojocau asked me "could you help me to repair the PECVD ?". I answered readily "Of course, the equipment is most important thing". What he told me "No". The most important thing is "person", and second, third one also "person". Thank you to him, currently leading our group nicely, NanoMaDe.

I would like to deeply thank my supervisor Jean-Luc Maurice for taking care of the advancement of my PhD, for guidance whenever it was necessary. His scientific curiosity inspired me a lot, thus I've always had a question and was motivated to solve the question. In fact, he actively supported me from the end of my master degree.

And I thank EGIDE(5[th]Blaise Pascal Scholarship, managed by France-Korea Government), Samsung Chair Project, ANR Project for financial support.

Finally, the biggest thanks go to my parents, my family, for, well, everything.

To my parents…

Outline

Chapter III. Graphene Growth Techniques............55

Chapter IV. Plasma-Assisted Graphene Growth 83

Chapter V. Ion Implantation 129

Chapter VI. Conclusions and Perspectives 158

Resume

The integration of graphene in microelectronics requires the ability to synthesize this material in a reproducible and low-cost manner. Early preparation methods, such as mechanical or chemical exfoliation of HOPG (highly ordered pyrolytic graphite), or epitaxial growth by high-temperature annealing of SiC (0001) in UHV (ultra-high vacuum), fall short in terms of reproducibility or scalability. In contrast, methods involving the catalytic crystallization of graphene on a metallic substrate may enable large-area fabrication and appear well adapted to meet the requirements for industrial application.

Chemical vapor deposition (CVD) on a metallic substrate is considered as one of the strong candidates for large-area and uniform graphene growth. Such a route, however, has two critical limitations (1) high-temperature processing(~1000 °C)– low-temperature is always preferable in an industrial perspective – and (2) necessity for a transfer on an insulating (functional) substrate, which introduces not only an additional step in the process, but also structural defects and chemical contamination.

In the present thesis work, we investigated new graphene growth techniques with the idea to limit or suppress those drawbacks. We focused on two techniques differentiated by the way the carbon atoms are introduced into the metal catalyst film: (i) direct-current plasma-enhanced CVD (dc-PECVD) and (ii) carbon ion implantation.

(i) The plasma-assisted graphene growth process first appeared in a 2007 paper, which inspired a lot of research groups including ours. Exposure of the metal film to highly reactive plasma introduces carbon atoms at and near the film surface; performing this at elevated temperature makes the carbon atoms to diffuse throughout the film. Our team had developed a large experience of dc-PECVD in the growth of vertically aligned carbon nanotubes. After adapting this method to graphene growth, it delivered graphene layers on Ni at 450 °C. Moreover, in addition to the top-surface layer, we obtained with this technique another graphene layer in-between Ni and the underlying insulating substrate (SiO_2 or glass). That second graphene layer placing itself directly on the insulating (functional) substrate, we developed a simple process for using it directly as a sensor without transfer. This was the main achievement of the present thesis work.

(ii) We were the first to propose carbon ion implantation for supplying carbon atoms to the Ni layer, prior to obtaining graphene upon annealing. By separating introduction and annealing, this technique allowed us to isolate important factors of a heat treatment. Thus, through precise control of carbon dose/implantation energy, we were able, by using this method, to get fundamental insight into the graphene growth mechanisms.

For most of the experiments, we employed nickel as catalyst, under the form of 200-nm thick films deposited by e-beam evaporation onto an insulating substrate. For PECVD, we used a high density and highly reactive plasma generated by the combination of CH_4 and H_2. We applied a procedure patented by our team, which postulated that two graphene layers could be formed (at the surface and at the interface).We thus confirmed this postulate and preliminary experiments. In such a process, the surface graphitic layer includes damages due to direct exposure to plasma. The underlying graphene on insulating substrate is protected from plasma exposure and requires no transfer for its use.

We have shown, with our implantation experiments, that carbon diffusion is very significant in redistributing carbon in Ni, especially through grain boundaries. In PECVD, grain boundaries would help driving C to the interface, but a complex mechanism related to plasma also has to be taken into account: we obtained interfacial graphene with PECVD while we did not get it with implantation. We now explain this absence of interface graphene after implantation by observing that carbon diffusion in Ni is quite fast, so that most of implanted carbon atoms will out-diffuse(within a few tens of seconds at 450 °C) rather than precipitate at interface. Thus the PECVD growth includes a complex – probably dynamic – mechanism that promotes precipitation at the interface.

Due to this fast diffusion, the final carbon distribution in a Ni film thus depends on the annealing treatment that is applied during or after carbon has been introduced. We show in particular that two kinds of graphitic materials are obtained after a given treatment: one under the form of single crystals of few-layer graphene/graphite, grown during the high temperature plateau, and a second under the form of nanocrystalline few-layer graphene, grown during cooling.

Finally, on the graphene grown by PECVD directly on glass at low temperature, we thus developed a humidity sensor, by direct electrode printing. Beyond this proof of concept, we need to further investigate growth mechanisms and annealing conditions for the development of various transfer-free, low-temperature, graphene applications.

As the present work comes to its end, we are investigating these mechanisms by using a new technique, which we call "Sub-plantation", where the carbon atoms are implanted at low energy into the metallic film. Our team started this development in order to reproduce some of the PECVD conditions in ultra-high vacuum and ultra-clean environment, after realizing that the carbon radicals had a significant kinetic energy in the dc-PECVD process (where the electric field reaches several hundreds of volts). The team thus designed an ultra-high vacuum (UHV) chamber jointly equipped with a carbon ion gun on the one hand and XPS, LEED and Auger analysis on the other hand: "FENIX" – Facility for Elaboration of Nanomaterials with In-situ analysis at Ecole Polytechnique (X). In FENIX, we can keep carbon contamination to a minimum, which is mandatory to understand the formation of graphene on the catalytic layer.

To conclude, we believe that the research carried out during this thesis work has brought a significant brick in the building and understanding of low-cost methods for making functional graphene devices.

Outline

Chapter I. Introduction

1.1. History of Carbon allotropes: From Graphite to Graphene

In the 15th century, a large quantity of graphite was discovered in England, which was extremely pure crystal. This remains the only large scale deposit of graphite ever found in this solid form. Graphite is the oldest known carbon allotrope with a crystalline phase which has the layered, planar structure of graphene. Each layer is composed by arranged carbon following hexagonal lattice, and weak van deer Waals forces exist in-between layers that link them to form a 3D structure. Such an interaction is generated by a delocalized π orbital. Without any doubt, graphite has revolutionized the world by the development of pencils (see in Figure 1.1.).
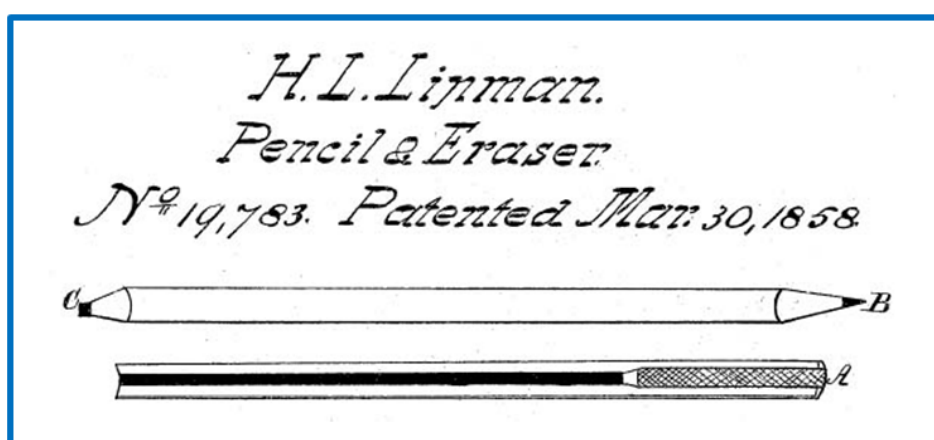
Figure 1.1. Hymen Lipman's pencil drawing in patent, which published in 1858[1].

For a long time, diamond and graphite were considered to be the only pure forms of carbon. In 1985 a new form of carbon, C_{60} named as fullerenes, was discovered by Kroto et al.[2] The 0-dimensional molecules have a particular shape like a "soccer ball". These fullerenes are made up of 60 carbon atoms arranged in pentagonal and hexagonal rings. In 1990, physicists W. Krätschmer and D.R. Huffman for the first time produced isolable quantities of C_{60} by causing an arc between two graphite rods to burn in a helium atmosphere and extracting the carbon condensate so formed using an organic solvent.

Then, in 1991, carbon nanotubes (CNTs) came out by Iijima's group, with a title of "Helical microtubules of graphitic carbon" in *Nature*[3]. CNTs are made of rolled up carbon layers and have 1-dimensional structure. Depending on the number of walls, CNTs can be categorized as single-walled CNTs (SWCNTs), double-walled CNTs (DWCNTs), and multi-walled CNTs (MWCNTs). Furthermore, according to rolling up angle ("*chiral vector*"), ithey are called armchair-, zigzag, and chiral-nanotubes. In fact, the discovery of CNTs has resulted in intense research on carbon-based materials due to the fact that they exhibit outstanding electrical and mechanical properties. This would be explained later closely connected to graphene.

Finally, in 2004, a single layer of carbon named "*graphene*" is isolated by Manchester group[4]. They simply put a flake of graphite on scotch tape, and repeatedly peel off until the thinnest flakes are found. Mechanical exfoliation provides high-quality graphene crystallites up to 100 μm in size, which is sufficient for most research purposes. It is worth to note that a few of the most important properties of the graphene monolayer were determined experimentally well before the year 2004, such a plasmon structure and the phonon dispersion branches[5, 6].

Figure 1.2 shows all carbon allotropes that we mentioned above, and how they formed. It is clear that (a) 2-dimensional graphene is a basic component of the others. For instance, (b) 0-dimensional fullerene is the form of wrapping up with 60 carbon atoms, (c) 1-dimensioanl CNTs can be formed by rolling up, and (d) 3-dimensional graphite is a crystal that stacked by graphene layer.
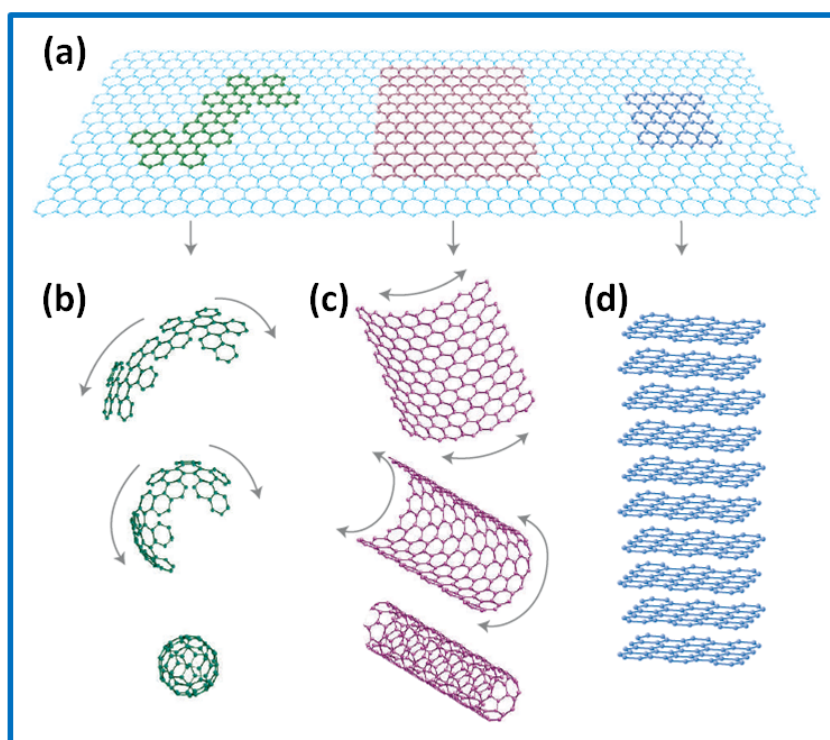
Figure 1.2. (a) Graphene is a mother of carbon allotropes and can be converted to (b) fullerene, (c) carbon nanotube, and (d) graphite. Citied from A.K. Geim et al., Nature Materials, **6**, 183-191 (2007)[7]

1.2. Background on graphene: Band Structure and Properties

1.2.1. Band Structure of Graphene

Graphite is a three-dimensional (3D) layered hexagonal lattice of carbon atoms. A single layer of graphite forms a two-dimensional (2D) material, called 2D graphite or a graphene layer. Even in 3D graphite, the interaction between two adjacent layers is small compared with intra-layer interactions, since the layer-layer separation of 3.35 Å is much larger than nearest-neighbor distance between two carbon atoms, a_{cc} = 1.42 Å. Thus the electronic structure of 2D graphite is a first approximation of that for 3D graphite.

The first tight-binding description of graphene was given by Wallace in 1947[8]. He considered nearest- and next-nearest-neighbor interaction for the graphene p_z orbitals, but neglected the overlap between wave functions centered at different atoms. The other- nowadays better known- tight binding approximation was nicely described by Saito et al.[9] It considers a nonfinite overlap between the basis functions, but includes only interactions between nearest neighbors within the graphene sheet.

1.2.1.1. Tight-Binding Approximation in Graphite
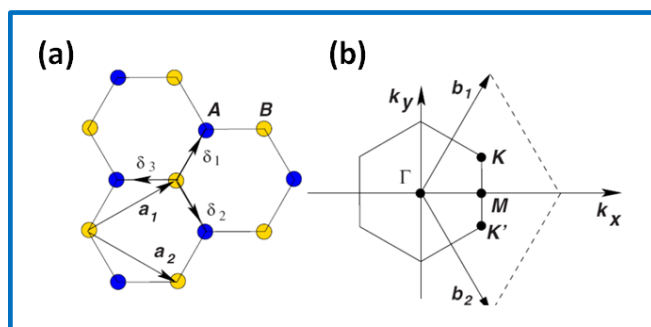
Figure 1.3. (a) The unit vectors in real space, a_1, a_2, and (b) the reciprocal lattice vector, b_1, b_2.

Graphite is a layered structure by graphene. In graphene lattice, see in Figure 1.3., we can identify two non-equivalent carbon atoms (A and B). Thus, using Bloch wave function of these two carbon atoms, we can obtain following energy dispersion,

$$E_{\pm}(k) = \frac{\varepsilon_{2p} \pm 2t\cos(ka/2)}{1 \pm 2s\cos(ka/2)}, \qquad (-\frac{\pi}{a} < k < \frac{\pi}{a}) \qquad \text{(Eq.1.1.)}$$

in which the (+) sign defines one branch and the (-) sign defines the other branch. The levels E_+ and E_- are degenerate at ka=±π. E_+(k) and E_-(k) are called bonding π and antibonding π^* energy band, respectively.

1.2.1.2. Tight-Binding Approximation in Graphene

From the Figure 1.3., we can define the unit vector, and the reciprocal lattice vectors. This calculation leads to following energy dispersion in graphene,

$$E_{g2D}(\vec{k}) = \pm t \left\{ 1 + 4\cos\frac{\sqrt{3}k_x a}{2}\cos\frac{k_y a}{2} + 4\cos^2\frac{k_y a}{2} \right\}^{1/2} \qquad \text{(Eq. 1.2.)}$$

In this case, the energies have the values of $\pm 3t$, $\pm t$ and 0, respectively at the high symmetry points, Γ, M and K in the Brillouin zone.

Figure 1.4. shows energy dispersion of graphene on momentum space. Especially, K points where valence band and conduction band are connected are called "***Dirac points***". This is an essential origin of amazing properties of graphene. Near the K and K' points, the energy dispersion has a circular cone shape which, to a first order approximation, is given by

$$E(\vec{k}) = \pm \hbar v_F |k|, \quad (v_F = 3ta/2\hbar \approx 10^6 ms^{-1}) \qquad \text{(Eq. 1.3.)}$$

Here, V_F is the Fermi velocity. Note that the wavevector k is measured from the K and K' points. This kind of energy dispersion is distinct from that of conventional 2D system (*m* is the electron mass), due to the fact than energy dispersion is not related to mass.

$$E(\vec{k}) = (\hbar^2 k^2 / 2m) \qquad \text{(Eq. 1.4.)}$$
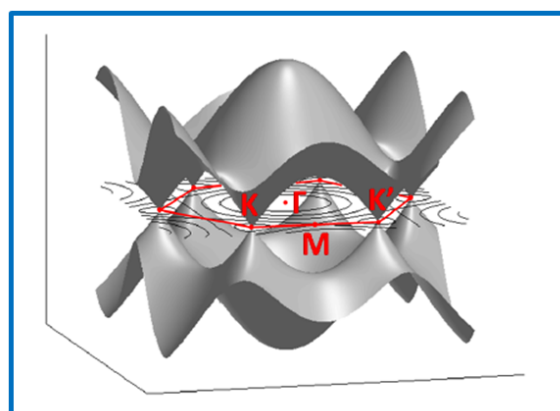
Figure 1.4. First Brillouin zone and band structure of graphene. The vertical axis is energy, while the horizontal

axis is momentum space on the graphene reciprocal lattice. The first Brillouin zone of graphene is illustrated in the horizontal plane and labeled with some points of interest. Especially, K and K' are known as the Dirac points, which connect the valence band and the conduction band. Citied from D.R. Cooper et al., arXiv:1110.6557v1[10]

1.2.2. Properties

Graphene is a versatile material that exhibiting superior properties in many-side. In this section, I'll briefly review featured properties of graphene.

One of the most attractive properties of graphene is the ultra-high charge mobility at room temperature. S.V. Morozov et al., reported that if extrinsic disorder is eliminated, charge mobility higher than 200,000 cm^2/Vs can be achieved with weak temperature dependence[11]. And charge mobility in excess of 200,000 cm^2/Vs (200 times higher than Si) observed by suspending single layer graphene at electron densities of 2 x 10^{11} cm^{-2}. Due to the fact that the presence of charge scattering by the underlying substrate and impurities or wrinkles in graphene, its charge mobility could be strongly affected[12].

Following Figure 1.5. shows electron mobility of various materials, including graphene, graphene nanoribbons, carbon nanotubes, Ge (bulk), Si (bulk), Si MOS (Metal-Oxide-Semiconductor), III-V compounds (bulk), and 4H-SiC (bulk)[13]. In fact, graphene possess the most high charge mobility, but introducing of bandgap by graphene nanoribbons makes suppression of charge mobility down to bulk phase of Si or even lower. This would be seriously considering in the field of application.
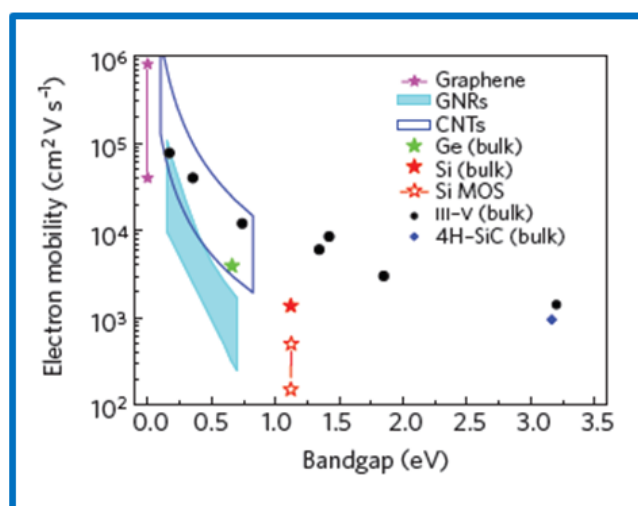
Figure 1.5. Electron mobility versus bandgap of various materials. Cited from F. Schwierz, Nature Nanotechnology **5**, 487 - 496 (2010)[13]

Graphene has a universal 2.3% linear optical absorption of incident white light[14], a consequence of graphene's unique electronic structure. And a room temperature thermal conductivity of about 6000 W/mK for a suspended monolayer graphene is predicted[15]. Single layer graphene has excellent mechanical properties with a Young's modulus of 1.0 TPa and a stiffness of 130 GPa[15]. It is also possible to carry high current density up to 3×10^8 A/cm^2 [16].
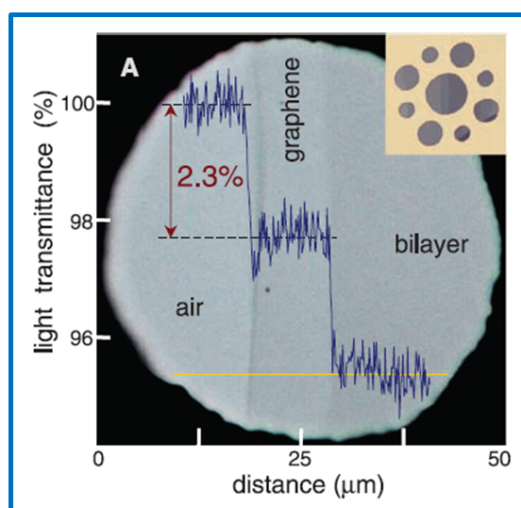
Figure 1.6. Light transmittance of single layer and bilayer graphene. Cited from R.R. Nair et al., Science **320**, 1308 (2008)[14]

Due to all above properties which can overcome current inherent limit of materials, as well as the performance of device, the research on graphene is getting expanding from fundamentals to the industrial applications.

1.3. Potential of graphene: Toward Applications

The appearance of 2-dimensional material, graphene, inspired a lot of theoretical physicists due to the fact that it exhibits amazing properties originating from Dirac point. Now, its potential toward applications is getting larger, including opto-electronics, bio-medical applications, surface coating for either anti-corrosion/oxidation or uniform heat dissipation etc.

1.3.1. Transistor

Semiconductor electronics are mainly composed of digital logic part and radio-frequency (RF) part. The former aims at switching electron signals, while the latter is to amplify the signals. In fact, monolayer graphene has no bandgap, which limits the on/off ratio in field-effect transistors, thus additional engineering of graphene to introduce a bandgap is required for digital logic application. In other words, graphene is more readily applicable in RF applications.

1.3.1.1. Digital Logic Components

A FET (Field Effect Transistor) consists of a gate, a channel region connecting source and drain electrodes, and a barrier separating the gate from the channel. The operation of a conventional FET relies on the control of the channel conductivity, and thus the drain current, by a voltage, V_{GS}, applied between the gate and source.
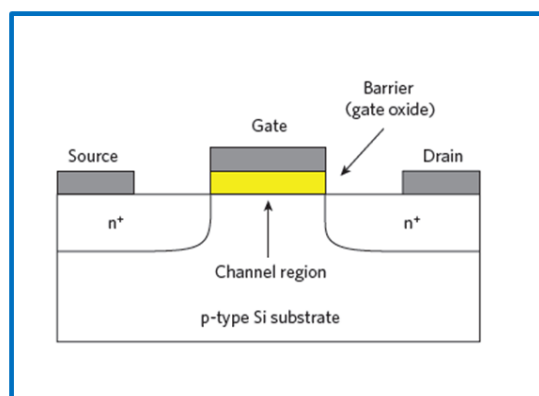
Figure 1.7. Schematic diagrams of conventional transistor structure. Cited from F. Schwierz, Nature Nanotechnology **5**, 487 - 496 (2010)[13]

Charge carriers in graphene process a very small effective mass, hence graphene shows extremely attractive material properties relevant to electronic devices. K.S. Novoselov et al., reported that charge mobilities of graphene obtained by micromechanical cleavage reached 15,000 cm^2/Vs for both electrons and holes[17]. Using epitaxially grown graphene, C. Berger et al. achieved a charge mobility of 27,000 cm^2/Vs in patterned graphene[18]. Extremely high charge mobilities reaching 200,000 cm^2/Vs are recorded from suspended graphene[19-21].

For the switching behavior, of course, we need a suitable bandgap in materials. Structural charge confinement is one of the ways that can open the bandgap in graphene, thus graphene nanoribbon (GNR), graphene nanomesh (GNM), and graphene quantum dot (GQD) are proposed. However, because of the

17

difficulties to make smooth edge, the introduction of bandgap might be partially related to Coulomb blockade which means that charge mobilities are strongly depressed. If the charge mobility is lowered down to the range of silicon, no more advantages are given in graphene transistors.

1.3.1.2. Radio-Frequency Transistors

The high mobility of charge carriers in graphene is ideal for obtaining fast switching and a high on current, I_{on}. Zero bandgap induces a large off current, however, so the on/off current ratios for graphene transistors are about 10^2, much lower than the $10^3 \sim 10^6$ required for mainstream logic applications[4]. But this relatively low on/off ratio is not a significant problem for high-frequency applications, such as radio-frequency switches.

Most applications for radio frequency (RF) transistors had been military oriented in the early 1980s, while wireless communication markets now prevail. The term RF stands for radio frequency and is commonly designated as electromagnetic waves with frequencies around and above 1 GHz. Thus RF transistors are devices with the capability to operate and amplify signals at GHz frequencies. RF transistors are used in a large range of different circuits, such as low-noise and power amplifiers, mixers, oscillators, frequency converters, etc.

This, together with the fact that radiofrequency circuits are much less complex than digital logic chips, has led to makers of radiofrequency chips being more open to new device concepts. An indication of this is the large variety of different transistor types and materials used in radiofrequency electronics: these include high-electron-mobility transistor (HEMTs) based on III-V semiconductors such as GaAs and InP, silicon n-channel MOSFETs, and different types of bipolar transistor.

In general, radio frequency transistor performance is characterized by two parameters: the cut off frequency f_T, and the maximum oscillation frequency f_{max}, where f_T and f_{max} represent how fast channel current and power transmission, respectively, are modulated by the gate. Cut-off frequency is defined as

$$f_T = \frac{g_m}{2\pi C_G}$$

(Eq. 1.5.)

where g_m is the intrinsic transconductance and C_g is the gate capacitance. Recently, graphene MOSFETs with gigahertz capabilities have been reported. So far, the highest measured f_T has been 300 GHz with Co_2Si-nanowire gates using exfoliated graphene[22]. At a wafer scale, 240 GHz has been reported using epitaxial graphene[23], compared with 200 GHz using chemical vapour deposition (CVD)[24].

The maximum oscillation frequency is:

$$f_{\max} = \frac{f_T}{2\sqrt{(g_D(R_G + R_{SD}) + 2\pi f_T R_G C_G)}} \ ,$$

(Eq. 1.6)

where g_D is the channel conductance, R_G is the gate resistance and R_{SD} is the source-drain resistance.

1.3.2. TCFs (Transparent Conducting Films)

It is predicted that the market size for TCFs will be 1.3 B€ in 2012[25]. 93% of that uses ITO (Indium Tin Oxide), primarily in display industry, such as LCD, OLED, e-paper, and touch screens.

However, the price of ITO is continuously increasing due to the limited supply of indium; even recycling ITO has become a big industry[26]. Since ITO is a ceramic material, it can crack and fracture at relatively low strains of 2~3%[27], therefore fails to integrate in flexible electronics. Another drawback of ITO is, see in Figure 1.7., strong spectral-dependent response[28, 29]. In particular, the transmittance drops rapidly near the UV (ultraviolet) region, which could be a serious problem for UV sensors and LEDs even if the transmittance is very high in the visible region[30]. The absorption spectrum of monolayer graphene is quite flat from 300 to 2,500 nm with a peak in the ultraviolet region (~270 nm), due to the exciton-shifted van Hove singularity in the graphene density of states[31]. These facts highlight uniform transmittance of graphene-based TCFs with a larger wavelength window than ITO films.
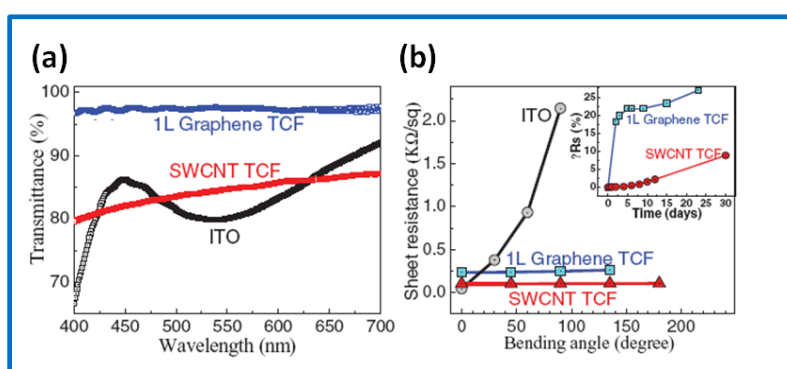
Figure 1.8. Performance of graphene-based TCFs compare to ITO and SWCNT. (a) Transmittance depend on wavelength. (b) Variation of sheet resistance with bending angle. Cited from C. Biswas and Y.H. Lee, Advanced Functional Materials **21**, 3806 - 3826 (2011)[30]

It is important to note that sheet resistance R_s and transmittance T are in fact linked. Both are

determined by the response of electrons to either static voltage or dynamic light electric field. The sheet resistance is ultimately controlled by the 3-dimensional DC conductivity, σ_{DC},

$$R_s = (\sigma_{DC}t)^{-1}$$

(Eq. 1.7.)

where t is the film thickness. The transmittance is controlled by the optical conductivity σ_{Op} which is following

$$T = (1 + \frac{Z_0}{2}\sigma_{Op}t)^{-2}$$

(Eq. 1.8.)

Here, Z_0 is the impedance of free space having 377 Ω. Note that optical conductivity is related to the Lambert – Beer absorption coefficient α by $\sigma_{Op} \approx 2\alpha/Z_0$. Then, we can combine these equations eliminating *t* to give a relationship between *T* and R_s for a thin conducting film,

$$T = (1 + \frac{Z_0}{2R_s}\frac{\sigma_{Op}}{\sigma_{DC}})^{-2}$$

(Eq. 1.9.)

Thus, the relationship between *T* and R_s is controlled by the conductivity ratio, σ_{Op}/σ_{DC}. High values of σ_{Op}/σ_{DC} result in the desired properties[32].

In fact, the transmittance of a freestanding monolayer graphene can be derived by applying the Fresnel equations in the thin-film limit for a material with a fixed universal optical conductance $G_0 = e^2/(4\hbar) \approx 6.08$ x 10^{-5} Ω^{-1}, to give[33]

$$T = (1 + 0.5\pi\alpha)^{-2} \approx 1 - \pi\alpha$$

(Eq. 1.10.)

where $\alpha = e^2/(4\pi\varepsilon_0\hbar c) = G_0/(\pi\varepsilon_0 c) \approx 1/137$ is the fine-structure constant[14].

There is a strong competition to replace ITO and its necessity is widely recognized. Other types of metal oxide, such FTO (Fluorine-doped Tin Oxide) and AZO (Aluminium Zinc Oxide) is already in market share with 6%, and various metal composites are also under investigation[34]. Graphene has strong advantages as we have seen above, but, for practical applications, the performance of devices should be further improved by the engineering of graphene films, such as through their synthesis, transfer, and doping. Graphene-based TCE could

be applicable in wide range of applications, including LED, display (LCD, OLED, and touch screen), lighting, etc.

1.3.3. Energy Harvesting and Storage

Energy harvesting and storage are both critical research domains where increasing demands for improved performance of energy devices and requirement for greener energy resources constitute an immense research interest. Graphene has a great potential to be implemented as electrodes/absorber in solar cells[35-41], electrochemical/thermal energy harvester[42-44], supercapacitor[45-51], electrodes in LIBs[52-57] (Li-Ion Batteries), hydrogen storage [58-60], bio-energy storage[61].

1.3.3.1. Battery

Technological improvements in rechargeable solid-state batteries are being driven by an ever-increasing demand for portable electronic devices. Lithium-ion batteries are the systems of choice, offering high energy density, flexible and lightweight design, and longer lifespan than comparable battery technologies. Currently the anode material employed for lithium based batteries is usually graphite because of its high ratio of the extracted Li to the inserted Li[55]. However, it has a limited theoretical capacity of 372 mAh/g which cannot meet the requirements of high energy capacity[62].

Graphene presents a variety of advantages compared with graphite or CNTs in battery applications. For instance, it has a theoretical specific surface area of 2675 m^2/g, much higher than that of CNTs and graphite with values of ~1300 m^2/g and 10-20 m^2/g. The large surface areas can provide more electrochemical reaction active sites for energy storage. Indeed, the edge sites of graphene could aid Li^+ adsorption and diffusion, consequently reducing charging time and increasing output power. Another distinguished point of graphene is a flexibility compared to fragile graphite, which is beneficial for fabricating flexible energy devices[48].

1.3.3.2. Supercapacitor

The research on novel, low-cost, eco-friendly, and excellent performance energy storage systems is under an ever-increasing demand. Due to the unique 2-dimensional structure and outstanding intrinsic physical properties of graphene, such as extraordinarily high electrical conductivity and large surface area compared to volume/weight (2675 m^2/g)[45], graphene-based materials exhibit great potential for applications in supercapacitors (also named electrochemical capacitors and ultracapacitors).

Supercapacitors store significantly higher amounts of energy density than conventional dielectric capacitors, but they have a similar cell structure as traditional ones except for the fact that the metal electrodes are replaced by highly porous electrodes[46]. Compared with batteries, supercapacitors are essentially

maintenance-free with longer life cycle, require a very simple charging circuit, and experience no memory effect with a rapid charging/discharging rate (within seconds or minutes) at high power densities[47]. Supercapacitors, which are generally much safer (than the other energy storage), could be adapted to batteries and fuel cells.

Depending on energy storage mechanisms, supercapacitors can be classified into (i) EDLCs (Electrochemical Double-Layer Capacitors) which store energy using the adsorption of both anions and cations, and (ii) pseudo-capacitors that store energy through fast surface redox reactions[49]. The capacitance in these EDLCs devices is stored as a build-up of charge in the layers of the electrical double-layer formed at the interface between at high surface area electrode and an electrolyte.

The group headed by R.S. Ruoff first explored graphene-based EDLCs utilizing CMG (chemically modified graphene) as electrode material[50]. Although the individual graphene sheets partially agglomerated into particles approximately 15~25 μm in diameter during the reduction process, the relatively high specific surface area of the graphene-based material aggregation (705 cm^2/g) still allows these electrodes to have high electrochemical performance. Large specific capacitance values of 135 and 99 F/g for aqueous and organic electrolytes, respectively, are achieved. Low degree of agglomeration can result in high capacitance of 205 F/g with a power density of 10 kW/kg in an aqueous electrolyte solution[51].

C. Liu et al. reported[49] that, via curved graphene electrode, supercapacitor having high energy density of 85.6 Wh/kg at room temperature can be achieved. This is significantly higher than typical level of 5~10 Wh/kg. The key to success was the ability to make full utilization of the highest intrinsic surface capacitance and specific surface area of single layer graphene by preparing curved graphene sheets that will not restack face-to-face. The curved morphology enables the formation of mesopores accessible to ionic liquids.

1.3.3.3. Solar Cells

Graphene can be utilized as transparent conducting electrode in solar cells, especially organic photovoltaics. Because, in addition to (i) uniform transmittance in a wide range of spectrum, and (ii) capability of utilize in flexible electronics, detrimental indium diffusion from ITO to active organic layer[63] could be avoided[40]. This could lead to fully realize the potential of organic solar cells as well as graphene.

Graphene has a hydrophobic surface of pristine graphene, so uniform coating of hole-transport layer, such a PEDOT:PSS, is challenging. It was found that AuCl$_3$ doping significantly improves the graphene OPV device performance, but also improves the surface wetting of the graphene electrodes, thus the device success rates are improved[41].

1.3.4. Sensors

Graphene provides the best surface to volume ratio of any material which means that every atom in graphene can interact with surrounding environments. If we use freestanding graphene, not on the supporting substrate, both sides of graphene surface could be an effective sensing area. All of these interactions, to some extent, will perturb the pristine nature of the graphene structural and electronic system, which then forms the basis for the detection of such interaction/binding events.

Note that the defect-free graphene layer has a nearly zero of electron transfer-rate constant. The edge of graphene has an electron transfer-rate constant, k_e, of 0.01 cm/s, while the basal plane exhibits electrochemically inert which below $k_b = 10^{-9}$ cm/s[64]. This means that some amount of defects should be intentionally introduced in graphene[65-67] or a strategic functionallization of the graphene surface should be preset so that it can react with target species.

Compared to CNTs (Carbon Naotubes), graphene does not include metallic impurities (catalyst metal is present in CNT tips). Graphene possess very high 2D electrical conductivity, in addition to large surface area, thus it is considered as an ideal material for electrochemistry.

1.3.4.1. Gas Sensor

Gas sensors based on graphene could make use of the change in electrical conductivity of graphene when gas molecules adsorb on the graphene's surface and act as donors or acceptors of electrons. Graphene-based gas sensor would result in ultimate detection limit, only single molecule[68].

When the graphene is exposed to various gasses, the response of device conductivity varies. Some cases such as NH_3 and CO dope the graphene with electrons while others such as NO_2 and H_2O dope it with holes, and to a different extent for different gasses, as shown in Figure 1.9.
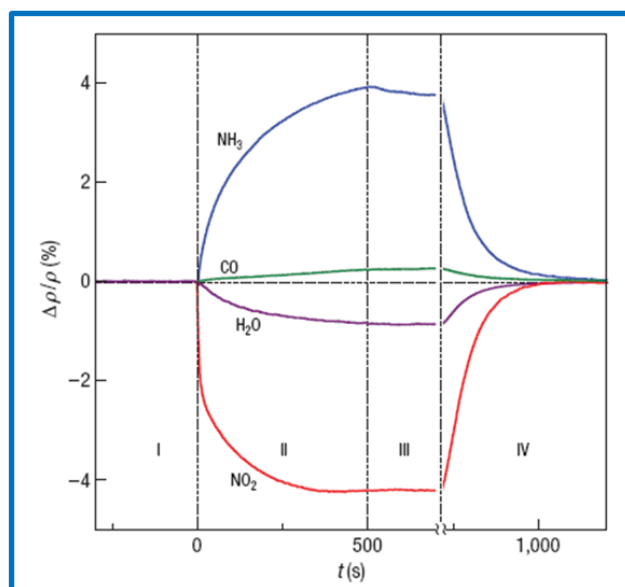
Figure 1.9. Resistivity changes in graphene-based gas sensor. Various gases diluted in concentration to 1 ppm are exposed. The positive sign of changes, (NH$_3$, CO), implies electron doping of graphene, while the other (NO$_2$, H$_2$O) means hole doping. Cited from F. Schedin et al., Nature Materials **6**, 652 - 655 (2007)[30]

To detect various gases, O$_2$[69], H$_2$[70-74], NO$_2$[75-77], H$_2$O$_2$ in food[78], and SO$_2$[79], a variety of graphene-derivative (graphene, graphene oxide, and reduced graphene oxide with metal-hybrid) are actively under investigation. In addition to gas sensor, several   graphene-based electrochemical[80, 81], mechanical (pressure[82], strain[83, 84]), bio (DNA[85-91], glucose[92, 93], peptide[94], bacteria[95], enzyme[96], etc.) sensors are proposed.

1.4. Conclusions

From the discovery of graphite, carbon allotropes are actively under investigating. The scientific research on graphite, which stacked structure of graphene layer, resulted in accumulation of fundamental insights. As the fullerene is appeared in 1985, the additional functionalities are given thanks to its 0-dimensional structure. And, carbon nanotubes come to the center of interest for such a long time. As the properties of CNT originating basically from graphene layer, now carbon-based materials are of great interest even with graphene.

Graphene exhibits unique electrical, optical, thermal, and mechanical properties, originating from linear energy dispersion at low energy, and this cover or surpass current industrialize materials. The potential of graphene is well-recognized from the fundamental insight to a variety of industries.

TCF still require more research to decrease sheet resistance, thus the understanding of graphene growth mechanism, advances in graphene transfer, and various doping/functionallization of graphene are required. In energy-related devices, such as supercapacitor, battery, and solar cell, graphene-metal hybrid electrodes are widely used to enhance the performance of devices. Graphene-based sensing platform is one of the most promising fields, but still remains unsolved the role of defects in graphene. The potential of graphene applications is still expanding, from those areas which we mentioned   above to anti-corrosion coating[97-100], gas/chemical barrier[101, 102], EMI shielding[103], water desalination[104, 105], field emission[106, 107], TEM grid[108, 109], heat dissipation[110-112], etc.

Only few years after from the discovery of material, graphene becomes surprisingly important material that gathering huge amount of funding from each government, global company, and academic institute. The situation is unprecedented in scientific research. The potential of graphene, in terms of fundamental and application, is hugely expanding as ever.

References

1.   Lipman, H. COMBINATION OF LEAD-PENCIL AND ERASER. *U.S. Patent* **19783** (1858)

2.   Kroto, H. W., Heath, J. R., O'Brien, S. C., Curl, R. F. and Smalley, R. E. C60: Buckminsterfullerene. *Nature* **318**, 162-163 (1985)

3.   Iijima, S. Helical microtubules of graphitic carbon. *Nature* **354**, 56-58 (1991)

4.   Novoselov, K. S., Geim, A. K., Morozov, S. V., Jiang, D., Zhang, Y., Dubonos, S. V., Grigorieva, I. V. and Firsov, A. A. Electric field effect in atomically thin carbon films. *Science* **306**, 666-669 (2004)

5.   Nagashima, A., Nuka, K., Itoh, H., Ichinokawa, T., Oshima, C., Otani, S. and Ishizawa, Y. Two-dimensional plasmons in monolayer graphite. *Solid State Communications* **83**, 581-585 (1992)

6.   Aizawa, T., Souda, R., Otani, S., Ishizawa, Y. and Oshima, C. Anomalous bond of monolayer graphite on transition-metal carbide surfaces. *Physical Review Letters* **64**, 768-771 (1990)

7.   Geim, A. K. and Novoselov, K. S. The rise of graphene. *Nat Mater* **6**, 183-191 (2007)

8.   Wallace, P. R. The Band Theory of Graphite. *Physical Review* **71**, 622-634 (1947)

9.   R. Saito, G. Dresselhaus, and M. S. Dresselhaus, Physical Properties of Carbon Nanotubes (Imperial, London, 1998)

10.   Cooper, D. R., D'Anjou, B., Ghattamaneni, N., Harack, B., Hilke, M., Horth, A., Majlis, N., Massicotte, M., Vandsburger, L., Whiteway, E. and Yu, V. Experimental review of graphene. arXiv:1110.6557 (2012)

11.   Morozov, S. V., Novoselov, K. S., Katsnelson, M. I., Schedin, F., Elias, D. C., Jaszczak, J. A. and Geim, A. K. Giant Intrinsic Carrier Mobilities in Graphene and Its Bilayer. *Physical Review Letters* **100**, 016602 (2008)

12.   Bolotin, K. I., Sikes, K. J., Jiang, Z., Klima, M., Fudenberg, G., Hone, J., Kim, P. and Stormer, H. L. Ultrahigh electron mobility in suspended graphene. *Solid State Communications* **146**, 351-355 (2008)

13.   Schwierz, F. Graphene transistors. *Nat Nano* **5**, 487-496 (2010)

14.   Nair, R. R., Blake, P., Grigorenko, A. N., Novoselov, K. S., Booth, T. J., Stauber, T., Peres, N. M. R. and Geim, A. K. Fine Structure Constant Defines Visual Transparency of Graphene. *Science* **320**, 1308 (2008)

15.   Zhu, Y., Murali, S., Cai, W., Li, X., Suk, J. W., Potts, J. R. and Ruoff, R. S. Graphene and Graphene Oxide: Synthesis, Properties, and Applications. *Advanced Materials* **22**, 3906-3924 (2010)

16.   Moser, J., Barreiro, A. and Bachtold, A. Current-induced cleaning of graphene. *Applied Physics Letters* **91**, 163513-3 (2007)

17.   Novoselov, K. S., Geim, A. K., Morozov, S. V., Jiang, D., Katsnelson, M. I., Grigorieva, I. V., Dubonos, S. V. and Firsov, A. A. Two-dimensional gas of massless Dirac fermions in graphene. *Nature* **438**, 197-200 (2005)

18.   Berger, C., Song, Z., Li, X., Wu, X., Brown, N., Naud, C., Mayou, D., Li, T., Hass, J., Marchenkov, A. N., Conrad, E. H., First, P. N. and de Heer, W. A. Electronic Confinement and Coherence in Patterned

Epitaxial Graphene. *Science* **312**, 1191-1196 (2006)

19. Bolotin, K. I., Sikes, K. J., Jiang, Z., Klima, M., Fudenberg, G., Hone, J., Kim, P. and Stormer, H. L. Ultrahigh electron mobility in suspended graphene. *Solid State Communications* **146**, 351-355 (2008)

20. Morozov, S. V., Novoselov, K. S., Katsnelson, M. I., Schedin, F., Elias, D. C., Jaszczak, J. A. and Geim, A. K. Giant intrinsic carrier mobilities in graphene and its bilayer. *Physical Review Letters* **100**, 016602-4 (2008)

21. Du, X., Skachko, I., Barker, A. and Andrei, E. Y. Approaching ballistic transport in suspended graphene. *Nat Nano* **3**, 491-495 (2008)

22. Liao, L., Lin, Y.-C., Bao, M., Cheng, R., Bai, J., Liu, Y., Qu, Y., Wang, K. L., Huang, Y. and Duan, X. High-speed graphene transistors with a self-aligned nanowire gate. *Nature* **467**, 305-308 (2010)

23. Avouris, P., Lin, Y. M., Xia, F., Mueller, T., Farmer, D. B., Dimitrakopoulos, C. and Grill, A. in Device Research Conference (DRC), 2010 205-206 (2010).

24. Jaeho, L., Hyun-Jong, C., Jaehong, L., Hyungcheol, S., Jinseong, H., Heejun, Y., Sung-Hoon, L., Sunae, S., Jaikwang, S., Chung, U. i., Inkyeong, Y. and Kinam, K. in Electron Devices Meeting (IEDM), 2010 IEEE International 23.5.1-23.5.4 (2010).

25. Thiele, C. and Das, R. Transparent Conductive Films 2012-2022. *Source: IDTechEx* (2012)

26. Hecht, D. S., Hu, L. and Irvin, G. Emerging Transparent Electrodes Based on Thin Films of Carbon Nanotubes, Graphene, and Metallic Nanostructures. *Advanced Materials* **23**, 1482-1513 (2011)

27. Cairns, D. R., Witte Ii, R. P., Sparacin, D. K., Sachsman, S. M., Paine, D. C., Crawford, G. P. and Newton, R. R. Strain-dependent electrical resistance of tin-doped indium oxide on polymer substrates. *Applied Physics Letters* **76**, 1425-1427 (2000)

28. Kim, H., Horwitz, J. S., Kushto, G., Pique, A., Kafafi, Z. H., Gilmore, C. M. and Chrisey, D. B. Effect of film thickness on the properties of indium tin oxide thin films. *Journal of Applied Physics* **88**, 6021-6025 (2000)

29. Agrawal, S., Frederick, M. J., Lupo, F., Victor, P., Nalamasu, O. and Ramanath, G. Directed Growth and Electrical- Transport Properties of Carbon Nanotube Architectures on Indium Tin Oxide Films on Silicon-Based Substrates. *Advanced Functional Materials* **15**, 1922-1926 (2005)

30. Biswas, C. and Lee, Y. H. Graphene Versus Carbon Nanotubes in Electronic Devices. *Advanced Functional Materials* **21**, 3806-3826 (2011)

31. Bonaccorso, F., Sun, Z., Hasan, T. and Ferrari, A. C. Graphene photonics and optoelectronics. *Nat Photon* **4**, 611-622 (2010)

32. De, S. and Coleman, J. N. Are There Fundamental Limitations on the Sheet Resistance and Transmittance of Thin Graphene Films? *ACS Nano* **4**, 2713-2720 (2010)

33. Kuzmenko, A. B., van Heumen, E., Carbone, F. and van der Marel, D. Universal Optical Conductance of Graphite. *Physical Review Letters* **100**, 117401 (2008)

34. Kumar, A. and Zhou, C. The Race To Replace Tin-Doped Indium Oxide: Which Material Will Win? *ACS*

Nano **4**, 11-14 (2010)

35.   Kalita, G., Kayastha, M. S., Uchida, H., Wakita, K. and Umeno, M. Direct growth of nanographene films by surface wave plasma chemical vapor deposition and their application in photovoltaic devices. *RSC Advances* **2**, 3225-3230 (2012)

36.   Li, X., Zhu, H., Wang, K., Cao, A., Wei, J., Li, C., Jia, Y., Li, Z., Li, X. and Wu, D. Graphene-On-Silicon Schottky Junction Solar Cells. *Advanced Materials* **22**, 2743-2748 (2010)

37.   Yan, X., Cui, X., Li, B. and Li, L.-s. Large, Solution-Processable Graphene Quantum Dots as Light Absorbers for Photovoltaics. *Nano Letters* **10**, 1869-1873 (2010)

38.   Ihm, K., Lim, J. T., Lee, K.-J., Kwon, J. W., Kang, T.-H., Chung, S., Bae, S., Kim, J. H., Hong, B. H. and Yeom, G. Y. Number of graphene layers as a modulator of the open-circuit voltage of graphene-based solar cell. *Applied Physics Letters* **97**, 032113-3 (2010)

39.   Xu, Y., Long, G., Huang, L., Huang, Y., Wan, X., Ma, Y. and Chen, Y. Polymer photovoltaic devices with transparent graphene electrodes produced by spin-casting. *Carbon* **48**, 3308-3311 (2010)

40.   Wan, X., Long, G., Huang, L. and Chen, Y. Graphene – A Promising Material for Organic Photovoltaic Cells. *Advanced Materials* **23**, 5342-5358 (2011)

41.   Park, H., Jill, A. R., Kim, K. K., Bulovic, V. and Kong, J. Doped graphene electrodes for organic solar cells. *Nanotechnology* **21**, 505204 (2010)

42.   Kang, T. J., Fang, S., Kozlov, M. E., Haines, C. S., Li, N., Kim, Y. H., Chen, Y. and Baughman, R. H. Electrical Power From Nanotube and Graphene Electrochemical Thermal Energy Harvesters. *Advanced Functional Materials* **22**, 477-489 (2012)

43.   Dhiman, P., Yavari, F., Mi, X., Gullapalli, H., Shi, Y., Ajayan, P. M. and Koratkar, N. Harvesting Energy from Water Flow over Graphene. *Nano Letters* **11**, 3123-3127 (2011)

44.   Yin, J., Zhang, Z., Li, X., Zhou, J. and Guo, W. Harvesting Energy from Water Flow over Graphene? *Nano Letters* **12**, 1736-1741 (2012)

45.   Xia, J., Chen, F., Li, J. and Tao, N. Measurement of the quantum capacitance of graphene. *Nat Nano* **4**, 505-509 (2009)

46.   Vivekchand, S., Rout, C., Subrahmanyam, K., Govindaraj, A. and Rao, C. Graphene-based electrochemical supercapacitors. *Journal of Chemical Sciences* **120**, 9-13 (2008)

47.   Simon, P. and Gogotsi, Y. Materials for electrochemical capacitors. *Nat Mater* **7**, 845-854 (2008)

48.   Pumera, M. Electrochemistry of graphene: new horizons for sensing and energy storage. *The Chemical Record* **9**, 211-223 (2009)

49.   Liu, C., Yu, Z., Neff, D., Zhamu, A. and Jang, B. Z. Graphene-Based Supercapacitor with an Ultrahigh Energy Density. *Nano Letters* **10**, 4863-4868 (2010)

50.   Stoller, M. D., Park, S., Zhu, Y., An, J. and Ruoff, R. S. Graphene-Based Ultracapacitors. *Nano Letters* **8**, 3498-3502 (2008)

51.   Stankovich, S., Dikin, D. A., Piner, R. D., Kohlhaas, K. A., Kleinhammes, A., Jia, Y., Wu, Y., Nguyen, S. T.

and Ruoff, R. S. Synthesis of graphene-based nanosheets via chemical reduction of exfoliated graphite oxide. *Carbon* **45**, 1558-1565 (2007)

52.   Vargas C, O. A., Caballero, A. and Morales, J. Can the performance of graphene nanosheets for lithium storage in Li-ion batteries be predicted? *Nanoscale* **4**, 2083-2092 (2012)

53.   Wu, Z.-S., Ren, W., Xu, L., Li, F. and Cheng, H.-M. Doped Graphene Sheets As Anode Materials with Superhigh Rate and Large Capacity for Lithium Ion Batteries. *ACS Nano* **5**, 5463-5471 (2011)

54.   Ji, L., Rao, M., Zheng, H., Zhang, L., Li, Y., Duan, W., Guo, J., Cairns, E. J. and Zhang, Y. Graphene Oxide as a Sulfur Immobilizer in High Performance Lithium/Sulfur Cells. *Journal of the American Chemical Society* **133**, 18522-18525 (2011)

55.   Liang, M. and Zhi, L. Graphene-based electrode materials for rechargeable lithium batteries. *Journal of Materials Chemistry* **19**, 5871-5878 (2009)

56.   Wang, H., Yang, Y., Liang, Y., Robinson, J. T., Li, Y., Jackson, A., Cui, Y. and Dai, H. Graphene-Wrapped Sulfur Particles as a Rechargeable Lithium?밧ulfur Battery Cathode Material with High Capacity and Cycling Stability. *Nano Letters* **11**, 2644-2647 (2011)

57.   Yang, S., Feng, X. and Müllen, K. Sandwich-Like, Graphene-Based Titania Nanosheets with High Surface Area for Fast Lithium Storage. *Advanced Materials* **23**, 3575-3579 (2011)

58.   Tozzini, V. and Pellegrini, V. Reversible Hydrogen Storage by Controlled Buckling of Graphene Layers. *The Journal of Physical Chemistry C* **115**, 25523-25528 (2011)

59.   Hussain, T., Pathak, B., Ramzan, M., Maark, T. A. and Ahuja, R. Calcium doped graphane as a hydrogen storage material. *Applied Physics Letters* **100**, 183902-5 (2012)

60.   Liu, C.-S. and Zeng, Z. Boron-tuned bonding mechanism of Li-graphene complex for reversible hydrogen storage. *Applied Physics Letters* **96**, 123101-3 (2010)

61.   Byun, K.-E., Choi, D. S., Kim, E., Seo, D. H., Yang, H., Seo, S. and Hong, S. Graphene - Polymer Hybrid Nanostructure-Based Bioenergy Storage Device for Real-Time Control of Biological Motor Activity. *ACS Nano* **5**, 8656-8664 (2011)

62.   Winter, M., Besenhard, J. O., Spahr, M. E. and Novák, P. Insertion Electrode Materials for Rechargeable Lithium Batteries. *Advanced Materials* **10**, 725-763 (1998)

63.   Schlatmann, A. R., Floet, D. W., Hilberer, A., Garten, F., Smulders, P. J. M., Klapwijk, T. M. and Hadziioannou, G. Indium contamination from the indium--tin--oxide electrode in polymer light-emitting diodes. *Applied Physics Letters* **69**, 1764-1766 (1996)

64.   Pumera, M., Ambrosi, A., Bonanni, A., Chng, E. L. K. and Poh, H. L. Graphene for electrochemical sensing and biosensing. *TrAC Trends in Analytical Chemistry* **29**, 954-965 (2010)

65.   Terrones, H., Lv, R., Terrones, M. and Mildred, S. D. The role of defects and doping in 2D graphene sheets and 1D nanoribbons. *Reports on Progress in Physics* **75**, 062501 (2012)

66.   Zhang, Y.-H., Chen, Y.-B., Zhou, K.-G., Liu, C.-H., Zeng, J., Zhang, H.-L. and Peng, Y. Improving gas sensing

properties of graphene by introducing dopants and defects: a first-principles study. *Nanotechnology* **20**, 185504 (2009)

67.   Araujo, P. T., Terrones, M. and Dresselhaus, M. S. Defects and impurities in graphene-like materials. *Materials Today* **15**, 98-109 (2012)

68.   Schedin, F., Geim, A. K., Morozov, S. V., Hill, E. W., Blake, P., Katsnelson, M. I. and Novoselov, K. S. Detection of individual gas molecules adsorbed on graphene. *Nat Mater* **6**, 652-655 (2007)

69.   Chen, C. W., Hung, S. C., Yang, M. D., Yeh, C. W., Wu, C. H., Chi, G. C., Ren, F. and Pearton, S. J. Oxygen sensors made by monolayer graphene under room temperature. *Applied Physics Letters* **99**, 243502-3 (2011)

70.   Ehemann, R., Krstic, P., Dadras, J., Kent, P. and Jakowski, J. Detection of hydrogen using graphene. *Nanoscale Research Letters* **7**, 198 (2012)

71.   Kumar, R., Varandani, D., Mehta, B. R., Singh, V. N., Wen, Z., Feng, X. and M체llen, K. Fast response and recovery of hydrogen sensing in Pd-Pt nanoparticle-Graphene composite layers. *Nanotechnology* **22**, 275719 (2011)

72.   Wang, J., Kwak, Y., Lee, I.-y., Maeng, S. and Kim, G.-H. Highly responsive hydrogen gas sensing by partially reduced graphite oxide thin films at room temperature. *Carbon* **50**, 4061-4067 (2012)

73.   Wu, W., Liu, Z., Jauregui, L. A., Yu, Q., Pillai, R., Cao, H., Bao, J., Chen, Y. P. and Pei, S.-S. Wafer-scale synthesis of graphene by chemical vapor deposition and its application in hydrogen sensing. *Sensors and Actuators B: Chemical* **150**, 296-300 (2010)

74.   Johnson, J. L., Behnam, A., Pearton, S. J. and Ural, A. Hydrogen Sensing Using Pd-Functionalized Multi-Layer Graphene Nanoribbon Networks. *Advanced Materials* **22**, 4877-4880 (2010)

75.   Ko, G., Kim, H. Y., Ahn, J., Park, Y. M., Lee, K. Y. and Kim, J. Graphene-based nitrogen dioxide gas sensors. *Current Applied Physics* **10**, 1002-1004 (2009)

76.   Yavari, F., Castillo, E., Gullapalli, H., Ajayan, P. M. and Koratkar, N. High sensitivity detection of NO2 and NH3 in air using chemical vapor deposition grown graphene. *Applied Physics Letters* **100**, 203120-4 (2012)

77.   Deng, S., Tjoa, V., Fan, H. M., Tan, H. R., Sayle, D. C., Olivo, M., Mhaisalkar, S., Wei, J. and Sow, C. H. Reduced Graphene Oxide Conjugated Cu2O Nanowire Mesocrystals for High-Performance NO2 Gas Sensor. *Journal of the American Chemical Society* **134**, 4905-4917 (2012)

78.   Zhang, B., Cui, Y., Chen, H., Liu, B., Chen, G. and Tang, D. A New Electrochemical Biosensor for Determination of Hydrogen Peroxide in Food Based on Well-Dispersive Gold Nanoparticles on Graphene Oxide. *Electroanalysis* **23**, 1821-1829 (2011)

79.   Ren, Y., Zhu, C., Cai, W., Li, H., Ji, H., Kholmanov, I., Wu, Y., Piner, R. D. and Ruoff, R. S. Detection of sulfur dioxide gas with graphene field effect transistor. *Applied Physics Letters* **100**, 163114-4 (2012)

80.   Chen, C.-H., Lin, C.-T., Lee, Y.-H., Liu, K.-K., Su, C.-Y., Zhang, W. and Li, L.-J. Electrical Probing of

Submicroliter Liquid Using Graphene Strip Transistors Built on a Nanopipette. *Small* **8**, 43-46 (2011)

81. Fu, W., Nef, C., Knopfmacher, O., Tarasov, A., Weiss, M., Calame, M. and Schönenberger, C. Graphene Transistors Are Insensitive to pH Changes in Solution. *Nano Letters* **11**, 3597-3600 (2011)

82. Xu, Y., Guo, Z., Chen, H., Yuan, Y., Lou, J., Lin, X., Gao, H., Chen, H. and Yu, B. In-plane and tunneling pressure sensors based on graphene/hexagonal boron nitride heterostructures. *Applied Physics Letters* **99**, 133109-3 (2011)

83. Wang, Y., Yang, R., Shi, Z., Zhang, L., Shi, D., Wang, E. and Zhang, G. Super-Elastic Graphene Ripples for Flexible Strain Sensors. *ACS Nano* **5**, 3645-3650 (2011)

84. Fu, X.-W., Liao, Z.-M., Zhou, J.-X., Zhou, Y.-B., Wu, H.-C., Zhang, R., Jing, G., Xu, J., Wu, X., Guo, W. and Yu, D. Strain dependent resistance in chemical vapor deposition grown graphene. *Applied Physics Letters* **99**, 213107-3 (2011)

85. Liu, X., Aizen, R., Freeman, R., Yehezkeli, O. and Willner, I. Multiplexed Aptasensors and Amplified DNA Sensors Using Functionalized Graphene Oxide: Application for Logic Gate Operations. *ACS Nano* **6**, 3553-3563 (2012)

86. Sathe, C., Zou, X., Leburton, J.-P. and Schulten, K. Computational Investigation of DNA Detection Using Graphene Nanopores. *ACS Nano* **5**, 8842-8851 (2011)

87. Choi, B. G., Park, H., Yang, M. H., Jung, Y. M., Lee, S. Y., Hong, W. H. and Park, T. J. Microwave-assisted synthesis of highly water-soluble graphene towards electrical DNA sensor. *Nanoscale* **2**, 2692-2697 (2010)

88. Postma, H. W. C. Rapid Sequencing of Individual DNA Molecules in Graphene Nanogaps. *Nano Letters* **10**, 420-425 (2010)

89. Yin, Z., He, Q., Huang, X., Zhang, J., Wu, S., Chen, P., Lu, G., Chen, P., Zhang, Q., Yan, Q. and Zhang, H. Real-time DNA detection using Pt nanoparticle-decorated reduced graphene oxide field-effect transistors. *Nanoscale* **4**, 293-297 (2011)

90. Venkatesan, B. M., Estrada, D., Banerjee, S., Jin, X., Dorgan, V. E., Bae, M.-H., Aluru, N. R., Pop, E. and Bashir, R. Stacked Graphene-Al2O3 Nanopore Sensors for Sensitive Detection of DNA and DNA-Protein Complexes. *ACS Nano* **6**, 441-450 (2011)

91. Hong, B. J., An, Z., Compton, O. C. and Nguyen, S. T. Tunable Biomolecular Interaction and Fluorescence Quenching Ability of Graphene Oxide: Application to "Turn-on" DNA Sensing in Biological Media. *Small*, n/a-n/a (2012)

92. Dong, X.-C., Xu, H., Wang, X.-W., Huang, Y.-X., Chan-Park, M. B., Zhang, H., Wang, L.-H., Huang, W. and Chen, P. 3D Graphene–Cobalt Oxide Electrode for High-Performance Supercapacitor and Enzymeless Glucose Detection. *ACS Nano* **6**, 3206-3213 (2012)

93. Kavitha, T., Gopalan, A. I., Lee, K.-P. and Park, S.-Y. Glucose sensing, photocatalytic and antibacterial properties of graphene - ZnO nanoparticle hybrids. *Carbon* **50**, 2994-3000 (2012)

94. Feng, L., Wu, L., Wang, J., Ren, J., Miyoshi, D., Sugimoto, N. and Qu, X. Detection of a Prognostic

Indicator in Early-Stage Cancer Using Functionalized Graphene-Based Peptide Sensors. *Advanced Materials* **24**, 125-131 (2011)

95. Mannoor, M. S., Tao, H., Clayton, J. D., Sengupta, A., Kaplan, D. L., Naik, R. R., Verma, N., Omenetto, F. G. and McAlpine, M. C. Graphene-based wireless bacteria detection on tooth enamel. *Nat Commun* **3**, 763 (2012)

96. Alwarappan, S., Boyapalle, S., Kumar, A., Li, C.-Z. and Mohapatra, S. Comparative Study of Single-, Few-, and Multilayered Graphene toward Enzyme Conjugation and Electrochemical Response. *The Journal of Physical Chemistry C* **116**, 6556-6559 (2012)

97. Prasai, D., Tuberquia, J. C., Harl, R. R., Jennings, G. K. and Bolotin, K. I. Graphene: Corrosion-Inhibiting Coating. *ACS Nano* **6**, 1102-1108 (2012)

98. Bunch, J. S., Verbridge, S. S., Alden, J. S., van der Zande, A. M., Parpia, J. M., Craighead, H. G. and McEuen, P. L. Impermeable Atomic Membranes from Graphene Sheets. *Nano Letters* **8**, 2458-2462 (2008)

99. Chen, S., Brown, L., Levendorf, M., Cai, W., Ju, S.-Y., Edgeworth, J., Li, X., Magnuson, C. W., Velamakanni, A., Piner, R. D., Kang, J., Park, J. and Ruoff, R. S. Oxidation Resistance of Graphene-Coated Cu and Cu/Ni Alloy. *ACS Nano* **5**, 1321-1327 (2011)

100. Singh Raman, R. K., Chakraborty Banerjee, P., Lobo, D. E., Gullapalli, H., Sumandasa, M., Kumar, A., Choudhary, L., Tkacz, R., Ajayan, P. M. and Majumder, M. Protecting copper from electrochemical degradation by graphene coating. *Carbon* **50**, 4040-4045 (2012)

101. Du, H., Li, J., Zhang, J., Su, G., Li, X. and Zhao, Y. Separation of Hydrogen and Nitrogen Gases with Porous Graphene Membrane. *The Journal of Physical Chemistry C* **115**, 23261-23266 (2011)

102. Hauser, A. W. and Schwerdtfeger, P. Nanoporous Graphene Membranes for Efficient 3He/4He Separation. *The Journal of Physical Chemistry Letters* **3**, 209-213 (2012)

103. Singh, A. P., Mishra, M., Chandra, A. and Dhawan, S. K. Graphene oxide/ferrofluid/cement composites for electromagnetic interference shielding application. *Nanotechnology* **22**, 465701 (2011)

104. Cohen-Tanugi, D. and Grossman, J. C. Water Desalination across Nanoporous Graphene. *Nano Letters*, Article ASAP (2012)

105. Cong, H.-P., Ren, X.-C., Wang, P. and Yu, S.-H. Macroscopic Multifunctional Graphene-Based Hydrogels and Aerogels by a Metal Ion Induced Self-Assembly Process. *ACS Nano* **6**, 2693-2703 (2012)

106. Wei, X., Bando, Y. and Golberg, D. Electron Emission from Individual Graphene Nanoribbons Driven by Internal Electric Field. *ACS Nano* **6**, 705-711 (2012)

107. Wu, Z.-S., Pei, S., Ren, W., Tang, D., Gao, L., Liu, B., Li, F., Liu, C. and Cheng, H.-M. Field Emission of Single-Layer Graphene Films Prepared by Electrophoretic Deposition. *Advanced Materials* **21**, 1756-1760 (2009)

108. Zhang, L., Zhang, H., Zhou, R., Chen, Z., Li, Q., Fan, S., Ge, G., Liu, R. and Kaili, J. A graphene oxide - carbon nanotube grid for high-resolution transmission electron microscopy of nanomaterials.

Nanotechnology **22**, 385704 (2011)

109.   Pantelic, R. S., Suk, J. W., Hao, Y., Ruoff, R. S. and Stahlberg, H. Oxidative Doping Renders Graphene Hydrophilic, Facilitating Its Use As a Support in Biological TEM. *Nano Letters* **11**, 4319-4323 (2011)

110.   Yan, Z., Liu, G., Khan, J. M. and Balandin, A. A. Graphene quilts for thermal management of high-power GaN transistors. *Nat Commun* **3**, 827 (2012)

111.   Shahil, K. M. F. and Balandin, A. A. Graphene–Multilayer Graphene Nanocomposites as Highly Efficient Thermal Interface Materials. *Nano Letters* **12**, 861-867 (2012)

112.   Bae, J. J., Lim, S. C., Han, G. H., Jo, Y. W., Doung, D. L., Kim, E. S., Chae, S. J., Huy, T. Q., Van Luan, N. and Lee, Y. H. Heat Dissipation of Transparent Graphene Defoggers. *Advanced Functional Materials*, n/a-n/a (2012)

Outline

Chapter II. Characterization of Graphene

2.1. Introduction

Graphene is an atomically thin 2-D material, which is composed of sp^2 carbon network, thus how to characterize this new material is of great importance, in addition to graphene synthesis. In this Chapter II., we will describe the techniques that we have used in graphene characterization and in determining its properties.

Scanning Electron Microscopy (SEM), and Atomic Force Microscopy (AFM) is commonly using to investigate its morphology and thickness of graphene, but it has a difficult to identify when the layer is fully continuous without cracks. The contrast/thickness difference is required to get the information. Transmission electron microscopy (TEM) provides the fact that atomic structure, uniformity at local area, vertical structure of sample with cross-section image, crystalline property of graphene with a relation of facing materials, and even size of crystal. However, this is a destructive measurement that relatively time-consuming/costly in preparation and limited at local place. Optical microscope revealed the possibility of detecting wrinkles/ripples or grain boundaries of graphene[1-3] as well as grain structure of catalyst metal[4, 5]. This supports a fast and simple investigation of samples. Raman spectroscopy is one of the most powerful tools in graphene analysis that bring the information of graphene's quality by position, width, and relative intensity of each peaks. This has a close relation to absorbents on surface, thickness, crystallite size, and stacking order of graphene. Furthermore, Raman mapping allows to demonstrate the uniformity of graphene layers. Optical transmittance can be measured using transferred graphene on glass substrate, and number of graphene layers can be roughly estimated. Lastly, the electrical properties of graphene are core interest, thus van der Pauw and TLM (Transfer Length Method) will be introduced. Additionally, our humidity sensing platform will be explained.

2.2. Scanning Electron Microscopy

Scanning Electron Microscopy (SEM) is one of the fast, non-destructive, and easily accessible characterization tools that provide useful information, such as identification of graphene position (compared to underlying substrate), and evolution of grain boundaries of catalyst metals at each process. SEM uses a focused beam of high energy electrons to generate a variety of signals at the surface of solid specimens. An Hitachi S-4800 FE-SEM working with conditions of 10 kV, 5 μA was employed to investigate the surface morphology of the samples (working distance < 10 mm).

Electron bombardment of a sample is unique to microprobe analysis and produces a large number of effects from the target material. The incident electrons interact with specimen atoms and are significantly scattered by them rather than penetrating the sample in a linear fashion. Most of the energy of an electron

beam will eventually end up heating the sample, however, before the electrons come to rest, they undergo two types of scattering: elastic and inelastic.

The most common imaging mode collects low-energy (less than 50 eV) *"secondary electrons"* that are ejected from the k-orbitals of the specimen atoms by inelastic scattering interaction with beam electrons[6-8]. Due to their low energy, these electrons originate within a few nanometers from the sample surface[9]. The topography of surface features influences the number of electrons that reach the secondary electron detector from any point on the scanned surface. This local variation in electron intensity creates the image contrast that reveals the surface morphology.

The mode of *"back scattered electron imaging"* provides image contrast as a function of elemental composition, as well as, surface topography[10]. Since the image is produced by elastic interaction (no energy lost) between the sample and the incident electron beam, in addition to high energy electrons, those electrons escape from much deeper than secondary electrons, so surface topography is not as accurately resolved as for secondary imaging. Secondary electrons are produced by inelastic interaction of beam electrons with electrons in the atom, while back scattering electrons generated by the elastic interaction of the beam electron with nuclei of atoms in the specimen.

When the contrast difference of objects in surface is significant, we can automatically distinguish each element and the numerical analysis is possible by support of *Image J* which is freeware image processing tool. Figure 2.1. shows the example of how we can automatically extract the area and the number of particles referred to image contrast. From the pristine SEM image, the area which has clearly black color can be selected by contrast difference, then the density of area and number of particles in image can be calculated.
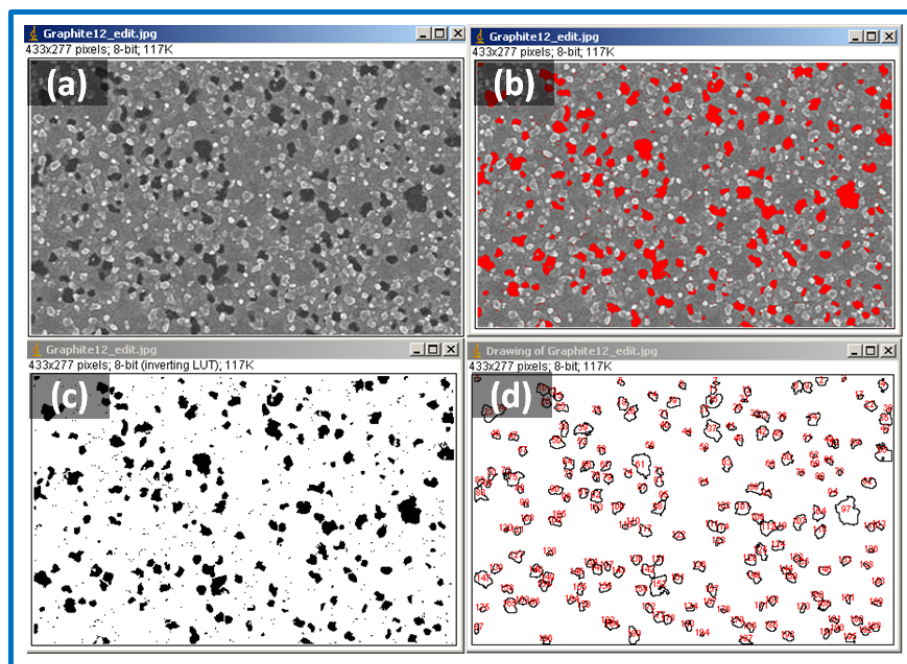
Figure 2.1. Surface analysis referred to contrast of image using Image J. (a) pristine SEM image, (b) filtered image by contrast, and calculation of (c) filtered area, (d) number of particles.

2.3. Atomic Force Microscopy

Atomic Force Microscopy (AFM) in the tapping mode is a commonly used tool to measure the thickness of graphene flakes on silicon oxide surfaces. We are using Veeco, Dimension^{TM} 3100 AFM system with a scan rate of 0.2 Hz over 10 μm x 10 μm surface, in general.

What is to consider in AFM data is the Instrumental offset. A. Gupta et al. investigated the height of a graphene deposit with estimated number of graphene layers by AFM[11]. From the following equation,

$$h = t \times n + t_0 \qquad\qquad\qquad \text{(Eq. 2.1.)}$$

where h is the height of graphene flakes (measured by AFM), n is the number of graphene layers (estimated by Raman), and t is the approximate theoretical thickness of a graphene layer, they inferred t_0 an AFM instrumental offset, independent of n. They obtained linear relationship, see in Figure 2.2., and extracted $t_0 = 0.33$ nm, i.e., a measurement of 0.7 nm height for a single layer[11]. This difference might result from the interaction between AFM tip and graphene, as compared to tip and SiO_2.
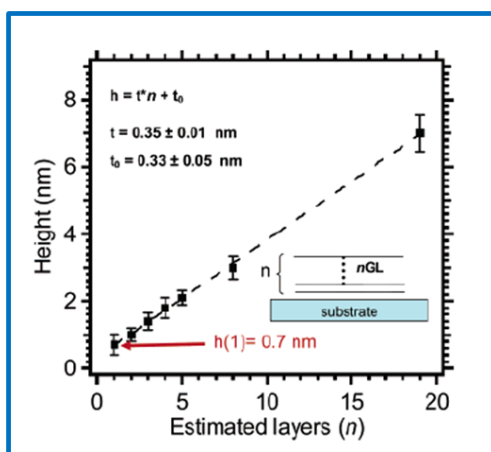
Figure 2.2. Thickness variation of graphene with estimated number of graphene layers. The straight line is a least-square fit to the data. Cited from A. Gupta et al. Nano Lett.**6**, 2667 (2006)[11]

Through AFM measurement before and after pre-annealing of metal for grain enlargement, the influence of catalyst grain (for example, size and flatness of grain) can be answered[4]. And some of structural defects, such as wrinkles, folded area, could be analyzed.

2.4. Transmission Electron Microscopy

Transmission electron microscopy (TEM) has been performed at either 120 kV, 200 kV using a high-resolution Topcon 002B (Courtesy of Thales R&T, Palaiseau, France) or a Jeol 2010 F (CIMEX, Écolepolytechnique) or at 300 kV using a FEI CM30 (CIMEX). TEM allowed us to study the morphologies of carbon-based materials and interfaced-layer in atomic resolution. The cross-sectional samples for TEM were prepared by slicing and polishing using the tripod technique down to the thickness of ~5 μm and then ion milling; the TEM plan-views were obtained by etching Ni, lifting-off of the graphene membrane, and depositing it on a holey carbon grid.

We use the diffraction line-width for measuring the average grain size of the graphene, following Scherrer formula. In 1918, P. Scherrer showed that, when parallel monochromatic radiation falls on a random oriented mass of crystals, the diffracted beam is broadened when the particle size is small[12-14]. By an approximation method he obtained an expression for the full width W of the diffracted beam in the form

$$W = \frac{K\lambda}{(L\cos \chi / 2)}$$

(Eq. 2.2.)

In which λ is the wavelength of the incident x-rays, L is the linear dimension of particle, χ/2 the Bragg

angle and K a numerical constant for which he obtained the value of $2(\ln2/\pi)^{1/2}$=0.93. In the case of TEM, where $\chi/2$ is small, the grain size L is, to a good approximation

$$L = \frac{K\lambda}{W} = \frac{Const.}{width(line)}$$

(Eq. 2.3.)

where K is the camera length of the microscope and B is the full width at half maximum, measured in units of length on the diffractogram. Particles having a width larger than the spatial coherency of the beam (up to several μm with field emission guns) will not increase the intrinsic line width.

2.5. Raman Spectroscopy

Raman spectroscopy has historically been used to study structural and electronic characteristics of carbon-basednanomaterials[15, 16], providing useful information on (i) the defects (D band), (ii) the degree of graphitization by in-plane vibration of sp^2-bound carbon atoms (G band), (iii) stacking order (2D band) as well as (iv) number of graphene layers via relative intensity ratio of each band. Raman spectra were acquired using a high-resolution (0.1 cm^{-1}) spectrometer (Labram HR800 from HORIBA Jobin Yvon) in a confocal microscope backscattering configuration. The objective used in this study was a 100× (NA = 0.9) objective from Olympus. Excitation was provided by a tunable Ar laser from Melles Griot (514-nm wavelength).
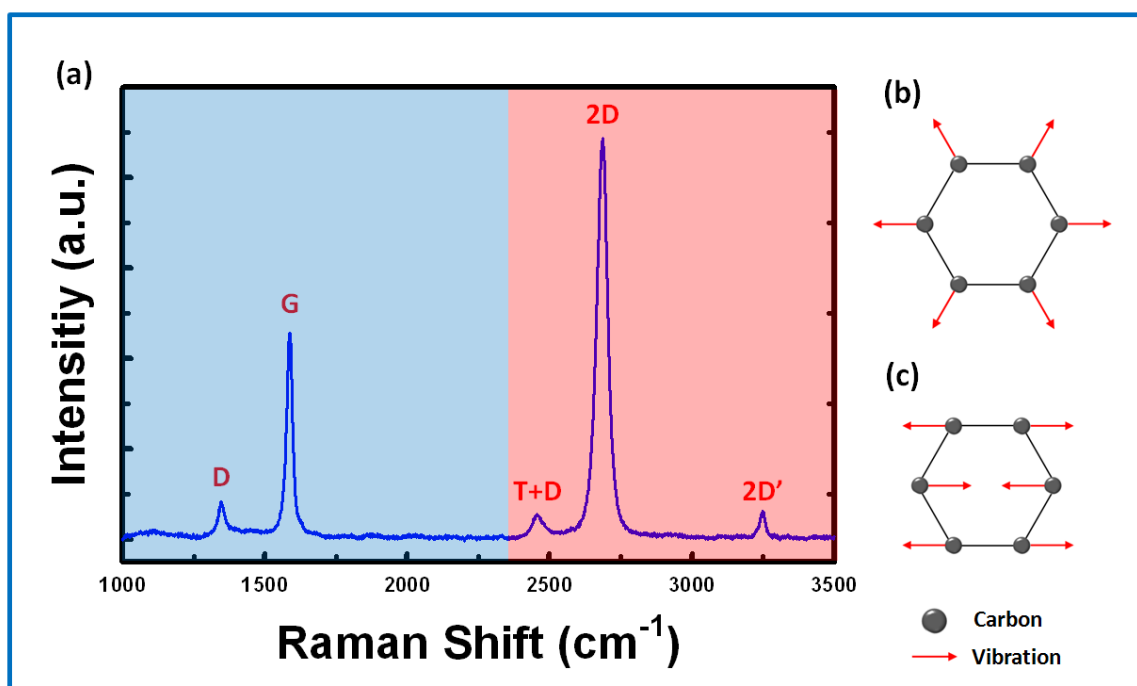

Figure 2.3. (a) Representative Raman spectrum of3 times layer-by-layer transferred single layers of graphene

from Cu foil. Note that, in high-quality graphene, D band is hardly detectable. In this case, D band is caused by the introduction of structural defects (wrinkles, folding, etc.) and chemical residue (metal etchants, polymers) comes from transfer process. Both first-order scattering (D, and G band in blue area) and 2nd-order scattering (T+D, 2D, and 2D' band in red area) are depicted. (b,c) carbon motions in the D and G mode, respectively.

The D peak located around 1350 cm^{-1} is a breathing mode of A$_{1g}$ symmetry involving phonons near the K zone boundary on the Brillouin zone. This mode is forbidden in *perfect graphite* and only becomes active by the presence of disorder. Note that the D mode is dispersive and thus depends on photon excitation energy, while the G peak is not dispersive. The G band originates from in-plane relative vibration of *sp^2* carbon atoms (see in Figure 2.3.(c)) and is a doubly degenerate (TO and LO) phonon mode (E$_{2g}$ symmetry) at the Brillouin zone center. The 2D band originates from a two phonon double resonance Raman process. The major Raman features of graphene and graphite are the so called G band (~1580 cm^{-1}) and 2D band (~2670 cm^{-1}).

The T+D peak can be ascribed to the combined dispersion of T ($\sim$ 1084 cm^{-1}) and D ($\sim$ 1350 cm^{-1}) modes at the Brillouin zone edge. The 2D' peak can be assigned to the second harmonic of D' peak ($\sim$ 1620 cm^{-1}), which does not require the existence of defects for its activation and is always present in the Raman spectrum of high-quality monolayer graphene.

2.5.1. Charge Doping

The in-plane vibrational G band of graphene is blue-shifted for both electron and hole doping, due to the nonadiabatic removal of the Kohn anomaly at the Γ point[17]. On the other hand, the 2D band is red-shifted for electron doping and blue-shifted for hole doping, due to the charge transfer induced modification of the equilibrium lattice parameter[18]. This makes Raman spectroscopy an effective technique to determine the doping type and dopant concentration in graphene.

A. Das et al., fabricated a back-gated graphene transistor for *in situ* Raman measurement[18], as shown in Figure 2.4. Referred to dirac voltage, 0.6 V here, electrostatic doping either p type (> 0.6 V) or n type (< 0.6 V) could be achieved. It is remarkable that G band frequency and width both exhibit symmetric changes relative to the value of 0.6 V. This symmetry is naturally linked to the symmetry of the electronic band structure that occurs at the Dirac point. In case of 2D band, shift is opposite direction for electron (redshift), and hole (blueshift).
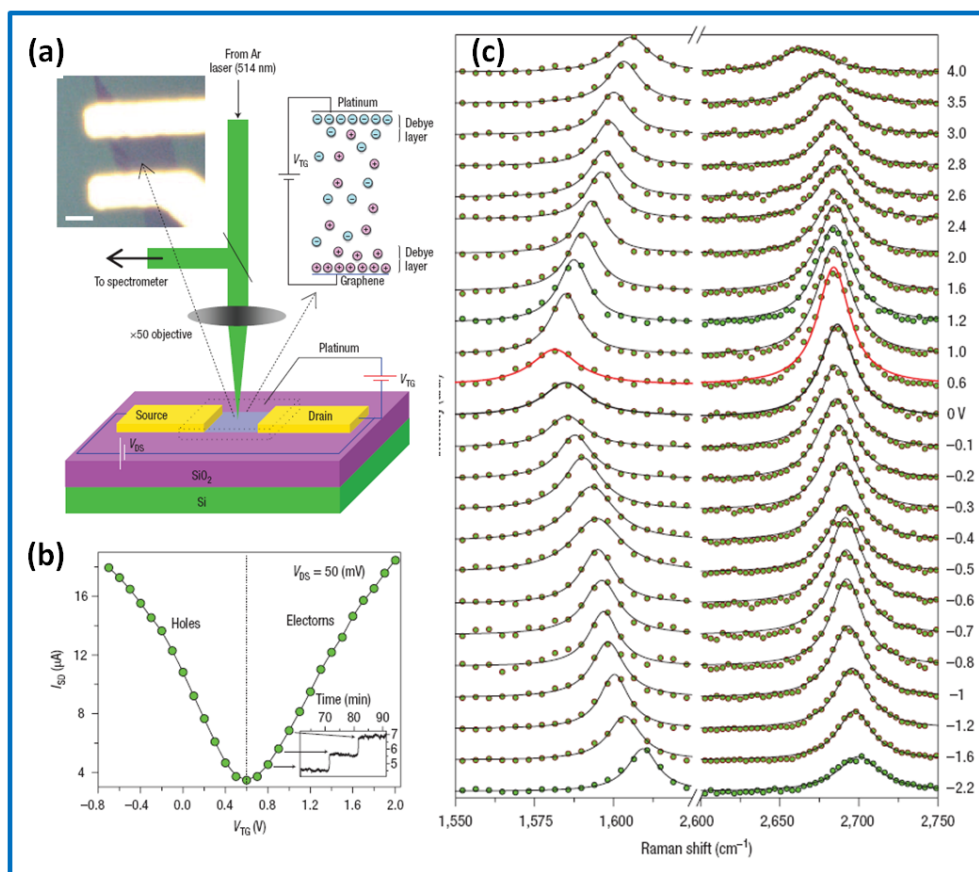
Figure 2.4. In-situ Raman measurement with electrostatic doping of graphene (a) Schematic diagram of the experimental setup. Between source and drain electrode, exfoliated-graphene flake is placed. (b) Drain current as a function of gate voltage. (c) Acquired in-situ Raman spectrum as a function of gate voltage. Cited from A. Das et al., Nat. Nanotechnol. **3**, 210 (2008)[18]

The integrated intensity ratio between 2D and G band, I_{2D}/I_G, is also known to be sensitive to charge doping. The strength of 2D band decreases with increasing charge density, while the strength of the G band remains rather constant[19]. This trend is confirmed for exfoliated and chemically grown ones[20].

2.5.2. Number of Graphene Layers

A strong Raman signal from single layer graphene on SiO$_2$/Si, comparable to that of bulk graphite, especially G band, has been observed by Y.Y. Want et al.[21]. The G peak originating from in-plane vibrations, the Raman intensity of G band should scale with the thickness of graphene/graphite samples up to the laser penetration depth, which is around 50 nm ($\sim$ 150 layers) for 532 nm laser.

However, Y. Y. Wang et al. found that the G band intensity of graphene sheets would decrease when the layers of graphene exceed certain value (see in Figure 2.5), while single layer graphene is comparable to that of graphite[21]. This is due to interferences of laser light in graphene sheets as well as the multi-reflection of Raman

light. Thus, they concluded that Raman signal of single graphene sheet can be enhanced 30 times by using a 269 nm SiO_2 above Si substrate.
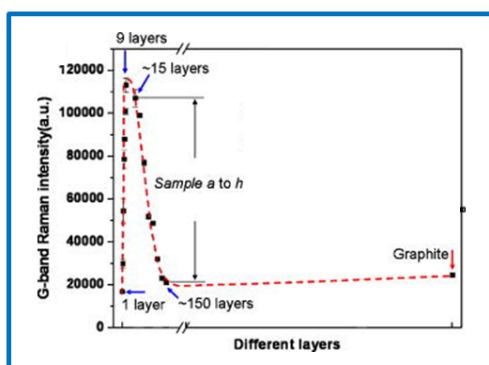
Figure 2.5. G band intensity of graphene sheets as a function of number of graphene layers (The data were collected using 532 nm radiation under ambient conditions). Cited from Y. Y. Wang et al., APL **92**, 043121 (2008) [21]

The intensity of the G band increases almost linearly as the graphene thickness increases in certain range. At the same time, G peak position is downshifted with increasing number of graphene layers. They prepared graphene layers from 1 to 20 on 100 nm-thick-SiO_2/Si wafer, via micromechanical cleavage using HOPG (Highly Oriented Pyrolytic Graphite). Raman spectra were then collected using 514.5 nm excitation under ambient conditions at low laser power (<2 mW). As they combined AFM system together in Raman spectroscopy, they can calculate the G peak shift, exactly. They found a linear relationship:

$$\omega_G = \omega_\infty + \beta / n \qquad\qquad \text{(Eq. 2.4.)}$$

where ω_G is the frequency of G peak, n is the number of graphene layers, and β is the constant value which is defined as 5.5 cm^{-1}. The differences in number of graphene layers, especially from 1 to 10 layers, result in blueshift of around 5 cm^{-1}
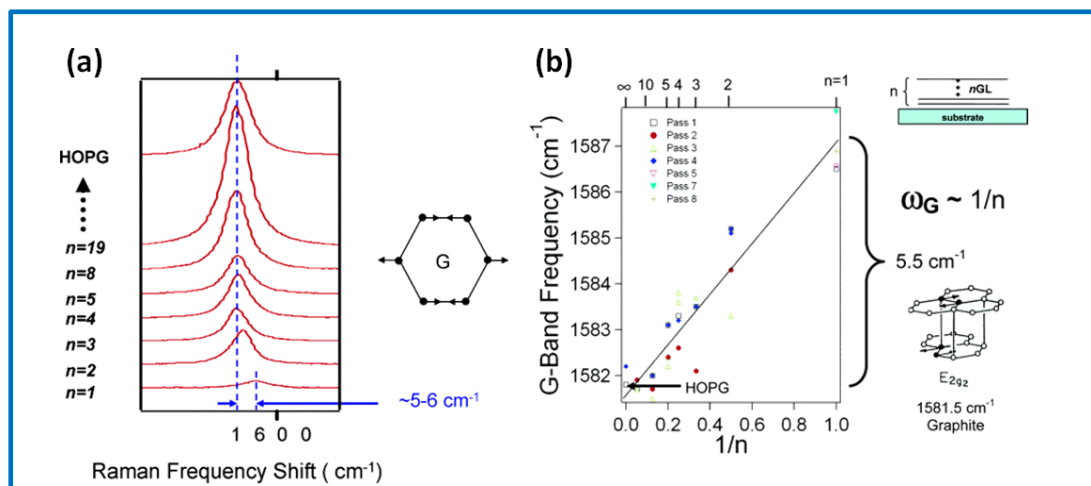
Figure 2.6. Effect of number of graphene layers on G peak intensity and peak shift. (a) Observed Raman spectra with increasing number of graphene layers and (b) extracted G peak position as a function of graphene thickness (The data were collected using 514.5 nm radiation under ambient conditions). Cited from A. Gupta et al., *Nano Lett.* **6**(12), 2667 (2006)[11]

The presence of symmetric 2D peak can be regarded as the fingerprint for the presence of monolayer graphene. The 2D band can also be used to count the number of graphene layers. The 2D band becomes broader and blueshifted when the graphene thickness increases from SLG to MLG[11].
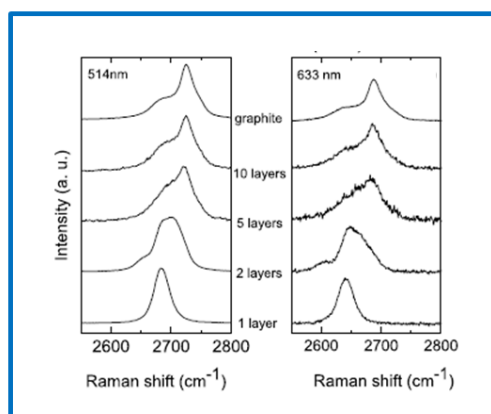
Figure 2.7. Evolution of the 2D peak at 514 nm and 633 nm with the number of graphene layers. Cited from A. C. Ferrari et al., Phys. Rev. Lett.**97**, 187401 (2006)[22]

2.5.3. Crystalline Size

Tuinstra and Koenig (TK) showed that the ratio between the D- and G-band Raman intensities (I_D/I_G) is directly related to the crystallite size (L_a) of 3D graphite[23, 24].

$$L_a = C(\lambda) * \frac{1}{(I_D / I_G)}$$

(Eq. 2.5.)

where C is a scaling coefficient

$$C(\lambda) \cong C_0 + \lambda_L * C_1$$

(Eq. 2.6.)

where C_0=-12.6 nm, C_1=0.033

if λ=514.5 nm,then C(λ)$\cong$4.379 nm

if λ=532.0 nm,then C(λ)$\cong$4.956 nm

2.5.4. Uniformity

A Raman spectrum of a solid contains information about its vibrational and electronic properties. Collecting spectral data with spatial resolution and encoding it in a 2D plot generates images with information complementary to optical and scanning force imaging. To investigate the uniformity as well as grain structure[25] of a graphene layer, Raman mapping is one of the best ways.

Q. Yu et al., present Raman mapping on single crystalline grain of graphene and nucleation sites/emerging area of two grains could be definitely found[25]. Such an investigation can bring the insights on the effect of grains of graphene on electronic/optical properties.
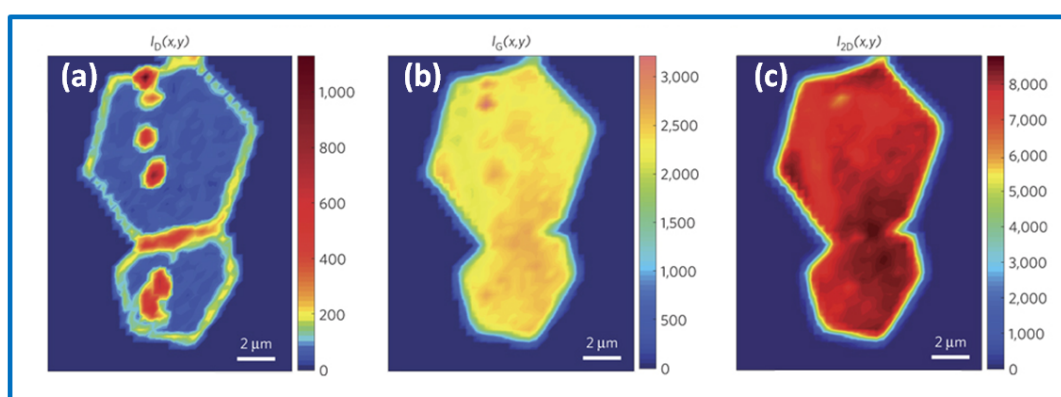
Figure 2.8. Raman mapping analysis on emerging single-crystalline graphene, referred to (a) D band, (b) G band, and (c) 2D band. Cited from Q. Yu et al., Nat. Mater. **10**, 443-449 (2011)[22]

Raman mapping is not only limited to each signal alone, but also possibly expand to correlation between two of them, even the bandwidth or position of peak can be used.

2.5.5. Stacking Order

Bilayer graphene (BLG), strongly coupled between two layers (AB stacking), has a similar integrated intensity of G and 2D band, while single layer graphene has much higher 2D band than that of G band[26-29]. However, when the stacking order of BLG is rotated, the interaction would be totally changed. Depend on degree of twist and coupling, relative intensity of G and 2D will be varied, this it would be a good indicator. Even mapping is possible to demonstrate the uniform stacking order.

C.H. Lui et al., reported that bernal (ABA stacking order) and rhombohedral (ABC order) trilayer graphene could be effectively identified by spatial Raman mapping (see in Figure 2.9.)[29]. Based on shape and width of 2D band, the distribution of stacking order can be determined. As the stacking order influences electrical properties of graphene, this would be a important measurement tools.
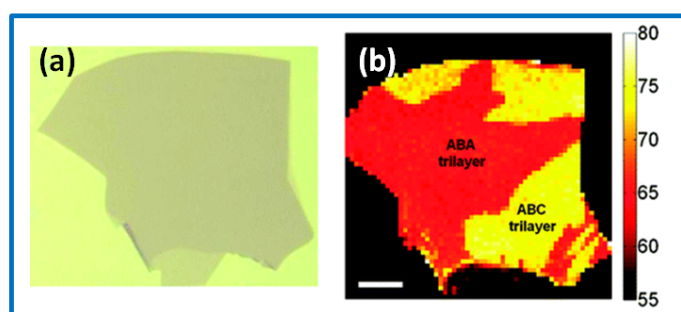
Figure 2.9. (a) Optical image and (b) corresponding spatial map of the spectral width of the Raman 2D-mode feature for trilayer graphene samples. The homogeneity of the optical images shows the uniformity of the layer thickness. The Raman images, taken with 514-nm excitation, are color coded according to the width of the Raman feature. Cited from C.H. Liu et al., Nano Lett. **11**, 164-169 (2011)[29]

2.6. Optical Transmittance

Single-layered graphene (SLG) absorbs only $\pi\alpha \approx$ 2.3 % of white light, where α ($= e^2 / \hbar c$) is the fine-structure constant[30, 31]. Thus, from the optical transmittance of grown-graphene, we can easily estimate the number of graphene layers. For optical transmittance measurement, we employed 6800 Double-Beam Spectrophotometer, JENWAY.

2.7. Electrical Characterization

2.7.1. Van der Pauw method

We have performed electrical characterization on transferred graphene layers. Especially, sheet resistance of graphene is of great importance and representative of two-dimensional entities. The van der Pauw method is a commonly used technique to measure the sheet resistance of materials, which was first proposed by L. J. van der Pauw in 1958[32].

In van der Pauw method, 4 point probes are directly located at the edges of graphene surface. Some of the scratches observed on uniform graphene surface can increase the sheet resistance. Since each probe is directly in contact with the graphene surface, calculated sheet resistance is sensitive to location and vibration during measurement.
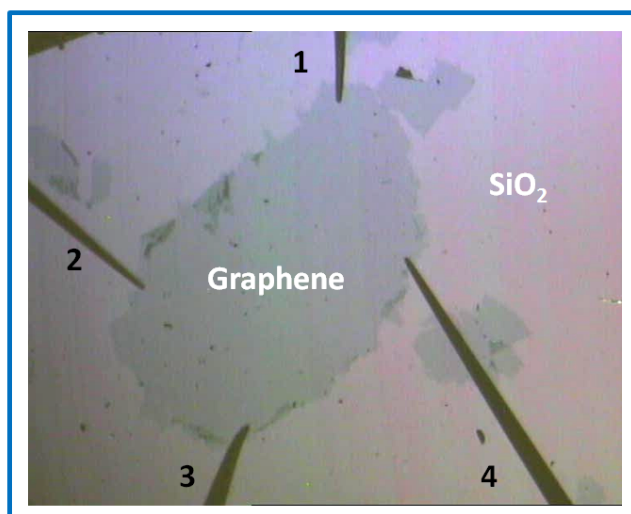
Figure 2.10. Optical image of graphene transferred on SiO_2 and van der Pauw measurement with 4 probe located at the edge of graphene flake.

To make a measurement, a current is caused to flow along one edge of the sample (for instance, I_{12}) and the voltage across the opposite edge (in this case, V_{34}) is measured. From these two values, a resistance (for this example, $R_{12,34}$) can be found using Ohm's law

$$R_{12,34} = \frac{V_{34}}{I_{12}}$$

(Eq. 2.7.)

van der Pauw discovered that the sheet resistance of samples with arbitrary shape can be determined from two of these resistances - one measured along a vertical edge, such as $R_{12,34}$, and a corresponding one measured along a horizontal edge, such as $R_{23,41}$. The actual sheet resistance is related to these resistances by

the van der Pauw formula

$$\exp(-\pi R_{12,34}/R_s) + \exp(-\pi R_{23,41}/R_s) = 1 \qquad \text{(Eq. 2.8.)}$$

From the reciprocity theorem, we can use following relation,

$$R_{AB,CD} = R_{CD,AB} \qquad \text{(Eq. 2.9.)}$$

Therefore, it is possible to obtain a more precise value for the resistances $R_{12,34}$ and $R_{23,41}$ by making two additional measurements of their reciprocal values $R_{34,12}$ and $R_{41,23}$ and averaging the results. We define here,

$$R_{vertical} = \frac{R_{12,34} + R_{34,12}}{2}, \quad R_{horizontal} = \frac{R_{23,41} + R_{41,23}}{2} \qquad \text{(Eq. 2.10.)}$$

Then, the van der Pauw formula becomes

$$\exp(-\frac{\pi R_{vertical}}{R_s}) + \exp(-\frac{\pi R_{horizontal}}{R_s}) = 1 \qquad \text{(Eq. 2.11.)}$$

A further improvement in the accuracy of the resistance values can be obtained by repeating the resistance measurements after switching polarities of both the current source and the voltage meter. Since this is still measuring the same portion of the sample, just in the opposite direction, the values of $R_{vertical}$ and $R_{horizontal}$ can still be calculated as the averages of the standard and reversed polarity measurements. The benefit of doing this is that any offset voltages, such as thermoelectric potentials due to the Seebeck effect, will be cancelled out. Combining these methods with the reciprocal measurements from above leads to the formulas for the resistances being

$$R_{vertical} = \frac{R_{12,34} + R_{34,12} + R_{21,43} + R_{43,21}}{2} \qquad \text{(Eq. 2.12.)}$$

$$R_{horizontal} = \frac{R_{23,41} + R_{41,23} + R_{32,14} + R_{14,32}}{2} \qquad \text{(Eq. 2.13.)}$$

The van der Pauw formula takes the same form as in the previous section. Both of the above procedures check the repeatability of the measurements. If any of the reversed polarity measurements don't agree to a sufficient degree of accuracy (usually within 3%) with the corresponding standard polarity measurement, then there is probably a source of error somewhere in the setup, which should be investigated

before continuing. The same principle applies to the reciprocal measurements—they should agree to a sufficient degree before they are used in any calculations.

In general, the van der Pauw formula cannot be rearranged to give the sheet resistance R_S in terms of known functions. The most notable exception to this is when $R_{vertical} = R = R_{horizontal}$; in this scenario the sheet resistance is given by

$$R_s = \frac{\pi R}{\ln 2}$$
(Eq. 2.14.)

X. Li et al., reported[33] that sheet resistance of graphene/PMMA stack under bending test via van der Pauw method, which in order of few hundred ohms per cm^2. H.J. Shin also performed van der Pauw measurement on doped graphene surface[34]. This method, van der Pauw, can be especially utilized in arbitrary shape of graphene flakes, so that appeared as useful technique.

2.7.2. Transfer Length Method

TLM (Transfer Length Method) can also be a useful method that can extract sheet resistance and contact resistance together. For TLM measurement, the array of silver electrode is directly printed on graphene surface, using Dimatix Material Printer DMP-2800 by FUJIFILM, USA.
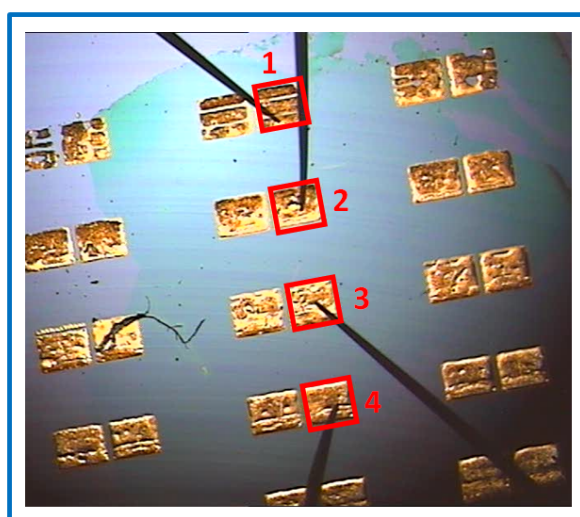
Figure 2.11. Optical image of graphene transferred on SiO$_2$ and TLM measurement with printed electrodes on graphene.

The ultra-low graphene-metal ohmic contact resistance (R_c) is crucial in the creation of high-

performance graphene transistors, which minimizes extrinsic source and drain charging delay and makes graphene FETs close to performing at their intrinsic speed[35]. In terms of contact resistance, TLM is much better than Van der Pauw method.

2.7.3. Humidity Sensing

Our group built up the platform for humidity sensing[36], see in Figure 2.8. The platform consists of (c) vacuum chamber with 4 point probes inside which are connected to (a) Keithley 4200-SCS for measurement. Below chamber, (d) a bottle of water is installed that can increase/decrease humidity by supplying water vapor through heated line. Setting humidity is measured by (f) Hygrometer (model: HC1000-400) which has an accuracy of 2.3% RH with a response time, less than 15 seconds.
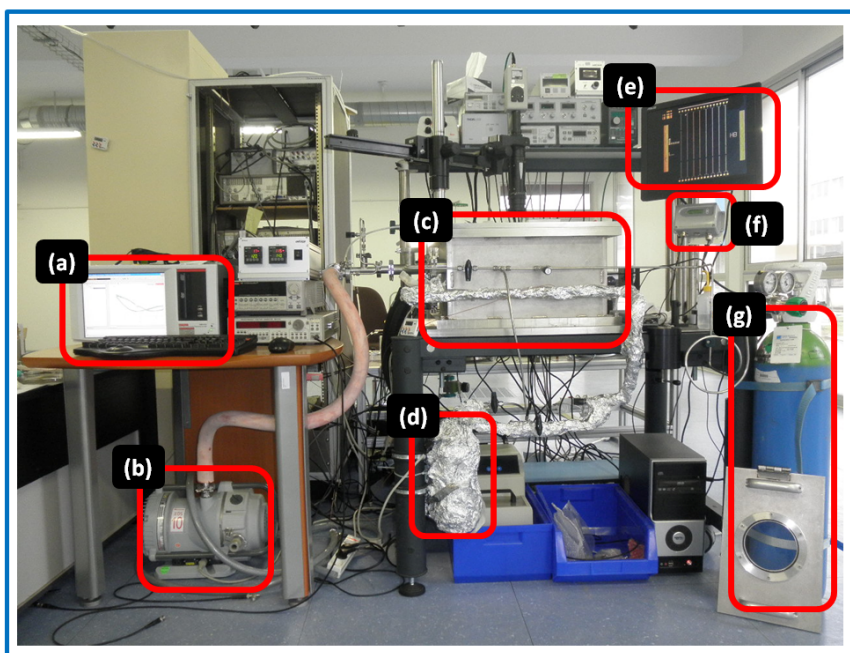
Figure 2.12. Photograph of test chamber for humidity sensing. (a) Keithley 4200-SCS, (b) Pump, (c) Test chamber, (d) Source of water vapor, (e) PC-monitor, (f)Hygrometer, and (g) dry gas. Credit: E. Norman, LPICM-Ecole Polytechnique

2.8. Conclusions

When the dimension of materials is reached down to nanoscale, even below nano, it is well-known that unusual properties can appear, as predicted by Richard Phillips Feynman (a lecture to the American Physical Society in 1959, titled "*There's Plenty of Room at the Bottom*"). For the research on sub-nano scale materials,

we need to develop accurate and reliable characterization methods.

Graphene, has a thickness of one atom, which has ever been reached before. Thus precise characterizations are mandatory to understand the properties and to progress in synthesis and applications. SEM, AFM and Raman are easily accessible tools with relatively fast measurements. However, SEM image, produced by second electron emission from species is a sort of virtual image, with a strong dependence on measurement environments, such as acceleration voltage, current, working distance, and substrate. On the other hand, AFM is a direct-imaging technique with a probe tip, but the Instrumental offset should be considered. Raman is a fast and non-destructive method that provides various useful data on graphene thickness, quality, doping, and interrelation with substrate. Raman system equipped with optical microscope, and mapping capability is now essential technique for graphene characterization.

Compare to above techniques, a TEM experiment is more powerful but also more time consuming. HR-TEM with atomic resolution is one of the direct measurements to characterize the crystal structure. Cross-sectional TEM is widely used to determine the structure of graphene at the interface between metal and substrate and the number of graphene layers.

Most of the graphene that we've synthesized is polycrystalline and it is widely assumed that grain boundaries of graphene are detrimental to charge transport. To identify the crystallite size, "*Tuinstra & Koenig (TK) equation*" in Raman (Eq. 2.5.) and "*Scherrer equation*" in TEM (Eq. 2.3.) can be used. From the comparison of two routes, the accurate estimation of crystallite size should be followed.

The monolayer graphene is absorbing only 2.3% of while light, thus optical transmittance measurement giving the information of graphene thickness. Sheet resistance of graphene (measured by Van der Pauw or TLM) is receiving a lot of attention from industries to compete with ITO (which is currently used as transparent conducting films). Of course, a trade-off should be found between the two factors, optical transmittance and sheet resistance, for each application, optimization depends on purpose of use.

Graphene is requiring an unheard-of precise characterization given the sensitivity of its properties to small variations. Thus in general as in the present work, multiple measurements are performed to correctly determine graphene thickness, quality, uniformity, and optical/electrical properties.

Reference

1.   Jung, I., Pelton, M., Piner, R., Dikin, D. A., Stankovich, S., Watcharotone, S., Hausner, M. and Ruoff, R. S. Simple Approach for High-Contrast Optical Imaging and Characterization of Graphene-Based Sheets. *Nano Letters* **7**, 3569-3575 (2007)

2.   Kim, D. W., Kim, Y. H., Jeong, H. S. and Jung, H.-T. Direct visualization of large-area graphene domains and boundaries by optical birefringency. *Nat Nano* **7**, 29-34 (2012)

3.   Wang, X., Zhao, M. and Nolte, D. D. Optical contrast and clarity of graphene on an arbitrary substrate. *Applied Physics Letters* **95**, 081102-3 (2009)

4.   Thiele, S., Reina, A., Healey, P., Kedzierski, J., Wyatt, P., Hsu, P.-L., Keast, C., Schaefer, J. and Jing, K. Engineering polycrystalline Ni films to improve thickness uniformity of the chemical-vapor-deposition-grown graphene films. *Nanotechnology* **21**, 015601 (2010)

5.   Liu, W., Chung, C.-H., Miao, C.-Q., Wang, Y.-J., Li, B.-Y., Ruan, L.-Y., Patel, K., Park, Y.-J., Woo, J. and Xie, Y.-H. Chemical vapor deposition of large area few layer graphene on Si catalyzed with nickel films. *Thin Solid Films* **518**, S128-S132 (2010)

6.   Seiler, H. Secondary electron emission in the scanning electron microscope. *Journal of Applied Physics* **54**, R1-R18 (1983)

7.   Park, M.-H., Kim, T.-H. and Yang, C.-W. Thickness contrast of few-layered graphene in SEM. *Surface and Interface Analysis*, n/a-n/a (2012)

8.   Kochat, V., Pal, A. N., Sneha, E. S., Sampathkumar, A., Gairola, A., Shivashankar, S. A., Raghavan, S. and Ghosh, A. High contrast imaging and thickness determination of graphene with in-column secondary electron microscopy. *Journal of Applied Physics* **110**, 014315-5 (2011)

9.   Goldstein, G. I., Newbury, D. E., Echlin, P., Joy, D. C., Fiori, C. and Lifshin, E. Scanning electron microscopy and x-ray microanalysis. New York: Plenum Press. ISBN 0-306-40768-X (1981)

10.   Venables, J. A. and Harland, C. J. Electron back-scattering patterns - A new technique for obtaining crystallographic information in the scanning electron microscope. *Philosophical Magazine* **27**, 1193-1200 (1973)

11.   Gupta, A., Chen, G., Joshi, P., Tadigadapa, S. and Eklund. Raman Scattering from High-Frequency Phonons in Supported n-Graphene Layer Films. *Nano Letters* **6**, 2667-2673 (2006)

12.   Scherrer, P. Bestimmung der Grösse und der inneren Struktur von Kolloidteilchen mittels Röntgenstrahlen. *Nachr. Ges. Wiss. Göttingen* **26**, 98 (1918)

13.   Langford, J. I. and Wilson, A. J. C. Scherrer after sixty years: A survey and some new results in the determination of crystallite size. *Journal of Applied Crystallography* **11**, 102 (1978)

14.   Patterson, A. L. The Scherrer formula for X-Ray particle size determination. *Physical Review* **56**, 978-982 (1939)

15.   Ferrari, A. C. and Robertson, J. Interpretation of Raman spectra of disordered and amorphous carbon. *Physical Review B* **61**, 14095-14107 (2000)

16.   Ferrari, A. C. and Robertson, J. Resonant Raman spectroscopy of disordered, amorphous, and diamondlike carbon. *Physical Review B* **64**, 075414 (2001)

17.   Pisana, S., Lazzeri, M., Casiraghi, C., Novoselov, K. S., Geim, A. K., Ferrari, A. C. and Mauri, F. Breakdown of the adiabatic Born-Oppenheimer approximation in graphene. *Nat Mater* **6**, 198-201 (2007)

18.   DasA, PisanaS, ChakrabortyB, PiscanecS, Saha, S. K., Waghmare, U. V., Novoselov, K. S., Krishnamurthy, H. R., Geim, A. K., Ferrari, A. C. and Sood, A. K. Monitoring dopants by Raman scattering in an electrochemically top-gated graphene transistor. *Nat Nano* **3**, 210-215 (2008)

19.   Shim, J., Lui, C. H., Ko, T. Y., Yu, Y.-J., Kim, P., Heinz, T. F. and Ryu, S. Water-Gated Charge Doping of Graphene Induced by Mica Substrates. *Nano Letters* **12**, 648-654 (2012)

20.   Kalbac, M., Reina-Cecco, A., Farhat, H., Kong, J., Kavan, L. and Dresselhaus, M. S. The Influence of Strong Electron and Hole Doping on the Raman Intensity of Chemical Vapor-Deposition Graphene. *ACS Nano* **4**, 6055-6063 (2010)

21.   Wang, Y. Y., Ni, Z. H., Shen, Z. X., Wang, H. M. and Wu, Y. H. Interference enhancement of Raman signal of graphene. *Applied Physics Letters* **92**, 043121-3 (2008)

22.   Ferrari, A. C., Meyer, J. C., Scardaci, V., Casiraghi, C., Lazzeri, M., Mauri, F., Piscanec, S., Jiang, D., Novoselov, K. S., Roth, S. and Geim, A. K. Raman Spectrum of Graphene and Graphene Layers. *Physical Review Letters* **97**, 187401 (2006)

23.   Matthews, M. J., Pimenta, M. A., Dresselhaus, G., Dresselhaus, M. S. and Endo, M. Origin of dispersive effects of the Raman D band in carbon materials. *Physical Review B* **59**, R6585-R6588 (1999)

24.   Tuinstra, F. and Koenig, J. L. Raman Spectrum of Graphite. *The Journal of Chemical Physics* **53**, 1126-1130 (1970)

25.   Yu, Q., Jauregui, L. A., Wu, W., Colby, R., Tian, J., Su, Z., Cao, H., Liu, Z., Pandey, D., Wei, D., Chung, T. F., Peng, P., Guisinger, N. P., Stach, E. A., Bao, J., Pei, S.-S. and Chen, Y. P. Control and characterization of individual grains and grain boundaries in graphene grown by chemical vapour deposition. *Nat Mater* **10**, 443-449 (2011)

26.   Rao, R., Podila, R., Tsuchikawa, R., Katoch, J., Tishler, D., Rao, A. M. and Ishigami, M. Effects of Layer Stacking on the Combination Raman Modes in Graphene. *ACS Nano* **5**, 1594-1599 (2011)

27.   Cong, C., Yu, T., Sato, K., Shang, J., Saito, R., Dresselhaus, G. F. and Dresselhaus, M. S. Raman Characterization of ABA- and ABC-Stacked Trilayer Graphene. *ACS Nano* **5**, 8760-8768 (2011)

28.   Zhan, D., Liu, L., Xu, Y. N., Ni, Z. H., Yan, J. X., Zhao, C. and Shen, Z. X. Low temperature edge dynamics of AB-stacked bilayer graphene: Naturally favored closed zigzag edges. *Sci. Rep.* **1** (2011)

29.   Lui, C. H., Li, Z., Chen, Z., Klimov, P. V., Brus, L. E. and Heinz, T. F. Imaging Stacking Order in Few-Layer Graphene. *Nano Letters* **11**, 164-169 (2011)

30.   Kuzmenko, A. B., van Heumen, E., Carbone, F. and van der Marel, D. Universal Optical Conductance of Graphite. *Physical Review Letters* **100**, 117401 (2008)

31.   Nair, R. R., Blake, P., Grigorenko, A. N., Novoselov, K. S., Booth, T. J., Stauber, T., Peres, N. M. R. and

Geim, A. K. Fine Structure Constant Defines Visual Transparency of Graphene. *Science* **320**, 1308 (2008)

32. Van der Pauw, L. J. A method of measuring specific resistivity and Hall effect of discs of arbitrary shape. *Philips Research Reports* **13**, 1-9 (1958)

33. Li, X., Zhu, Y., Cai, W., Borysiak, M., Han, B., Chen, D., Piner, R. D., Colombo, L. and Ruoff, R. S. Transfer of Large-Area Graphene Films for High-Performance Transparent Conductive Electrodes. *Nano Letters* **9**, 4359-4363 (2009)

34. Shin, H.-J., Choi, W. M., Choi, D., Han, G. H., Yoon, S.-M., Park, H.-K., Kim, S.-W., Jin, Y. W., Lee, S. Y., Kim, J. M., Choi, J.-Y. and Lee, Y. H. Control of Electronic Structure of Graphene by Various Dopants and Their Effects on a Nanogenerator. *Journal of the American Chemical Society* **132**, 15603-15609 (2010)

35. Xia, F., Perebeinos, V., Lin, Y.-m., Wu, Y. and Avouris, P. The origins and limits of metal-graphene junction resistance. *Nat Nano* **6**, 179-184 (2011)

36. Lebental, B., Moujahid, W., Lee, C. S., Maurice, J.-L. and Cojocaru, C. S. Graphene-based resistive humidity sensor for in situ monitoring of drying shrinkage and intrinsic permeability in concrete. *NICOM4: 4th Int. Symp. Nanotechnology in Construction* (2012)

Outline

Chapter III. Graphene Growth Techniques 55

Chapter III. Graphene Growth Techniques

History: Behind the curtain

Band theory of graphene was first explored by Philip R. Wallace in 1947 as a starting point for understanding the electronics properties of more complex structure, 3-dimensional graphite[1]. In fact, graphene has been experimentally studied for over 40 years. In 1962, Hanns-Peter Boehm et al., described single-layer carbon foils[2]. During 1970s, the fundamental aspects of carbon reaction with Ni, including segregation, precipitation and crystallization, have been reported. These all lay groundwork for understanding of graphene growth mechanisms on transition metals[3-5]. The term *"graphene"*, coined as a combination of *"graphite"* and the suffix *"–ene"*, has first appeared in 1987 to describe single sheets of graphite within graphite intercalation compounds (GICs)[6].

Before the isolation of graphene, there were a number of previous attempts to make atomically thin graphitic films by using exfoliation techniques. Rodney S. Ruoff et al., reported tailoring graphite with the goal of achieving single sheets. They've fabricated graphite islands by oxygen plasma etching on HOPG, then ,simply by rubbing the HOPG surface against the surface of other substrates, the thin graphite can be easily cleaved along the basal plane[7]. This technique led to finally electric-field-dependent transport measurements of extremely thing graphite by P. Kim et al.[8]

3.1. Exfoliation General

Exfoliation of graphite can be considered as the reverse process of stacking graphene into graphite. The stacking process is the result of chemical bonding between adjacent graphene sheets. The lowest energy and thus most common stacking is "*Bernal stacking*", in which adjacent graphene sheets are rotated with an angle of 60° relative to each other about the stacking axis. This results in the formation of two sublattices of atoms. For the sublattice consisting of A atoms, for every A atom there is another A atom positioned in the adjacent sheet below, whereas for the other sublattice consisting of B atoms, there are no respective B atoms below them in the adjacent sheet. The intersheet spacing in the stacking direction (or c direction) is 3.354 Å. The adjacent sheets are bonded through the overlap of partially filled p_z (or π) orbitals perpendicular to the plane, also known as van der Waals force. Due to the large lattice spacing and weak bonding in the c direction as compared to the small lattice spacing and much stronger σ bonding in the hexagonal lattice plane, it has long been tempting to obtain graphene sheets through exfoliation of graphite. Experimentally, exfoliation of graphite has been investigated and realized by using various techniques, including chemical/solution, mechanical, and thermal methods.

3.1.1. Mechanical Exfoliation (or Mechanical Cleavage)

The best quality graphene, in terms of structural integrity and electronic performance, is obtained by mechanical cleavage of highly oriented pyrolytic graphite (HOPG). In this procedure, a layer is peeled off the HOPG crystal with Scotch tape and transferred onto a silicon substrate. This was the first way to demonstrate ideal graphene, i.e. only single atomic layer, and the observation of field effect in graphene has led to Novel Prize in Physics 2010.

Obtaining graphene with a fabricating method which is simple and easy has lead to a variety of fundamental studies. However, although exfoliated graphene has very low concentration of structural defects, the flake thickness, size, and location are largely uncontrollable, which prevents the use of such a graphene out of laboratories. So, several strategies are presently being pursued to achieve reproducible and scalable graphene on various substrates.

3.2.2. Chemical Exfoliation

One of the key challenges in the synthesis of large quantities of graphene sheets is to overcome the strong cohesive van der Waals energy of the π-stacked layers in graphite[9]. A popular chemical method to prepare single layer graphene (SLG) is the reduction of graphene oxide in chemical solution.

Like mechanical exfoliation, chemical exfoliation of graphite is also an old technique. The primary advantage of chemical exfoliation over the mechanical approach lies in its high-yield and scalability. The chemical exfoliation is generally accomplished in two process steps. The first step is to enlarge the interlayer spacing between graphene sheets by forming graphite intercalated compounds (GICs). The GICs can be formed in many different forms, depending on the types of the intercalants, although not all of them are suitable for the subsequent exfoliation process.

One of the popular methods to form GICs for exfoliation purpose is to soak graphite for an extended period of time in mixtures of sulfuric and nitric acid. After an appropriate duration of soaking, the acid molecules penetrate into the graphite, forming alternating layers of graphite and intercalant. The thickness of the graphite layers decreases with time, with a possibility down to a few layers, though the yield of obtaining few layer graphene sheets is typically quite low. After the intercalation, the second step is to exfoliate the thin graphite sheets via rapid evaporation of the intercalated material at elevated temperature. The extent of exfoliation can be further enhanced by subjecting the thermal annealed GICs to treatments like ball milling and ultrasonication. Although this technique is simple, the graphite nanoplatelets obtained via this method usually exhibit thicknesses ranging from a few to a few hundreds of layers. In order to obtain SLG, the intercalation and exfoliation processes have to be repeated by using different intercalating and exfoliating chemistry and

processes. Alternatively, one can also oxidize the graphite completely to form GOs. The GOs can be subsequently exfoliated to form very thin GO sheets using different techniques. A chemical, thermal, or electrochemical reduction process is then followed to convert the GOs into graphene sheets. Some typical experiments are described below.

Fabrication of graphene sheets via chemical routes has potential but presents several challenges. Efforts are required for both gaining an understanding of the intercalation, oxidation, exfoliation, reduction, fictionalization, and dispersion processes and developing new starting materials and reaction routes. More details can be found in a recent review[10].

3.2. Sublimation of SiC at high temperature, under UHV

The growth of graphene on SiC has the primary advantage of growth on large area insulating or semiconducting substrates. SiC is a wide band gap semiconductor (3.2 eV for 4H-SiC and 3.0 eV for 6H-SiC) with both cubic and a number of hexagonal crystalline structures. It is important to realize that SiC has two polar faces perpendicular to the c-axis. The SiC (0001) Si-terminated face (Si-face) has one dangling Si bond per Si atom, while the SiC ($000\bar{1}$) C-terminated face (C-face) has one C dangling bond per C atom. Because of the relationship between graphene and SiC lattice constants, there are a large number of possible orientations of a graphene lattice that lead to nearly commensurate structures with the SiC (0001) and ($000\bar{1}$) surfaces. The two commonly used polytypes of hexagonal SiC are 6H and 4H, as unit cells are shown in Figure 3.1. In both cases the cells are composed of Si-C bilayers with different stacking arrangements.

The pioneering investigations into graphite formation on 6H-SiC (0001) and ($000\bar{1}$) surfaces were performed by van Bommel et al.[11] They performed heat treatment of SiC crystal surface in temperature range between 1000 ^{o}C and 1500 ^{o}C, and found carbon rich surface through LEED and AES measurements. It was also clear from these early works that graphene formation on the two polar surfaces was clearly different. Graphene growth on the Si-face is much slower compared to growth on C-face. In addition, Si-face graphene is epitaxial with a phase rotated 30° relative to the SiC while C-face films can have multiple-orientation phases. Because of the orientational disorder in C-face grown graphene, most structural, growth and electronic studies of epitaxial graphene focused on Si-face graphene.

From stoichiometry alone the formation of a single graphene sheet requires the carbon contained in SiC bilayers. Liberating this much carbon requires the removal, and subsequent sublimation into the vacuum, of Si from more than three SiC bilayers. This presents a serious challenge because even at temperatures of 1440 ^{o}C (well above the graphitization temperature), the diffusion of Si or C in bulk SiC is essentially zero.

Another stoichiometric consequence of the SiC bilayer carbon concentration is that when Si is removed from the SiC/graphene interface, so that enough carbon has been liberated to form a single graphene sheet, there must be a partial SiC bilayer left at the carbon-graphene interface. We can assume that a graphene layer forms only when the areal density of carbon is equal to the areal density of graphene and all the carbon comes from the SiC substrate. A plot of the excess carbon as a function of SiC bilayers consumed during Si sublimation reveals a periodic minimum every $\sim$7 graphene layers.

Epitaxial graphene on both the ($000\overline{1}$) (C-face) and the (0001) (Si-face) of SiC not only comparable to the structural and impurity quality of exfoliated graphene but is scalable to large scale circuits as well[12-14].

3.3. Metal-Catalyzed Growth

In this Section 3.3., we will describe metal-catalyzed growth of graphene which is widely investigated now[15-25].

3.3.1. Surface vs Interface

SLG or MLG sheets can be readily formed on selected metal surfaces via either surface segregation of carbon atoms or thermal decomposition of carbon-containing molecules.

In the first method, the source of carbon can either be (i) the small amount of carbon impurities[26] or (ii) the intentionally introduced carbon through implantation[27-30] or (iii) in contact with solid-phase carbon source (amorphous carbon[18, 31], amorphpous SiC[32], polymer[33, 34], diamond[19], graphite, and even waste[35]). Then, annealing of the carbon containing metals causes the carbon to segregate to the surface. Depending on the annealing conditions (temperature, duration, surrounding gas, cooling rate, etc.), the segregated carbon can be in the form of MLG or SLG on the metallic surface. The former is formed when the segregated carbon reaches thermal equilibrium with the metal.

In the second method, the metal surface is exposed to carbon-containing molecules at elevated temperature. For example, the hydrocarbon, such methane and acetylene, is widely using as a carbon source, given that thermal decomposition of molecules supported by catalytic effect result in absorption on/in substrate to form graphene.

Depend on whether (i) carbon atoms are pre-included or supplied in high temperature process and (ii) carbon atoms are dissolved into metallic substrate or directly react with surface, the underlying growth mechanisms need to be clarified.

In the field of graphene synthesis, the research paradigm is changing amazingly fast. Our group suggested that carbon atoms could diffuse through ($\sim$ 200 nm-thick) catalyst layer, which means that graphene could be located at the opposite side. Such a graphene, placing at interface between catalyst and underlying insulating substrate, could be directly used in device application, which is the most attractive advantage in this technique.

There are some reports on graphene growth without catalyst layer, but, in general, a metallic substrate is widely required. Furthermore, the interfacial graphene layer grown by carbon diffusion passing through catalyst layer might open new capabilities in development of graphene-based applications. This will be pointed out in later.

3.3.2. Chemical Vapor Deposition

Graphite segregation at surfaces and grain boundaries of metals has been studied for a long time[36]. At high temperature, Ni can dissolve relatively large amount of carbon compare to at room temperature, and during cooling process, excess carbon in nickel should be out-diffused, namely segregation/precipitation process, so that graphene layers could be formed on catalyst surface. However, the number of graphene layers thus segregated and high temperatures cannot be preserved at ambient temperature due to nonequilibrium segregation of carbon while cooling down. To overcome this limitation, a variety of efforts were followed, especially focused on cooling rate. In their experiments by Qingkai Yu et al.[37], carbons are dissolved into Ni at 1000 $^{\circ}$C, and then, the sample is cooled down by mechanically pushing the sample holder to a lower temperature. The cooling rate was monitored by a thermocouple on the sample holder, and corresponded to fast (20 $^{\circ}$C/s), medium (10 $^{\circ}$C/s), and slow (0.1 $^{\circ}$C/s). The Raman spectra (Figure 4.1.(b)) show the quality of graphene segregated at Ni surfaces. Several layers of high quality graphene could be synthesized on Ni surface with optimized medium cooling rates, while higher cooling rates resulted in the formation of graphite with more defects[37].
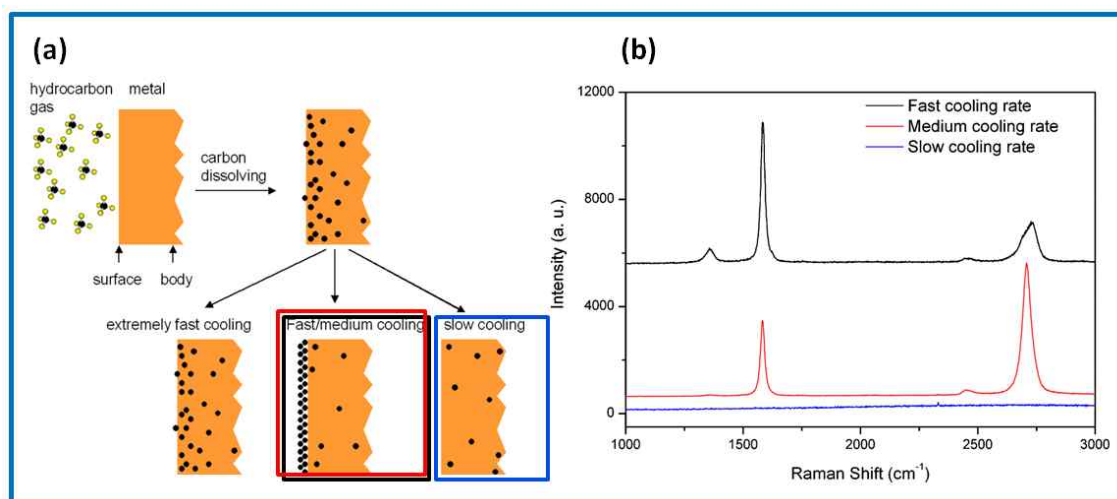
Figure 3.1. Approach to overcome the nonequilibirm carbon segregation in Ni for uniform graphene growth. (a) Illustration of carbon segregation at metal surfaces, and (b) its corresponding Raman spectra (excited by an Argon laser operating at 514 nm wavelength) depending on cooling rate. Citied from Qingkai Yu et al., APL, **93**, 113103 (2008)[37]

CVD is a technique used for such a long time. Since the most of current semiconductor industry has CVD-based infrastructure, the importance of this route is worthy of being highlighted. In this section, I will introduce a variety of CVD technique, such as thermal CVD (T-CVD), dc-PECVD, MW-PECVD and HW-CVD, from the viewpoint of comparison with some examples.

3.3.2.1. Thermal-CVD

The first report on few layer graphene (FLG) synthesized by CVD appeared in 2006. P. R. Somani et al.,employed a natural, eco-friendly, low cost precursor, namely camphor, and after they evaporated/pyrolyzed in CVD furnace, few layer graphene sheets on Ni foils were observed. Graphene, thus produced, was found to have multiple folds and estimated to have approximately 35 layers of graphene sheets. This study opened up a new processing route for graphene synthesis, though several issues like controlling the number of layers, minimizing the folds etc, were yet to be solved[38].

Reliable transfer of large-area monolayer graphene onto arbitrary substrates is a critical step in the use of CVD-grown graphene for most practical applications. J. Kong et al.[39, 40] have reported, for the first time, the large scale transfer of graphene layers by using of PMMA, as in the case of CNTs[41].

Problems associated with large-scale pattern growth of graphene constitute one of the main obstacles to using this material in device applications. B. H. Hong et al., presented that graphene could be grown on pre-patterned Ni surface and be transferred to another substrate. Especially, they realized its full potential toward stretchable, transparent electrodes[24].

One of the revolutions in CVD-graphene came out in 2009, by Rodney S. Ruoff and his team. They employed Cu as a catalyst metal, instead of Ni, and they succeed in obtaining large area, high quality, and uniform single layer graphene[25]. As the Cu has low carbon solubility, having almost negligible value (0.001~0.008 wt.% at 1084 ^{o}C[23]), the self-limiting mechanism proposed in which graphene growth process. This means that only surface react with supplying gas to form graphene layers. The coverage of single layer graphene was more than 95 %, and the rest was two- or three-layer graphene. In addition, Cu has a relatively large grain size, with respect to Ni, which results in low density of grain boundaries in graphene. This means that high quality graphene, in term of electrical properties with reduced charge scattering, could be obtained.

Again, B. H. Hong *et al.* show significant step forward on graphene applications by roll-to-roll (R2R) process[42]. They grow large scale graphene on 30 inch Cu foils at high temperature with their CVD process, and then they load Graphene/Cu foil in R2R system. By using combination of polymer coating, Cu etching, and releasing polymer support on a target substrate, large area graphene can be transferred simply and finally succeed in operating touch screen with transferred graphene. From the industrial aspects, it is one of the most breaking results, and it has been attracting worldwide attention.

The strong interest in graphene has motivated the scalable production of high-quality graphene and graphene devices. As the large-scale graphene films synthesized so far are typically polycrystalline, consisting of many single-crystalline grains separated by grain boundaries, it is important to characterize and control grain boundaries, generally believed to degrade graphene quality[43].
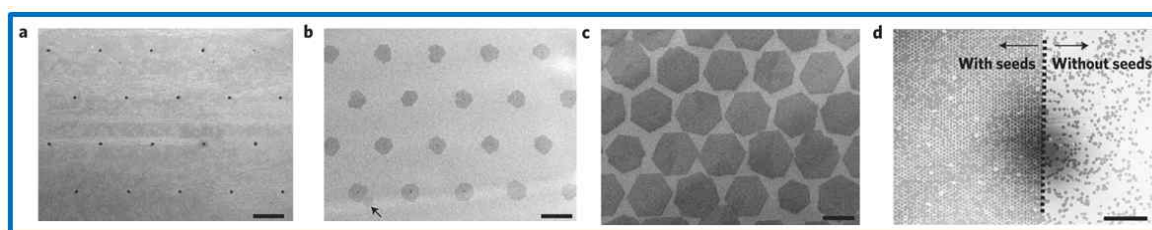
Figure 3.2. SEM images showing; (a) An array of seed crystal patterned form a pre-grown multilayer graphene film on Cu foil by e-beam lithography. The size of each seed is about 500 nm, and period of array is 16 µm. Typical graphene grain array grown from an array of seed crystals (b) for 5 minutes, and (c) for 15 minutes, respectively. (d) Effect of seed array on graphene growth. Scale bar is 10 µm for (a-c), and 200 µm for (d). Cited from Q. Yu et al., Nat. Mater. **10**, 443-449 (2011)[43]

Controlled growth of high-quality graphene is still the bottleneck of practical applications. The widely used chemical vapour deposition process generally suffers from an uncontrollable carbon precipitation effect that leads to inhomogeneous growth and strong correlation to the growth conditions. Indeed, a rather narrow

process window should be enlarged, in terms of growth temperature & duration, gas ratio & type etc. Zhongfan Liu et al. demonstrated that, through rational design of a binary metal alloy, they can effectively suppress the carbon precipitation process and activate a self-limited growth mechanism for homogeneous monolayer graphene[44]. The key of their strategy is to utilize a molybdenum (Mo) component in a binary alloy to trap all of the dissolved excess carbon species in the form of molybdenum carbides, which are chemically stable throughout the high-temperature growth process. This type of process engineering has been used to grow strictly single-layer graphene with 100% surface coverage and excellent tolerance to variations in growth conditions. With simplicity, scalability and a very large growth window, the presented approach may facilitate graphene research and industrial applications.

3.3.2.2. dc-PECVD

In another approach, 1 to 2 nm thick well-ordered graphene sheet was reported to be grown on Ni substrate by plasma-assisted CVD (PECVD), while the same treatment failed to synthesize graphene on Si. DC plasma is ignited by a mixture of methane and hydrogen, and they found atomically smooth micrometer size regions, separated by ridges. This paper demonstrated, for the first time, which PECVD can be used to grow graphene layers[45]*.*

However, dc-PECVD is the main technique used for growing graphene in the present work. We present the setup we have used and the results we obtained in Chapter V.

3.3.2.3. MW-PECVD

A. Malesevic et al. presented a possible route for the mass production of freestanding few-layered graphene (FLG) by means of MW-PECVD[46]. Micrometer-tall flakes of 4 to 6 layers stacked graphene sheets were synthesized by controlled recombination of carbon radicals in microwave plasma. However, the resulting graphene flakes are aligned vertically to the substrate, see in Figure 2. 2., like carbon nanowalls. This would be suitable only for field emission devices.
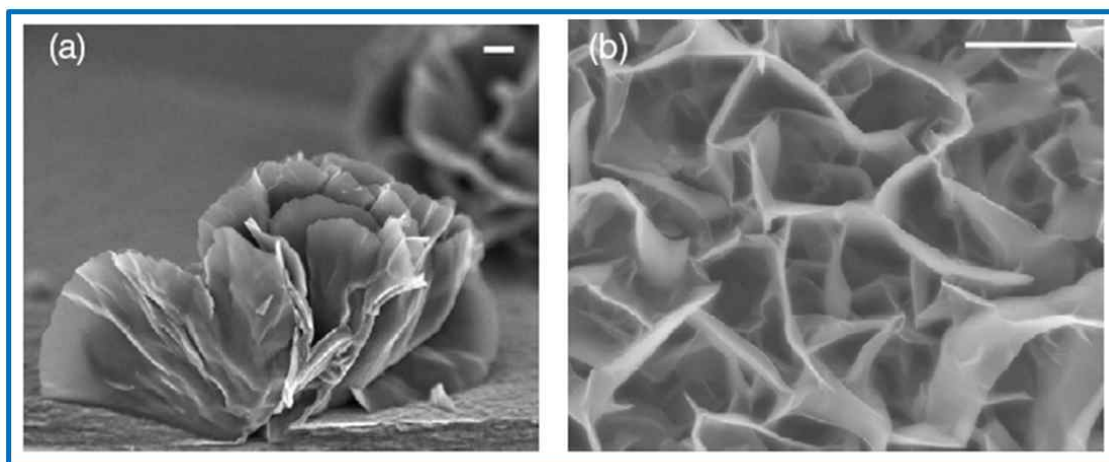
Figure 3.3. (a) Schematics of the microwave PECVD system for graphene growth. (b) SEM images of transferred on Cu grid. Cited from A. Malesevic et al., Nanotechnology **19**, 305604 (2008)[46]

In 2009, the researchers from City University of Hong Kong reported that high-quality graphene sheets could be synthesized on stainless steel substrates at 500 ^{o}C by microwave plasma enhanced chemical vapor deposition (MW-PECVD) in an atmosphere of methane/hydrogen mixture[47].
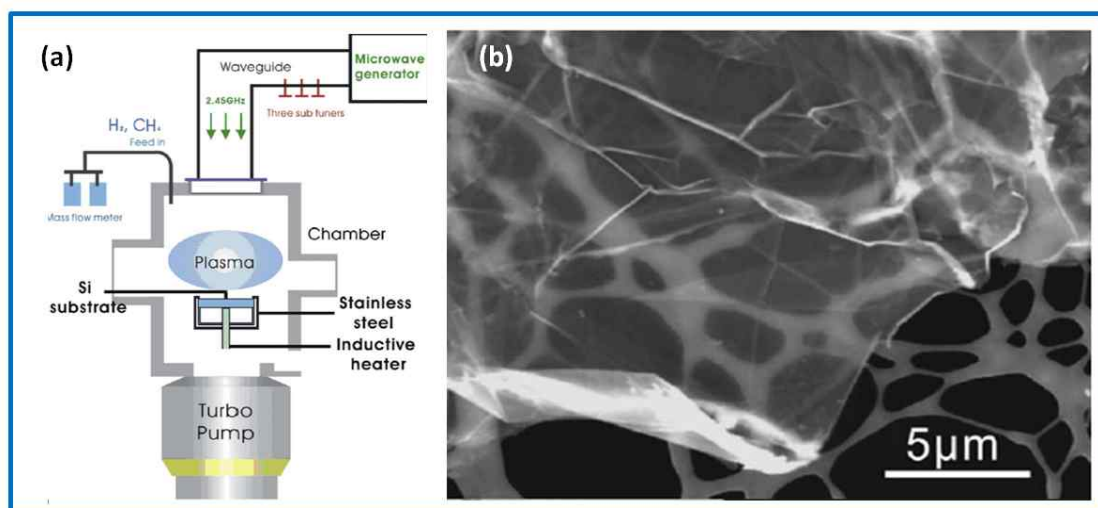
Figure 3.4. (a) Schematics of the microwave PECVD system for graphene growth. (b) SEM images of transferred on Cu grid. Cited from G. D. Yuan et al., Chem. Phys. Lett. **467**, 361-364 (2009)[47]

MW-PECVD systems allow to grow graphene layers on both metallic and insulating substrate. However, strong in-plane stress arising from high power like 2kW, is still remained challenging.

3.3.2.4. HW-CVD

Hot-wire CVD (HW-CVD) is also useful technique to grow the carbon nanostructures. In a typical CVD

(namely Thermal CVD), gas decomposition occurs by applied thermal energy, while HW-CVD has the advantages to lower the process temperature thanks to helical hot-wire (made by tungsten). Hot-wire is generally installed in front of gas inlet to chamber, thus incoming gas could be decomposed as reactive species.

To the best of our knowledge, no significant result has been reported by HW-CVD. However, we believed that this technique also would be in competition of graphene research.

3.3.3. Carbon Ion Implantation

Ion implantation is a mature technique, widely using in microelectronics industry. The carbon density in single layer graphene (SLG) is $\sim 3.8 \times 10^{15}$ atoms/cm^2, corresponding to a dose easily accessible to ion implantation. Therefore, through precise control of the amount of carbon implanted in metals, we have the possibility of controlling the number of graphene layers, as well as we can elucidate graphene growth mechanisms by trace of carbon movement. In addition, implantation is not affected by solubility, any metal can be used in principle, substantially widening the choice of substrate.

J. A. Golovchenko et al., report an ion implantation method for the large-scale synthesis of high quality films with controllable thickness[27]. They implant 2.0×10^{15} ions/cm^2, 4.0×10^{15} ions/cm^2, 7.9×10^{15} ions/cm^2, and 1.3×10^{16} ions/cm^2 in 500 nm-thick Ni, which corresponds approximately to the surface atomic thickness of carbon contained in 0.5, 1, 2 and 3 graphene monolayers, respectively. The average carbon ion penetration depth is around 40 nm with an acceleration voltage of 30 keV. The shallow ion implantation at the above doses does not perturb crystalline grain structure of a metallic substrate. After high temperature annealing for 1 hour at 1000 ^{o}C, samples are slowly cooled down to room temperature with a cooling rate of 5~20 ^{o}C/min. From the sample with carbon density of 7.9×10^{15} ions/cm^2, they claim that more than 75% of surface is covered by 1~2 layer graphene, which is however not remarkable compared to the results of CVD. Contrary to initial purpose, they finally report no thickness control by carbon dose.
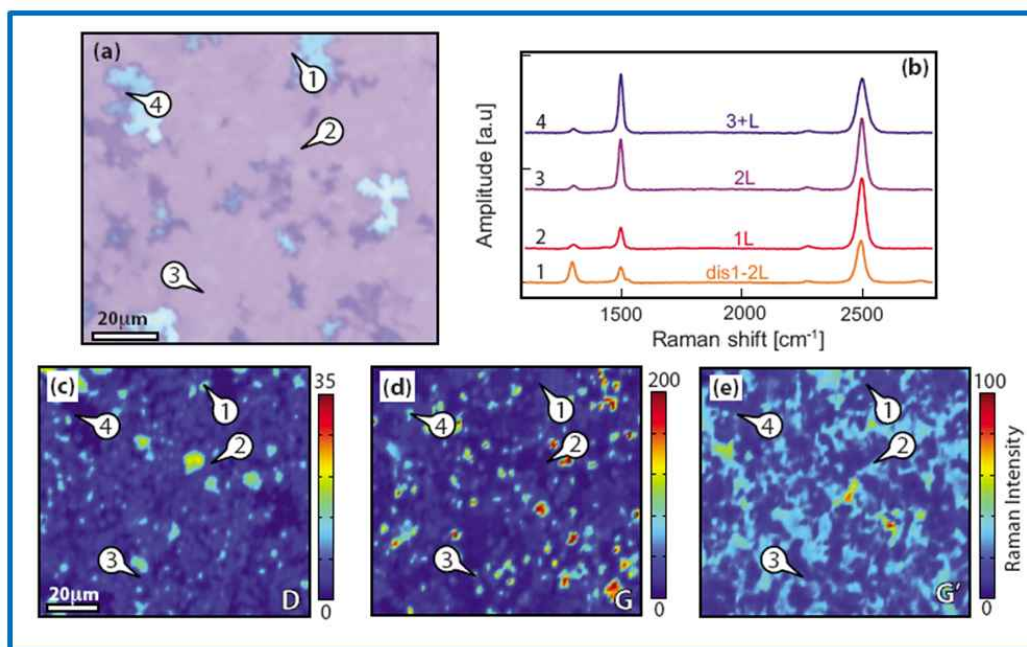
Figure 3. 1. Optical image of graphene film grown on nickel implanted with 7.9 x 10^{15} C atoms/cm^2 (which corresponds to 2 monolayer graphene), and subsequently transferred to Si/SiO$_2$ substrate. (b) Raman spectrum taken on marked positions in the optical image. (c-e) Spatial maps of D, G, and G' Raman peak intensities, repectively, in the same field of view as the optical image. Cited from S. Garaj et al., APL **97**, 183103 (2010)[27]

We have used carbon ion implantation in the present thesis work to decipher growth mechanisms. Ion implantation for graphene growth is an emerging technique that can open up a new route towards functional devices. Extensive research is still required to achieve its goals - high-quality, large area graphene with controllable thickness. This will be discussed in detail in Chapter V where we present our own results on graphene from implanted carbon.

3.3.4. Low-Energy Ion Bombardment and MBE

While thermal methane molecules do not decompose on the Pt(111) surface easily, it has been found that methane molecules decompose efficiently at normal kinetic energies higher than the threshold of about 200 meV[48]. H. Ueta et al. presented that the surface reaction on Pt(111) induced by the collision of supersonic methane molecules with a sufficiently high kinetic energy (670 meV) results in huge domains of highly oriented monolayer graphite without any unidentified carbon-related materials, and that the monolayer graphite completely covers the Pt(111) surface[49].

J. M. Garcia et al. Found that few-layered graphene could be grown using a molecular beam deposition technique in ultra-high vacuum by evaporation of atomic carbon and subsequent annealing of the samples at 800 ~ 900 ^{o}C. The graded thickness layers are grown on strip-shaped oxidized silicon substrates which are covered with 300 nm thick nickel films deposited by e-beam evaporation. The thickness of the deposited

carbon layers changes continuously from 70 Å to less than 4 Å. The relatively narrow optical phonon bands in Raman spectroscopy reveal that good quality multilayer graphene films form on the Ni surface[50].

One of the advantages of this technique is the ultraclean atmosphere of chamber that will allow *in-situ* preparation of ultra-high purity metal layers (Ni or Cu) and high quality graphene layers. In addition, this is compatible with *in-situ* vacuum characterization techniques such as x-ray photoelectron spectroscopy (XPS), Auger electron spectroscopy (AES), and low energy electron diffraction (LEED).

3.3.5. Deposition Techniques used in the Present Work

Our group owns well-established home-made PECVD systems for CNT/CNF growth that allow precisely controlling the plasma flux into samples. We get started to grow graphene layers using PECVD, especially at low temperature. We developed low-temperature and transfer-free process. We present the results of our own PECVD experiments in Chapter V.

In parallel, we investigated ion implantation technique with further annealing process. Annealing condition was first targeted to indentify the thermodynamical behavior of carbon in the nickel. From these results, we can obtain fundamental insights on growth mechanism of graphene. We present the results of our own implantation experiments in Chapter V.

Lastly, we are constructing a new graphene growth system with low-energy carbon beams in ultra-high vacuum, where we develop the growth process based on "sub-plantation". This system minimizes contaminations, as the metal catalyst film is grown in situ by molecular beam epitaxy. Moreover, this system is equipped with x-ray photoelectron spectroscopy (XPS), Auger electron spectroscopy (AES), and low energy electron diffraction (LEED), thus it allows us to directly characterize graphene layers in-situ. We present the results of our sub-plantation experiments in Chapter VII.

3.4. Current issues on graphene synthesis

In this part, I will briefly discuss some of the central issues in the development and application of graphene. First point is the band gap engineering. This part includes structural charge confinement and electrostatic doping effect in bilayer graphene. Second issue is the graphene growth directly on insulating substrate, and last point is to lower the growth temperature.

3.4.1. Main issues 1. Band Gap engineering

In the past few years, unprecedented efforts to demonstrate the practical use of graphene have been made for electronic device applications. The charge carriers in graphene behave like massless Dirac fermions,

and graphene shows ballistic charge transport turning it into an ideal material for circuit fabrication. However, graphene lacks a bandgap around the Fermi level, which is the defining concept for semiconducting materials and essential for controlling the conductivity by electronic means.

A variety of methods for introducing a gap in graphene have been proposed, including by structural modifications like graphene nanoribbons (GNRs), graphene nanomeshs (GNMs), and graphene quantum dots(GQDs), by substrate/molecular/electrostatic doping, and by interactions in-between graphene layers.

3.4.1.1. GNRs/GNMs/GQDs or porous graphene

Before 2006, there are theoretical predictions that the bandgap in graphene can be opened. Y. W. Son et al, found that the ground state of the zigzag-edge GNRs has a bandgap inversely proportional to the ribbon width, when the number of carbon chain is less than 8 in parallel direction with length[51]. V. Barone et al., explained that armchair GNRs with a width large than 8 nm could present a maximum band gap of 0.3 eV, while for ribbons with a width 80 nm, the maximum possible band gap is 0.05 eV[52].

In 2006, researchers in Intel Corporation theoretically predict band gap opening of GNR, compared to CNT circumference. They show GNRs don't keep superior charge mobility in large bandgap (with quite thinner width), while it supposed to have the charge mobility of 10^4 cm^2/Vs with less than 0.25 eV bandgap[53].

Graphene itself is a two-dimensional, zero-gap semiconductor with extremely interesting electronic properties. In addition to the 2D confinement, the graphene electrons can be further confined by forming narrow ribbon. The width confinement is expected to result in a split of the original 2D energy dispersion of graphene into a number of one-dimensional modes. Depending on the boundary conditions, some sets of these 1D modes do not pass through the intersection point of the conduction and valence band, and these quasi-1D graphene ribbons become semiconductors with a finite energy gap. The properties of GNRs would be quite different from those of graphene, for example, the carrier mobility is expected to decrease as the gap increase.

Z. Chen et al., reported graphene nanoribbons which has a width ranging from 20 nm to 500 nm, and its temperature-dependent charge transport coupled with 1/f noise[54]. By mechanical exfoliation of HOPG, they obtained graphene sheet on 200 nm-thick SiO$_2$/Si substrate. Then, GNR-based field effect transistors (FETs) were fabricated by an e-beam lithography followed by an oxygen plasma etching. Resistivity increase with narrower GNR was found for the reason that the effect of edge scattering would be dominant in narrow path. Current patterning technology is not fully suitable for GNR fabrication with smooth edge to minimize charge scattering. This would be negligible when the width is large enough, i. e. more than 50 nm. State-of-the-art lithographical and etching techniques do not allow atomic-level resolution control and result in patterned lines

with roughness on the order of a few nanometers. Figure 2. 6. (b,c) shows temperature-dependent charge transport in 100 nm, and 20 nm width of GNR-based FETs, as a function of back gate voltage. The minimum current of the 100 nm width GNR device differs by less than a factor of two between 300 K and 4 K data. On the other hand, 20 nm width GNR shows only about a factor of two current in current variation at 400 K, but exhibits more than 1.5 orders of magnitude variation at 4 K. This difference clearly states that confinement in the 20 nm ribbon opens a finite semiconductor gap in graphene. The gap is rather small and the off-state of the semiconductor is deteriorated by thermal carriers at high temperature and only appears at low enough temperature. From Arrhenius plot of the minimum current with $1/T$ (1/K), they extracted 28 meV for 20 nm GNR.
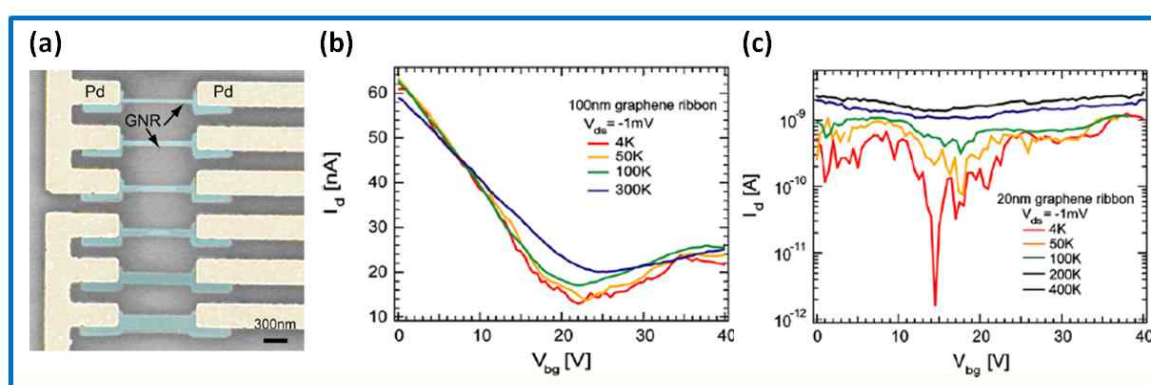
Figure 3. 2. GNR-based FETs characteristics (a) SEM image of GNR devices fabricated on a 200 nm-thick SiO$_2$ substrate. Temperature-dependent electrical characteristics as a function of gate voltage with (b) 100 nm, (c) 20 nm width of GNR, respectively. Cited from Z. Chen et al., Physica E **40**, 228-232 (2007)[54]

In 2008, a chemical route to produce GNR with width below 10 nm has been developed by Stanford University[55, 56]. Unlike single-walled carbon nanotubes (SWCNTs), all of the sub-10 nm GNRs produced were semiconductors and afforded graphene filed effect transistors with on/off ratios of about 10^7 at room temperature. They exfoliated commercial expandable graphite by brief heating to 1000 ^{o}C in forming gas. The resulting exfoliated graphite was dispersed in a 1,2-dichloroethane (DCE) solution of poly(m-phenylenevinylene-co-2,5-dioxtoxy-p-phenylenevinylene) (PmPV) by sonication for 30 min to form a homogeneous suspension. Centrifugation then removed large pieces of materials from the supernatant. Room temperature on/off current switching (I$_{on}$/I$_{off}$) induced by the gate voltage increased exponentially as the GNR width decreased, with I$_{on}$/I$_{off}$ ~1, ~5, ~100, and more than 10^5 for 50 nm, 20 nm, 10 nm, and sub-10 nm width GNRs, respectively. (see in Figure 2. 7.)
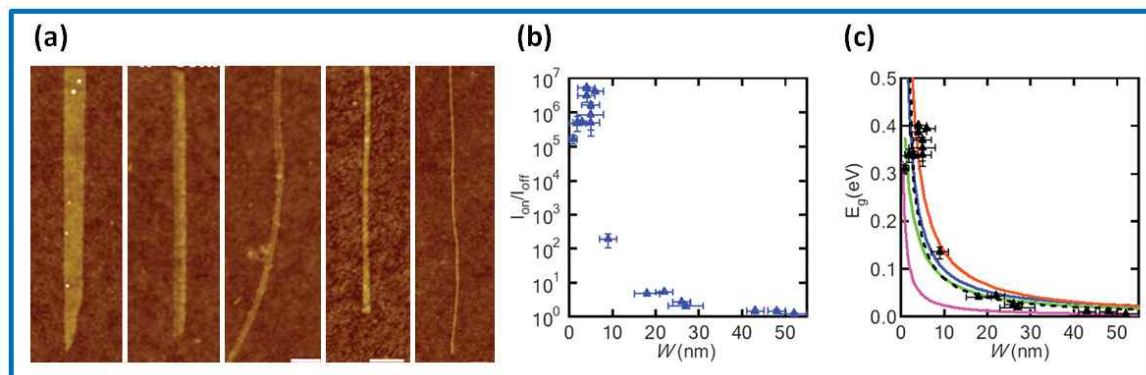
Figure 3. 3. Chemically derived, ultrasmooth graphene nanoribbons down to sub-10 nm width and electrical characterization of GNR-based FETs. (a) AFM images of selected GNRs with widths in the 50 nm, 30 nm, 20 nm, 10 nm, and sub 10 nm from left to right. (b) I_{on}/I_{off} ratio (under V_{ds}=0.5V) for GNRs of various ribbon widths. (b) E_g extracted from experimental data for various GNRs versus ribbon width. The black dashed line is a fit of experimental data into an empirical form of E_g(eV)=0.8/W (nm). The purple, blue, and orange solid lines are first-principle calculations for three types of armchair-edged GNRs respectively, and the green solid line is calculations for zigzag-edged GNRs. Cited from X. Li et al., Science **319**, 1229-1231 (2008)[55]

In metal-intrinsic semiconductor junction, the lowest current, I_{off}, is generated when the mid-gap of semiconductor (Fermi level) is completely aligned with work function of metals. In this situation, the current is only governed by thermally activated carriers, which has the probability related to term "exp(-E_g/k_bT)". Thus, I_{on}/I_{off} could be expressed as follow;

$$I_{on}/I_{off} \propto \exp(E_g/k_BT)$$

where k_B is the Boltzmann's constant and T is temperature. The band gaps extracted this way were fit into an empirical form of

$$E_g(eV) = 0.8/W(nm)$$

, which was consistent with the exponential increase in I_{on}/I_{off} of GNR FETs as ribbon width decreased.

It has been predicted that both armchair nanoribbons and zigzag nanoribbons (the two ideal types of nanoribbon) have a bandgap that is, to a good approximation, inversely proportional to the width of the nanoribbon. The opening of a bandgap in nanoribbons has been verified experimentally for widths down to about 1 nm, and theory and experiments both reveal bandgaps in excess of 200 meV for widths below 20 nm.

To open a bandgap useful for conventional field-effect devices, very narrow nanoribbons with well-defined edges are needed. This represents a serious challenge given the semiconductor processing equipment

available at the moment. Recently, nanoribbons that were uniform in width and had reduced edge roughness were produced by 'unzipping' carbon nanotubes. However, even a perfect nanoribbon is not perfect for electronics applications. In general, the larger the bandgap that opens in a nanoribbon, the more the valence and conduction bands become parabolic (rather than cone-shaped): this decreases the curvature around the K point and increases the effective mass of the charge carriers, which is likely to decrease the mobility.

Having graphene nanoribbons with smooth edges, however, is extremely difficult. The existence of an energy gap in graphene nanoribbons may be understood in terms of Coulomb blockade, due not to lateral confinement. In details, the roughness of the edges creates nano-islands where charges are isolated. Localized electrons behave as like tunneling under applied voltage [57].

3.4.1.2. Biased BLG

The electronic bandgap is an intrinsic property of semiconductors and insulators that largely determines their transport and optical properties. A tunable bandgap would be highly desirable because it would allow great flexibility in design and optimization of such devices, for instance, p-n junctions, transistors, photodiodes and lasers. The possibility of tunning by applying a variable external electric field appears particularly interesting. However, in conventional materials, the bandgap is fixed by the crystalline structure, preventing such bandgap control.

Bilayer graphene is also gapless (see Figure 2. 8. (iii) case), and its valence and conduction bands have a parabolic shape near the K point. If an electric field is applied perpendicular to the bilayer, it introduces a potential difference between the two planes of the bilayer graphene resulting in the opening of a bandgap[58, 59]. This opening was calculated by tight-binding model in the presence of a potential difference between layers. The dependence of the asymmetry gap $\Delta(n)$ is roughly linear with n with the addition of density $n \sim 10^{12}$ cm^{-2} yielding a gap $\Delta \sim 10$ meV.
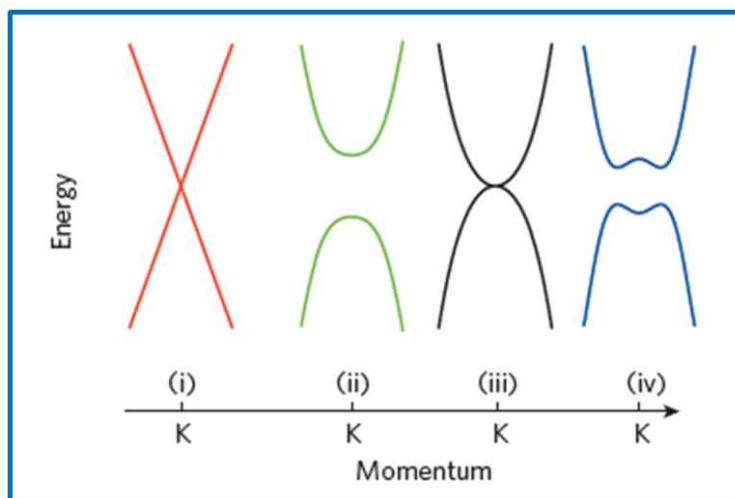
Figure 3. 4. Band structure around the K point of (i) large-area graphene, (ii) graphene nanoribbons, (iii) unbiased bilayer graphene, and (iv) bilayer graphene with an applied perpendicular filed**.**
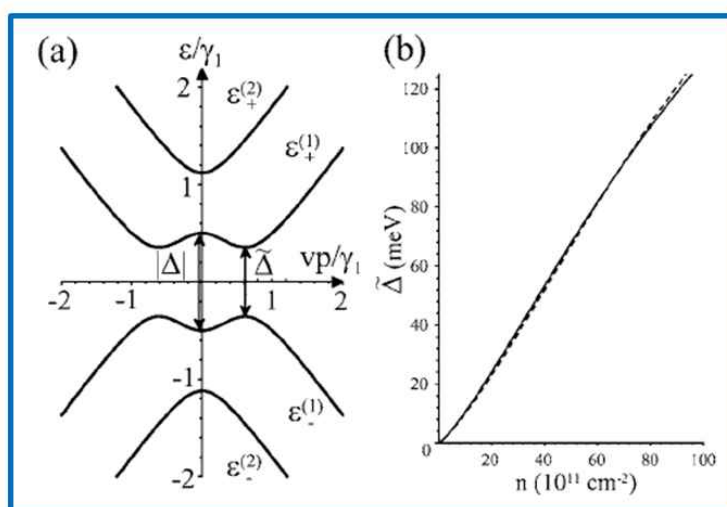
Figure 3. 5. (a) Schematic of the electronic bands near the K point in the presence of finite layer asymmetry Δ (for illustrative purposes a very large asymmetry $\Delta = \gamma_1$ is used); (b) numerically calculated dependence $\tilde{\Delta}(n)$ (solid line) compared with analytic expression (dashed line) using Eq. (1). For these values of density $\Delta = \sim\Delta$.

      T. Ohta et al., described the synthesis of bilayer graphene thin films deposited on insulating silicon carbide and report the characterization on their electronic band structure using angle-resolved photoemission[60]. By selectively adjusting the carrier concentration in each layer, changes in the Coulomb potential led to control of the gap between valence and conduction band. Y. Zhang et al., demonstrated consciously tunable bandgap of up to 250 meV by gate-control[61]. Upon dual-electrical gating, the top and bottom electrical displacement fields, D_t and D_b, would affect following two physical/chemical properties;

      (i) The difference of the two, $\delta D = D_t - D_b$, leads to a net carrier doping, that is, a shift of the Fermi

energy (E_f).

(ii) The average of the two, $\overline{D} = (D_t + D_b)/2$, breaks the inversion symmetry of the bilayer and generates a non-zero bandgap.

Thus, by setting δD to zero and varying $\overline{D}$, they can successfully tune the bandgap while keeping the bilayer charge neutral. By varying δD above or below zero, we can inject electrons or holes into the bilayer and shift the Fermi level without changing bandgap. The drain electrode is grounded and the displacement fields D_t and D_b are tuned independently by top and bottom voltages (V_t and V_b) through the relations $D_b = +\varepsilon_b(V_b - V_b^0)/d_b$ and $D_t = +\varepsilon_t(V_t - V_t^0)/d_t$. Here, ε and d are the dielectric constant and thickness of the dielectric layer and V^0 is the effective offset voltage due to initial environment induced carrier doping. As they keep $\delta D = 0$, uncontrolled chemical doping effect is excluded and bandgap tuning by $\overline{D}$ is explicitly achieved up to 250 meV, for high field of 3 x 10^7 V/cm.
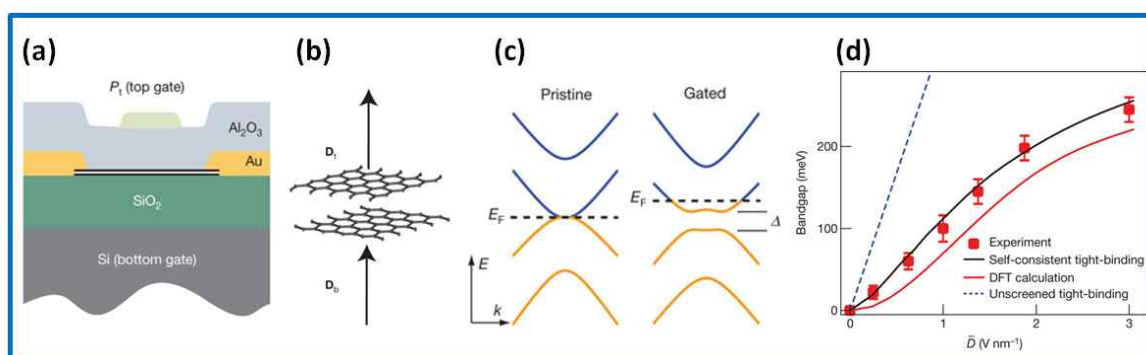
Figure 3. 6. (a) Illustration of a cross-sectional side view of the dual-gated device, especially based on bilayer graphene. (b) Sketch showing how gating of the bilayer induces top (D_t) and bottom (D_b) electrical displacement fields. (c) The electronic structure of (left) pristine and (right) gated bilayer graphene, respectively. (k denotes the wavevector) (d) Electric-field dependence of tunable energy bandgap in graphene bilayer. Experimental data with red squares are compared to theoretical predictions based on self-consistent tight-binding (black trace), *ab initio* density functional (red trace), and unscreened tight-binding calculations (blue dashed trance). Cited from Y. Zhang et al., *Nature* **459**, 820-823 (2009)[61]

3.4.2. Main issues 2. Transfer-free or Direct-growth processes

With the CVD technique as well as with other types of carbon supply, the metal substrate is supposed to be essential, not only for decomposing hydrocarbon gas or solid-state organic layer, but also to conduct low-temperature crystallization of graphene. As grown-graphene is itself layered on conducting substrate, it should be resettled on insulating surface for device applications.

Transfer introduces indeed a variety of defects. Large-area uniform graphene growth through CVD

technique, coupled with PMMA-assisted transfer is well established. However, (i) there are inevitable organic contaminations originating from PMMA (even in photolithographic process for device fabrications)[62, 63], (ii) significant amounts of cracks, defects, and wrinkles are generated[64], and (iii) substantial amounts of time/cost are unavoidable[65]. For the above reasons, a new paradigm in graphene synthesis is desired.

Direct growth of graphene on an insulating substrate thus has two major advantages: (1) it allows one to skip transfer and keep the as-grown quality and (2) it drastically simplifies the process.

In this section, we will focus on the direct growth of graphene on an insulating substrate, where no transfer is required.

3.4.2.1. SAM (or solid-state carbon source) pre-deposition

H. J. Shin et al., introduced a method for transfer-free growth of few-layer graphene on a dielectric substrate based on pyrolysis of a self-assembled monolayer (SAM) of carbon materials squeezed between a catalytic metal and a substrate[66]. The metal/SAM/substrate structure provides advantages not only for the robust removal of the top-most catalyst after growth, but also in preventing the SAM material from being evaporated at high temperature, which is crucial for high-quality graphene growth without creating additional defects, wrinkles, and tears. They found clear relationship between the amount of carbon atoms in SAM and that in graphene layers.
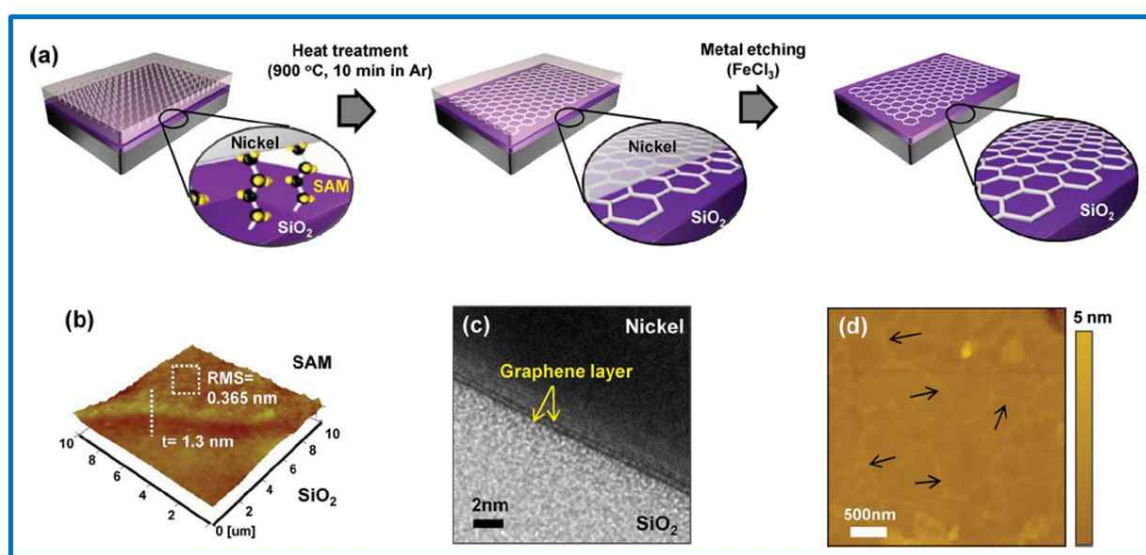
Figure 3. 7. (a) Schematic illustration for transfer-free growth of graphene on a substrate. (b) AFM image (tapping mode) of octyl-SAM on a SiO_2/Si substrate. A step was formed by removing half of the SAM layer with UV/ozone cleaning. (c) Cross-sectional HR-TEM image after pyrolysis of octyl-SAM, yielding bilayer graphene. (d) AFM image of graphene originated by octyl-SAM on the substrate after metal etching. Cited from H. J. Shin

et al., *Adv. Mater.* **23**, 4392-4397 (2011)[66]

The group lead by Prof. J. M. Tour, also presented a similar process where they pre-deposit solid carbon source, such as poly(2-phenylpropyl)methysiloxane, poly(methyl methacrylate), polystyrene, and poly(acrylonitrile-co-butadiene-co-styrene), and subsequently 500 nm-thick Ni on top of it. Through annealing at 1000 ^{o}C under low pressure, bilayer graphene is formed in-between metal and various insulating substrates[67]. However, as graphene thickness doesn't depend on the solid carbon layer thickness, nor on the nature of carbon source, a couple of questions regarding the mechanisms of this process remain in abeyance.

3.4.2.2. Direct graphene formation on insulating substrate without catalyst metal

There are some reports on direct graphene growth on insulating substrate without catalyst layer. The possibility of graphene formation anchored at step edges on MgO(100) or ZrO$_2$ surface is experimentally demonstrated with support from density functional theory (DFT) investigations. Cyclohexane (C$_6$H$_{12}$) or acetylene (C$_2$H$_2$) is used as carbon feedstock, and substrate is heated in CVD system with Ar gas[68]. Indeed, mica[69], sapphire[70], and silicon dioxide[71] are also demonstrated as potential substrates for graphene growth without catalyst.

However, because of the lack of direct evidence of the catalytic chemical reaction of the insulating substrates, the growth mechanisms are still controversial. J. Sun et al. suggested that C clusters could be formed by the pyrolysis of the hydrocarbon precursor and that the self-assembly of these clusters could result in graphene formation[72].

3.4.2.3. Grain boundary-based Carbon Diffusion

Grain boundaries of a polycrystalline metal can be a strong pathway for carbon diffusion compared to *through grains*. The importance of grain boundary-based diffusion of carbon in graphene growth has first been demonstrated by our group[73, 74]. It is now getting more attention with an increasing number of related papers [75-77]. We discuss grain-boundary diffusion in Chapter V on ion implantation.

Here, it is worth to note that the effect of bulk diffusion is negligible in case of copper, mainly due to the absence of carbon solubility. Copper has the lowest affinity to carbon as reflected by the fact that it does not form any carbide phases and has very low carbon solubility compared to Co and Ni (0.001~0.008 wt.% at 1084 ^{o}C for Cu, while ~0.6 wt.% at 1326 ^{o}C for Ni, and ~0.9 wt.% at 1320 ^{o}C for Co)[23, 78, 79]. Please say a little more about the work of Su et al.

3.4.3. Main issues 3. Low-temperature, CMOS-compatible processes

To date, high quality graphene is generated at remarkably high temperature, up to 1500 ^{o}C for epitaxial

way, and at 1000 ^{o}C for CVD system. The high growth temperatures impose limitations on the choice of substrates. For example, flexible PET (polyethylene terephthalate), PI (polyimide), and glass substrate will be seriously damaged. Moreover, such high temperatures cannot be used in current CMOS (complementary metal–oxide–semiconductor) process.

Low temperature process for graphene synthesis would timely be indispensable for applications of graphene in electronic devices. Therefore, there is still a need to develop a reliable and reproducible method for low temperature synthesis of high-quality graphene that is suitable for the full exploitation of graphene properties and application potentials.

Plasma-assisted process has a strong benefit to lower the growth temperature, thanks to its highly reactive species, as we witness in research for carbon nanotubes. The differences in binding energy of carbon feeding gas could be considered as one of the key to decrease the temperature.

Reference

1.   Wallace, P. R. The Band Theory of Graphite. *Physical Review* **71**, 622-634 (1947)

2.   Boehm, H. P., Clauss, A., Fischer, G. O. and Hofmann, U. Das Adsorptionsverhalten sehr dünner Kohlenstoff-Folien. *Zeitschrift für anorganische und allgemeine Chemie* **316**, 119-127 (1962)

3.   Eizenberg, M. and Blakely, J. M. Carbon monolayer phase condensation on Ni(111). *Surface Science* **82**, 228-236 (1979)

4.   Eizenberg, M. and Blakely, J. M. Carbon interaction with nickel surfaces: Monolayer formation and structural stability. *The Journal of Chemical Physics* **71**, 3467-3477 (1979)

5.   Shelton, J. C., Patil, H. R. and Blakely, J. M. Equilibrium segregation of carbon to a nickel (111) surface: A surface phase transition. *Surface Science* **43**, 493-520 (1974)

6.   S. Mouras, et al. 1987. Synthesis of first stage graphite intercalation compounds with fluorides. Revue de Chimie Minerale. 24:572

7.   Xuekun Lu and Minfeng Yu and Hui Huang and Rodney, S. R. Tailoring graphite with the goal of achieving single sheets. *Nanotechnology* **10**, 269 (1999)

8.   Zhang, Y., Small, J. P., Pontius, W. V. and Kim, P. Fabrication and electric-field-dependent transport measurements of mesoscopic graphite devices. *Applied Physics Letters* **86**, 073104-3 (2005)

9.   Schniepp, H. C., Li, J.-L., McAllister, M. J., Sai, H., Herrera-Alonso, M., Adamson, D. H., Prud'homme, R. K., Car, R., Saville, D. A. and Aksay, I. A. Functionalized Single Graphene Sheets Derived from Splitting Graphite Oxide. *The Journal of Physical Chemistry B* **110**, 8535-8539 (2006)

10.   Park, S. and Ruoff, R. S. Chemical methods for the production of graphenes. *Nat Nano* **4**, 217-224 (2009)

11.   Van Bommel, A. J., Crombeen, J. E. and Van Tooren, A. LEED and Auger electron observations of the SiC(0001) surface. *Surface Science* **48**, 463-472 (1975)

12.   Berger, C., Song, Z., Li, T., Li, X., Ogbazghi, A. Y., Feng, R., Dai, Z., Marchenkov, A. N., Conrad, E. H., First, P. N. and de Heer, W. A. Ultrathin Epitaxial Graphite:??2D Electron Gas Properties and a Route toward Graphene-based Nanoelectronics. *The Journal of Physical Chemistry B* **108**, 19912-19916 (2004)

13.   Berger, C., Song, Z., Li, X., Wu, X., Brown, N., Naud, C., Mayou, D., Li, T., Hass, J., Marchenkov, A. N., Conrad, E. H., First, P. N. and de Heer, W. A. Electronic Confinement and Coherence in Patterned Epitaxial Graphene. *Science* **312**, 1191-1196 (2006)

14.   SprinkleM, RuanM, HuY, HankinsonJ, Rubio Roy, M., ZhangB, WuX, BergerC and de Heer, W. A. Scalable templated growth of graphene nanoribbons on SiC. *Nat Nano* **5**, 727-731 (2010)

15.   Rodríguez-Manzo, J. A., Pham-Huu, C. and Banhart, F. Graphene Growth by a Metal-Catalyzed Solid-State Transformation of Amorphous Carbon. *ACS Nano* **5**, 1529-1534 (2011)

16.   Pinggang, P., Dan, X., Yi, Y., Changjian, Z., He, T., Tingting, F., Xiao, L., Tianling, R. and Hongwei, Z. in Nano/Micro Engineered and Molecular Systems (NEMS), 2012 7th IEEE International Conference on 7-10 (2012).

17.   Ji, H., Hao, Y., Ren, Y., Charlton, M., Lee, W. H., Wu, Q., Li, H., Zhu, Y., Wu, Y., Piner, R. and Ruoff, R. S. Graphene Growth Using a Solid Carbon Feedstock and Hydrogen. *ACS Nano* **5**, 7656-7661 (2011)

18.   Zheng, M., Takei, K., Hsia, B., Fang, H., Zhang, X., Ferralis, N., Ko, H., Chueh, Y.-L., Zhang, Y., Maboudian, R. and Javey, A. Metal-catalyzed crystallization of amorphous carbon to graphene. *Applied Physics Letters* **96**, 063110-3 (2010)

19.   García, J. M., He, R., Jiang, M. P., Kim, P., Pfeiffer, L. N. and Pinczuk, A. Multilayer graphene grown by precipitation upon cooling of nickel on diamond. *Carbon* **49**, 1006-1012 (2010)

20.   Lahiri, J., Travis, S. M., Ross, A. J., Adamska, L., Oleynik, I. I. and Batzill, M. Graphene growth and stability at nickel surfaces. *New Journal of Physics* **13**, 025001 (2011)

21.   Loginova, E., Norman, C. B., Feibelman, P. J. and McCarty, K. F. Evidence for graphene growth by C cluster attachment. *New Journal of Physics* **10**, 093026 (2008)

22.   Coraux, J., Alpha, T. N. D., Engler, M., Busse, C., Wall, D., Buckanie, N., Heringdorf, F.-J. M. z., Gastel, R. v., Poelsema, B. and Michely, T. Growth of graphene on Ir(111). *New Journal of Physics* **11**, 023006 (2009)

23.   Mattevi, C., Kim, H. and Chhowalla, M. A review of chemical vapour deposition of graphene on copper. *Journal of Materials Chemistry* **21**, 3324-3334 (2011)

24.   Kim, K. S., Zhao, Y., Jang, H., Lee, S. Y., Kim, J. M., Kim, K. S., Ahn, J.-H., Kim, P., Choi, J.-Y. and Hong, B. H. Large-scale pattern growth of graphene films for stretchable transparent electrodes. *Nature* **457**, 706-710 (2009)

25.   Li, X., Cai, W., An, J., Kim, S., Nah, J., Yang, D., Piner, R., Velamakanni, A., Jung, I., Tutuc, E., Banerjee, S. K., Colombo, L. and Ruoff, R. S. Large-Area Synthesis of High-Quality and Uniform Graphene Films on Copper Foils. *Science* **324**, 1312-1314 (2009)

26.   Kang, D., Kim, W.-J., Lim, J. A. and Song, Y.-W. Direct Growth and Patterning of Multilayer Graphene onto a Targeted Substrate without an External Carbon Source. *ACS Applied Materials & Interfaces* (2012)

27.   Garaj, S., Hubbard, W. and Golovchenko, J. A. Graphene synthesis by ion implantation. *Applied Physics Letters* **97**, 183103-3 (2010)

28.   Zhang, R., Zhang, Z., Wang, Z., Wang, S., Wang, W., Fu, D. and Liu, J. Nonlinear damage effect in graphene synthesis by C-cluster ion implantation. *Applied Physics Letters* **101**, 011905-4 (2012)

29.   Mun, J. H., Lim, S. K. and Cho, B. J. Local Growth of Graphene by Ion Implantation of Carbon in a Nickel Thin Film followed by Rapid Thermal Annealing. *Journal of The Electrochemical Society* **159**, G89-G92 (2012)

30.   Baraton, L., He, Z., Lee, C. S., Maurice, J.-L., Cojocaru, C. S., Gourgues-Lorenzon, A.-F., Lee, Y. H. and Didier, P. Synthesis of few-layered graphene by ion implantation of carbon in nickel thin films. *Nanotechnology* **22**, 085601 (2011)

31.   Orofeo, C., Ago, H., Hu, B. and Tsuji, M. Synthesis of large area, homogeneous, single layer graphene films by annealing amorphous carbon on Co and Ni. *Nano Research* **4**, 531-540 (2011)

32.   Hofrichter, J., Szafranek, B. u. N., Otto, M., Echtermeyer, T. J., Baus, M., Majerus, A., Geringer, V., Ramsteiner, M. and Kurz, H. Synthesis of Graphene on Silicon Dioxide by a Solid Carbon Source. *Nano Letters* **10**, 36-42 (2009)

33.   Sun, Z., Yan, Z., Yao, J., Beitler, E., Zhu, Y. and Tour, J. M. Growth of graphene from solid carbon sources. *Nature* **468**, 549-552 (2010)

34.   Turchanin, A., Weber, D., Büenfeld, M., Kisielowski, C., Fistul, M. V., Efetov, K. B., Weimann, T., Stosch, R., Mayer, J. and Gölzhäuser, A. Conversion of Self-Assembled Monolayers into Nanocrystalline Graphene: Structure and Electric Transport. *ACS Nano* **5**, 3896-3904 (2011)

35.   Ruan, G., Sun, Z., Peng, Z. and Tour, J. M. Growth of Graphene from Food, Insects, and Waste. *ACS Nano* **5**, 7601-7607 (2011)

36.   A. Hayes and J. Chipman, Trans. Am. Inst. Min., Metall. Pet. Eng. 135, 85 (1939)

37.   Yu, Q., Lian, J., Siriponglert, S., Li, H., Chen, Y. P. and Pei, S.-S. Graphene segregated on Ni surfaces and transferred to insulators. *Applied Physics Letters* **93**, 113103-3 (2008)

38.   Somani, P. R., Somani, S. P. and Umeno, M. Planer nano-graphenes from camphor by CVD. *Chemical Physics Letters* **430**, 56-59 (2006)

39.   Reina, A., Jia, X., Ho, J., Nezich, D., Son, H., Bulovic, V., Dresselhaus, M. S. and Kong, J. Large Area, Few-Layer Graphene Films on Arbitrary Substrates by Chemical Vapor Deposition. *Nano Letters* **9**, 30-35 (2008)

40.   Reina, A., Son, H., Jiao, L., Fan, B., Dresselhaus, M. S., Liu, Z. and Kong, J. Transferring and Identification of Single- and Few-Layer Graphene on Arbitrary Substrates. *The Journal of Physical Chemistry C* **112**, 17741-17744 (2008)

41.   Jiao, L., Fan, B., Xian, X., Wu, Z., Zhang, J. and Liu, Z. Creation of Nanostructures with Poly(methyl methacrylate)-Mediated Nanotransfer Printing. *Journal of the American Chemical Society* **130**, 12612-12613 (2008)

42.   Bae, S., Kim, H., Lee, Y., Xu, X., Park, J.-S., Zheng, Y., Balakrishnan, J., Lei, T., Ri Kim, H., Song, Y. I., Kim, Y.-J., Kim, K. S., Ozyilmaz, B., Ahn, J.-H., Hong, B. H. and Iijima, S. Roll-to-roll production of 30-inch graphene films for transparent electrodes. *Nat Nano* **5**, 574-578

43.   Yu, Q., Jauregui, L. A., Wu, W., Colby, R., Tian, J., Su, Z., Cao, H., Liu, Z., Pandey, D., Wei, D., Chung, T. F., Peng, P., Guisinger, N. P., Stach, E. A., Bao, J., Pei, S.-S. and Chen, Y. P. Control and characterization of individual grains and grain boundaries in graphene grown by chemical vapour deposition. *Nat Mater* **10**, 443-449

44.   Dai, B., Fu, L., Zou, Z., Wang, M., Xu, H., Wang, S. and Liu, Z. Rational design of a binary metal alloy for chemical vapour deposition growth of uniform single-layer graphene. *Nat Commun* **2**, 522

45.   Obraztsov, A. N., Obraztsova, E. A., Tyurnina, A. V. and Zolotukhin, A. A. Chemical vapor deposition of thin graphite films of nanometer thickness. *Carbon* **45**, 2017-2021 (2007)

46.   Alexander Malesevic and Roumen Vitchev and Koen Schouteden and Alexander Volodin and Liang Zhang and Gustaaf Van Tendeloo and Annick Vanhulsel and Chris Van, H. Synthesis of few-layer

graphene via microwave plasma-enhanced chemical vapour deposition. *Nanotechnology* **19**, 305604 (2008)

47.   Yuan, G. D., Zhang, W. J., Yang, Y., Tang, Y. B., Li, Y. Q., Wang, J. X., Meng, X. M., He, Z. B., Wu, C. M. L., Bello, I., Lee, C. S. and Lee, S. T. Graphene sheets via microwave chemical vapor deposition. *Chemical Physics Letters* **467**, 361-364 (2009)

48.   Kondo, T., Sasaki, T. and Yamamoto, S. Dissociative chemisorption of CH4 on a cesiated Pt(111) surface studied by supersonic molecular beam scattering techniques. *The Journal of Chemical Physics* **116**, 7673-7684 (2002)

49.   Ueta, H., Saida, M., Nakai, C., Yamada, Y., Sasaki, M. and Yamamoto, S. Highly oriented monolayer graphite formation on Pt(111) by a supersonic methane beam. *Surface Science* **560**, 183-190 (2004)

50.   Garcia, J. M., He, R., Jiang, M. P., Yan, J., Pinczuk, A., Zuev, Y. M., Kim, K. S., Kim, P., Baldwin, K., West, K. W. and Pfeiffer, L. N. Multilayer graphene films grown by molecular beam deposition. *Solid State Communications* **150**, 809-811 (2010)

51.   Son, Y.-W., Cohen, M. L. and Louie, S. G. Half-metallic graphene nanoribbons. *Nature* **444**, 347-349 (2006)

52.   Barone, V., Hod, O. and Scuseria, G. E. Electronic Structure and Stability of Semiconducting Graphene Nanoribbons. *Nano Letters* **6**, 2748-2754 (2006)

53.   Obradovic, B., Kotlyar, R., Heinz, F., Matagne, P., Rakshit, T., Giles, M. D., Stettler, M. A. and Nikonov, D. E. Analysis of graphene nanoribbons as a channel material for field-effect transistors. *Applied Physics Letters* **88**, 142102-3 (2006)

54.   Chen, Z., Lin, Y.-M., Rooks, M. J. and Avouris, P. Graphene nano-ribbon electronics. *Physica E: Low-dimensional Systems and Nanostructures* **40**, 228-232 (2007)

55.   Li, X., Wang, X., Zhang, L., Lee, S. and Dai, H. Chemically derived, ultrasmooth graphene nanoribbon semiconductors. *Science* **319**, 1229-1232 (2008)

56.   Wang, X., Ouyang, Y., Li, X., Wang, H., Guo, J. and Dai, H. Room-Temperature All-Semiconducting Sub-10-nm Graphene Nanoribbon Field-Effect Transistors. *Physical Review Letters* **100**, 206803 (2008)

57.   Stampfer, C., Güttinger, J., Hellmüller, S., Molitor, F., Ensslin, K. and Ihn, T. Energy gaps in etched graphene nanoribbons. *Physical Review Letters* **102**, 056403 (2009)

58.   McCann, E. Asymmetry gap in the electronic band structure of bilayer graphene. *Physical Review B* **74**, 161403 (2006)

59.   McCann, E. and Fal'ko, V. I. Landau-Level Degeneracy and Quantum Hall Effect in a Graphite Bilayer. *Physical Review Letters* **96**, 086805 (2006)

60.   Ohta, T., Bostwick, A., Seyller, T., Horn, K. and Rotenberg, E. Controlling the Electronic Structure of Bilayer Graphene. *Science* **313**, 951-954 (2006)

61.   Zhang, Y., Tang, T.-T., Girit, C., Hao, Z., Martin, M. C., Zettl, A., Crommie, M. F., Shen, Y. R. and Wang, F. Direct observation of a widely tunable bandgap in bilayer graphene. *Nature* **459**, 820-823 (2009)

62.   Ishigami, M., Chen, J. H., Cullen, W. G., Fuhrer, M. S. and Williams, E. D. Atomic Structure of Graphene

on SiO2. *Nano Letters* **7**, 1643-1648 (2007)

63.   Pirkle, A., Chan, J., Venugopal, A., Hinojos, D., Magnuson, C. W., McDonnell, S., Colombo, L., Vogel, E. M., Ruoff, R. S. and Wallace, R. M. The effect of chemical residues on the physical and electrical properties of chemical vapor deposited graphene transferred to SiO2. *Applied Physics Letters* **99**, 122108-3 (2011)

64.   Lin, Y.-C., Jin, C., Lee, J.-C., Jen, S.-F., Suenaga, K. and Chiu, P.-W. Clean Transfer of Graphene for Isolation and Suspension. *ACS Nano* **5**, 2362-2368 (2011)

65.   Liang, X., Sperling, B. A., Calizo, I., Cheng, G., Hacker, C. A., Zhang, Q., Obeng, Y., Yan, K., Peng, H., Li, Q., Zhu, X., Yuan, H., Hight Walker, A. R., Liu, Z., Peng, L.-m. and Richter, C. A. Toward Clean and Crackless Transfer of Graphene. *ACS Nano* **5**, 9144-9153 (2011)

66.   Shin, H.-J., Choi, W. M., Yoon, S.-M., Han, G. H., Woo, Y. S., Kim, E. S., Chae, S. J., Li, X.-S., Benayad, A., Loc, D. D., Gunes, F., Lee, Y. H. and Choi, J.-Y. Transfer-Free Growth of Few-Layer Graphene by Self-Assembled Monolayers. *Advanced Materials* **23**, 4392-4397 (2011)

67.   Yan, Z., Peng, Z., Sun, Z., Yao, J., Zhu, Y., Liu, Z., Ajayan, P. M. and Tour, J. M. Growth of Bilayer Graphene on Insulating Substrates. *ACS Nano* **5**, 8187-8192 (2011)

68.   Scott, A., Dianat, A., Borrnert, F., Bachmatiuk, A., Zhang, S., Warner, J. H., Borowiak-Palen, E., Knupfer, M., Buchner, B., Cuniberti, G. and Rummeli, M. H. The catalytic potential of high-kappa dielectrics for graphene formation. *Applied Physics Letters* **98**, 073110-3 (2011)

69.   Lippert, G., Dabrowski, J., Lemme, M., Marcus, C., Seifarth, O. and Lupina, G. Direct graphene growth on insulator. *physica status solidi (b)* **248**, 2619-2622 (2011)

70.   Fanton, M. A., Robinson, J. A., Puls, C., Liu, Y., Hollander, M. J., Weiland, B. E., LaBella, M., Trumbull, K., Kasarda, R., Howsare, C., Stitt, J. and Snyder, D. W. Characterization of Graphene Films and Transistors Grown on Sapphire by Metal-Free Chemical Vapor Deposition. *ACS Nano* **5**, 8062-8069 (2011)

71.   Bi, H., Sun, S., Huang, F., Xie, X. and Jiang, M. Direct growth of few-layer graphene films on SiO2 substrates and their photovoltaic applications. *Journal of Materials Chemistry* **22**, 411-416 (2012)

72.   Sun, J., Lindvall, N., Cole, M. T., Teo, K. B. K. and Yurgens, A. Large-area uniform graphene-like thin films grown by chemical vapor deposition directly on silicon nitride. *Applied Physics Letters* **98**, 252107-3 (2011)

73.   Lee, C. S., Baraton, L., He, Z., Maurice, J.-L., Chaigneau, M., Pribat, D. and Cojocaru, C. S. in Carbon Nanotubes, Graphene, and Associated Devices III 77610P-7 (SPIE, San Diego, California, USA) (2010)

74.   Baraton, L., He, Z., Lee, C. S., Cojocaru, C. S., Chatelet, M., Maurice, J.-L., Lee, Y. H. and Pribat, D. On the mechanisms of precipitation of graphene on nickel thin films. *EPL (Europhysics Letters)* **96**, 46003 (2011)

75.   Su, C.-Y., Lu, A.-Y., Wu, C.-Y., Li, Y.-T., Liu, K.-K., Zhang, W., Lin, S.-Y., Juang, Z.-Y., Zhong, Y.-L., Chen, F.-R. and Li, L.-J. Direct Formation of Wafer Scale Graphene Thin Layers on Insulating Substrates by Chemical Vapor Deposition. *Nano Letters* **11**, 3612-3616 (2011)

76.   Peng, Z., Yan, Z., Sun, Z. and Tour, J. M. Direct Growth of Bilayer Graphene on SiO2 Substrates by

Carbon Diffusion through Nickel. *ACS Nano* **5**, 8241-8247 (2011)

77.   Kaplas, T., Sharma, D. and Svirko, Y. Few-layer graphene synthesis on a dielectric substrate. *Carbon* **50**, 1503-1509 (2012)

79.   López, G. A. and Mittemeijer, E. J. The solubility of C in solid Cu. *Scripta Materialia* **51**, 1-5 (2004)

Outline

Chapter IV. Plasma-Assisted Graphene Growth 83

Chapter IV. Plasma-Assisted Graphene Growth

4.1. Introduction

Since the discovery of carbon nanotubes (CNTs), it has gathered a lot of attention from academic institutes to industries by producing numerous numbers of scientific papers. Among those efforts, the introduction of plasma in synthesis resulted in strong impact on the lowering of growth temperature. Because the plasma include a variety of reactive species for reaction with/on desired substrate. The history of carbon nanotubes (CNTs) would be a best guideline for graphene research. The research on graphene synthesis is actively under investigating with some of possible ways that described in Chapter III., and especially chemical vapor deposition (CVD) is widely using for growing large-area, high-quality graphene layer. However, it is suffering from high temperature process, more than 1000 °C, thus there are strong requirements to lower growth temperature at least down to CMOS-compatible range. Development of graphene growth based on plasma is timely, as CNTs do, to overcome current limitations of temperature. And it may have the benefits that can accelerate the research, because CNTs already pioneered in plasma atmosphere and resulted in accumulation of knowledge.

As we described in *Chapter I.3.*, the plasma-assisted graphene growth process is first appeared in 2007[1]. This paper inspired a lot of research group including us, allowing low temperature process, which is favorable for industrial aspects. In this *Chapter IV.*, we will describe the development of plasma-assisted graphene growth, and a lowering growth temperature, as well as, direct graphene growth on arbitrary insulating substrate. It is worth to highlight that direct growth on insulating substrate can even bring new paradigm in the research of graphene synthesis due to the fact that transfer process is not necessary anymore. These are mainly contributed to reactive plasma environment, and will be explain later.

The possibility to grow graphene in PECVD system is already appeared in the field of CNT synthesis. There are some reports on the formation of vertical carbon nanowalls (CNWs)[2-8] that have the structure of few layer graphene partially pushed out (toward out-of-plane) by strain. One can expect that, with appropriate engineering of perpendicular strain to surface, we can probably obtain flat graphene on catalyst surface. A group leading by Michael Höltig demonstrated that homogenous CNWs can be grown by PECVD over large area at low temperature ($\sim$500 $^{\rm o}$C)[9], see in Figure 4.1.
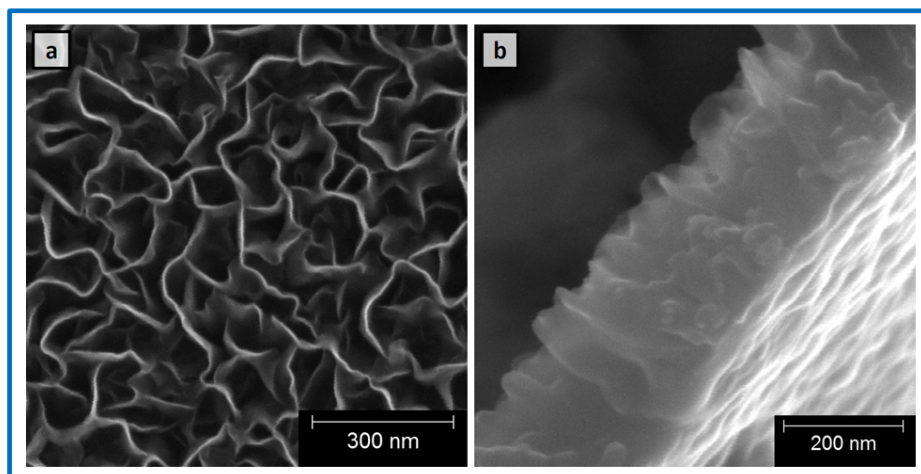
Figure 4.1. (a) Surface and (b) cross-sectional SEM image of CNWs. Credit: Hamburg University[9]

In fact, we found another type of graphene at underneath of catalyst metal, connected to the walls of CNFs obtained by PECVD (see in Figure 4.2.(c)). In detail, vertically aligned carbon nanofibers (CNFs) were grown in a home-made dc PECVD system, using 4 nm-thick Ni catalyst layers on TiN/Si wafers. The growth temperature was set at 650 °C with only 5 minutes growth time. A mixture of water vapor (H_2O) and isopropyl alcohol (C_2H_2OH) was used as the reactive gas source. This aims both to develop new chemistry for CNFs growth based on water vapor and to investigate initial growth process, such as nucleation step, with short exposure time. The applied voltage between anode and cathode in the triode-type chamber was kept at a constant value of 500 V, and with a current intensity of 0.2 A. The extraction voltage and current were precisely adjusted and stabilized at 54 V and 54 mA, respectively (PECVD set up is described in Section 4.2.2. PECVD Setting).
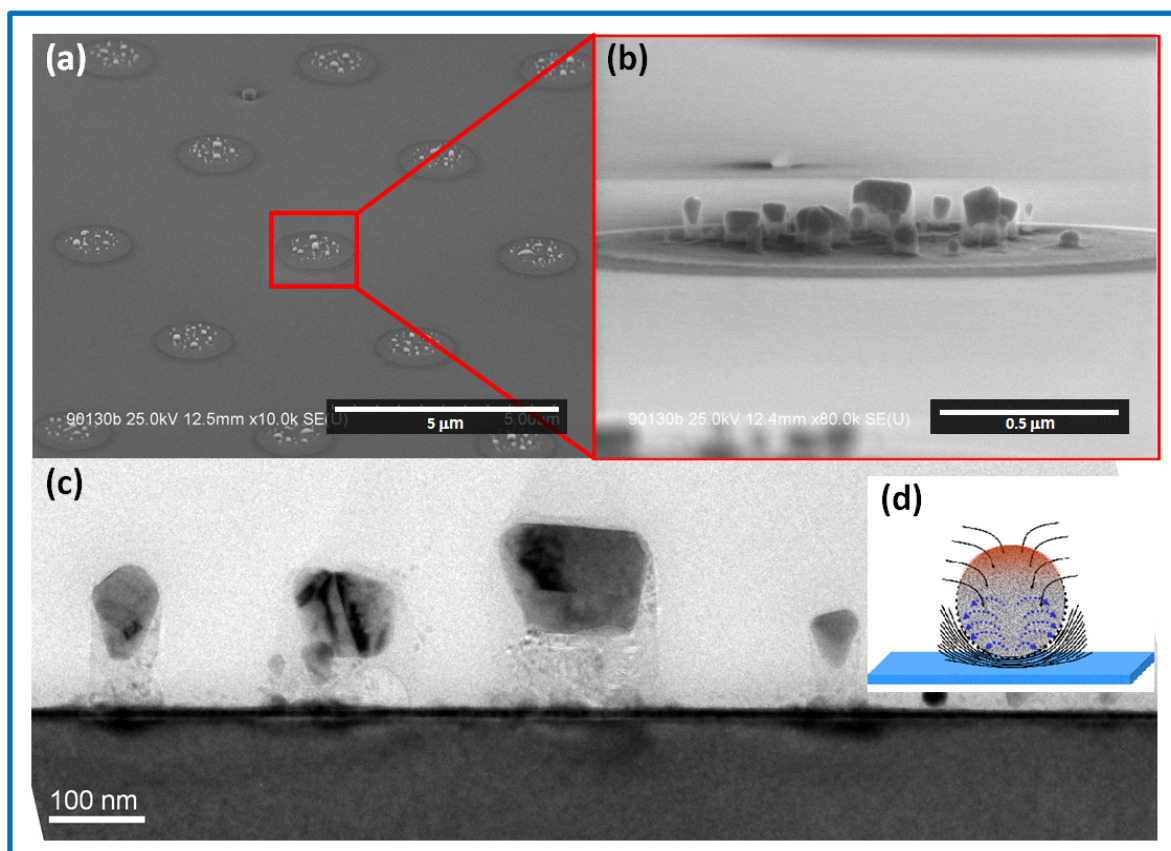
Figure 4.2. (a) SEM image of CNFs. and (b) its magnified image with perpendicular direction to CNFs. (c) TEM image showing stacks of horizontal graphene layers connected to CNF walls. (d) Schematic of graphitization at underneath of catalyst particle. Cited from C.S. Cojocaru et al., J. Nanosci. Nanotechnol. **6**(5), 1331 (2006)[10]

Thus, dc-PECVD allows one to prepare graphene at the interface between an insulating layer and a metal catalyst film. We shall see in the following that it does this together with growing graphene on top of the metal film.

4.2. Generalities

The development of graphene growth process based on PECVD is quite new, even to understand its growth mechanism. Thus, a careful consideration on experimental conditions is required. In this section, we will describe the PECVD set up and sample preparation process for all experiments. This would be a reference point to further develop new growth manner.

4.2.1. Substrates used, Wafer Cleaning and Catalyst Preparation

The substrates used for the present dc-PECVD study are either (100) silicon wafers with 300-nm thermally grown oxide or standard glass. To clearly investigate the graphene growth process, we need to avoid the carbon supply from unintended external source, such as organic contaminations, impurities, etc. For this reason, we give a special care to cleaning the substrate before the evaporation of nickel. The substrate is first dipped into trichloroethylene (Alfa Aesar, L14474, 98%) under the heating in 100 $^{\circ}$C for 30 minutes. Then, rinsing by acetone, isopropyl alcohol, and deionized (DI) water follow in order, consequently, substrate is fully dried by nitrogen gas. A mixture of sulfuric acid (Sigma Aldrich, 339741, 99.9%) and hydrogen peroxide, namely piranha solution(H_2SO_4:H_2O_2=3:1), is then used to clean organic residues off substrates for more than 30 minutes on hot plate with 150 °C. After rinsing by deionized (DI) water, drying by nitrogen, nickel is directly evaporated with a deposition rate lower than 0.3 nm/sec, under a base pressure of 2 x 10^{-7} torr. Figure 4.3. shows uniform and clean as-deposited Ni layer by SEM (with a special care to focus on surface). The RMS roughness is estimated less than 3.0 nm, while sputtered one show higher value of 4.4 nm[11].
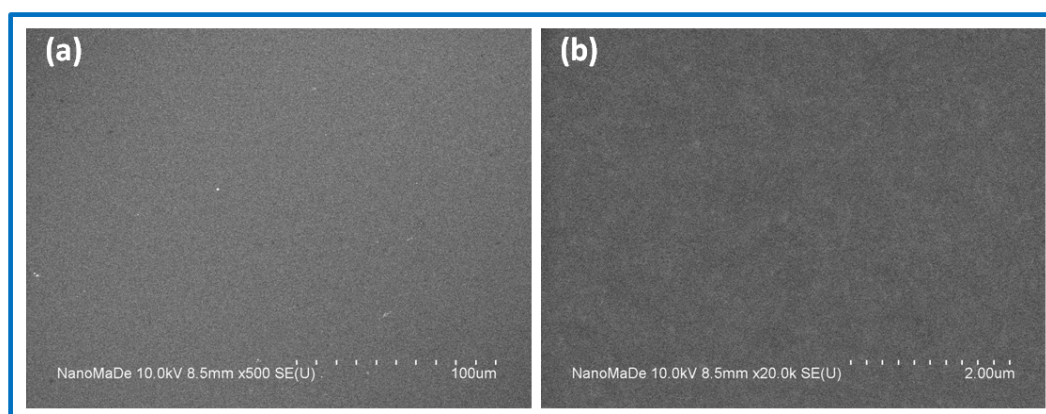
Figure 4.3. (a) Low and (b) high magnification SEM image of as-deposited Ni films with 200 nm-thick on SiO_2/Si wafer.

4.2.2. PECVD setting

Our home-made triode type plasma-assisted chemical vapor deposition (PECVD) system allows to control precisely the density of plasma flux on the substrate. Figure 5.4. presents a schematic of our PECVD set up with a photograph of plasma generation. Basically, we have triode-type PECVD system and we can apply the dc voltage on both in-between anode-grid, and grid-cathode. The sample is placed on the cathode, which is made of graphite. First, as the gas are diffused into anode-grid, the plasma can be ignited with relatively high power, and by delicate control of second voltage between grid and cathode, plasma can be diffused through porous grid and reached into the sample surface. Our chamber is equipped with optical emission spectroscopy (OES) for monitoring the plasma and thermocouple is installed at behind the cathode for temperature control.
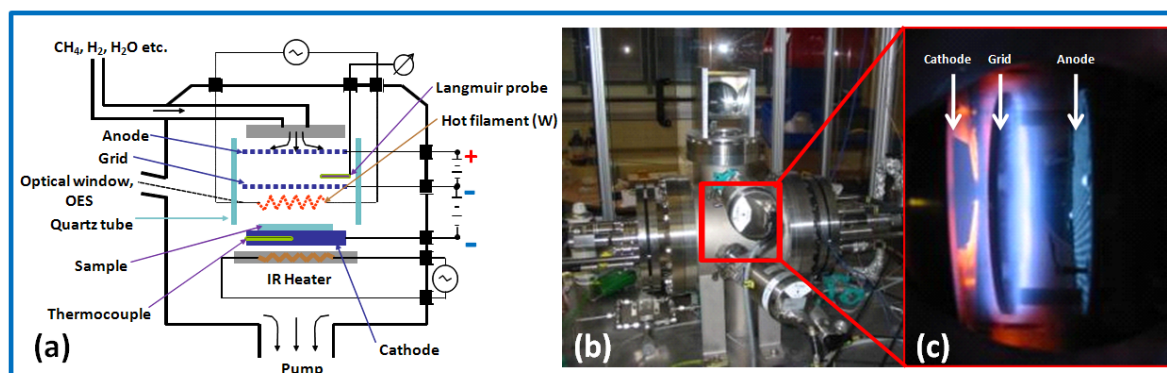
Figure 4.4. (a) Schematic and (b) Photograph of PECVD set up. Our PECVD is installed in lateral direction. (c) Photograph of plasma state via optical window (red square in b). Cathode, grid and anode are pointed out by white arrow.

4.2.3. Growth and Etching Process

In this section, we will deal with general graphene growth procedure as well as etching process for further engineering of sample using water vapor (sort of oxygen plasma etching process).

4.2.3.1. Chamber Cleaning by Water Vapor Plasma

To keep the chamber inside clean from organic contaminations, we are using water vapor plasma with inversed bias (contrast to working conditions) in-between each process. Plasma containing oxygen component is an effective, economical, environmentally safe method for critical cleaning.

In plasma, gas atoms are excited to higher energy states and also ionized. As the atoms and molecules 'relax' to their normal, lower energy states they release a photon of light, this results in the characteristic "glow" or light associated with plasma. Different gases give different colors. For example, oxygen plasma emits a light blue color. And this color corresponds to UV energy. the vacuum ultra violet (VUV) energy, which is generated by the plasma is very effective in the breaking of most organic bonds of contaminations, such as C-H, C-C, C=C, C-O, and C-N. A second cleaning action is carried out by the oxygen species created in the plasma (O_2^+, O_2^-, O_3, O, O^+, O^-, ionized ozone, metastable excited oxygen, and free electrons). These species react with organic contaminants to form H_2O, CO, CO_2, and low molecular weight hydrocarbons. These compounds have relatively high vapor pressures and are evacuated from the chamber during processing. Therefore, inside of chamber remained ultra-clean[12-15].

Water vapor plasma is an interesting possibility to address the decontamination issues[16], due to the fact that water vapor discharges are considerably cheaper, safer, and easier to handle than high-purity

commercial gas mixtures of hydrogen or oxygen. In later case, there is a demand for the installation of expensive precision gas delivery systems and safety protocols due to fire and explosion hazards, while a process based on water vapor may need only a simple dry vacuum evaporator tank. Water vapor plasma might represent an interesting trade-off between low costs and efficacy as long as the decontamination efficiency of such plasmas is of the same order of magnitude as the one obtained with oxygen-based gas mixtures. In terms of generation of oxide films, water vapor plasma has higher oxidative properties in comparison to oxygen plasma[17].

Thus, additional bottle containing H_2O is simply installed in PECVD system and both of bottle and inlet line are under heating for evaporating water molecules/for keeping its vapor phase. Through Mass Flow Controller (MFC), we can precisely control the amount of water vapor (0 ~ 10 sccm) that is introduced to chamber.

For cleaning process, the pressure is set at 2 mbar with an introduction of 10 sccm water vapor. Then, the plasma is generated by putting conditions, 0.18 kW, 850 V, 0.33 A (power, voltage and current in order). Initially, plasma has shallow purple color (because, initially, inside of chamber is not fully filled by water vapor) and finally shallow blue. As the plasma is stabilized, the extraction voltage and current are applied in-between grid and cathode. In general, the cleaning process by plasma takes 30 minutes.

4.2.3.2. General Growth Process in PECVD

The sample is first attached to cathode, and the chamber is pumped out to its base pressure which is 2 x 10^{-5} mbar. Then, the hydrogen gas (50 sccm) is introduced during temperature increase at 2 mbar. In general, our working temperature is 450 °C (with an increase rate of +25 °C/min), which is significantly lower than conventional case. This would have a couple of benefits, such as wide-range substrate adaptation (i.e. glass) and compatibility with current CMOS process.

Prior to beginning graphene growth process, diffusive hydrogen plasma is exposed to the sample surface from anode-grid regime. In detail, hydrogen plasma is ignited in between anode and grid, by putting values, 0.18 kW, 650 V, 0.07 A (power, voltage and current in order). Actual values are recorded as 0.02 kW, 340~360 V, 0.06 A. (These values are always monitored for checking the abnormal atmosphere inside of reactor. From now on, I'll only mention setting values.). We need to remind that, here, no extraction voltage/current is applied, which means plasma itself diffuses through porous mesh to sample surface. This incoming plasma flux by diffusion is softer than extraction under control, so it aims to avoid any physical damage on catalyst surface. Pre-treatment by hydrogen plasma for 2 minutes aims to minimize the surface oxide of catalyst metal, which is inactive for graphene growth. This step is widely-accepted in CNT synthesis[18-21].

Once hydrogen plasma process has been done, 40 sccm of CH_4 (as a reference condition) is introduced into chamber. By launching DC generator (0.17 kW, 650 V, 0.20 A) for anode-grid, plasma by a mixture of CH_4 and H_2 is ignited. At the same time, the other DC generator used for extraction in grid-cathode is also under operation. Extraction current is fixed at 50 mA coupled with voltage fluctuation.
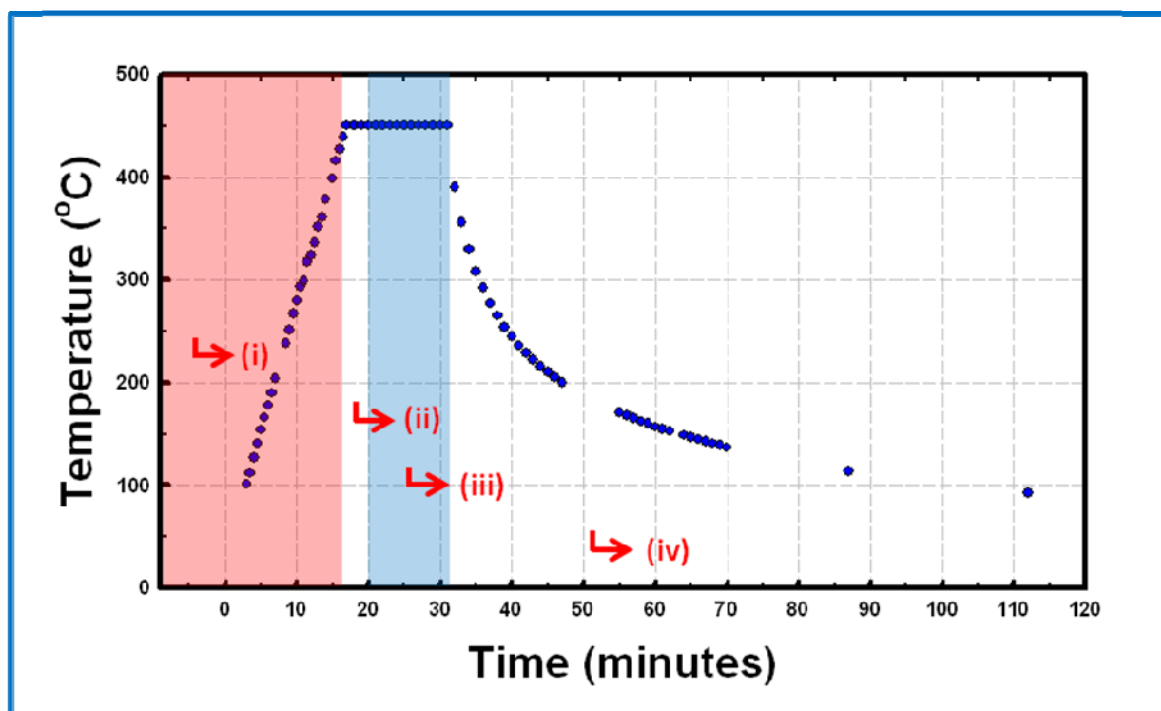
Figure 4.5. General PECVD process for graphene growth. (i) Temperature increase with a ramping speed of +25 °C/min., under H_2 atmosphere. (ii) H_2 plasma pre-treatment for removal of native oxide layer on catalyst. (iii) Graphene growth process by plasma exposure with a mixture of CH_4 and H_2. (iv) Natural cooling under vacuum.

The decomposition temperature is determined by C-H bond energy of carbon source. Among hydrocarbon sources (widely using for the growth of carbon-based materials), methane has a relatively low C-H bond energy, 410 kJ/mol, while ethylene and acetylene has 443 kJ/mol, 506 kJ/mol. Thus, methane is preferable for development of low-temperature process[22].

4.2.3.3. Plasma Etching Process

To minimize the amorphous carbon on metal surface, we can use oxygen-based plasma treatment. As usual, the plasma is first generated in-between anode and grid, with a condition of 0.18 kW, 650 V, 0.29A Keeping the pressure at 2 mbar with 10 sccm water vapor, plasma is extracted to sample surface for 2 minutes. Extraction voltage and current is 20 V, 50 mA, respectively. Due to the plasma ion bombardment, temperature of cathode is increasing up to 125 °C. This process will be used in annealing treatment at high temperature (see

section 4.2.5.).

Plasma exposure which has oxygen component is favorable for etching carbon-based materials. Here, we employed water vapor plasma with high power to etch both amorphous carbon and formed graphene on Ni surface. Plasma conditions are similar with previous case, except for extraction conditions 40 V, 80 mA and process time (10 minutes); they result in higher surface temperature, 175 °C.

4.2.4. PECVD parameters

Our home-made PECVD allow to control a variety of parameters, not limited to exposure time, temperature, gas flow, but also distance between two electrodes inside of chamber. In fact, plasma-based growth system is rather complicated than simple thermal CVD. Therefore, we need to simplify as much as possible that could lead to understand of graphene growth process.

Temperature would be a strongly influencing factors that controlling the quality of materials. S.J. Chae et al., demonstrated that, with increasing growth temperature from 700 °C to 1000 °C at intervals of 100 °C, the D band in Raman spectrum gradually disappeared[23]. The graphene layer was the thinnest at 1000 °C for the temperature used, indicating that there are complicated growth process rather than simple temperature-dependent growth process. A group leading by R.S. Ruoff investigated the low-temperature range graphene growth[24]. With a growth temperature of 300 °C, sparse domains are observed on the Cu foil surface, whereas more graphene domains per unit area are observed for the 400 °C growth. Domains grown at 500 °C, and 600 °C have a rectangular shape. It is estimated that growth temperature mainly affects its growth rate. In other words, a simple comparison of quality by Raman spectrum is not allowed due to the existence of high density of graphene grains.

It is worth to note that temperature increasing/cooling rate is also important parameters[25-28]. Y. Miyata compared the effect of cooling: one is cooled down from 900 °C to 560 °C for around 10 second, and the other one is for 20 minutes, naturally. In later case, they have never been observed graphene at same growth conditions. Fast cooling rate is considered as a crucial factor to grow thin graphene layers. However, when the cooling rate is too fast with same amount of carbon concentration, no graphene is observed in some cases. This means that cooling rate has upper/lower limit with a correlation of dissolved carbon into catalyst. And cooling rate seems to be more important that increasing rate, because it actually interact with carbon for graphene growth.

Especially, the atmosphere when sample is cooled down should be cared. In such a case, when hydrogen is kept alone in cooling procedure, it might plan an important role in etching edges and corners of

graphene flakes[24]. If the graphene films are cooled in hydrogen alone, the graphene film could be reduced locally at high surface energy locations[29]. However, it has even possibility to minimize amorphous carbon with a suitable optimization process.

In PECVD process, there is a special factor that could affect on graphene growth. The change of pressure leads to shift of reactive plasma close to or far from the samples, as well as the density of gases like in T-CVD process. In the following section, we will investigate some of the factors to grow graphene.

4.2.5. Annealing treatment

Using PECVD process, we developed a novel graphene growth technique at low temperature. In addition to this, we designed annealing process at high temperature for further increasing graphene quality. Moreover, this allowed us to better understand the role of carbon diffusion/precipitation in the growth process. We thus focus in the present section on the effect of annealing treatments on the graphene layers that have developed on the top surface of the metal film. The PECVD process applied was standard condition that previously mentioned in Section 4.2.3.2.

We employed simple furnace system (see in Figure 4.6. below), which has cooling & heating zone. Quartz boats carrying the samples could be pushed/pulled by load lock between cooling & heating zone. Especially, heating zone is covered by tungsten (W) wire with temperature controller (Carbolite 1200 °C Split Tube furnace, types HST & VST). And gas inlet is installed for introducing gases, such as hydrogen.
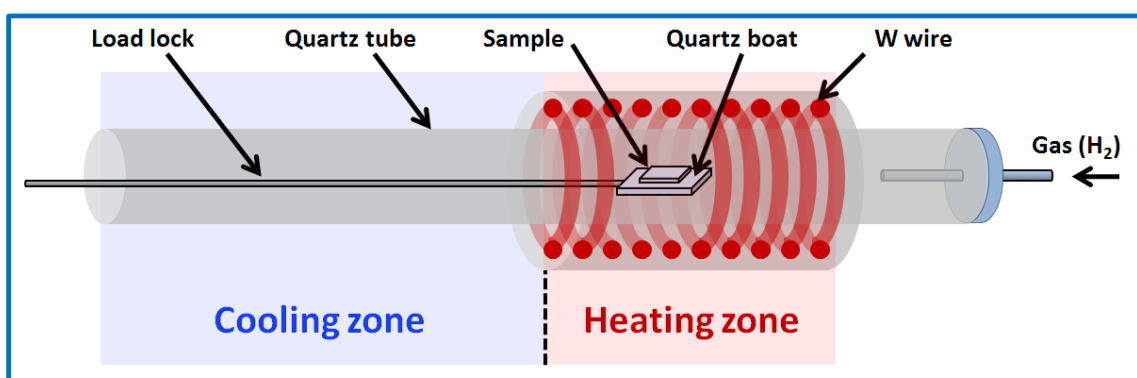
**Figure 4.6.** Schematics of furnace system for high temperature treatment.

First, the sample is loaded in cool zone and the chamber is heated up to 900 °C with a ramping speed of +20 °C per minute. All process in furnace has been done under vacuum (base pressure: 2.0×10^{-5} mbar). Then, using load lock, sample is transferred to the pre-heated zone. After annealing process for 18 minutes,

temperature controller turns off without introducing any gases. When the temperature reaches 750 °C, the sample is quenched out to cool zone. In fact, these conditions are set-up from graphene growth by ion implantation, which will be explained in next Chapter V.
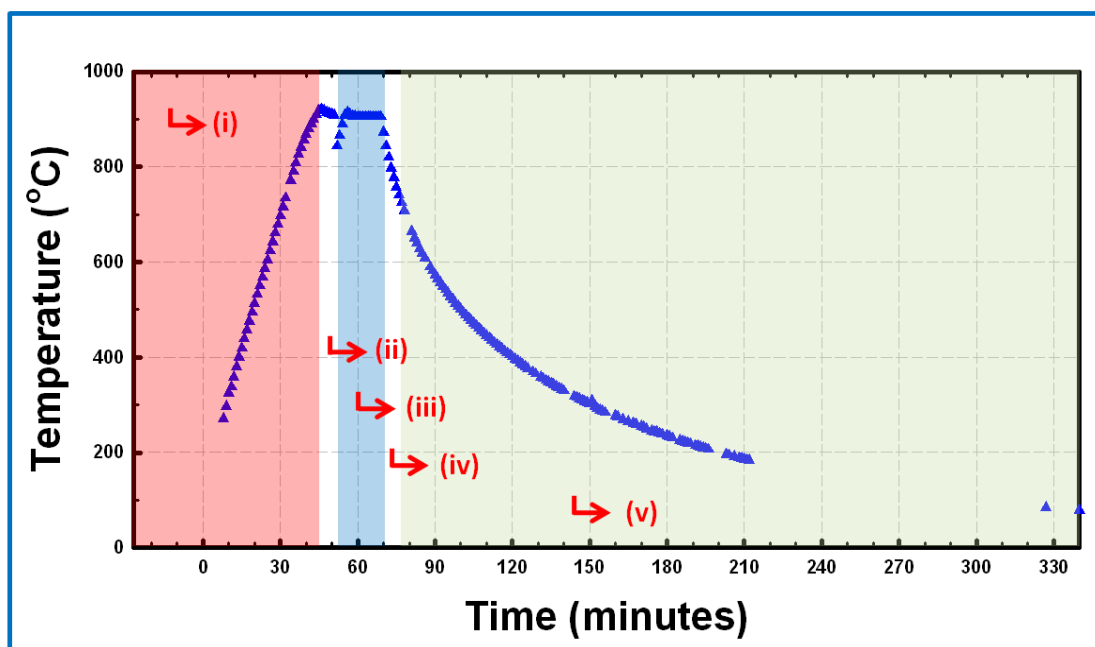
Figure 4.7. Annealing treatment in furnace. First, the quartz boat carrying the sample is loaded in cool zone. (i) Temperature increase with a ramping speed of +20 °C/min., under vacuum ($10^{-4} \sim 10^{-5}$ mbar). (ii) Waiting for temperature stabilization at 900 °C. (iii) Pushing the sample into heating of furnace zone by load lock and annealing process at high temperature. (iv) Turn off the temperature controller and slow cool down in heated zone. (v) Quenching of quartz boat to cool zone for rapid cooling.

First, we adopt reference conditions (as described in section 4.2.3.2. General Growth Process in PECVD) using 200 nm-thick $Ni/SiO_2/Si$. Figure 4.8. (below) shows the surface images after plasma exposure, followed by annealing process. On the SEM images, we can clearly identify extreme contrasts (black and white particles, indicated by green arrow "3", and "4"). As we maximize the contrast of image, we notice that nickel surface excluding extreme part has the contrast difference, roughly grain by grain. In a magnified image, Figure 4.8.(b), black particles are expected to be graphene/graphite-like, because of the presence of corner angle with 120°.

It is worth to note that the boundary of dark contrast estimated both graphene and relatively thick graphite via SEM measurement. The other dark particles which has non-specific angle might be covered by surrounding Ni. Clear identification on surface image will be discussed.
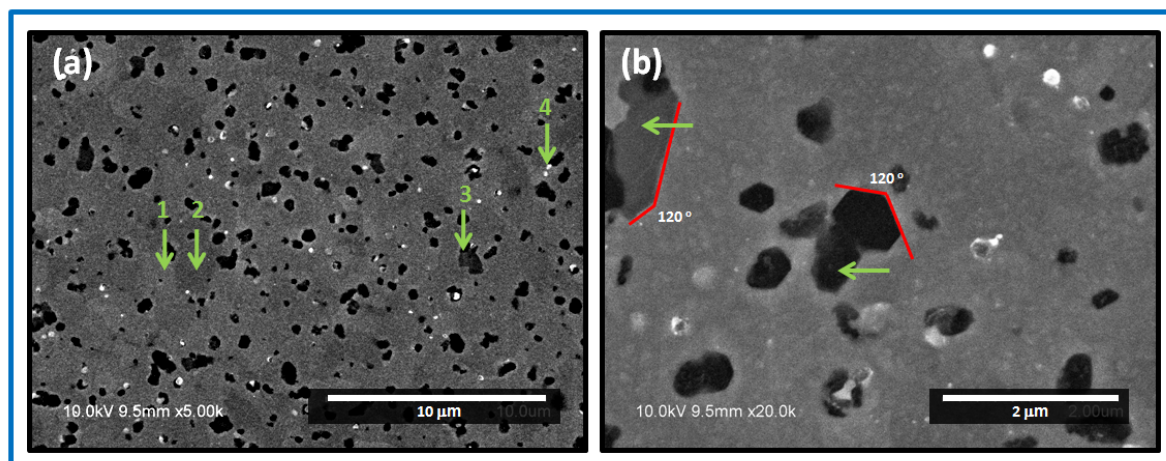
Figure 4.8. Graphene growth by PECVD: Scanning electron microscope images on plasma-exposed sample followed by high temperature annealing, measured at different magnifications (a) x 5k (here, contrast is maximized to clearly distinguish the area "1" and "2" indicated by green arrow) and (b) x 20k, respectively.

In an early stage of development, we focused on annealing conditions at high temperature, especially annealing time and quenching process. A standard PECVD process has been performed first (unless otherwise noted), then the experiment on annealing treatment followed.

Thus, standard PECVD process has been performed, unless otherwise noted. Figure 4.9. shows Raman spectrum on annealed sample for 25 minutes without quenching process. Note that when we cooled naturally down the samples, we will describe as "*without quenching*" to highlight the effect of quenching process. The quartz boat carrying the sample remained in hot zone after turning off the temperature controller.

We found three representative peaks related to graphene. In details, D and G peak centered at 1351.9 cm^{-1} and 1587.5 cm^{-1}, respectively, with an integrated ratio of $I_D/I_G=0.95$. However, full width at half maximum (FWHM) of each peak is around 100 cm^{-1}, which is too broad for classical interpretation schemes[30]. The last is 2D peak (centered at 2703.5 cm^{-1}), which originates from two phonon double resonance Raman process (see *Chapter II. Characterization of Graphene*). It exhibits relatively narrow FWHM of 77.8 cm^{-1}, with an integrated ratio of $I_G/I_{2D}=2.14$. Peak position and FWHM are extracted using LabSpec Version 5.25.15.
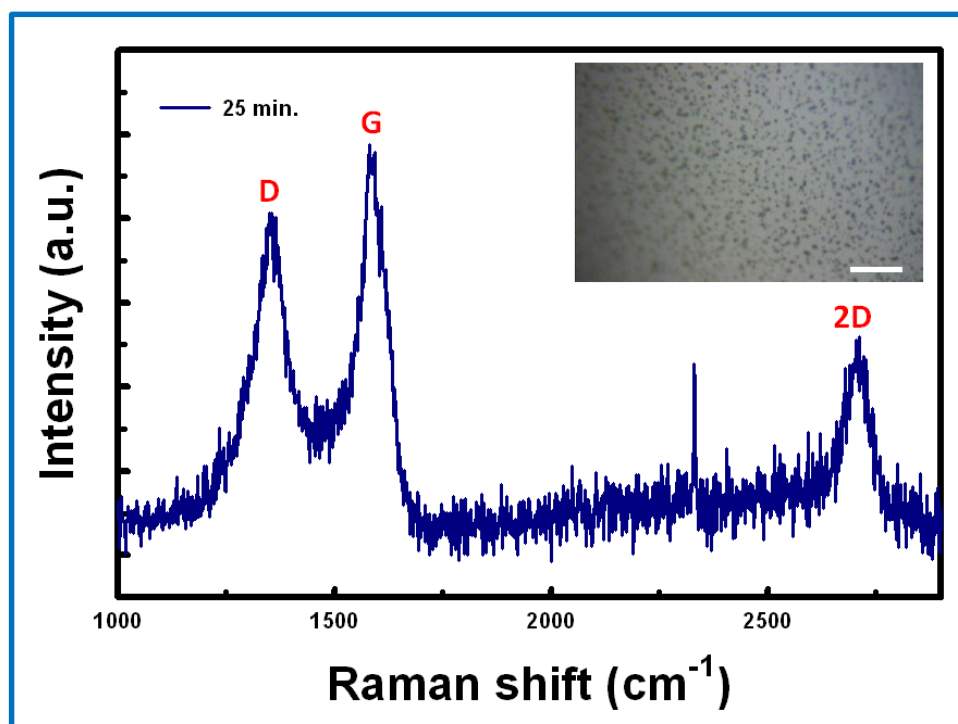
Figure 4.9. Raman spectrum (excited by 514 nm laser) for graphene layers, where D, G, and 2D peaks are indicated in the figure. Standard PECVD process including 25 minutes annealing without quenching has been performed. (Inset) Optical microscope image of samples. Scale bar represent 10 μm.

4.2.6. Growth at surface and at interface

Graphene is generally growing on metal surface, thus electrical isolation via transfer process is mandatory for device fabrication. While many efforts have been made to improve transfer process[31-33], organic residues that come from PMMA and chemical etchant still remain on graphene surface, which results in impeding its intrinsic performance[34, 35]. In addition, transfer causes mechanical stress, which generates structural defects[36, 37].

For above reasons, developing graphene growth directly on insulating substrate for device application, without transfer process, is of great importance for future development. Thus, most of our efforts have been devoted to understanding carbon diffusion through nickel, and growth of interfacial graphene layers in-between nickel and silicon oxide. However, in order to understand diffusion, and the relationships between precipitation at surface and interface, we started our study by the analysis of growth on the top surface.

4.3. Growth at nickel surface

To date, graphene growth on metal surface has been extensively studied. Based on thermal CVD (T-CVD) technique, effect of growth temperature, feeding gas rate/ratio/type in combination with hydrogen or argon gas, growth time, cooling condition, and type of catalyst have been investigated for growth of high quality graphene.

In contrast to T-CVD, plasma enhanced CVD (PECVD) process is not well understood yet. Here, growth temperature, pressure as well as gas mixture ratio are systematically investigated to understand growth mechanisms of PECVD process.

4.3.1. Effect of Annealing: Quenching Process

As we see in Figure 4.8., surface topography varies quite significantly: Raman spectra has the capability to reflect the information of local structure. Therefore, we precisely investigated the Raman response from the positions. After standard PECVD growth, we varied annealing conditions;

Case (i)   (a,b) 25 min. annealing without quenching process.
Case (ii)   (c,d) 18 min. annealing without quenching process.
Case (iii)   (e,f) 18 min. annealing with quenching process.

as presented in Figure 4.10. below. First of all, we can clearly see the difference in Raman response by local positions (Left column is obtained on uniform surface as like green arrow "1" or "2" in Figure 4.8., and right one corresponds to probably thick graphene flakes with dark contrast.). Uniform surface has relatively intense D band signal compare to G band, while 2D band is much more remarkable on thick graphene flakes, for all cases.

Annealing duration might be a factor that can control the carbon diffusion. Here, we compared only two cases, 18 min. vs 25 min. annealing without quenching process. The integrated intensity ratio between G and D (I_G/I_D) represents the order of graphitization, recorded as 1.25 for 25 minutes, it has lower value with 1.06 after 18-min annealing. Moreover, clear 2D peak is found in Case (i). However, distinct differences are not observed, even much similar spectra is recorded on thick graphene with dark color.

Carbon diffusivity D_T *(cm^2/s)* at temperature *T(K)* is expressed as;

$$D_T = D_0 \exp(-E_D / kT)$$

(Eq. 4.1.)

where D_0 is an entropic pre-factor and E_D the diffusion activation energy. Lander et al., found that $D_0 = 2.48$ cm^2/s, $E_D = 1.74$ eV (their activation temperatures in kelvins have again been translated into activation energies in eV per atom)[38]. The diffusion length is as follow;

$$L = 2\sqrt{D_T \tau}$$

(Eq. 4.2.)

Here, τ is the diffusion time, and diffusion length varies as the square root of time. Thus, annealing time wouldn't be a critical factor influencing graphene growth.
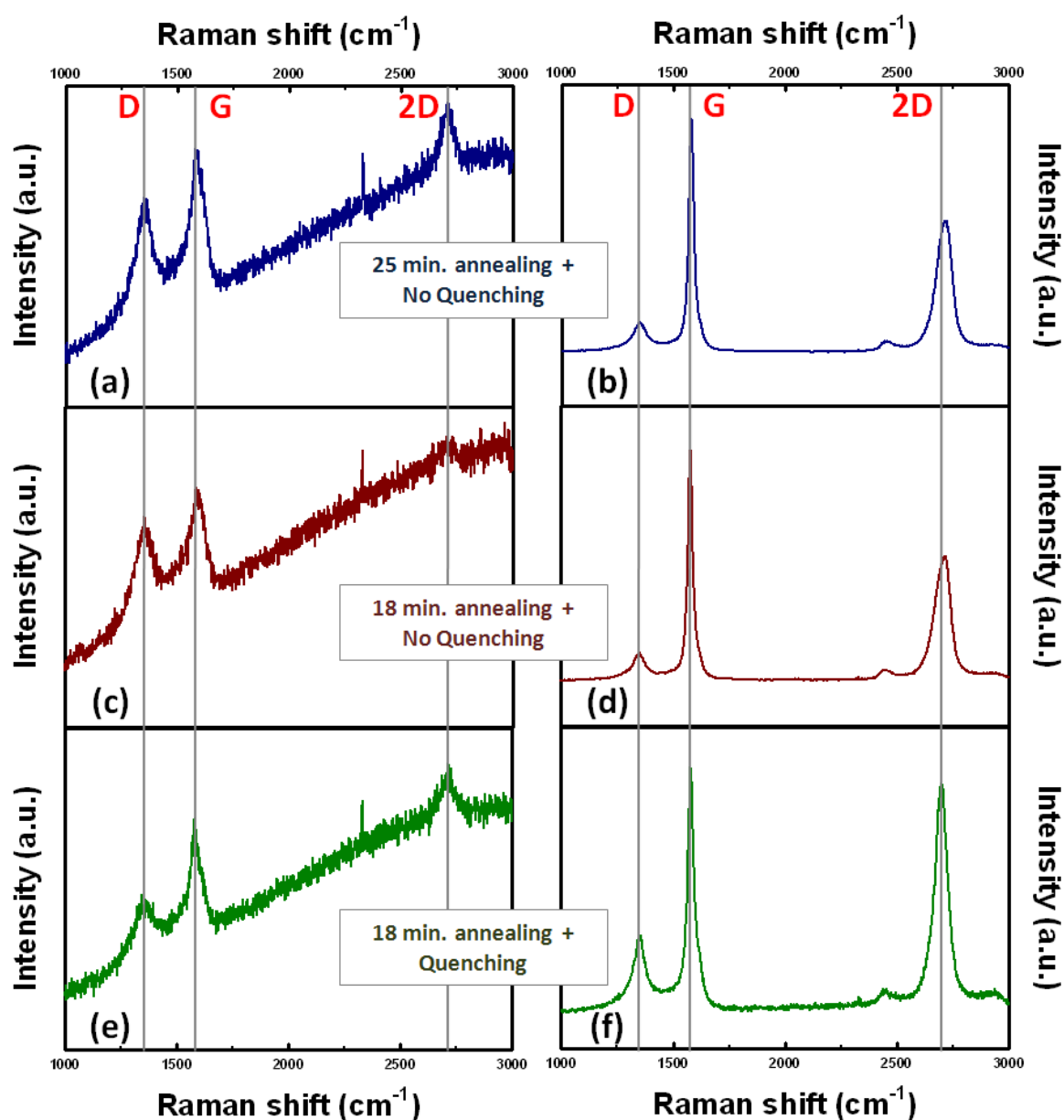

Figure 4.10. Raman spectra (excited by 514 nm laser) of graphene layers as a function of annealing conditions.

(a,b) 25 min. annealing without quenching process, (c,d) 18 min. annealing without quenching process, and (e,f) 18 min. annealing with quenching process at 750 °C. Left column (a,c,e) measured on uniform surface, while right column (b,d,f) corresponds to graphite-like particles with dark contrast.

Comparing Case (ii) and Case (iii), we our aim is to figure out the effect of quenching process. With quenching process at 750 °C, we can obtain a narrow 2D peak with the intensity ratio I_{2D}/I_G of 0.95 in Figure 4.10.(f). Less defect inclusions from uniform surface (e) and more defects from dark surface (f) indicating that relatively uniform graphene layers are formed on Ni surface. As the discrepancy between surface and dark particle is getting closure, this quenching process is favored. Especially, the FWHM of 2D peak is 67.8 cm^{-1} which corresponds to 4~5 graphene layer[39, 40]. It is noted that, unlike 2D band positions and intensity, the FWHM is less affected by excitation energy, charge impurity[41-43].

Blueshift of 2D peak position could be also an evidence for thinning of graphene layers, coupled with higher I_{2D}/I_G[39, 44-46]. For examples, for case (iii) with quenching process which has I_{2D}/I_G=0.95 with narrow G peak, this could correspond to 4~5 graphene[39]. From dark particles, which are estimated as well-organized graphitic structure, fairly narrower and sharper G peak appears, compared to those spectra obtained from uniform surface.
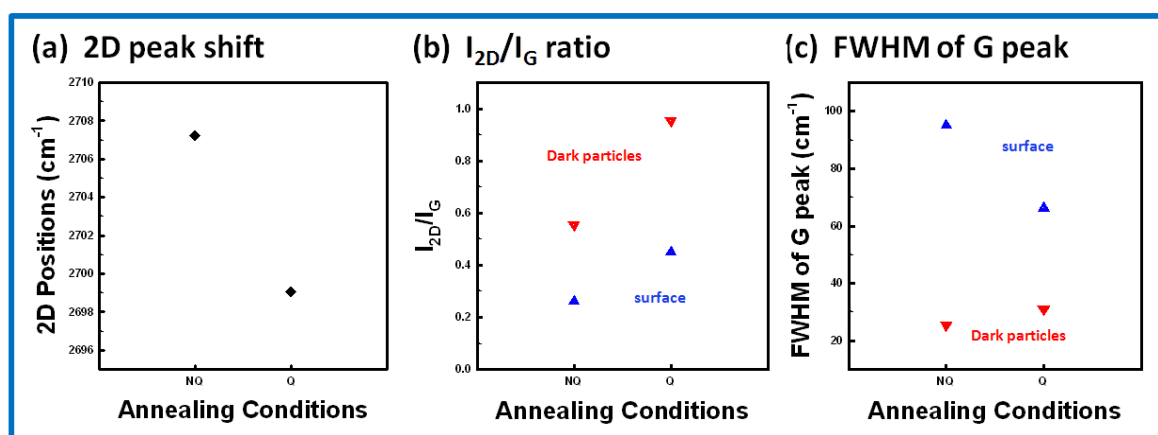
Figure 4.11. Intensity ratio between 2D and G band depends on with/without quenching process. (Q and NQ on x axis mean with Quenching and No Quenching, respectively.) (a) 2D peak position extracted from peak deconvolution. (b) Integrated intensity ratio, I_{2D}/I_G, (c) FWHM of G peak calculated from each on surface and on dark particles.

At high temperature, i.e. 900 °C, transition metal can dissolve considerable amount of carbon atoms into bulk with high carbon solubility. In cooling process, carbon solubility of Ni is lowered so the rest of carbon atoms should be diffused out from bulk to surface. Quenching process doesn't give them enough time to move around as they want, so those carbons near Ni surface could escape but the rest of carbon atoms would be

freeze out inside of Ni. That's the reason why here we can obtain much thin and uniform Raman signals. This will be explained again in next Chapter V, with numerical analysis.

The importance of rapid cooling has been investigated by Yu et al[25]. They found that segregation behaviors depend on cooling rate, strongly affecting the thickness and quality of the graphene films. Different cooling rates, corresponding to fast 20 °C/s, medium 10 °C/s, and slow 0.1 °C/s, were employed, and the structural characteristics of graphene formed on Ni substrates were studied by transmission electron microscopy (TEM) and Raman spectroscopy. Extremely fast cooling rate results in a quench effect in which the solute atoms lose the mobility before they can diffuse, while extremely slow cooling rate gives carbon enough time to make large graphite precipitates, so there will not be enough carbon segregated at the surface.

Through this first experiment using PECVD coupled with annealing process, we found two distinct regions; one is a uniform surface with relatively high intensity of defects, and the other is well-ordered thick graphene. And quenching process seems to be preferential that decrease the thickness of graphene by freezing additional carbon diffusion out. Here, we designed two step processes, from PECVD to annealing process, thus we need to simplify the procedure to understand better.

4.3.2. Mild Water Vapor Exposure for Annealing

Raman spectra after PECVD process (especially, broad and high D peak signal) indicate that Ni surface might be partially covered by amorphous carbon. Thus, to minimize amorphous carbon on Ni, we applied mild water plasma exposure for 2 minutes (see section 4.2.3.3.). Figure 4.12. shows how water vapor plasma does affect the surface morphology. After standard PECVD process for 4 minutes on 200 nm-thick Ni, typical surface of Ni observed. Then, sample is cut into 2 pieces, (b) one is for mild water plasma treatment, and (c) the other one is just annealed together with (b) according to standard conditions. From SEM images, we can clearly see the effect of mild water plasma than can decrease the amount of dark particles, which suspected as graphite. As we decrease the amount of amorphous carbon on Ni, carbon supply into Ni during annealing process has been reduced. So, with less introduction of graphite/carbon, we can have much uniform carbon distributions.

Polycrystalline Ni itself has a high amount of nucleation sites for graphene growth, (due to the possibility of facing steps with incoming carbon species on Ni surface) and, in our plasma process, high density of carbon flux also be a reason for local structural deformations. These are lead to formation of graphite particles during annealing/cooling process, which is not intended to get.
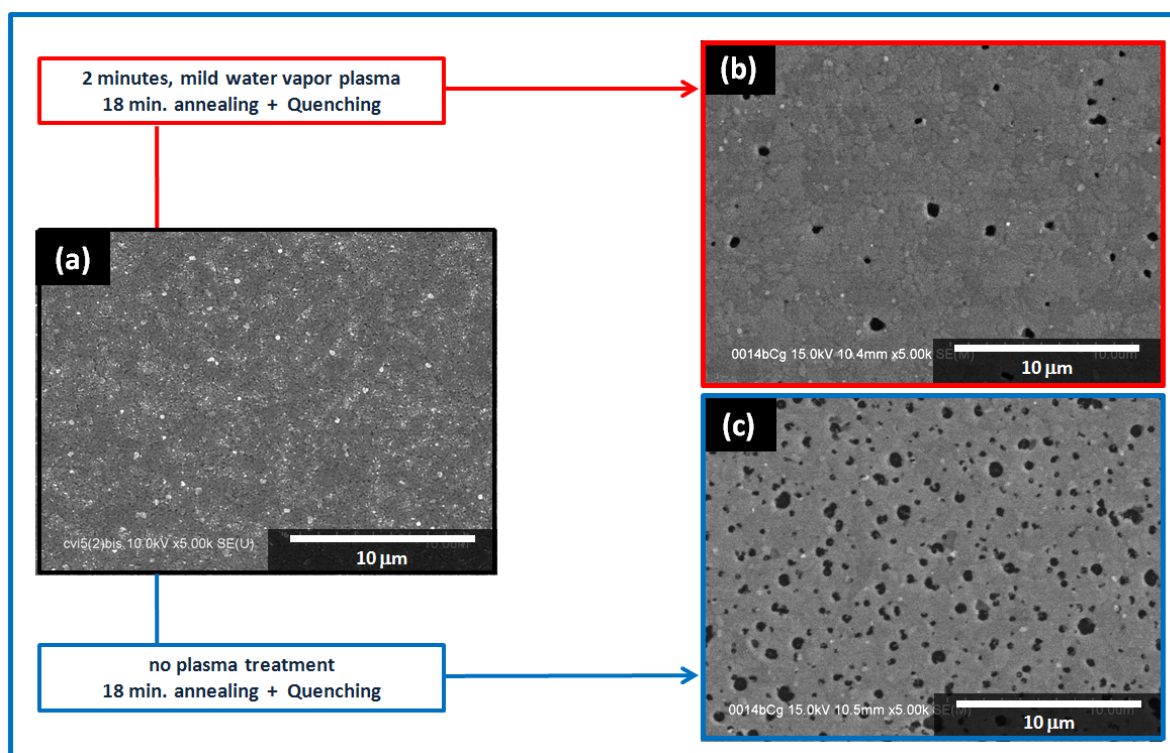
Figure 4.12. Effect of mild water vapor plasma process. Scanning electron microscope images after (a) General PECVD process for 4 minutes. Then, sample is cut into 2 pieces, (b) one is treated by mild water vapor plasma for 2 minutes, and (c) the other one is not exposed by plasma. Both samples are annealed at high temperature, following standard conditions, which mentioned in Figure 4.10. Case (iii); 18 minutes annealing followed by quenching process at 750 °C.

4.3.3. Gas mixture

In this section, our efforts will be devoted to simplify the process to understand better its growth mechanism, which means annealing process won't be applied here.

Competition between carbon feeding gas (C_2H_2, C_2H_4, and CH_4 etc.) and hydrogen has been paid attention for a long time. Another carbon allotrope with 1-dimension, namely carbon nanotube, can be synthesized by a mixture of methane and hydrogen. In this chemistry, dissociated carbon from CH_4 can be incorporated in metal films (or metal particles) and hydrogen can be an etchant for amorphous phase of carbon[47, 48]. Balancing their activities, high quality carbon nanotube with fast growth rate can be obtained.

In graphene synthesis, which is analogous to that of carbon nanotubes, the gas ratio is also of great importance as it can control the quality of materials. Here, we need to point out that other groups are

introducing only few tens of ppm (parts per million) of carbon feeding gas compare to hydrogen and argon gas, or even less[49, 50]. Our working conditions are using extremely high percentage of CH_4 compare to hydrogen, this opens up a route to new fundamental insight.

The amount of hydrogen is fixed as 50 sccm, and methane is varied from 10, 20, 40 and 80 sccm. The other conditions are kept just same as reference. After plasma exposure for 4 minutes, top-view SEM images are taken (Figure 4.13). Working temperature and pressure are the same, but a change in extraction voltage is unavoidable.

Figure 4.13. below shows the surface images of plasma exposed samples, as a function of gas ratio; (a) 10:50, (b) 20:50, (c) 40:50, and (d) 80:50 sccm for CH_4 and H_2. From (a) and (b), we can assume that nickel surface is getting affected by income flux of carbon. Green arrow indicates the flat Ni surface, while red arrow shows the introduction of carbon-materials on/into Ni. Those incorporated carbon often shows angular shape. Lastly, the arrow with blue color means growing part, perpendicular to surface. In case of 20 sccm of H_2, flat Ni surface is getting changed to carbon incorporated surface. Moreover, when we supply high percentage of CH_4, like 40 and 80 sccm cases, it seems fully covered by carbon and surface morphologies is totally changed.
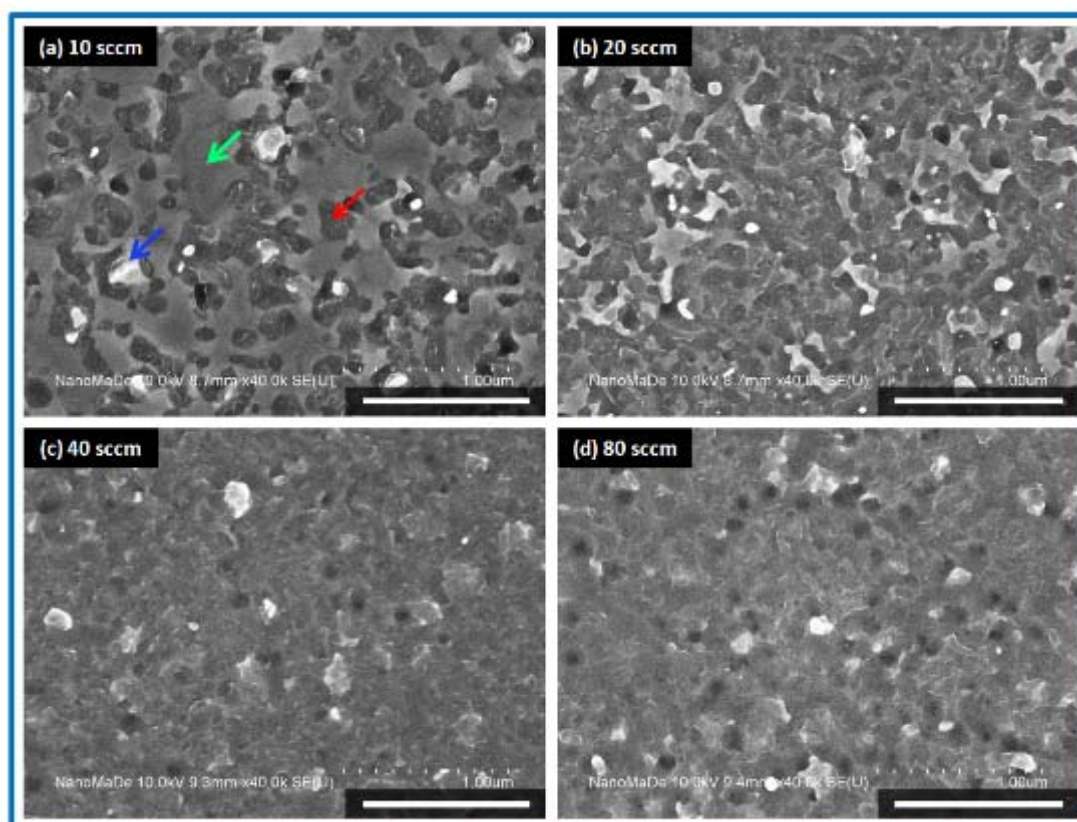
Figure 4.13. Top-view SEM images after PECVD process with a mixture of 50 sccm hydrogen and (a) 10 sccm, (b) 20 sccm, (c) 40 sccm, and (d) 80 sccm of methane, respectively. The other conditions are kept just same as

reference. All scale bars represent 1 μm length.

Raman spectra (Fig. 4.14) are acquired using 514.5 nm laser with power of 0.90 mW. We note a slight increase of D peak signal as a function of the amount of methane in the mixture.
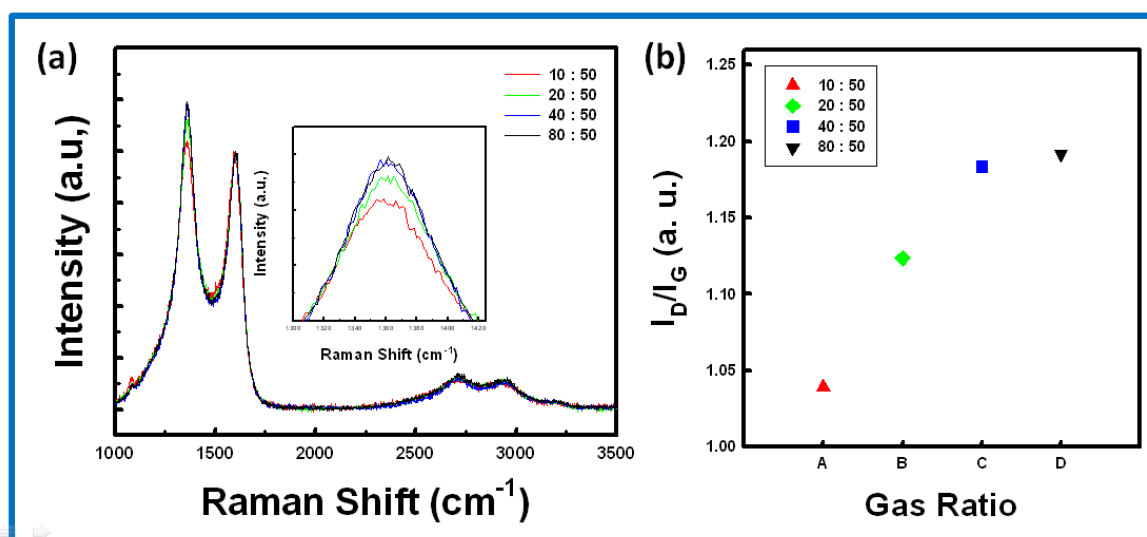
Figure 4.14. (a) The change of Raman spectra with a gas ratio between methane and hydrogen. Inset shows the magnified D peak, which appeared around 1365 cm^{-1}. (b) Evolution of I_D/I_G with gas ratio.

As we mentioned in Chapter II., crystallite size (L_a) of graphene can be extracted from the intensity ratio I_d/I_G (Eq. 2.5.). In fact, the gas ratio makes a small effect on L_a, which is of the order of the uncertainty. This means that our growth with a gas ratio (10 : 50 ∼ 80 : 50 of CH_4 : H_2) is always in conditions of high methane concentration where crystallite size remains out of control.   In other respects, the density of nucleation sites, which is closely related to crystallite size, depends on the nickel crystal quality. Controlling graphene crystal size by gas ratio should be possible if we use pre-annealed Ni (which has enlarged grain size) with relatively small amount of CH_4.

However, our primitive work, apart from the control of crystallite size, aims to grow graphene layers at low temperature that could be used without transfer process, thus at the interface between catalyst and substrate. This high methane concentration introduces a high flux of carbon atoms in the nickel that, after diffusion, ends up as a significant interface precipitation. This will be further discussed in next Chapter V.

Regardless of gas ratio, now we annealed sample at high temperature without quenching process. From Raman measurement, we calculated I_D/I_G and I_G/I_{2D}, as plotted in Figure 4.15.(a). In graph, "AP" means "**A**fter **P**ECVD process", "AA_S" means "**A**fter **A**nnealing process and measured on uniform **S**urface", and "AA_P" means "**A**fter **A**nnealing process and measured on graphite **P**articles". First, slight decreasing of D band signals

is observed by annealing process. Graphite particles, especially formed by annealing process, deliver quite low D band signals. But that ratio between G and 2D is under similar range. Crystallite sizes calculated from I_D/I_G (Eq. 2.5., Figure 4.15(b)) indicate that the annealing process doesn't significantly affect the crystallinity of the graphene that uniformly covers the surface. Uniform surface has fairly high density of nucleation sites with small grains, it couldn't be properly rearranged or healed[51, 52]. On the other hand, graphite particles get enlarged: their crystal size reaches up to 82 nm in lateral dimensions.
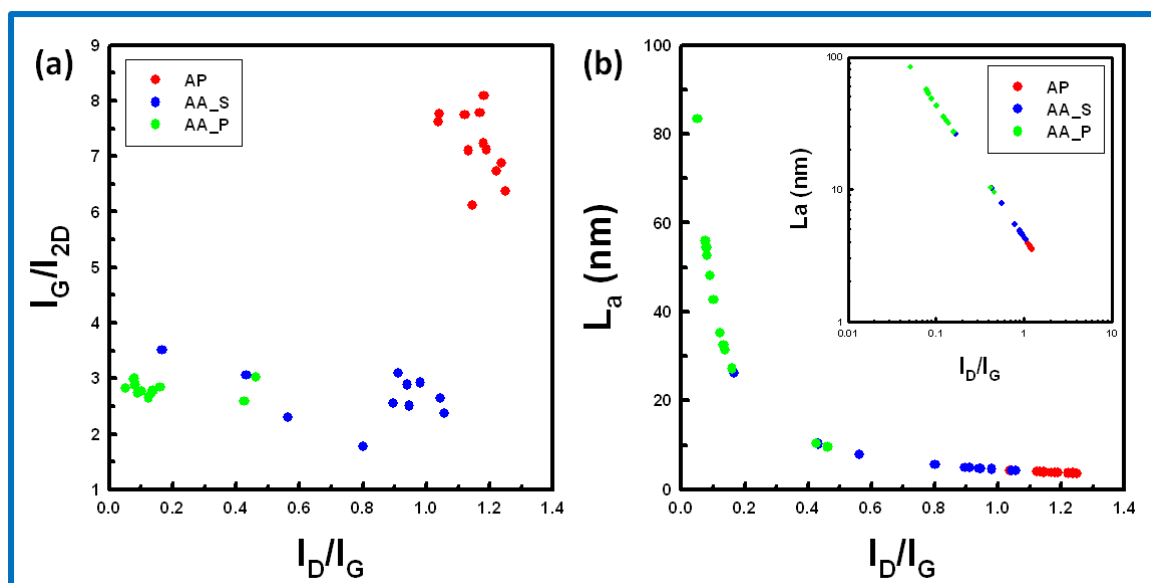
Figure 4.15. (a) I_G/I_{2D} versus I_D/I_G, calculated from Raman spectra. AP means "After Plasma process" with red color. AA_S/AA_P means "After Annealing process at high temperature" and taken on uniform surface and black particle, which is considered as graphite. (b) Crystallinity size calculated from I_D/I_G (Eq. 2.5.). Inset shows log vs log scale graph.

Our growth conditions seem not perfect for high quality graphene on Ni surface, but their potential toward transfer-free and low-temperature growth will be discussed. And we will see (4.4. Growth directly on insulating substrate) that they are quite useful for growth at the interface between the nickel and the insulating substrate.

4.3.4. Growth Time

Time-dependent dynamics can deliver useful information on graphene growth mechanism. In this section, I will present the effect of growth time on graphene formation.

4.3.4.1. Plasma Exposure

Keeping the H_2 pretreatment just as same, plasma exposure time by a mixture of CH_4 and H_2 varied

from 1 min., to 2 min., 4 min., 8 min., and 12 min. Figure 4.16. below shows scanning electron microscope (SEM) images of Ni surface after plasma exposure. All the images are taken at same working conditions of 5 K magnification and around 9 mm working distance at 10 kV acceleration voltage. Here, we can recognize the surface change with bright contrast.
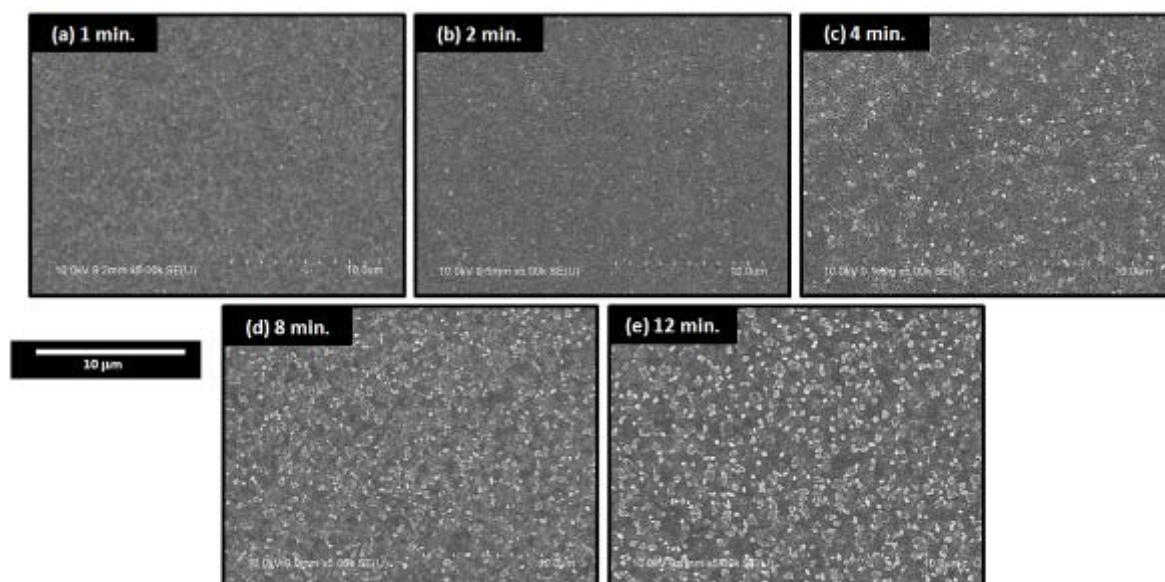
Figure 4.16. Growth time-dependent surface evolution taken by scanning electron microscope. Plasma ignited by a mixture of CH_4 and H_2 exposed to samples for (a) 1 min., (b) 2 min., (c) 4 min., (d) 8 min., and (e) 12 min., respectively. (5 K magnification for all images)

By recording tilted SEM images (Figure 4.17.), we see that bright spots in fig. 4.16 actually correspond to extruded particles. And their size is getting larger with increasing number of particles. This will now be closely investigated for understating surface changes.
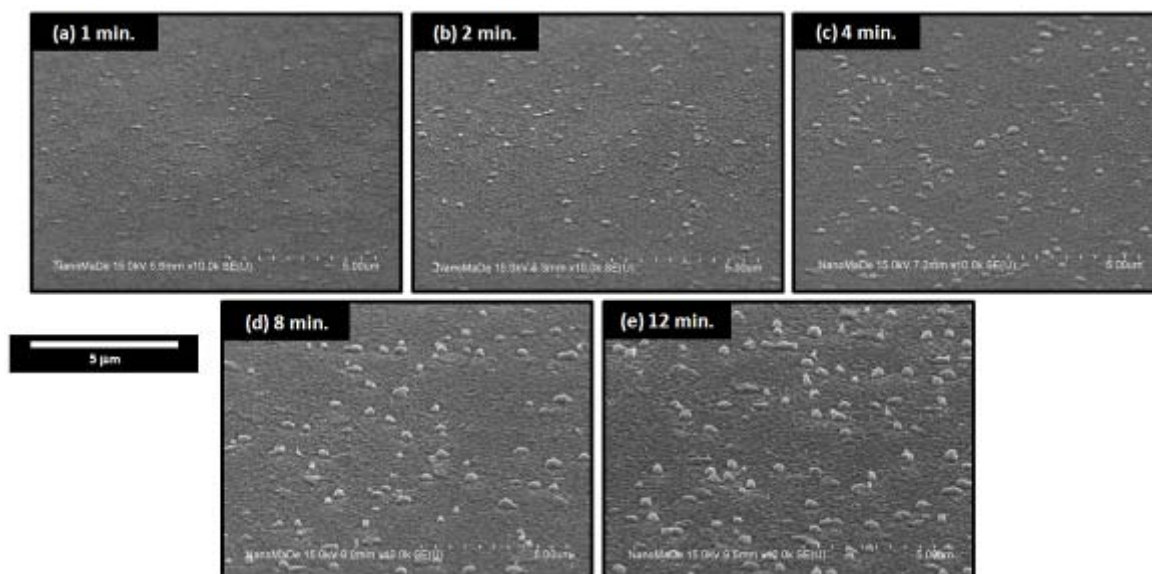
Figure 4.17. Growth time-dependent surface evolution taken by tilted scanning electron microscope. Plasma ignited by a mixture of CH_4 and H_2 exposed to samples for (a) 1 min., (b) 2 min., (c) 4 min., (d) 8 min., and (e) 12 min., respectively. (10 K magnification for all images)

4.3.4.2. Annealing Process

For all previous samples in Figures 4.16 and 4.17., we applied mild water vapor plasma for 2 minutes, and annealing process is followed by standard conditions (see section 4.2.2.3. for mild water vapor plasma, and section 4.2.5. for annealing process). And Figure 4.18. below shows surface changes compared to previous images. Graphite with dark contrast has been formed and still bright contrast has appeared on surface.
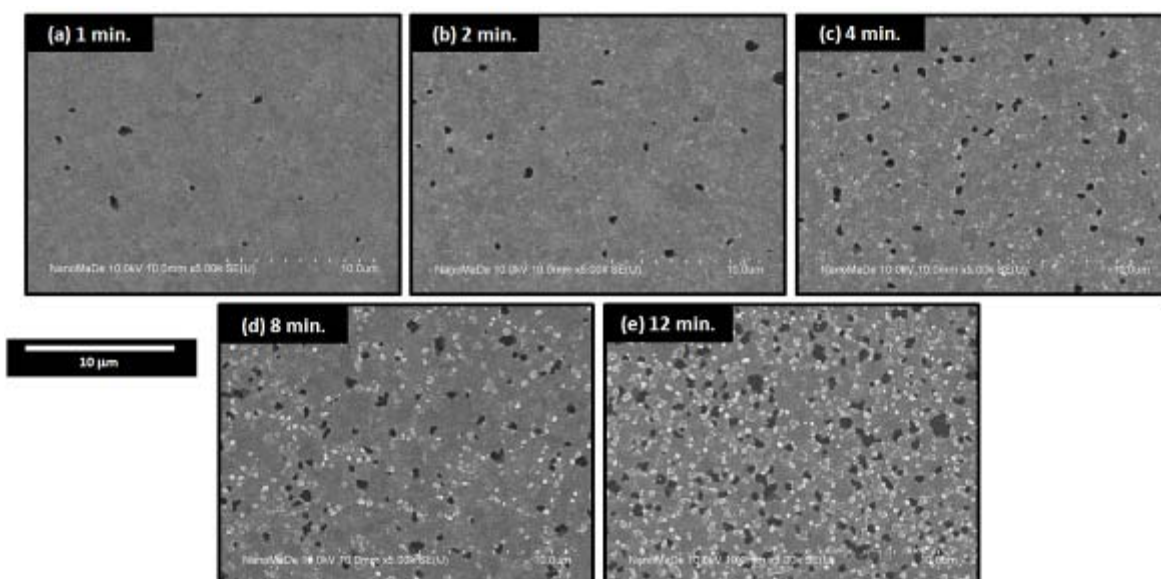

Figure 4.18. Growth time-dependent surface evolution taken by scanning electron microscope. Plasma ignited by a mixture of CH_4 and H_2 exposed to samples for (a) 1 min., (b) 2 min., (c) 4 min., (d) 8 min., and (e) 12 min.,

respectively, after annealing for 18 min. at 900 °C. (5 K magnification for all images)

First, the numerical analysis on graphite inclusions has been performed by support of *Image J* which is freeware image processing tool. Based on the differences in contrast, number of graphite particles and relative area of graphene inclusions are automatically extracted, as shown in Figure 4.19. below. Time-dependant evolution of graphite is evidently revealed by linear relationship with plasma exposure time. In fact, the introduction of graphite particles might be related to both polycrystalline nature of Ni and high percentage of carbon feeding gas compared to hydrogen. The presence of grain boundaries in Ni could lead to non-homogeneous carbon diffusion, and crystallization as they give energetically favorable sites. To obtain a homogeneous graphene, we need to minimize the number of graphite particles, as much we can.
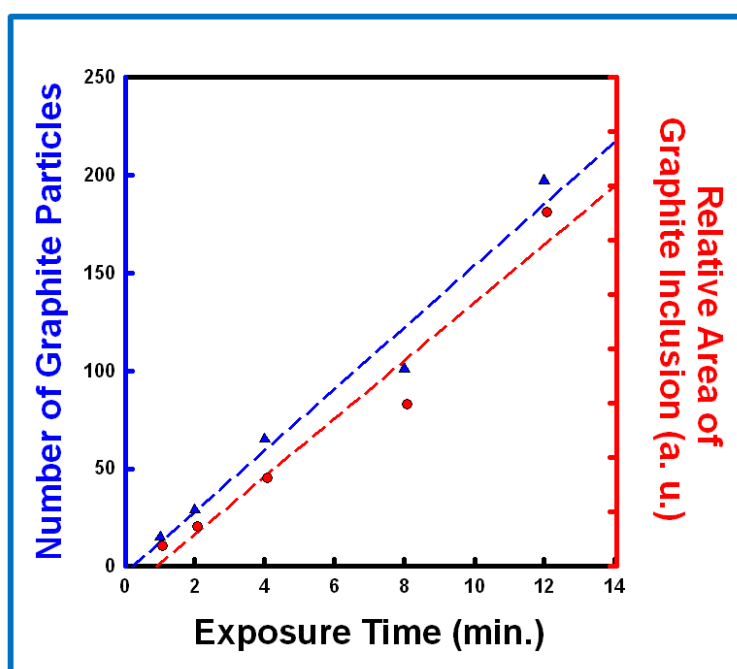
Figure 4.19. Graphite inclusions with plasma exposure time. Using "Image J", the number of graphite particles and relative area of graphite are extracted and marked with blue and red color, respectively. Both factors are well accord with linear relationship. This shows obviously that graphite is enlarging (both total number and its size) with time-dependency.

4.3.4.3. Structural Deformation

To identify the emerging particles visible on SEM images, we performed atomic force microscope (AFM) measurements with line profiles. Figure 4.20.(a-c) corresponds to samples exposed to plasma process for 12 minutes, then annealed following our standard condition (see section 4.2.5.). SEM is compared to AFM at the same scale (10 µm x 10 µm). Referred to uniform surface, the particles with brighter contrast have a height up to 200 nm by line profile extraction. Here, I would like to recall that initial Ni layer is 200 nm-thick, which is

similar with height of these particles. Graphite is located with a depth of ~80 nm. For the sample exposed 8 minutes to plasma (the rest conditions are exactly same), the trend is similar for a xx min exposition to plasma with 200-nm height, and ~50-nm depth, for bright particles, and for graphite, respectively. Then, the question arising is: what happened to the amount of Ni on graphite particles, which corresponds to a thickness of 50~100 nm? This can be explained with magnified SEM images coupled with backscattering measurements.
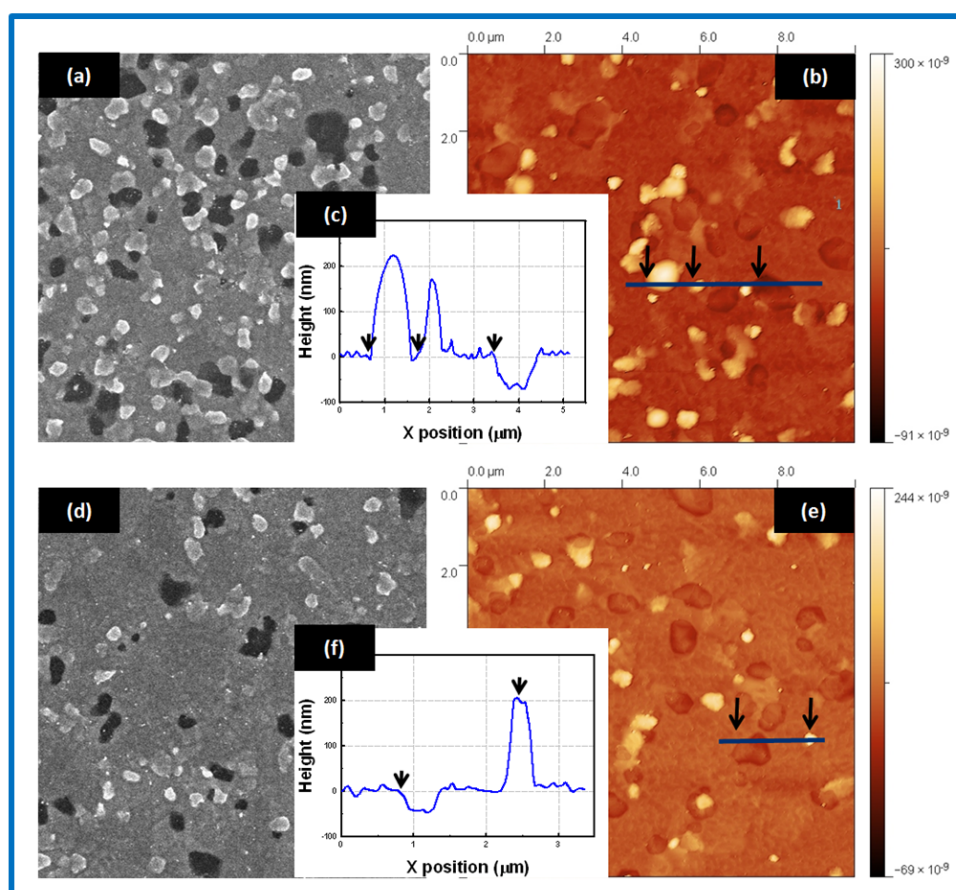
Figure 4.20. SEM, AFM, and line profile from marked line in AFM data, of plasma exposed samples (a-c) for 12 minutes, (d-f) for 8 minutes, respectively. After PECVD process, general annealing process has been done. SEM and AFM has same scale bar with 10 μm x 10 μm size, for compassion of surface morphologies.

Regardless of plasma exposure time, from 1 min. to 12 min., graphite-like particles with a specific angle, approximately 120 °C at each corner side, have been found, as shown in Figure 4.21. Tilted images with higher magnification indicate that a strong structural deformation has occurred, especially on graphite particles. As graphite structure is generated inside of Ni, some of Ni must be pushed up. This process could lead to CNT-like growth, perpendicularly to substrate, as marked by green arrows in (f,g). When we closely look at the red arrows, we can always see an underlying dark contrast, which can be suspected to be graphite.
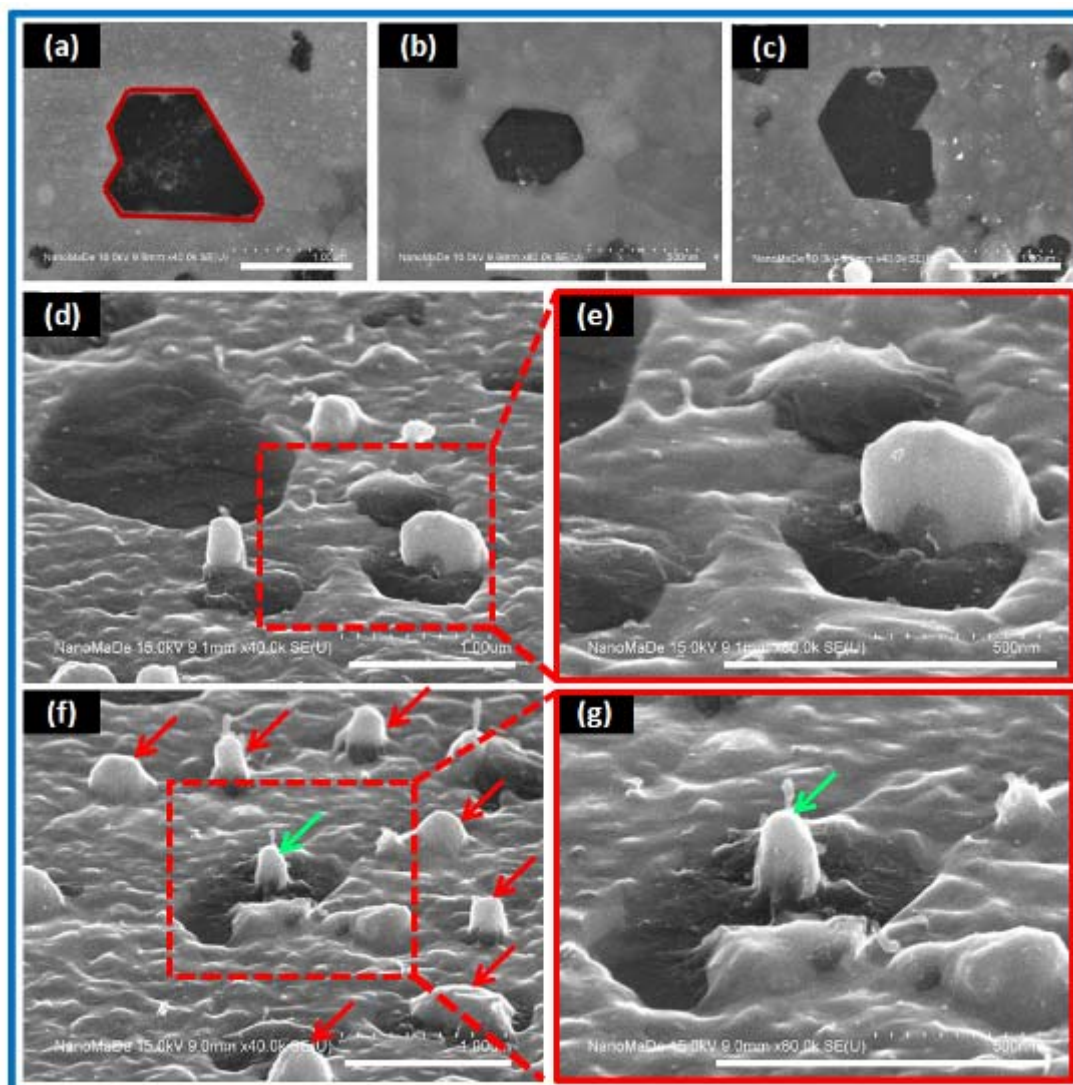
Figure 4.21. SEM images with high magnifications for various cases. Top-view surface images focused on graphite particles, showing specific angles at each corner close to 120°, for exposure times (a-c) 1, 8, 12 minutes, respectively, with 40K, 60K, and 40K magnification. (d-g) Tilted SEM images of 12 minutes exposed samples with (d,f) 40K, and (e,g) 80K. Red arrows in (f) indicate surface deformation, like CNT growth. As growth is perpendicular to surface, a dark contrast appears in the underlying area. Green arrows in (f,g) indicate a strong Ni deformation on graphite surface. Scale bars represent 1 μm in all cases (and not the values indicated by the SEM).

To analyze those growing structures, we have performed back scattering measurements, as shown in Figure 4.22. Brighter contrast in secondary electron SEM image, which means strong surface deformations, appears as Ni in backscattering regime. This is a good agreement with previous hypothesis.
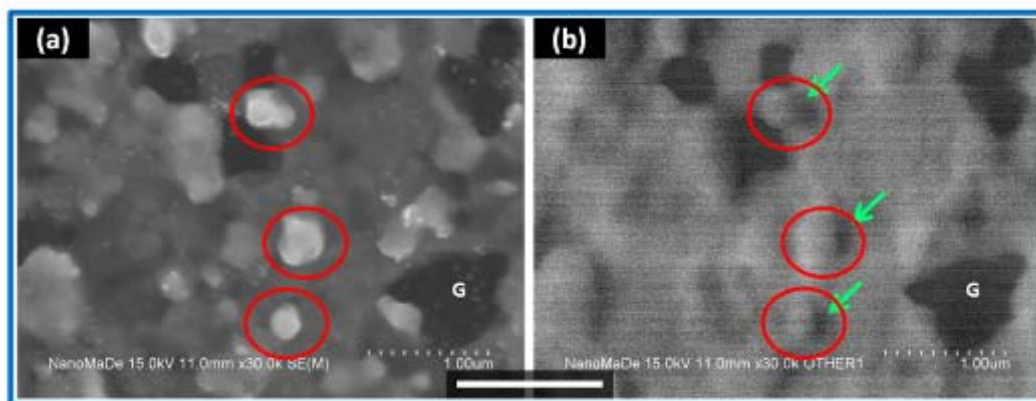
Figure 4.22. (a) SEM secondary electron image, and (b) back scattering image for same local position. Red circles point out highly deformed positions, as shown in previous tilt-SEM images. Scale bar is 1 μm for both.

4.3.4.4. Graphene Transfer

Graphene being placed on metal surface, transfer process is needed for investigation of electrical/optical properties. For the graphene transfer, basically, we employed floating transfer method. We fabricated a template made of Teflon, which, being hydrophobic, helps to obtain graphene floating on the etchant surface. Commercial nickel etchant (Nickel Etchant TBF - Transene) is poured in beaker with template, and the sample is softly placed in etchant. As Ni layer is etched away thanks to in-plane diffusion of etchant, graphene remains on the surface of etchant, while, on the other hand, an insulating substrate is immersed into etchant. Thus, floating graphene can be picked up on a new, functional, substrate.

Figure 4.23. shows top-view scanning electron microscope images after transfer of graphene layers on new SiO_2/Si substrate. In fact, here, we can identify three elements; (i) uniform graphene surface, (ii) graphitic particles, and (iii) exposed SiO_2 surface. In case of only 1 minute exposed sample, graphene surface is quite uniform and just few of particles are observed. As the plasma exposure time is increasing, the number of particles, which are graphite, appear more and more. Consequently, because of the interactions with graphite particles, graphene layer could be partially torn out and SiO_2 surface appears. This point will be discussed more in next chapter regarding interfacial graphene.
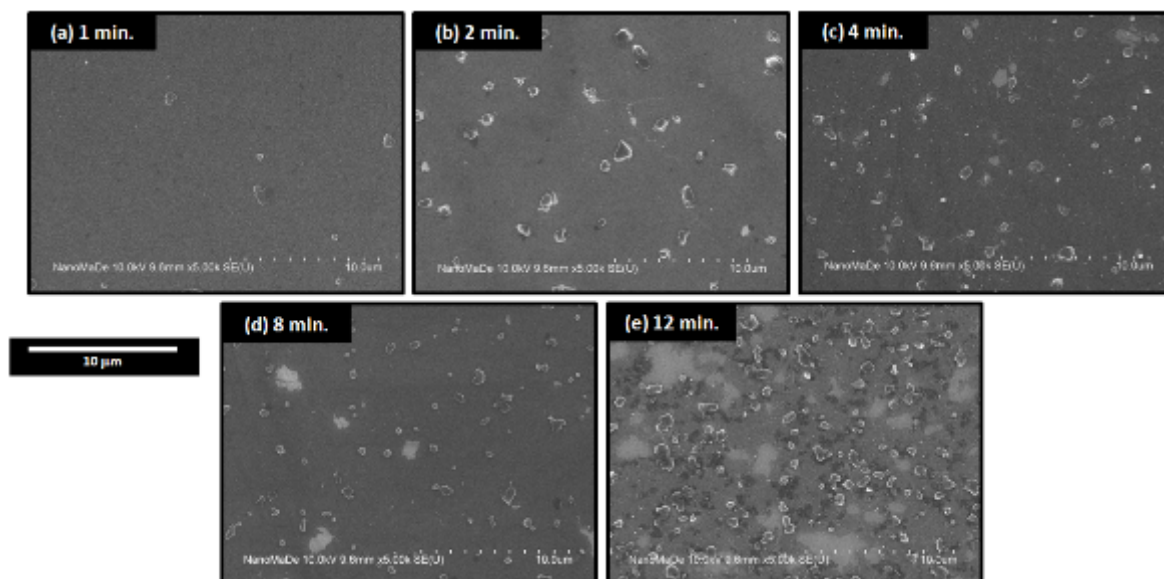
Figure 4.23. Scanning electron microscope images on transferred graphene layers, with plasma exposure time (a) 1 min., (b) 2 min., (c) 4 min., (d) 8 min., and (e) 12 min. All images are taken at same conditions.

The samples presented in Fig. 4.24. are taken again with specific angle of tilt. To visualize the graphene layers onto the SiO_2 substrate, images are taken intentionally at the edge of graphene layers, as we can see in Figure 4.25. Referred to contrast, folded areas are found in the 1-mn exposed sample, marked by green arrows, and the boundary between graphene and SiO_2 can be clearly distinguished thanks to substrate cleanliness.
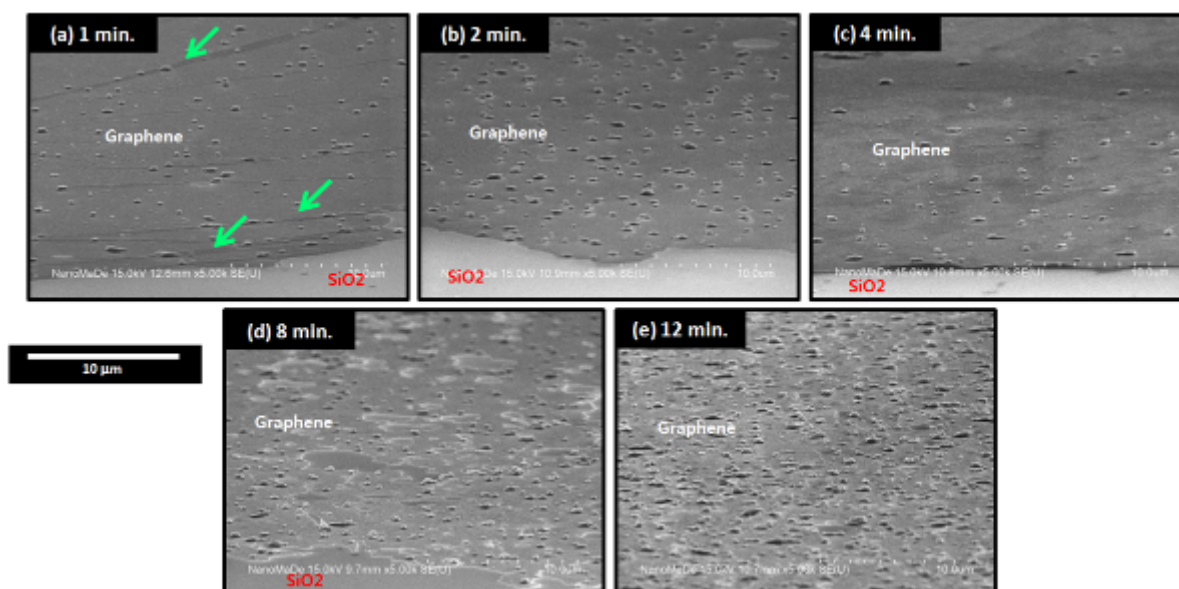
Figure 4.24. Tilted scanning electron microscope images on transferred graphene layers, with plasma exposure time (a) 1 min., (b) 2 min., (c) 4 min., (d) 8 min., and (e) 12 min. All images are taken in the same conditions.

109

4.3.4.5. Electrical Characterizations

Depending on plasma exposure time, which is closely related to the number of graphene layers, the sheet resistance varies from 17.66 kΩ/sq. to 161.53 kΩ/sq. From linear fitting the data, the following equation can be extracted

$$\text{S. R.(van der Pauw)} = y_0 + \alpha \cdot P_t \qquad \text{(Eq. 4.3.)}$$
$$= 142.12 - 10.47 \cdot P_t$$
$$= 142.12 - 12.47 \cdot N$$

where y_0 is the pre-factor extracted from point of contact with y axis, α is the linear dependency factor extracted from slope in Figure 4.25.(c), P_t is the plasma exposure time, and N is the number of estimated graphene layers (referred to Raman data).

In TLM measurement, the sheet resistance of 4 minutes exposed sample is 7.57 kΩ/sq., 8 times lower than previous case of 60.97 kΩ/sq. This is mainly attributed to contact electrode formation, yielding extraction of contact resistance of 12.14 kΩ. Therefore, metal electrode with better contact is additionally required for further engineering of graphene. Linear dependency of sheet resistance on exposure time and thickness of graphene layer can be expressed same with van der Pauw case, as following,

$$\text{S. R.(TLM)} = y_0 + \alpha \cdot P_t \qquad \text{(Eq. 4.4.)}$$
$$= 21.31 - 1.69 \cdot P_t$$
$$= 21.31 - 2.03 \cdot N$$

Note that all the values here are empirically defined from those data in Figure 4.25.(c). And silver electrode has a work function of 4.73 eV, which is quite similar with graphene, around 4.5 eV.
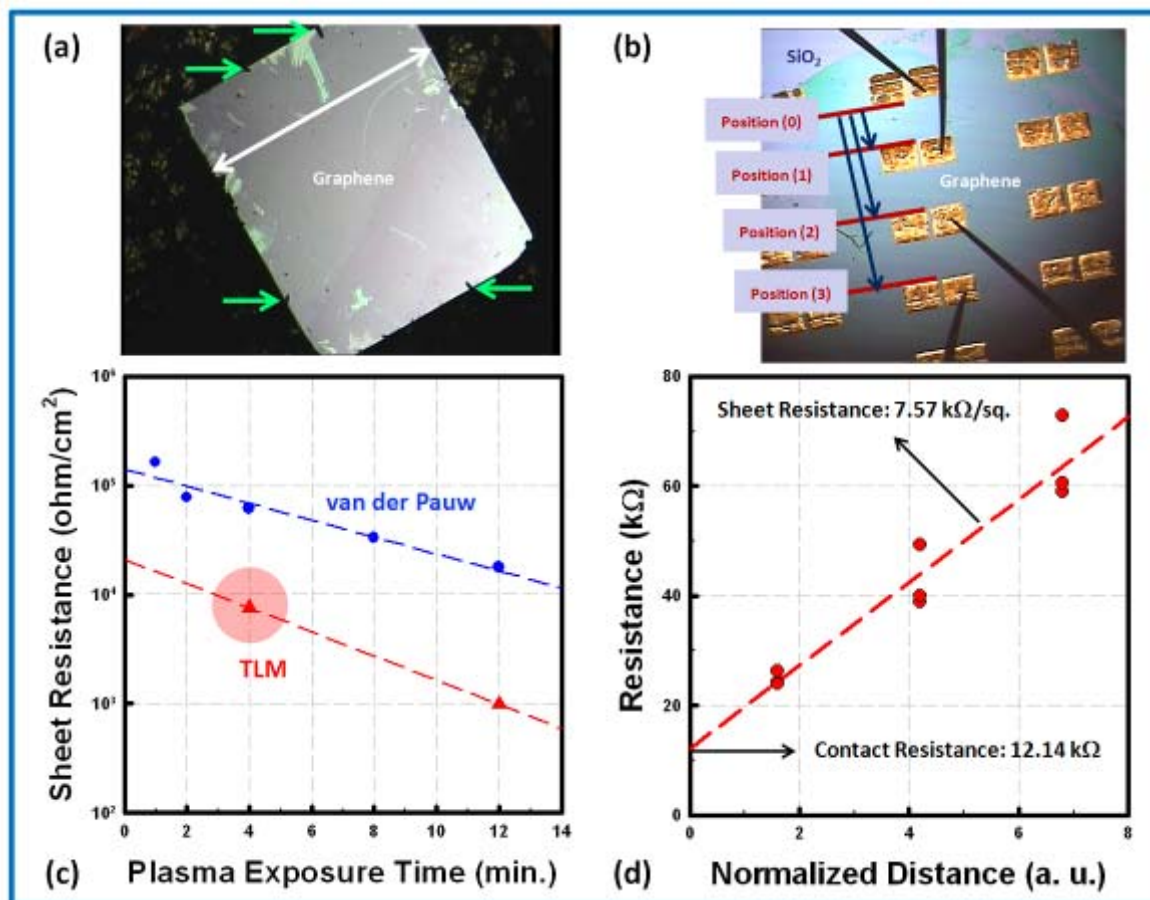
Figure 4.25. Electrical characterization of graphene films (a) Optical image of graphene in van der Pauw measurement. Graphene is covered on SiO$_2$ wafer with 0.5 cm scale width (white arrow), and green arrows indicate the 4 prove locations. (b) Optical image of graphene in TLM method. Array of (rectangular shape) silver electrode with a dimension of 1.00 mm x 0.75 mm is printed on graphene with a 1.2 mm pitch. (c) Sheet resistance depends on plasma exposure time from 1 to 12 minutes, measured by (blue color) van der Pauw and (red color) TLM method. Dotted lines for each method represent the linear dependency. (d) TLM measurement on graphene samples exposed by plasma for 4 minutes corresponds to the point of light red circle in (c). Along the normalized distance (distance between probes / width of contact pad perpendicular to the measuring direction), resistance can be measured between two electrodes. Sheet resistance can be extracted from the slope of graph, 7.57 kΩ/sq. and contact resistance can be recorded from the point of contact in y axis, 12.14kΩ.

4.4. Growth directly on insulating substrate

After etching out the nickel film (for transfer of graphene layer by floating method), we find a varying contrast on the surface of the silicon oxide wafer immersed into liquid. As we measure SEM and Raman on these samples, we surprisingly find that there is also a graphene layer. To surely confirm this layer, where it

comes from, new procedures are required.

4.4.1. Graphene Growth directly on Insulating substrates

Following our hypothesis[53], two graphene layers exist. One is on Ni surface, and the other is at interface between Ni and SiO_2. During transfer process, they could easily interact by van der Waals force, so that the film observed at the end on the SiO_2 would actually have formed on the top surface. Thus we need to first eliminate the carbon-related materials on Ni surface.

We simply apply strong water plasma with higher power and longer time, compare to mild plasma conditions gas mix, pressure, plasma power, time?. Effect of strong water plasma is confirmed by Raman, as shown in Figure 4.26. All the peaks, related to carbon signals, have disappeared. During the 10 minutes process, substrate temperature is slightly increased from R.T. to 175 ^{o}C.
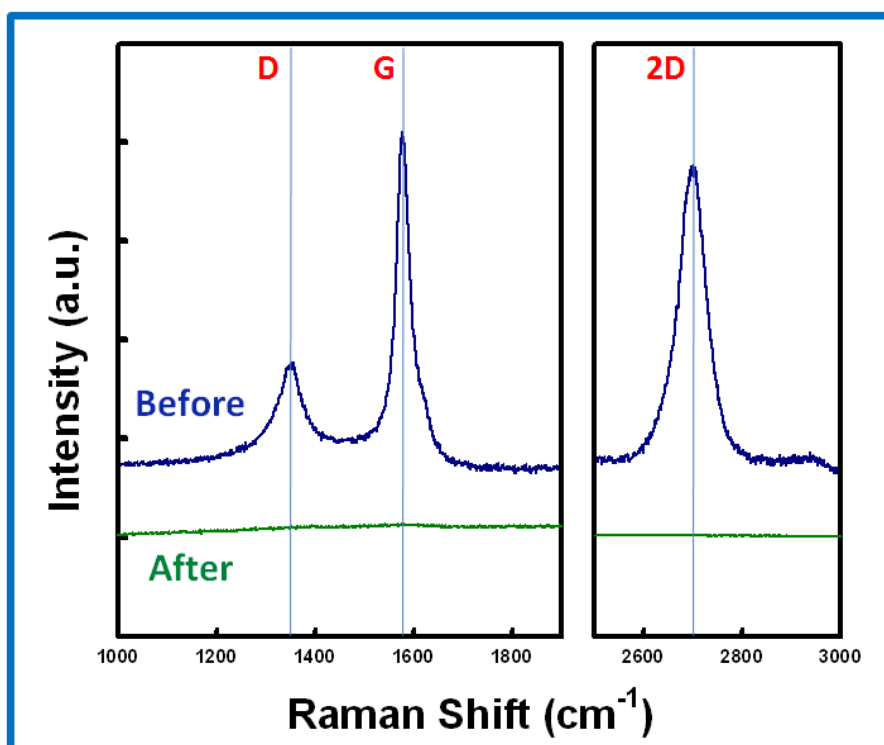
Figure 4.26. Effect of strong water plasma exposure for removal of carbon on Ni surface. Clear disappearance of D, G, and 2D peaks, which are representative of graphene, is observed by Raman measurement.

4.4.2. Plasma exposure time

Now, we applied this strong water vapor plasma to previous series of samples, in Figure 4.27. The time,

marked in figure captions, means process plasma by a mixture of methane and hydrogen. And annealing process at high temperature has been followed (900 °C for 18 minutes, and rapidly cooled down under vacuum, see more details in section 4.2.5.). Here, the development of graphite particles is highlighted as height difference is getting larger.
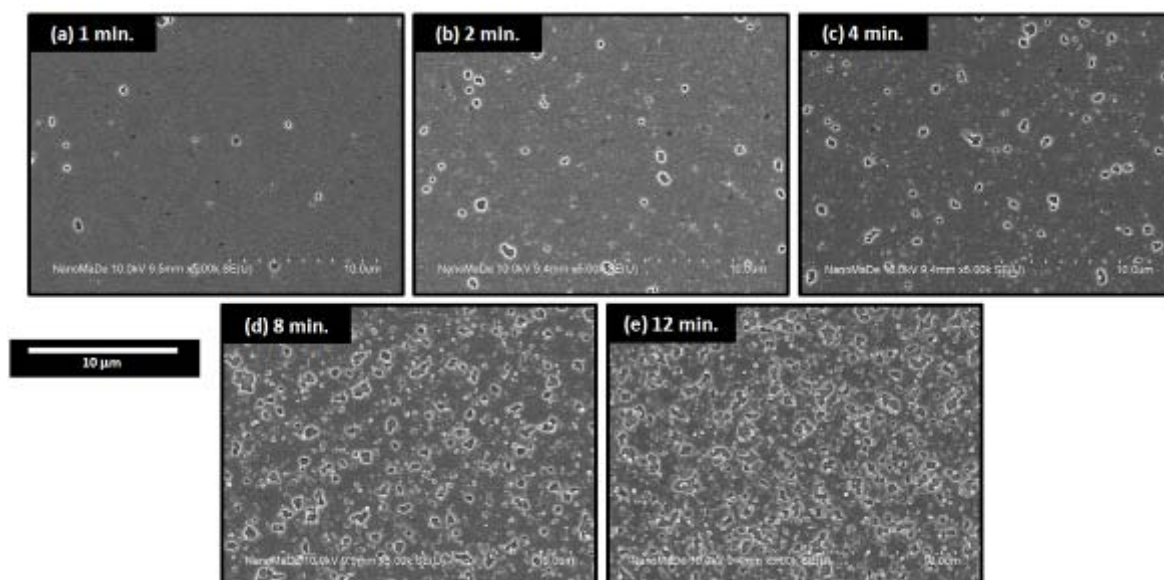
Figure 4.27. Scanning electron microscope images of top nickel surface? after strong water vapor plasma exposure and annealing. Those samples are prepared graphene with plasma exposure time by a mixture of methane and hydrogen for (a) 1 min., (b) 2 min., (c) 4 min., (d) 8 min., and (e) 12 min. All images are taken at same conditions.

Then, finally we etched away remained Ni using commercial etchant. And another set of SEM is taken as follows.
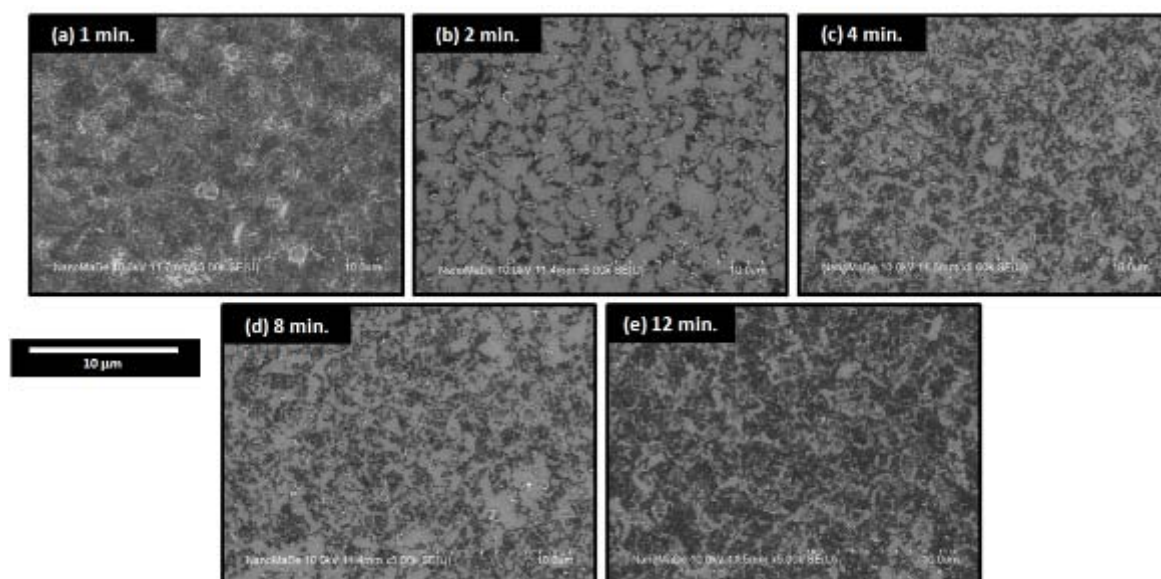
Figure 4.28. Demonstration of interfacial graphene with plasma exposure time. (a) 1 min., (b) 2 min., (c) 4 min., (d) 8 min., and (e) 12 min. All images are taken in the same conditions.

4.4.3. Effect of Annealing process

Figure 4.29. shows the Raman spectra of the graphene layers at each step ("AP" = After PECVD process, "AA" = After annealing process) and at each position ("TLG" = Top layer graphene on nickel surface, "IG" = Interfacial graphene after sequential etching of TLG, and nickel.) with a comparison of two nickel thicknesses. Each Raman spectrum is normalized by the maximum intensity of G peak.

In case of TLG, we find significant suppression of D peak by annealing process at high temperature independent of Ni thickness. Thinner nickel with 50 nm is only exposed to carbon-containing plasma for 4 minutes, due to relatively low potential to digest incoming carbon. We analyze the integrated intensity ratio of G peak compare to D peak, I_G/I_D. The I_G/I_D is significantly increased from 0.81 to 3.50 and from 0.84 to 5.33, for 200 nm and for 50 nm nickel layer, respectively. I can hardly believe this. I would like to see those samples and redo the Raman.

P. Jacobson et al., performed the investigation of structural evolution of graphene on Ni(111) as a function of growth temperature by scanning tunneling microscopy (STM)[51]. Low temperature (400~500 °C) growth results in a continuous but defective film with small ordered graphene domains and disordered domains composed of Stone-Wales (SW)-like defects. As the growth temperature is increased, the disordered domains shrink leaving small clusters of defects alongside epitaxially matched graphene. Following their density functional theory (DFT) calculations, the crucial role of the metallic support for the healing of SW defects, as the interaction with the substrate leads to a

stabilization of the reaction intermediate. The defect concentration in graphene is strongly governed by the effect of the graphene-substrate interaction on the temperature dependence.

S. Karoui also pointed out that an isolated graphene sheet can anneal a large number of defects in temperature range of 1000~2500 K suggesting that their healings are thermally activated[54]. Especially, in the presence of a nickel substrate, the perfect graphene layer can be obtained. The nickel-carbon chemical bonds keep breaking and reforming around defected carbon zones, providing a direct interaction, necessary for healing. Thus, the action of Ni atoms is found to play a key role in the reconstruction of the graphene sheet by annealing defects.

Here, we need to note that the origin of D band from our graphene. Our graphene is grown via PECVD at low temperature, and composed of nanocrystalline phase including numerous grain boundaries. These structural defects are re-crystallized by thermal energy in combination of Ni. Maybe, but we first need to be sure that what we measure is not the development of graphite flakes but indeed the healing of graphene.

The atomic rearrangement at grain boundaries (GBs) is typified by the formation of Stone-Wales (SW) defects consisting of pentagon-heptagon pairs. Grain boundaries in graphene are major defects that influence electrical, optical, and thermal properties, thus, for a detailed investigation of GBs, a reliable production method is encouraged. For this purpose, nanocrystalline graphene growth based on PECVD would be quite useful.

Now we are going to focus on interfacial graphene which is of great interest toward transfer-free graphene development. We remark that the interfacial graphene is poorly dependent on annealing process. The I_G/I_D ratio of interfacial graphene is not changed a lot by annealing process, from 0.70 to 0.90 for 200 nm nickel and from 0.84 to 1.31 for 50 nm nickel, respectively.

The interfacial graphene is not fully continuous, as we can see in Figure 4.28 (above SEM image), thus basically intense D band appears. Due to the fact that surface of interfacial graphene is covered by Ni (not air as in the case of top layer graphene), the healing effect (or re-arrangement) by high-temperature annealing might be diminished.

The quality of graphene by PECVD does not appear to depend on nickel thickness, carbon exposure time, or growing position (see red line in Figure 4.29.). This may mean, again, that our growth conditions are quite extreme regarding methane concentration, as we showed above, and maybe other parameters, .
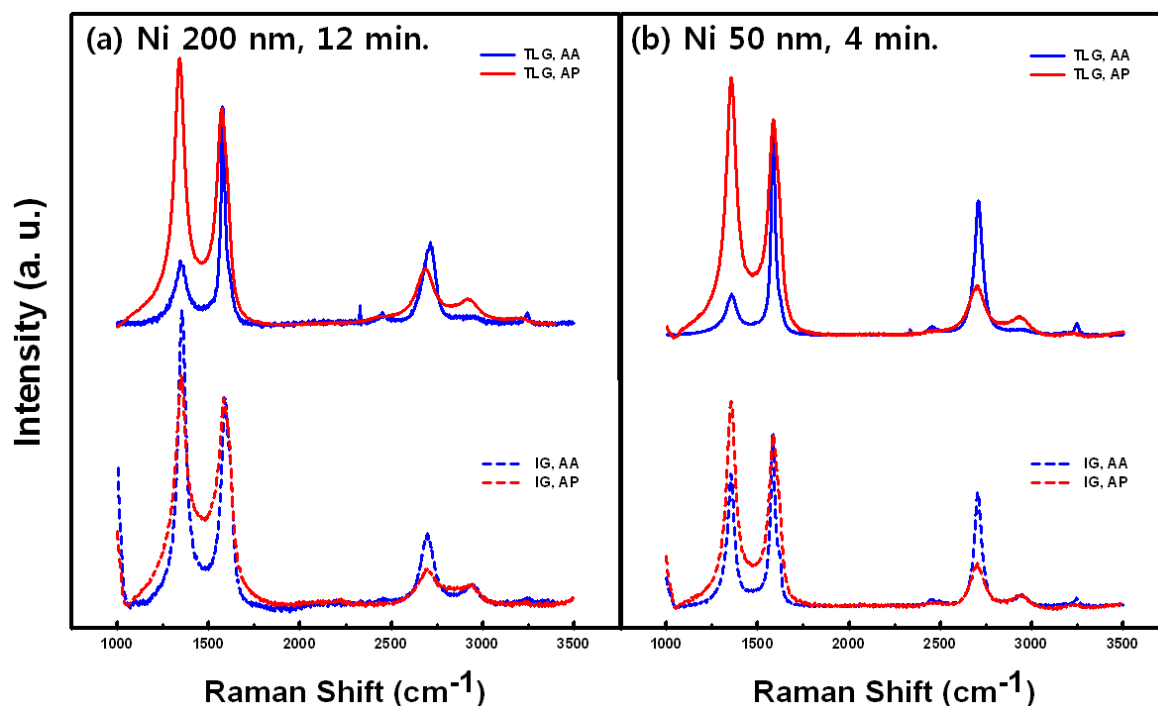
Figure 4.29. Direct comparison of the quality of graphene layers at each step and at each position.

In this section, we confirmed the healing effect of high-temperature annealing supported by Ni. Such an effect would be influenced by surrounding environment, such as type of catalysts, crystallographic orientation of each grain, type of gases, and temperature.

4.4.5. Transmission electron microscopy (TEM)

This section is devoted to clearly confirm (i) formation of interfacial graphene, and (ii) demonstration of nanocrystalline graphene, together.

Figure 4.34 shows TEM observations of samples at different stages of our process. Interfacial graphene is found to be present after PE-CVD exposure as well as after annealing. The graphene films appear continuous over areas as large as several tens of nm and, quite surprisingly, more so before the additional annealing step. Plan-views of the top layer films transferred on TEM amorphous carbon holey grids, indicate that the films consist of two phases: (1) a continuous background, and (2) bulky graphite blocks. Annealing has a visible effect on the latter: numerous and with nanometer size before annealing, they are larger but fewer after annealing. Moreover, their structure consists in pillars or onions, with (002) planes parallel to the beam before annealing (002 diffraction spots visible in Figure 4.34.(b2)), while they are flat with (002) planes in the substrate plane after annealing (no 002 diffraction spots visible in Figure 4.34.(d2)). On the other hand, the graphene films exhibit similar contrasts before and after annealing (but appear more sensitive to the electron beam before

116

annealing). The selected area electron diffraction patterns (Figure 4.34 (b1) and (d1)) show no obvious effect of the annealing on the structure of that background graphene: it appears in the two cases to consist of nano-crystalline grains, with random orientations in the plane. The line width indicates a coherence length smaller than 4 nm, which gives an order of magnitude of the size of the nano-grains. The absence of the 002 and 004 reflections confirm that the graphene crystallites are all oriented in the plane, as shown by the cross-sectional views.
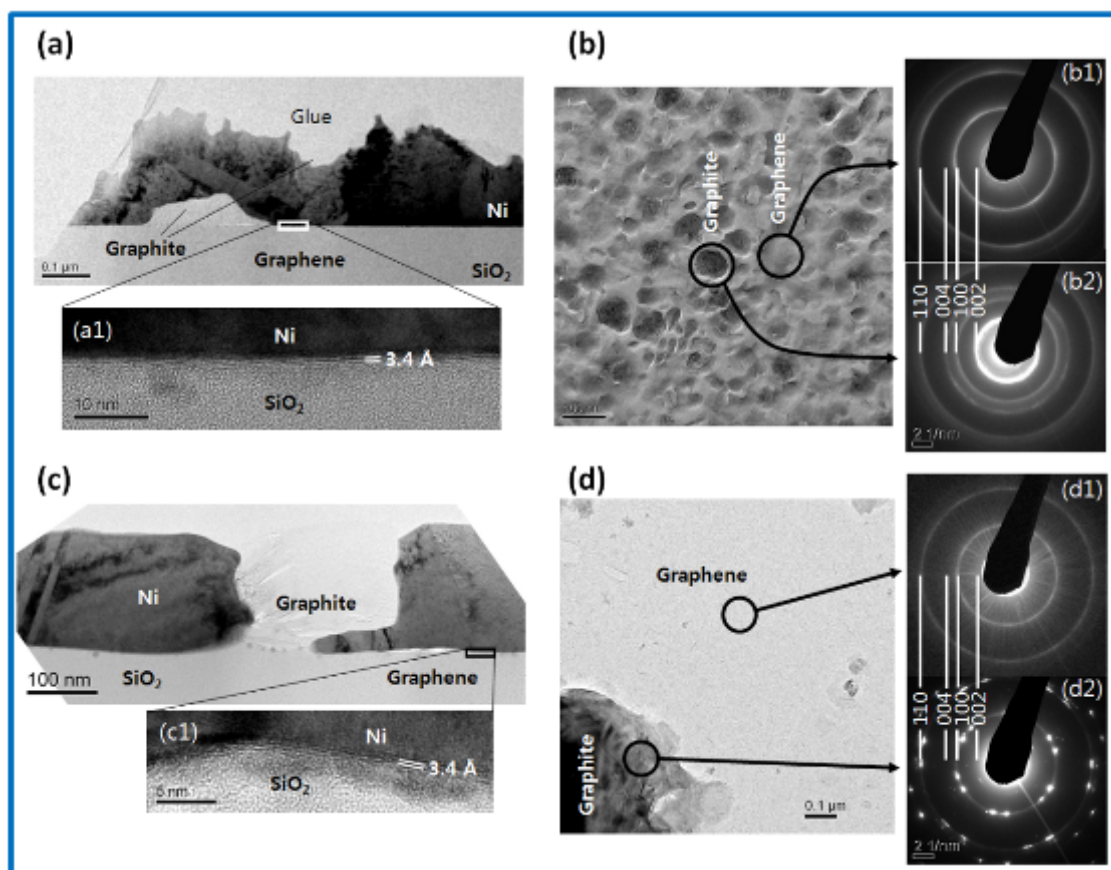
Figure 4.44. TEM images of the samples after growth by PE-CVD at 450 °C for 12 min (a,b), and after an additional annealing treatment in vacuum at 900 °C for 18 min (c,d). (a, c) Cross-sections where graphite blocks can be seen, together with interfacial graphene in the two cases. The latter (a1, c1) appears continuous over several tens of nm, and more so before annealing. (b, d) plan views obtained after Ni etching, and depositing the remaining layer on a TEM holey-carbon grid. Images recorded in holey regions (no contribution of amorphous carbon). The diffraction patterns (b1 and d1) indicate that the background consists of nano-crystalline graphene, with random orientation of the nano-grains in the plane. Note the absence of 002 and 004 reflections indicating a good alignment of the graphene layers in the plane. The graphite blocks are small pillars or onions, with (002) planes parallel to the beam before annealing (b2), while they are flat with no (002) planes visible after annealing (d2).

4.4.6. Toward Humidity Sensing

This section illustrates our efforts toward realizing the practical potential of PECVD process for graphene growth. We show here that interfacial graphene can be grown on glass substrate, and that a humidity sensing platform can be developed on it without transfer-process.

Standard PECVD process is performed for 12 minutes, as usual, then strong water vapor plasma is applied to chemically etch away carbon-related materials from Ni surface. Figure 4.45. shows clearly how efficiently this process can be adopted for any substrate, from SiO_2 to glass. Insets shows SEM images (blue outline, left) before and (red outline, right) after H_2O plasma exposure. The particles obtained after graphene growth, disappear after water vapor plasma as we can see in right inset. Note that H_2O plasma process is sensitive to sample contact with cathode, atmosphere inside of chamber in terms of contaminations. If the contact between sample and cathode is fairly good, we see a highly glowingsample surface in plasma process, compared to the cathode surface. This means that reactive ions/electrons are focused on sample surface with high concentrations. When the chamber is not properly cleaned, H_2O plasma is unstable.
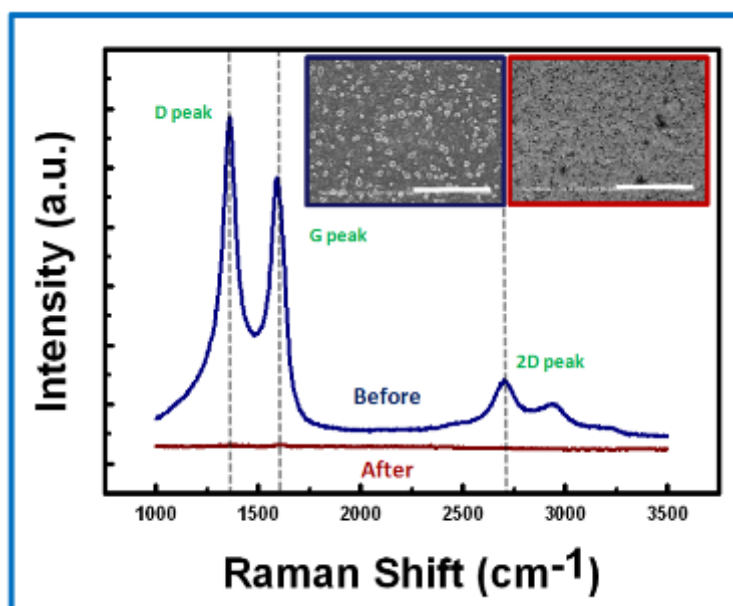
Figure 4.45. Etching of top-surface graphene by strong water-vapor plasma. Raman spectra before (a, in blue) and after (b, in red) plasma exposure. Insets show SEM images of nickel before and after plasma treatment (Scale bar is 5 μm).

The TEM sample was prepared by transferring onto a gold TEM grid a part of the film that was floating in the Ni-etchant. The film appears to be made of regions of ca. 200 nm in diameter (Figure 4.46.(a)) bordered by bent areas (Figure 4.46.(b)), where the number of graphene layers appears to be 10 to 30 (Figure 4.46.b), which is more than the average number deduced from transmittance measurements (see below). This local

bending of the flakes causes the thickness to vary with a ~200 nm characteristic distance. Such a wavelength remaining below the visible range, this roughness is not optically visible. Electron diffraction (Figure 4.46.(c)) indicates that the film is perfectly crystalline, but with nanometric grains: applying the Scherrer formula to the 100 line width gives a size of coherently diffracting areas (~grain size) of ~3 nm (see Chapter II. Characterization of Graphene).
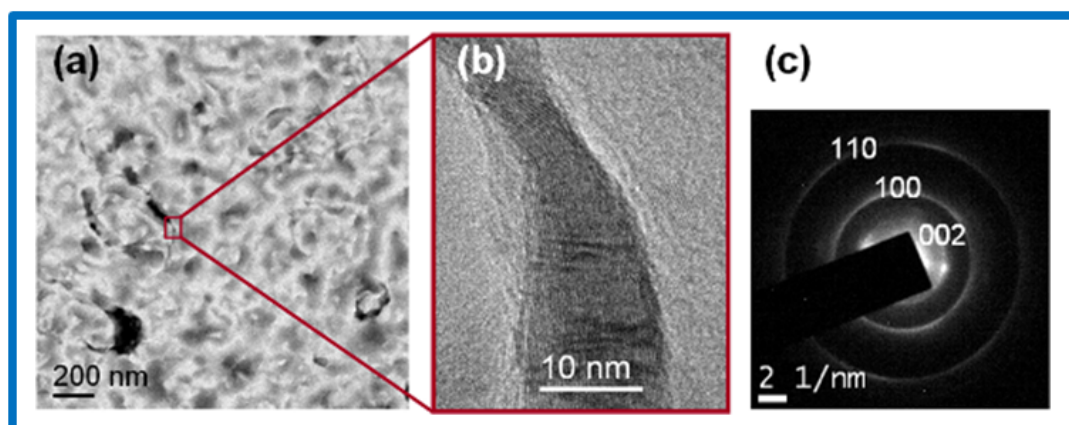
Figure 4.46. Plan-view TEM of a graphene film grown at 450 °C with the 12 minutes plasma treatment. (a) Low-magnification image. (b) High-resolution image showing a bent part exhibiting the stack of graphene layers the film is made of. (c) Electron diffraction pattern recorded over an area of 0.2 μm in diameter. The 100 and 110 rings are characteristic of nanocrystalline graphene; the 002 dots come from bent parts such as that in (b).

Combined optical and Raman observations (Figure 4.47.) give a clear evidence of the formation of an interfacial graphene layer. Except for a fold that probably formed during the drying process (green arrow in (Figure 4.37.(a)), we observe that this graphene layer (red arrow in Figure 4.47.(a)) is uniformly covering the glass substrate (the blue arrow indicates glass substrate in figure 5.xx.a). Figure 4.47.(b) exhibits a Raman spectrum typical of the layer, acquired over an area of 1 μm^2. The G band (Figure 4.47.(b)), originating from in-plane vibrations of sp^2 carbon bonds, is observed at 1597 cm^{-1}. The defect signal is relatively important (D in Figure 4(b), I_D/I_G = 1.18), while the 2D band remains weak (I_G/I_{2D} = 3.54). The D band is most probably due to the high density of distorted bonds associated with the boundaries between the nano-grains. The weakness of the 2D peak might in addition be related to the thickness of our samples, which may be locally significant.
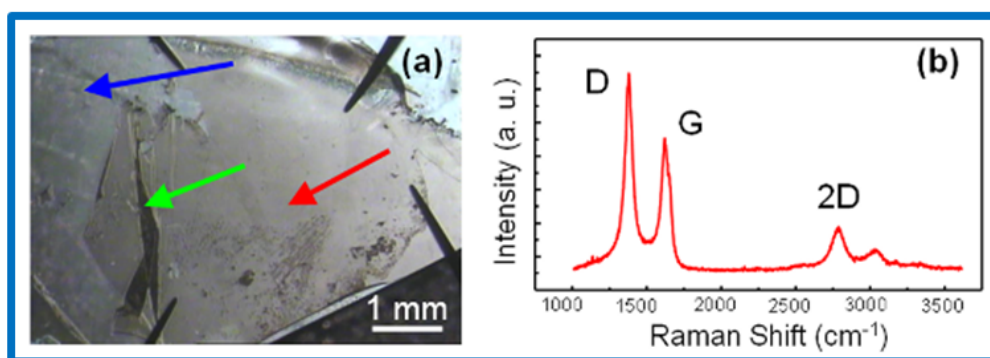
Figure 4.47. (a) Optical image of the interfacial FLG film, after water plasma exposure and subsequent nickel etching. The red arrow indicates graphene, the blue one, glass, and the green one, a folded area in the FLG film. (b) Raman spectrum typical of the film.

The optical transmittance of the FLG films was measured in the visible and near infra-red range (Figure 4.48) is found to be respectively 78.4 % and 67.3 % at 650 nm, for plasma exposure times of 6 and 12 minutes. The dependence of the transmittance on wavelength remains small, which is quite remarkable given the relative simplicity of the process (low-temperature synthesis and transfer-free fabrication). Although the nanocrystalline structure of our material differs from that of true graphene, one may get an order of magnitude of the number of layers by using the 2.3 % decrease of transmittance by layer. We thus estimate the average number of layers to respectively ~9 and ~15 for the 6 minutes and 12 minutes deposits. Thus, the number of layers measured by TEM (Figure 4.46.(b)) would be characteristic of the bent parts; the flat parts would be thinner.
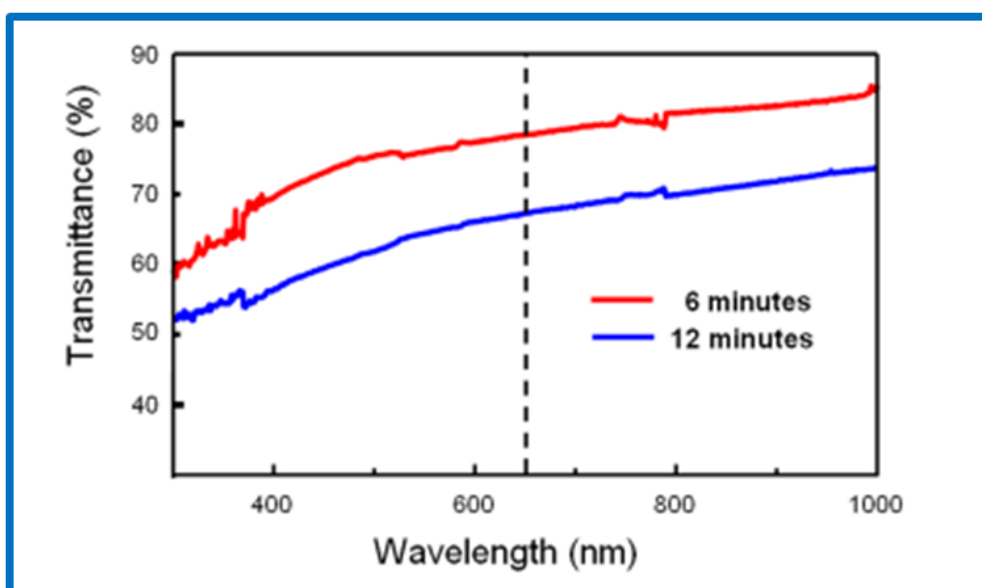
Figure 4.48. Optical transmittance in the 300 to 1000-nm range, for two plasma exposure times. The vertical dotted line indicates the 650-nm wavelength.

As the graphite sheets are grown directly on an insulating substrate, they do not need to be transferred before measuring the sheet resistance. We directly ink-jet printed series of four 500 µm x 1000 µm parallel rectangular electrodes separated by 500 µm using INKTEC TEC-IJ-010 silver ink in a Dimatix DMP-2800 materials printer (Figure 4.49.(a)). We measured a sheet resistance as low as 500 Ω/sq. on a 12-minute sample. Sheet resistances vary significantly depending on the location on the samples, which is attributed to inhomogeneous thickness. Quite interestingly, the sample exposed only 6 minutes to the growth plasma, which presents 78.4 % transmittance at 650 nm (Figure 4.48.), exhibits an average sheet resistance of 5±1.2 kΩ/sq.

Sensitivity of materials to gas is often related to defects site density[55], which makes a priori our material an outstanding candidate for gas sensing. We characterized two 12-minute sheets under increasing relative humidity (RH). For both devices, the sensitivity to humidity is clear, especially above 40 % RH. For the best conductive material, the sheet resistance increases by almost 700 Ω from 3.3 to 4.0 kΩ/sq. (+ 20 %) between 5 % and 63 % relative humidity (Figure 4.49.b); for the other sheet, the resistance increases by 3 kΩ from 45 to 48 kΩ/sq. (+7 %) between 4 % and 86 % RH. These variations appear large enough to be measured by discrete electronic components, thus paving the way toward actual graphene-based integrated humidity sensors.
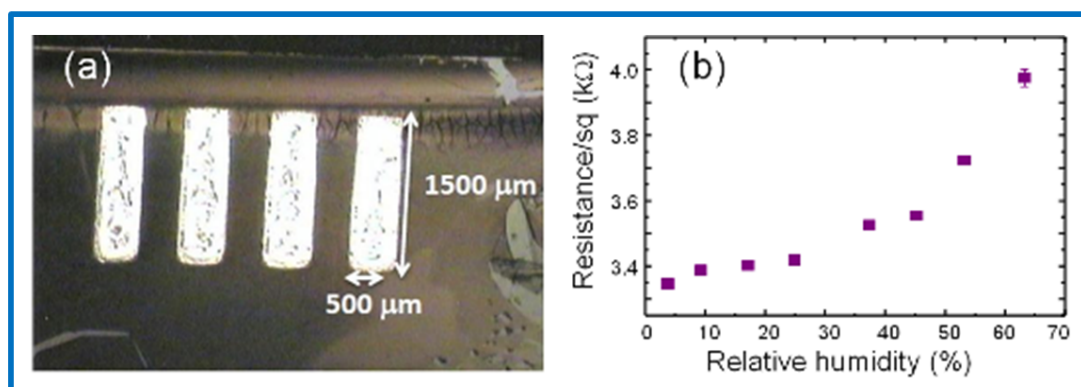
Figure 4.49. (a) The inkjet printed silver electrodes; (b) sheet resistance versus relative humidity for a 12-mn plasma exposure.

4.5. Conclusions

Currently, numerous methods investigated for high quality graphene growth over large area, are based on classical thermal-CVD technique. The realization of graphene in practical application is still far, however, due to the fact that this method needs: (i) time-consuming complex transfer process, and (ii) unfavorable high temperature at around 1000 °C. The graphene grown on transition metals should be transferred to insulating substrate by polymer-based technique. Mechanical stress and chemical residues leads to serious

structural/chemical damage on graphene, which reduce its optical/electrical properties. In addition to this, the high temperature process is not compatible with most of the current optoelectronic device fabrication.

Our research is devoted to opening up new growth technique, capable of solving above problems. Here, using a plasma-enhanced chemical vapor deposition process, we demonstrated the graphene formations (i) on metal surface and (ii) at interface with insulating substrate, especially at low temperature. Compared to simple thermal CVD process, the growth temperature is successfully lowered, thanks to reactive plasma phase. Especially, the latter case, the interfacial graphene, can be directly used for device fabrication without transfer process.

In our first experiment, we annealed the plasma-exposed samples at high temperature. We found that cooling condition (especially cooling rate) is much more important than annealing time. Fast cooling makes the carbon atoms freeze out inside of Ni layer, and only limited amount near Ni surface can be diffused out. This leads to rater uniform graphene precipitation. Additionally, it is worth to note that even sample holder is pulled cooling zone out, inner space is connected to heat zone and even quartz boat which carrying sample is heated. Thus, sample holder need to be equipped with cooling system and direct temperature measurement. Precise temperature cooling will allow to interpret by how do carbon diffusion is determined.

After annealing process, we identified a large amount of thick graphene flakes on Ni surface. Thus, we designed mild water vapor plasma treatment to minimize the amount of amorphous carbon. With only 2 minutes exposure in diffusive plasma (plasma comes itself by diffusion through grid without extraction voltage and current), we can avoid surface damage by relatively strong plasma, as well as successfully minimize the amorphous carbon. This makes much lower density of thick flakes.

The ratio of gas mixture, between carbon feeding gas and etching agent, is of great importance in carbon-based material synthesis. Our working condition, means gas composition, is quite different with others, in general. We need to point out that other groups are introducing only few tens of ppm (parts per million) of carbon feeding gas compare to hydrogen and argon gas, or even less. Thus, our working conditions are using extremely high percentage of CH_4 compare to hydrogen. We varied a gas ratio ($10 : 50 \sim 80 : 50$ of $CH_4 : H_2$), and surface morphologies as well as crystallite size are analyzed by SEM and Raman spectroscopy, respectively. It appeared that Ni surface is getting covered by amorphous carbon, but the crystallize size (determined by Raman) is not affected a lot. This could be explained somehow as we are using high percent of methane comparing to hydrogen, its growth process with such a range of methane composition is under saturation regime.

In fact, we try to lower growth temperature, which compatible current industry, thus, the effect of temperature is not investigated. What we seriously have a look is the time-dependent evolution of graphene

growth. After PECVD process for $1 \sim 12$ minutes, a mild water vapor plasma and an annealing process at high temperature followed. Here, we found linear increase of graphitic flakes and roughly increase of number of graphene layers. Furthermore, the interfacial graphene which located in-between Ni and SiO_2 was found. There was a time-dependant evolution of coverage, but underlying mechanisms is complicated. Due to the fact that high reactive plasma exposure with high amount of methane, carbon atoms can diffuse to the interface, especially through Ni graphene boundaries. From the cross-sectional TEM, we found that graphitic flaks can be formed on both side, near surface and near interface. It assumed that some of vacancies, defects, and structural voids at interface could lead to nucleation and growing of graphitic flakes. Interfacial graphene has a great potential over transfer process, but owing to complicated underlying mechanism, it suffers from the lack of possible parameter-dependence.

We successfully grow the continuous & interfacial graphene layer on glass, especially at low temperature. To the best of our knowledge, this is first time that a large continuous graphene layer is obtained directly on insulating substrate at 450°C. After nickel etching, we are able to measure the optical transmittance of the layers without any transfer. We also measured their sheet resistance directly and after ink-jet printing of electrical contacts: it is locally as low as 500 Ω/sq. The interfacial graphene contains relatively high amount of defects, but, in other words, our graphene is highly activated for sensing system. Those defects, mainly grain boundaries originated from nanocrystalline, can be utilized. Finally, we developed a humidity sensor based on highly activated & directly grown graphene on insulating substrate. It has the possibilities to expand on various substrates and to control the sensitivity depends on degree of crystallinity. These results herald the prototyping of actual low-cost graphene sensors for civil and urban engineering applications.

Reference

1.   Obraztsov, A. N., Obraztsova, E. A., Tyurnina, A. V. and Zolotukhin, A. A. Chemical vapor deposition of thin graphite films of nanometer thickness. *Carbon* **45**, 2017-2021 (2007)

2.   Hiramatsu, M., Shiji, K., Amano, H. and Hori, M. Fabrication of vertically aligned carbon nanowalls using capacitively coupled plasma-enhanced chemical vapor deposition assisted by hydrogen radical injection. *Applied Physics Letters* **84**, 4708-4710 (2004)

3.   Wu, Y., Qiao, P., Chong, T. and Shen, Z. Carbon Nanowalls Grown by Microwave Plasma Enhanced Chemical Vapor Deposition. *Advanced Materials* **14**, 64-67 (2002)

4.   Malesevic, A., Vizireanu, S., Kemps, R., Vanhulsel, A., Haesendonck, C. V. and Dinescu, G. Combined growth of carbon nanotubes and carbon nanowalls by plasma-enhanced chemical vapor deposition. *Carbon* **45**, 2932-2937 (2007)

5.   Kurita, S., Yoshimura, A., Kawamoto, H., Uchida, T., Kojima, K., Tachibana, M., Molina-Morales, P. and Nakai, H. Raman spectra of carbon nanowalls grown by plasma-enhanced chemical vapor deposition. *Journal of Applied Physics* **97**, 104320-5 (2005)

6.   Shiji, K., Hiramatsu, M., Enomoto, A., Nakamura, M., Amano, H. and Hori, M. Vertical growth of carbon nanowalls using rf plasma-enhanced chemical vapor deposition. *Diamond and Related Materials* **14**, 831-834 (2005)

7.   Banerjee, D., Mukherjee, S. and Chattopadhyay, K. K. Synthesis of amorphous carbon nanowalls by DC-PECVD on different substrates and study of its field emission properties. *Applied Surface Science* **257**, 3717-3722 (2010)

8.   Krivchenko, V. A., Dvorkin, V. V., Dzbanovsky, N. N., Timofeyev, M. A., Stepanov, A. S., Rakhimov, A. T., Suetin, N. V., Vilkov, O. Y. and Yashina, L. V. Evolution of carbon film structure during its catalyst-free growth in the plasma of direct current glow discharge. *Carbon* **50**, 1477-1487 (2012)

9.   Höltig, M. http://www.chemie.uni-hamburg.de/pc/mews/research/nanotubes_print.html.

10.   Cojocaru, C. S., Senger, A. and Normand, F. L. A nucleation and growth model of vertically-oriented carbon nanofibers or nanotubes by plasma-enhanced catalytic chemical vapor deposition. *Journal of nanoscience and nanotechnology* **6**, 1331 (2006)

11.   Thiele, S., Reina, A., Healey, P., Kedzierski, J., Wyatt, P., Hsu, P.-L., Keast, C., Schaefer, J. and Jing, K. Engineering polycrystalline Ni films to improve thickness uniformity of the chemical-vapor-deposition-grown graphene films. *Nanotechnology* **21**, 015601 (2010)

12.   Chen, C.-H., Arnett, D. and Liu, D. Plasma cleaning method for removing residues in a plasma treatment chamber. *United States Patent*, Patent number: 5356478 (1994)

13.   O'Kane, D. F. and Mittal, K. L. Plasma cleaning of metal surfaces. *Journal of Vacuum Science and Technology* **11**, 567-569 (1974)

14.   Oneill, J. A. and Singh, J. Role of the chamber wall in low‐pressure high‐density etching plasmas. *Journal of Applied Physics* **77**, 497-504 (1995)

15. Korzec, D., Rapp, J., Theirich, D. and Engemann, J. Cleaning of metal parts in oxygen radio frequency plasma: Process study. *Journal of Vacuum Science & Technology A: Vacuum, Surfaces, and Films* **12**, 369-378 (1994)

16. Fumagalli, F., Kylián, O., Amato, L., Hanuš, J., and Rossi, F. Low-pressure water vapour plasma treatment of surfaces for biomolecules decontamination. *Journal of Physics D: Applied Physics* **45**, 135203 (2012)

17. Suzuki, T., Sawado, Y. and Fujii, Y. Characterization of oxide films generated on stainless steel in water vapor and oxygen plasmas. *Surface and Coatings Technology* **200**, 284-287 (2005)

18. Ren, Z. F., Huang, Z. P., Xu, J. W., Wang, J. H., Bush, P., Siegal, M. P. and Provencio, P. N. Synthesis of Large Arrays of Well-Aligned Carbon Nanotubes on Glass. *Science* **282**, 1105-1107 (1998)

19. Jian, S.-R. Effects of H2 plasma pretreated Ni catalysts on the growth of carbon nanotubes. *Materials Chemistry and Physics* **115**, 740-743 (2009)

20. Choi, W. S., Choi, S.-H., Hong, B., Lim, D.-G., Yang, K.-J. and Lee, J.-H. Effect of hydrogen plasma pretreatment on growth of carbon nanotubes by MPECVD. *Materials Science and Engineering: C* **26**, 1211-1214 (2006)

21. Jian, S.-R., Chen, Y.-T., Wang, C.-F., Wen, H.-C., Chiu, W.-M. and Yang, C.-S. The Influences of H_2 Plasma Pretreatment on the Growth of Vertically Aligned Carbon Nanotubes by Microwave Plasma Chemical Vapor Deposition. *Nanoscale Research Letters* **3**, 230-235 (2008)

22. Luo, Y.-R. Comprehensive Handbook of Chemical Bond Energies. *CRC Press* (2007)

23. Chae, S. J., Güneş, F., Kim, K. K., Kim, E. S., Han, G. H., Kim, S. M., Shin, H.-J., Yoon, S.-M., Choi, J.-Y., Park, M. H., Yang, C. W., Pribat, D. and Lee, Y. H. Synthesis of Large-Area Graphene Layers on Poly-Nickel Substrate by Chemical Vapor Deposition: Wrinkle Formation. *Advanced Materials* **21**, 2328-2333 (2009)

24. Zhang, B., Lee, W. H., Piner, R., Kholmanov, I., Wu, Y., Li, H., Ji, H. and Ruoff, R. S. Low-Temperature Chemical Vapor Deposition Growth of Graphene from Toluene on Electropolished Copper Foils. *ACS Nano* **6**, 2471-2476 (2012)

25. Yu, Q., Lian, J., Siriponglert, S., Li, H., Chen, Y. P. and Pei, S.-S. Graphene segregated on Ni surfaces and transferred to insulators. *Applied Physics Letters* **93**, 113103-3 (2008)

26. Miyata, Y., Kamon, K., Ohashi, K., Kitaura, R., Yoshimura, M. and Shinohara, H. A simple alcohol-chemical vapor deposition synthesis of single-layer graphenes using flash cooling. *Applied Physics Letters* **96**, 263105-3 (2010)

27. Reina, A., Thiele, S., Jia, X., Bhaviripudi, S., Dresselhaus, M., Schaefer, J. and Kong, J. Growth of large-area single- and Bi-layer graphene by controlled carbon precipitation on polycrystalline Ni surfaces. *Nano Research* **2**, 509-516 (2009)

28. Chen, S., Cai, W., Piner, R. D., Suk, J. W., Wu, Y., Ren, Y., Kang, J. and Ruoff, R. S. Synthesis and Characterization of Large-Area Graphene and Graphite Films on Commercial Cu - Ni Alloy Foils. *Nano Letters* **11**, 3519-3525 (2011)

29. Qi, Y., Eskelsen, J. R., Mazur, U. and Hipps, K. W. Fabrication of Graphene with CuO Islands by Chemical Vapor Deposition. *Langmuir* **28**, 3489-3493 (2012)

30. Ni, Z., Wang, Y., Yu, T. and Shen, Z. ChemInform Abstract: Raman Spectroscopy and Imaging of Graphene. *ChemInform* **41**, no-no (2010)

31. Reina, A., Son, H., Jiao, L., Fan, B., Dresselhaus, M. S., Liu, Z. and Kong, J. Transferring and Identification of Single- and Few-Layer Graphene on Arbitrary Substrates. *The Journal of Physical Chemistry C* **112**, 17741-17744 (2008)

32. Reina, A., Jia, X., Ho, J., Nezich, D., Son, H., Bulovic, V., Dresselhaus, M. S. and Kong, J. Large Area, Few-Layer Graphene Films on Arbitrary Substrates by Chemical Vapor Deposition. *Nano Letters* **9**, 30-35 (2008)

33. Liang, X., Sperling, B. A., Calizo, I., Cheng, G., Hacker, C. A., Zhang, Q., Obeng, Y., Yan, K., Peng, H., Li, Q., Zhu, X., Yuan, H., Hight Walker, A. R., Liu, Z., Peng, L.-m. and Richter, C. A. Toward Clean and Crackless Transfer of Graphene. *ACS Nano* **5**, 9144-9153 (2011)

34. Pirkle, A., Chan, J., Venugopal, A., Hinojos, D., Magnuson, C. W., McDonnell, S., Colombo, L., Vogel, E. M., Ruoff, R. S. and Wallace, R. M. The effect of chemical residues on the physical and electrical properties of chemical vapor deposited graphene transferred to SiO[sub 2]. *Applied Physics Letters* **99**, 122108-3 (2011)

35. Lin, Y.-C., Lu, C.-C., Yeh, C.-H., Jin, C., Suenaga, K. and Chiu, P.-W. Graphene Annealing: How Clean Can It Be? *Nano Letters* **12**, 414-419 (2012)

36. Alemán, B. n., Regan, W., Aloni, S., Altoe, V., Alem, N., Girit, C. l., Geng, B., Maserati, L., Crommie, M., Wang, F. and Zettl, A. Transfer-Free Batch Fabrication of Large-Area Suspended Graphene Membranes. *ACS Nano* **4**, 4762-4768 (2010)

37. Kang, J., Hwang, S., Kim, J. H., Kim, M. H., Ryu, J., Seo, S. J., Hong, B. H., Kim, M. K. and Choi, J.-B. Efficient Transfer of Large-Area Graphene Films onto Rigid Substrates by Hot Pressing. *ACS Nano* **6**, 5360-5365 (2012)

38. Lander, J. J., Kern, H. E. and Beach, A. L. Solubility and Diffusion Coefficient of Carbon in Nickel: Reaction Rates of Nickel-Carbon Alloys with Barium Oxide. *Journal of Applied Physics* **23**, 1305-1309 (1952)

39. Hao, Y., Wang, Y., Wang, L., Ni, Z., Wang, Z., Wang, R., Koo, C. K., Shen, Z. and Thong, J. T. L. Probing Layer Number and Stacking Order of Few-Layer Graphene by Raman Spectroscopy. *Small* **6**, 195-200 (2010)

40. Grüneis, A., Attaccalite, C., Wirtz, L., Shiozawa, H., Saito, R., Pichler, T. and Rubio, A. Tight-binding description of the quasiparticle dispersion of graphite and few-layer graphene. *Physical Review B* **78**, 205425 (2008)

41. Malard, L. M., Nilsson, J., Elias, D. C., Brant, J. C., Plentz, F., Alves, E. S., Castro Neto, A. H. and Pimenta, M. A. Probing the electronic structure of bilayer graphene by Raman scattering. *Physical Review B* **76**,

201401 (2007)

42.   Ni, Z. H., Yu, T., Luo, Z. Q., Wang, Y. Y., Liu, L., Wong, C. P., Miao, J., Huang, W. and Shen, Z. X. Probing Charged Impurities in Suspended Graphene Using Raman Spectroscopy. *ACS Nano* **3**, 569-574 (2009)

43.   Casiraghi, C., Pisana, S., Novoselov, K. S., Geim, A. K. and Ferrari, A. C. Raman fingerprint of charged impurities in graphene. *Applied Physics Letters* **91**, 233108 (2007)

44.   Ferrari, A. C., Meyer, J. C., Scardaci, V., Casiraghi, C., Lazzeri, M., Mauri, F., Piscanec, S., Jiang, D., Novoselov, K. S., Roth, S. and Geim, A. K. Raman Spectrum of Graphene and Graphene Layers. *Physical Review Letters* **97**, 187401 (2006)

45.   Ni, Z., Wang, Y., Yu, T. and Shen, Z. Raman spectroscopy and imaging of graphene. *Nano Research* **1**, 273-291 (2008)

46.   Gupta, A., Chen, G., Joshi, P., Tadigadapa, S. and Eklund. Raman Scattering from High-Frequency Phonons in Supported n-Graphene Layer Films. *Nano Letters* **6**, 2667-2673 (2006)

47.   Lee, C.S., Ryu, J.H., Lim, H.E., Min, K.Y., Jeong I.O., Manivannan, S., Jang, J., and Park, K.C. Electron Emission from Robust CNTs Grown by Resist-Assisted Patterning, J. Korean Phys. Soc. 53, 2735 (2008)

48.   Teo, K. B. K., Chhowalla, M., Amaratunga, G. A. J., Milne, W. I., Pirio, G., Legagneux, P., Wyczisk, F., Olivier, J. and Pribat, D. Characterization of plasma-enhanced chemical vapor deposition carbon nanotubes by Auger electron spectroscopy. *Journal of Vacuum Science & Technology B: Microelectronics and Nanometer Structures* **20**, 116-121 (2002)

49.   Li, X., Magnuson, C. W., Venugopal, A., Tromp, R. M., Hannon, J. B., Vogel, E. M., Colombo, L. and Ruoff, R. S. Large-Area Graphene Single Crystals Grown by Low-Pressure Chemical Vapor Deposition of Methane on Copper. *Journal of the American Chemical Society* **133**, 2816-2819 (2011)

50.   Yu, Q., Jauregui, L. A., Wu, W., Colby, R., Tian, J., Su, Z., Cao, H., Liu, Z., Pandey, D., Wei, D., Chung, T. F., Peng, P., Guisinger, N. P., Stach, E. A., Bao, J., Pei, S.-S. and Chen, Y. P. Control and characterization of individual grains and grain boundaries in graphene grown by chemical vapour deposition. *Nat Mater* **10**, 443-449 (2011)

51.   Jacobson, P., Stöger, B., Garhofer, A., Parkinson, G. S., Schmid, M., Caudillo, R., Mittendorfer, F., Redinger, J. and Diebold, U. Disorder and Defect Healing in Graphene on Ni(111). *The Journal of Physical Chemistry Letters* **3**, 136-139 (2012)

52.   Liu, L., Rim, K. T., Eom, D., Heinz, T. F. and Flynn, G. W. Direct Observation of Atomic Scale Graphitic Layer Growth. *Nano Letters* **8**, 1872-1878 (2008)

53.   Baraton, L., Cojocaru, C. S. and Pribat, D. Process for controlled growth of graphene films. International Patent 0805769-2008 (2008)

54.   Karoui, S., Amara, H., Bichara, C. and Ducastelle, F. o. Nickel-Assisted Healing of Defective Graphene. *ACS Nano* **4**, 6114-6120 (2010)

55.   Yong-Hui Zhang and Ya-Bin Chen and Kai-Ge Zhou and Cai-Hong Liu and Jing Zeng and Hao-Li Zhang and Yong, P. Improving gas sensing properties of graphene by introducing dopants and defects: a first-principles study. *Nanotechnology* **20**, 185504 (2009)

Outline

Chapter V. Ion Implantation

5.1. Introduction

Chemical vapour deposition (CVD) is one of the most promising techniques to grow large-area, high-quality graphene layers onto transition metals, which is favourable for current industrial aspects[1-4]. Despite the fact that numerous experimental works have been performed, we are still suffering from the lack of understanding on growth mechanisms. For further advance in graphene synthesis and realization of its potential to application fields, this should be elucidated by various growth techniques, multiple in-situ measurements, and ultra high resolution analysis tools. In this *Chapter V*, we will introduce a novel route for graphene synthesis that could bring fundamental insight on growth mechanisms.

Carbon atoms, needless to say, are necessary to synthesize graphene layers. In CVD technique, those carbons come from a vapour source, which can either be gas[1-4] or liquid[5-8]. Even though we put specific amount of carbon via MFC (Mass Flow Controller) valve in CVD chamber, actual carbon which react with metallic substrate and result in graphene growth would be influenced by plenty of factors, such as pressure[9-11], temperature[11], type of transition metals (carbon solubility/diffusivity and its thickness)[1] and its roughness[12]/crystallinity[13].

Because of the complexity due to a variety of influencing factors, understanding of graphene growth mechanism is still veiled. Our group, for the first time, has designed carbon ion implantation technique[14]; (i) to precisely control the amount of carbons inside of metals, (ii) to elucidate the graphene growth process, thanks to simplifying the process. Shortly speaking, carbon ion implantation allows a precise control in terms of carbon dose and implantation depth (energy), which permits in turn an accurate study of the precipitation processes. In the present *Chapter V*, we expose our systematic investigation of graphene growth processes based on the implantation of various doses followed by annealing process at high temperature.

5.1.1. Ion Implantation

At the beginning of the semiconductor industry back in the 1950s, ion implantation was among many processes identified and explored. Since then, ion implanters have developed to low- and medium-current implanters in the early 1970s and medium- and high-current machines at low energies in the 1980s. High-energy implanters are in growing demand recently. Conclusively, ion implantation is a robust technique, developed over the past ~40 years by the microelectronics industry[15, 16]. It is worth to note that ion implantation process is the most precise, reliable, and reproducible processing technique currently being used in commercial semiconductor chip fabrication[17].

129

The main advantage of ion implantation in graphene synthesis is that we can precisely control (i) the amount of carbon implanted, and (ii) the depth to be implanted. This means that we can implant carbon doses in desired depth corresponding exactly to 1 layer, 2 layers or even more of graphene. Through annealing process, we can find how carbon diffuses in Ni and precipitate at Ni surface.

Using TRIM (TRansport of Ions in Matter) simulation, we can estimate how deep and how much carbon is implanted from the carbon dose and implantation energy[18-20].

5.1.2. Metallic Substrate

The metallic substrate has a couple of roles in graphene synthesis. One is mechanical supporting layer for graphene, and the other is the catalytic effect to decompose hydrocarbon gases and to crystallize carbon atoms into graphene.

The catalytic growth of graphene has first appeared using Ni thin films[21], which were widely used in CNT synthesis. Ni has high carbon solubility as well as high carbon diffusivity[18, 22]. Thus, thermally decomposed carbon-containing species could be absorbed and diffused on/into Ni layer. This state is explained as *"metastable solid solution"*. Then, crystallization of carbon atoms onto the metal surface to form graphene can follow. Using ion implantation technique, carbon atoms can be stored in advance. That is to say, we can focus on diffusion-precipitation step, apart from binding energy of carbon precursor[6, 10], decomposition rate of gas[24-26], and optimization of CVD temperature/pressure/cooling etc[5, 9, 27-30].

5.1.2.1. Carbon Solubility/Diffusivity

The choice of metallic substrate is of great importance that can determine graphene growth pathway. This is closely related to carbon solubility and diffusivity of metals, as well as lattice mismatch. In this section, we will focus on the formal point with phase diagram between metal and carbon.

Figure 5.1. shows (inset) the Ni-C phase diagram, and an enlargement of the metal-rich side within a temperature range from 600 K to 1800 K. At a given temperature T_1 (see right y axis), if carbon atoms are constantly supplied to the surface of a nickel film, they will dissolve into it, up to a certain concentration represented by point A in the phase diagram (solubility limit at T_1). Above this concentration, the excess carbon will precipitate in graphite form. This is typically the reaction path for the formation of carbon nanotubes (blue plain arrow on Figure 5.1.), provided the nickel material is in the form of small clusters of nanometric dimensions. Now, still at T_1, if a limited amount of carbon is supplied to the nickel surface, corresponding to a concentration below the solubility limit (once dissolved in the nickel film), and if the solid solution is allowed to cool down, carbon will again precipitate, in the form of graphite, as the temperature crosses the solubility line

(T_C on Figure 5.1.). If the amount of dissolved carbon in the nickel at high temperature is carefully controlled, graphite precipitation can yield graphene or few layers graphene films on the surface of the nickel after cooling down to room temperature.
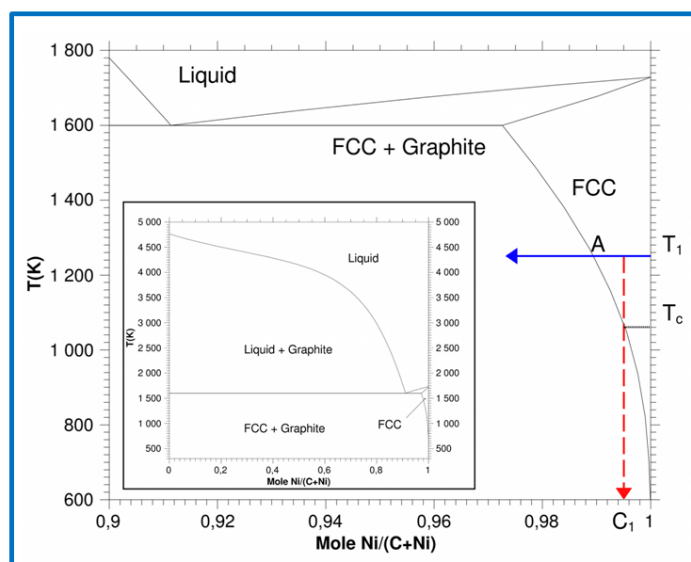
Figure 5.1. Metal rich part of the Nickel-Carbon phase diagram (inset is the full phase diagram). When carbon is supplied to a nickel layer heated at T_1, the carbon dissolves into it until the carbon concentration reaches a value corresponding to the A point. When the carbon concentration increases further, the supplied carbon precipitates as graphite. If the carbon supply is stopped at concentration C_1 and the nickel layer is allowed to cool down, the carbon starts to precipitate as graphite when the temperature T_c is reached.

In contrast to Ni, the transition metals which have low carbon solubility, for example Cu, show totally different growth process. Cu has negligible carbon solubility, of 0.008 weight % at 1084 °C[31-33], its reaction mechanism is only limited around surface[34]. This means that as the surface is getting covered by graphene, the process can be done by self-limited mechanism.

131
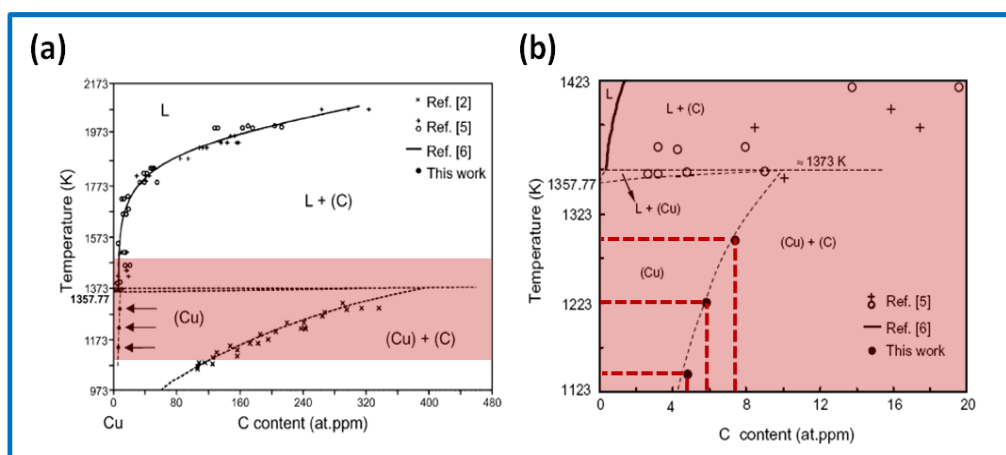
Figure 5.2. (a) Cu-C equilibrium phase diagram at the Cu-rich side, and (b) magnified phase diagram in temperature range from 1123 K to 1423 K (marked area of (a) by reddish color). Cited from G.A. López and E.J. Mittemeijer, Scr. Mater. **51**(1), 1-5 (2004)[32]

In fact, Cu has the most stable electron configuration of $[Ar]3d^{10}4s^1$ (along with $[Ar]3d^54s^1$). This allows symmetric electron dispersion which minimizes the electron-electron repulsion. Thus, only soft bonds with carbon (via charge transfer from the π electrons in the sp^2 hybridized carbon to the empty 4s state of copper) can be formed[33, 35, 36]. Co and Ni have an electron configuration of $[Ar]3d^74s^2$ and $[Ar]4s^23d^8$, respectively. Fe ($[Ar]3d^64s^2$) is the most unstable one and Cu is the most stable one that stabilize carbon on their surface by forming weak bonds.

Table 5.1. Electron configuration of some representative catalyst metal for graphene growth. Carbon solubility and melting temperature are listed together. [*]α-Fe transforms to FCC γ-Fe at 912 °C, [**]γ-Fe transforms to δ-Fe at 1395 °C.

Atomic Number & Electron Configuration	Symbol	Carbon Solubility	Melting Temperature
26 - $[Ar]3d^64s^2$	α-Fe[*]	0.02 wt. % at 723 °C	-
	γ-Fe[**]	2.08 wt. % at 1148 °C	-
	δ-Fe	0.09 wt. % at 1495 °C	1538 °C
27 - $[Ar]3d^74s^2$	Co	0.9 wt. % at 1320 °C[33]	1495 °C
28 - $[Ar]4s^23d^8$	Ni	0.6 wt. % at 1326 °C[33]	1453 °C
29 - $[Ar]3d^{10}4s^1$	Cu	0.008 wt. % at 1084 °C[31, 33, 37]	1085 °C

In previous *Chapter IV*, we introduced the interfacial graphene located in-between Ni and SiO$_2$ substrate. Through ion implantation technique, we are able to get closer by high implantation energy and subsequent carbon diffusion. An idea of ion implantation is thus also to possibly enhance the part of precipitation that

takes place at the interface.

5.1.2.2. Lattice Mismatch

Graphene grown on transition-metal surfaces typically exhibits a moiré pattern due to the lattice mismatch between graphene and the underlying metal surface. This has an important role in defining the structure characteristic of grown-graphene[38, 39]. The lattice mismatch is defined as follows;

$$\text{Lattice Mismatch (L.M.)} = (L_M - L_G)/L_M \qquad \text{(Eq. 5.1.)}$$

where L_M, L_G are the lattice constants of metal and graphene, respectively. Lattice constant of graphene is 2.46 Å[40]. In the following table 5.2., we can see all catalyst metals that reported for graphene growth. Lattice mismatch is calculated from its lattice constant, L_M.

Table 5.2. Lattice constant of metal and its lattice mismatch compare to graphene.

Atomic Number	Symbol	Lattice Constant L_M (Å)	Lattice Structure	Lattice mismatch (%)
28	Ni(111)	2.49	FCC	1.20
27	Co(0001)	2.51	Hexagonal	1.99
29	Cu	2.55	FCC	3.63
45	Rh(111)	2.69	FCC	8.55
44	Ru(0001)	2.71	Hexagonal	9.23
77	Ir(111)	2.72	FCC	9.56
46	Pd(111)	2.75	FCC	10.57
78	Pt(111)	2.77	FCC	11.19
79	Au	2.88	FCC	14.73

Unlike the case of epitaxial growth of a typical semiconductor material on lattice mismatched substrate, in which pseudomorphic growth can be achieved through the introduction of lattice strains under a certain critical thickness, graphene cannot be strained so easily on metal due to the large anisotropy in chemical bonding strength between the basal plane and vertical direction. Therefore, except for graphene on Ni(111) in which (1 x 1) structure is formed due to the small lattice mismatch, in most other cases, graphene supercells are formed on metallic substrate. In general, pseudomorphic growth is predicted to be preferred for small-mismatched interfaces, while incommensurate films are favoured for large-mismatched interfaces[41].

Depend on how strongly the graphene layer interacts with the underlying metal substrates, the degree of corrugation in graphene on lattice-mismatched transition-metal can be determined[42]. For example, Ir(111) and Pt(111) surfaces weakly interact with the graphene layer[43, 44]. On the other hand, on Ru(0001) and Ni(111)

surfaces, the graphene band structure is strongly modified[36].

5.1.2.3. Linear Thermal Expansion Coefficient

Materials expand because an increase in temperature leads to greater thermal vibration of the atoms and hence to an increase in the average separation distance of adjacent atoms. Solids mostly expand in response to heating and contract on cooling. The linear coefficient of thermal expansion α describes by how much a material will expand for each degree of temperature increase, as given by the formula,

$$dl = L_0 \times \alpha(T_1 - T_0) \qquad \text{(Eq. 5.2.)}$$

where *dl* is the change in length of material in the direction being measured (meter), L_0 is the initial length of material (meter), *α is the linear thermal expansion coefficient*, and T_0, T_1 are initial, final temperature.

Table 5.3. shows the list of linear thermal expansion coefficients, especially of those metals related to graphene growth. It is worth to note that the difference in linear thermal expansion coefficient (between graphene and metal substrate) is one of possible reasons introducing ripples (or wrinkles) on graphene grown at surfaces[45, 46].

Table 5.3. Linear thermal expansion coefficient compared to graphite *Note that the value corresponds to in-plane graphite.

	Coefficient of Linear Thermal Expansion ($10^{-6}/°C$)
SiO_2	-
Graphite*	**7.9**
Ir	6.4
Pt	9.0
Pd	11.8
Ni	13.0
Au	14.2
Cu	16.6
Al	22.2

5.2. Experimental

In this section, we will describe how we prepared sample for implantation, from wafer cleaning to Ni evaporation. Then, the precise information on implantation, such as implantation energy and carbon does, will be explained.

5.2.1. Wafer Cleaning and Catalyst Preparation

For the wafer cleaning and catalyst preparation, we followed sample process which described in Chapter 4.2.1. Briefly, 4 inch wafer purchased from SILTRONIX (300 nm-thick SiO_2/Si) is dipped into trichloroethylene (Alfa Aesar, L14474, 98%) under the heating in 100 °C for 30 minutes. Then, rinsing by acetone, isopropyl alcohol, and deionized (DI) water follow in order. Consequently substrate is fully dried by nitrogen gas. A mixture of sulfuric acid (Sigma Aldrich, 339741, 99.9%) and hydrogen peroxide (Sigma Aldrich), namely piranha solution, is used to clean organic residues off substrates for more than 30 minutes on hot plate with 150 °C. After rinsing by deionized (DI) water, drying by nitrogen, nickel is directly evaporated with a deposition rate lower than 0.3 nm/sec, under 2 x 10^{-7} torr in vacuum.

5.2.2. Ion Implantation from ibs

We prepared 200 nm-thick Ni on SiO_2/Si substrate, then transferred samples to company, ion beam services (ibs)[47] for the implantation of carbon with specific carbon does and acceleration voltage.

5.2.3. Ion Implantation from Université de Strasbourg

Carbon implantation at different carbon doses and energies were performed on a *200kV EATON ion implanter* which installed in InESS (L'Institut d'Électronique du Solide et des Systèmes), Université de Strasbourg. Following table 5.4. shows basic information on the equipment.

Table 5.4. General information on 200kV EATON ion implanter

200kV EATON ion implanter	
Acceleration Voltage	10 ~ 200 kV
Ion Energy	10 ~ 200 keV
Source	Freemann equipped
Current	~ μA
Beam size	5 mm
Implantation Temperature	- 200 °C ~ +600 °C

In this work, there are mainly two series, according to the location of the implantation tuned by the ion energy. One is for graphene formation on metal surface, thus we employed low implantation energy. Implanted carbon ions will be strongly distributed at near surface. These carbon ions could be engineered to out-diffuse for precipitation. The other is that we are aiming to introduce carbon ions near interface, between metal and underlying SiO_2. It would therefore require high implantation energy to penetrate roughly 150 nm-thick metals, referred to 200 nm-thick cases. The latter case, interfacial graphene, can support previous work in Chapter IV. with more fundamental insights.

5.3. Results and Discussions, Part (I)

In this section, we will describe our experiments on graphene growth on polycrystalline Ni thin films by using ion implantation of carbon ions. The carbon density in monolayer graphene is $\sim 3.8 \times 10^{15}$ atoms/cm^2, corresponding to a dose easily accessible/controllable by ion implantation, thus fundamental insights on growth mechanisms can be obtained through precise injection of carbon atoms.

5.3.1. Carbon Ion Implantation and Annealing

Figure 5.3. shows the schematic procedure followed in this work. We have used 200-nm thick nickel films deposited by e-beam evaporation on oxidized silicon wafers (SiO_2 thickness $\sim$300 nm). Carbon implantation in those Ni films was performed at an energy of 80 keV (yielding a $\sim$ 100 nm projected range) using doses of {8 16, 24 and 32} $\times 10^{15}$ atoms/cm^2 which correspond to the equivalent of $\sim$ 2, 4, 6 and 8 graphene layers assuming a uniform precipitation of the total implanted C upon.
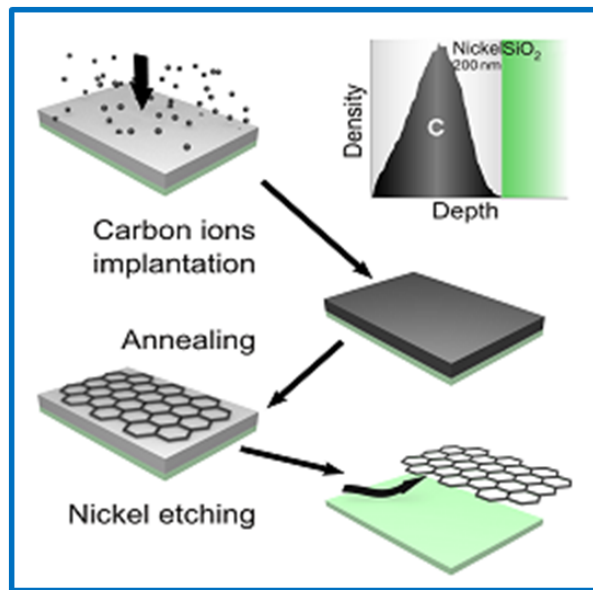
Figure 5.3. Schematic representation of the procedure used in this work. The inset shows the calculated carbon distribution through the thickness of the Ni film after ion implantation at an energy of 80 keV

Simulations ran with the SRIM 2008 software indicated that no carbon is implanted in the silicon oxide layer[48]. The ion implantation energy was determined using classical simulation means. We have first calculated the projected range of carbon ions in nickel for different energies (see in Figure 5.4.). In order to obtain a projected range around 100 nm (i.e., centered in the middle of the thin Ni film), a 80 keV energy was chosen. Once the implantation energy was calculated, an implantation simulation using the SRIM 2008 software has been performed to check that the entire carbon dose is contained inside the nickel layer (no C lost in the SiO_2 layer, Figure 5.4.(b)).
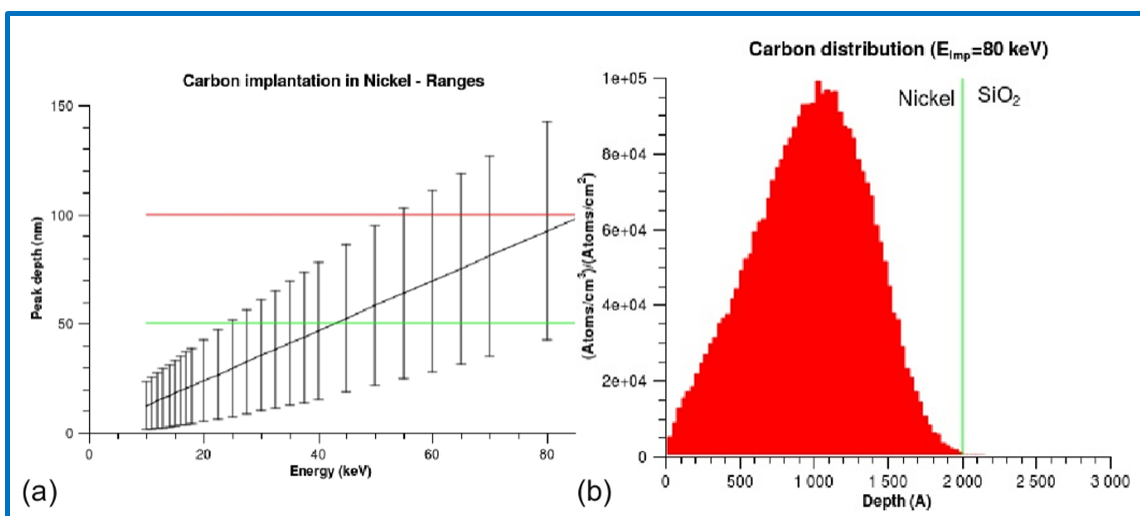
Figure 5.4. (a) Projected range of ion implanted carbon in nickel as a function of implantation energy. (b) Simulated concentration profile of carbon in nickel for a 80 keV implantation energy

5.3.2. Carbon Out-Diffusion from Polycrystalline Ni

The implanted substrates were annealed under vacuum ($\sim 10^{-5}$ mbar) using different starting and stopping temperature. The annealing was performed by pushing the samples (loaded on a quartz boat) with a stainless steel rod into the furnace which was preheated to the setting temperature. The stainless steel rod was also used to rapidly remove the samples from the furnace, thus providing rapid quenching process. (See in Section 4.2.5.)

From the results of Lander et al[49], we have evaluated the C solubility in a 200 nm thick Ni film at different temperatures. We have transformed the data of Lander ($\ln S = 2.480 - 4.880/T$ where S is the carbon solubility in weight % C into Ni) into C atoms per cm^3 of Ni, yielding

$$S_T = 5.33 \times 10^{22} \exp(4880/T) \text{ atoms/cm}^3 \qquad \text{(Eq. 5.3.)}$$

where S_T is the carbon solubility expressed in atoms/cm^3 at temperature T. From this formula, we have deduced the C solubility in atoms/cm^2 in our 200 nm thick Ni films. Some values of interest for the present study are listed in table 5.5.

Table 5.5. Some C solubility values in a 200 nm-thick Ni film.

Temperature (°C)	C solubility (x 10^{15} atoms/cm^2)
725	8
900	16
1000	23

In order to avoid complications with the kinetics of carbon out-diffusion from the Ni film due to the decrease of solubility as the temperature drops[50], the following procedure was adopted after ion implantation: (i) annealing was first performed at 900 °C over 30 min, in order to dissolve all the implanted carbon in the Ni thin film (the carbon solubility in Ni at 900 °C is $\sim 16 \times 10^{15}$/cm^2, see in table 5.5.) and (ii) the furnace temperature was then slowly decreased to 725 °C (at a rate of 0.5 °C/s). During this temperature decrease, the carbon solubility in Ni evolves from 16×10^{15}/cm^2 down to 8×10^{15}/cm^2, which means that the equivalent of ~ 2 graphene layers should out-diffuse and precipitate. Finally, (iii) the samples were rapidly quenched from 725 °C, thus trapping the residual carbon inside the Ni. In this manner, we can control the amount of precipitated carbon at high temperature without knowing the details of kinetics of carbon out-diffusion from Ni at moderate to low temperature.

Figure 5.5. shows a Raman spectrum taken on a sample processed as explained above (16 x 10^{15} cm^{-2}, annealing at 900 °C and quenching from 725 °C) and still standing on top of the Ni film. It exhibits the now classical features of graphene, i.e., a low D band (~1350 cm^{-1}), a strong G band (~1590 cm^{-1}) and a 2D band (~2700 cm^{-1}) emerging from a double resonant scattering phenomenon[51].

The D band activated by defects is negligible, indicating that well-organized *sp^2* network is formed with high I_G/I_D ratio of 4.9. The other relationship between I_{2D}/I_G is also important factors that can bring the information on number of graphene layers. The intensity ratio, I_{2D}/I_G, is recorded as 1.39 which closes to ~ 5 layers. However, wide 2D peak is not fully suitable to conclude its thickness exactly. The peak position, especially 2D peak, reflects its electronics structure, as we mentioned in Section 4.1.2.2. As the Raman signal is collected on Graphene/Ni surface, p type doping effect resulting in 2D peak redshift[52]. In addition, it is worth to mention that increase of graphene thickness can make same situation.
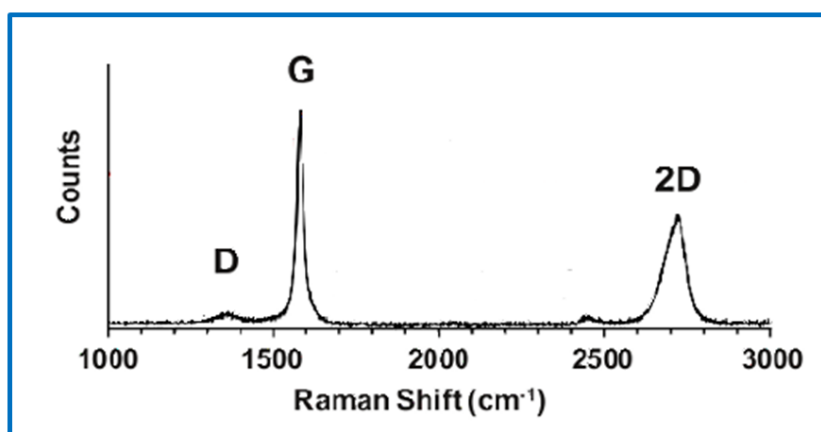
Figure 5.5. Raman characterization (at 514 nm excitation) of a graphene film still standing on top of the Ni catalyst.

Next, we examined the surface structure of the Ni films after annealing, using electron backscatter diffraction (EBSD) in the scanning electron microscope (SEM) and transmission electron microscopy (TEM). First of all, we observed that the Ni films were strongly (111) textured after ion implantation and annealing (Figure 5.6.). Also, the grain size was rather small, varying typically between 0.5 and 1 µm. Preferential growth of (111) direction is widely reported via high temperature (1000 °C) annealing, as well as grain size can be reached to ~10 µm. Small grain size of Ni, in our case, might be attributed to rather low temperature process (900 °C) and the effect of pre-implanted carbon. Along the grain boundaries, carbon diffusivity is much higher than the other part. Thus, grains are carbon segregation places, which disturb grain growth of Ni.
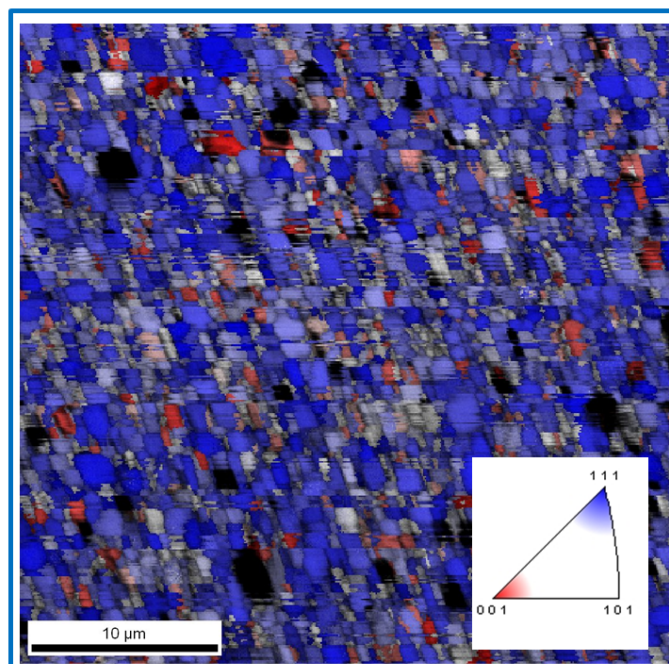
Figure 5.6. SEM image of a Ni film after carbon ion implantation and annealing. The local crystallographic orientation at each pixel has been measured using electron backscatter diffraction (EBSD). The dominant blue colour indicates that more than 80% of the Ni grains are oriented within 15° of <111>.

5.3.3. HR-TEM study

In order to understand the poor electrical properties of the graphene films, we characterized the fine structure of the films using transmission electron microscopy experiments. After the annealing procedure described above, we have transferred some graphene layers to holey carbon-coated TEM grids. Figure 5.7. shows a typical high resolution TEM image of a layer obtained after implantation with a dose of 24 x 10^{15} cm^{-2}. The graphene flakes appear to cover several squared micrometers, i.e., more than the typical nickel grain size. Their being folded allows one to count the number of layers on their edges: between two and four, again, in that case (inset in Figure 5.7.). As summarized in Figure 5.7., two types of carbon structures are observed: (a) well crystallized graphite flakes and few layers graphene (FLG) and (b) nanometric graphene crystals arranged in films. The observation of two different carbon structures on the same sample suggests the existence of at least two mechanisms.
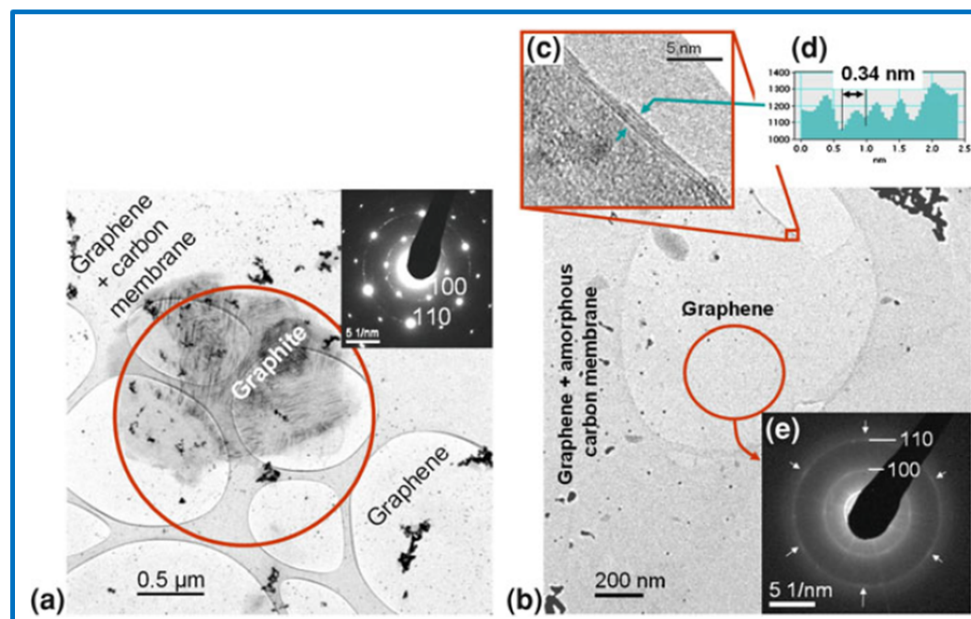
Figure 5.7. TEM micrographs of graphene film transferred onto a TEM grid. (a) Plan-view of a graphite flake and electron diffraction pattern (EDP, inset) recorded over the circled area. (b) General view of the graphene. (c) High magnification TEM image of the edge of the film, where a local folding allows to count the number of graphene layers. (d) Intensity profile of the image in (c), indicating a distance of 0.34nm between the graphene layers. (e) Selected area EDP (circle in (c)) exhibiting 100 and 110 graphene reflections with a distribution of orientations. A given orientation appears to be favoured as the diffracted intensity is enhanced with six-fold symmetry (arrows)

It therefore seems that, during high temperature annealing, the implanted carbon diffuses towards dedicated nucleation sites, from where growth takes place, and that some grains are totally depleted of carbon by this diffusion process. This carbon redistribution indicates that the graphene thickness (number of monolayers) is determined by the topography of the nucleation sites (probably steps or bunches of them at the boundary of (111)-oriented Ni grains), rather than by the amount of carbon present in the Ni films, which points toward further study of the graphene nucleation mechanism on Ni thin films. This tendency of graphene to produce a non-uniform film thickness when synthesized on Ni has already been reported[34] but not really explained yet.
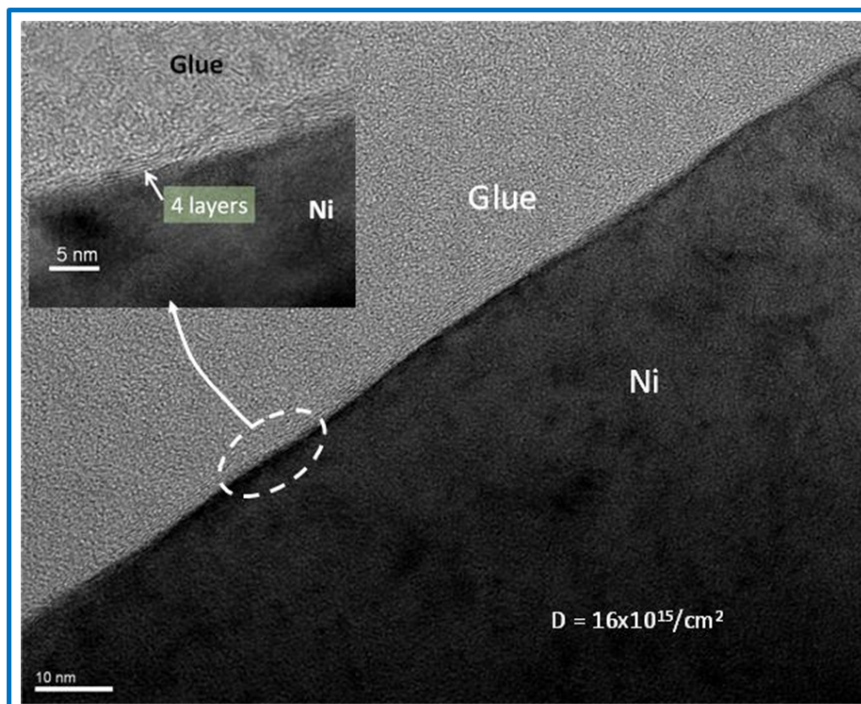
Figure 5.8. Cross sectional HRTEM image showing part of a graphene film with a thickness of 4 to 5 layers, extending over the whole top surface of a Ni grain. The inset is a higher magnification picture showing a particular area where 4 layers can be counted.

Graphite flakes and FLG are always seen at the grain boundaries (GBs). During the annealing, the nickel film is strongly deformed and, in particular, undergoes a substantial grain growth. This suggests that graphite flakes/FLG grow at GBs and that, similarly to what is observed in the case of the growth of nanotubes[53], the metal is displaced by the growing graphite. Furthermore, those graphite flakes are always oriented with the c-axis perpendicular to the surface: as growth proceeds laterally, this tends to indicate that growth started from a grain wall. As shown in Figure 5.9., in certain topological conditions, FLG is grown. This requires GBs with a high curvature (and thus a high density of atomic steps) acting as nucleation centres for the lateral growth of FLG. The fact that we found some places with graphite flakes, some places with FLG and others with no graphene, as well as the large variations in the thickness of the observed graphitic objects, indicates that the initially uniform density of carbon atoms is strongly redistributed during annealing procedure. In fact, we calculated from Lander et al. data[49] that, for an annealing of one second at 725 °C, the diffusion length of carbon atoms in nickel is 1.2 μm.
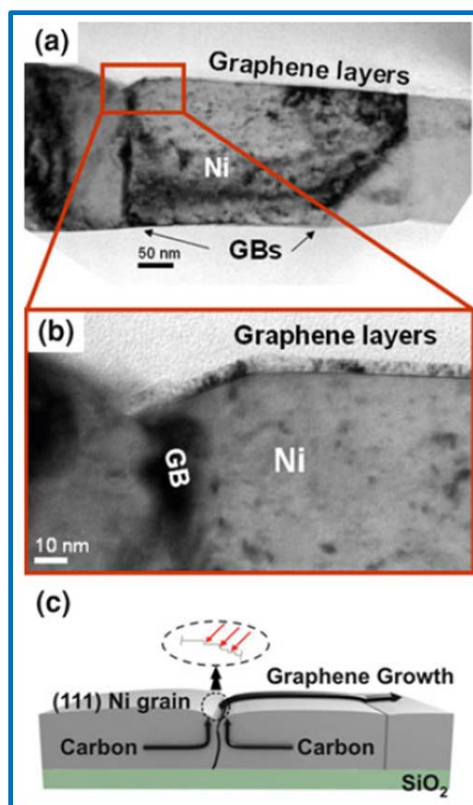
Figure 5.9. TEM cross-section of graphene or graphite on nickel grains. Sample implanted with 16×10^{15} atoms/cm^2 dose of carbon, annealed at 900 °C for 30 min, slowly cooled to 725 °C, and then quenched. (a) TEM images showing the connection between a nickel grain boundary and graphene layers at the surface of the film. (b) Schematic representation of the nucleation and growth mechanism of graphene over nickel. Nucleation preferentially occurs in regions of high curvature of the (111) grain surface, where the step concentration is high (blue arrows in inset), and graphene subsequently grows parallel to the grain surface.

5.3.3. Growth Mechanisms

Step flow growth (see in Figure 5.9.(a)) has indeed been observed for individual graphene layers, in the case of carbon nanofibres grown with Ni catalyst[54-57], in the case of epitaxy of graphene on Ru(111)[58], and in the nucleation of single-walled carbon nanotubes on Co[59]. The lateral growth that occurs here then recalls again the mechanism observed in multiwall carbon nanotube growth[53, 60, 61], especially when the metal is in the form of nail-shaped particles, where the surface under the head of the nail delivers the graphene layers, and its body then guides them in the form of nanotube/nanofibres[53, 61]. Such a scheme would explain why large graphite flakes seem in some occurrences to have just replaced a certain thickness of nickel: expending nickel grains would offer room on their surface for graphite to grow laterally.

So the less energetic path for graphite formation would be that summarized in Figure 5.10.(a), where

grain boundaries accelerate the diffusion of carbon atoms toward nucleation sites, from which graphite/FLG films grow laterally (Figure 5.10.(b), below), as the GB drifts away. It is interesting to note that the graphite thickness in that case depends on the depth of the groove associated with the GB, and on the local surface curvature. As quoted above, FLG films are also synthesized according to the same mechanism[62], when the surface topography is favourable, i.e., when the intersection of the grain boundary with the Ni surface exhibits a large radius of curvature and only a few atomic steps are available for graphene nucleation there.

The quasi-absence of long-range order in our nanocrystalline-graphene films (see the rings in the diffraction patterns; Figure 5.10.(a)) indicates that the mechanism at the origin of their existence is quite different from that discussed above: there is little correlation between the crystal orientation at one place and another. Thus, the nucleation rate in that case must have been extremely high, and it has obviously involved a very high density of nucleation sites, which is compatible with the fact that the Ni surface is far from perfect. Thus, this process has implied only local transport of carbon atoms (Figure 5.10.(b)).

An explanation is that the nanocrystalline graphene has most probably developed during quenching, below 725 °C, because of the very high supersaturation, associated with still significant carbon diffusivity[49] (Figure 5.10.(b)). Data from the literature indicate that such a disorder is indeed possible even in a constant-temperature regime, as, for example, in the case of C-segregation at the surface of platinum (100)[63]. The key word again is high supersaturation. Such conditions are essentially opposite to the unsaturated regime with which Blakely and coworkers observed single-crystal graphene formation[64]. Our 8×10^{15} atoms/cm^2 dose, which was aimed at obtaining Blakely and co-workers' graphene "segregation"[64-66], thus, did not deliver it.

A major difference between the work of Blakely and coworkers[64-66] and the present one resides in the presence of grain boundaries here and their absence there. In our samples, GBs are at the origin of a very strong re-distribution of carbon throughout the Ni films. Whatever the exact cause of that redistribution, we did observe it with all the doses, including 8×10^{15} atoms/cm^2 one. Thus, in reality, the local carbon concentration in the nickel in the present samples is everywhere different from the concentration imposed by implantation. As the carbon concentration window for graphene "segregation" on Ni surface is quite narrows, the regions of the sample where the concentration condition is fulfilled are probably very few
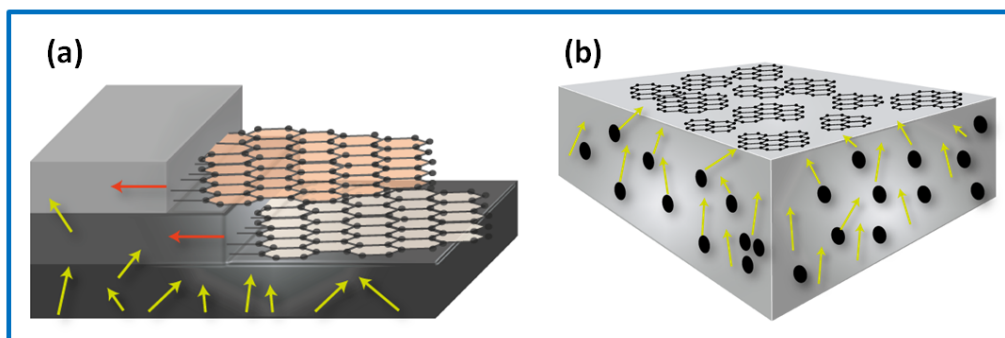
Figure 5.10. Two types of growth processes starting from carbon atoms dissolved into Ni: (a) Lateral growth of high quality graphite/few layered graphene. (b) Growth of nanocrystalline graphene after surface precipitation of carbon atoms.

5.4. Results and Discussions, Part (II)

In previous section, we opened up new possibilities for graphene growth. Ion implantation technique has a variety of factors that could affect graphene growth, such as carbon dose, implantation energy, and catalyst metals, so investigation of those parameters are necessary. In this section, carbon ion implantation at different carbon doses and energies were performed on a 200kV EATON Implanter that is installed at Université de Strasbourg, France.

5.4.1. Effect of Implantation Conditions

After PECVD growth (Chapter 4.), we found interfacial graphene layers in-between Ni and SiO$_2$/Si. We have discussed its advantages for transfer-free, low-temperature graphene applications. For these reasons, our goal with ion implantation is not only to elucidate graphene growth mechanism in general but also to precisely understand interfacial graphene formation.

Through Rutherford Backscattering spectroscopy (RBS) which is performed with 2 MeV He[+] at an incidence angle of 160° in a Van de Graaff accelerator, the interfaces and the thicknesses of the layers were determined. As shown in Figure 5.11., steep interfaces between Ni/SiO$_2$ and SiO$_2$/Si(100), respectively, were obtained. The thicknesses obtained are in good agreement with the expected thicknesses for Ni (190 instead of 200 nm) and SiO$_2$ (290 instead of 300 nm), calculated with the density expected for Ni (8.91 g/cm^3) and SiO2 (2.33 g/cm^3).
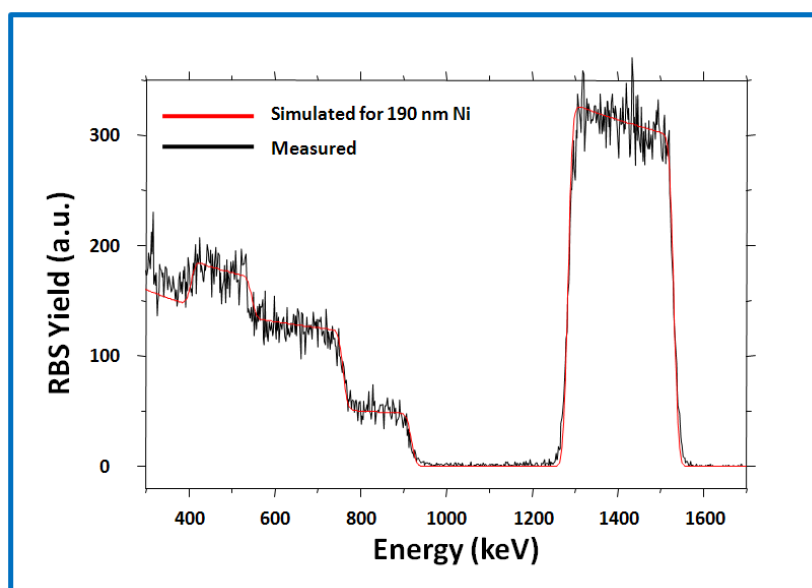
Figure 5.11. Rutherford Backscattering spectroscopy (RBS) measurement on Ni-evaporated sample. The thickness of Ni layer is expected to 190 nm, instead of 200 nm.

Our first trials with carbon implantation were performed at 80 keV, with the aim of centring the carbon distribution at equal distance from the top surface and the bottom interface. We performed TRIM (Transport of Ions in Matter) simulation to estimate how many and how deeply carbons are implanted into Ni films at 20 and 120 keV (Figure 5.12.). Ni layer (200 nm-thick) is directly deposited, as before, on chemically-cleaned SiO_2/Si by e-beam evaporation. Carbon dose is fixed as 5 x 10^{15}/cm^2 which corresponds to 1.3 graphene monolayer and only the implantation energy is changed. At 20 keV the maximum of carbon concentration occurs at around 30 nm below the surface (almost no carbon appears after 85 nm depth), whereas at 120 keV the wide and weak maximum of concentration occurs around 140 ~ 170 nm, far from the surface but near the interface with SiO_2 (300 nm)/Si. We can also note that a small amount of carbon is implanted into SiO_2 layer with high energy. We assumed that these carbons may be possible to enhance adhesion of nickel films with SiO_2 and to participate as nucleation centre for graphene formation at interface. Let us put some emphasis again on the case of high energy implantation with 120 keV that aims to promote formation of interfacial graphene layers.
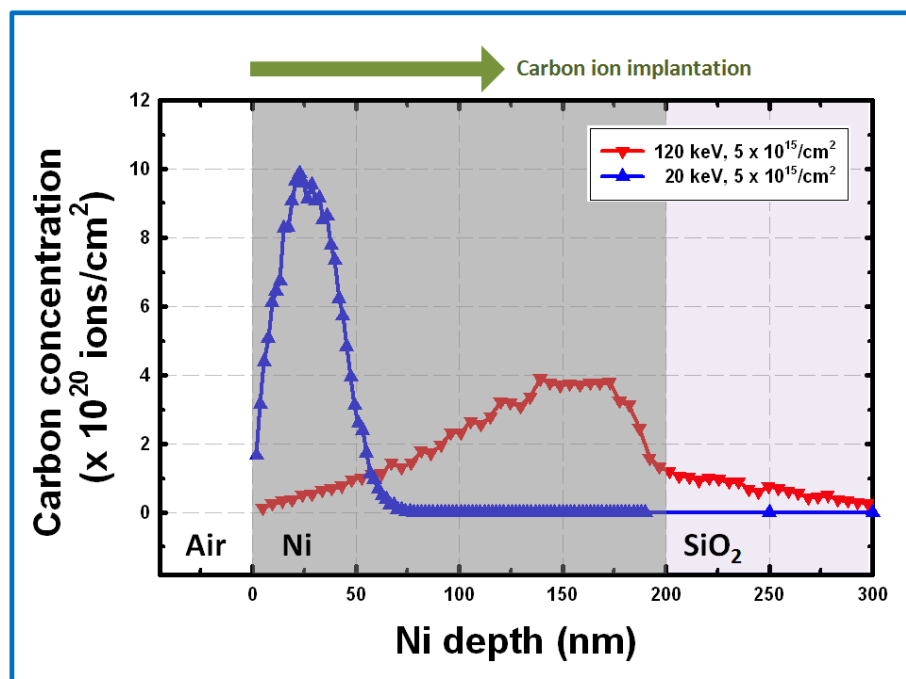
Figure 5.12. Depth profile of implanted carbon using 200 nm-thick Ni on SiO$_2$(300 nm)/Si sample by TRIM simulation.

5.4.2. Study on Annealing Conditions

One of the most dominant factors that influence carbon diffusion is the annealing temperature, thus we have investigated its impact.

Figure 5.13. shows top-view scanning electron microscope (SEM) images of annealed samples at 450 ^{o}C, 750 °C, and 900 °C. In the annealing system, we have two separated regions; one is heating zone surrounded by tungsten wire for heating and the other is cooling zone which is outside of quartz tube and exposed to air. This system enables us to push/pull the substrate in-between heating and cooling zone.

First, sample is loaded in cooling zoon and evacuated down to 2.0 x 10^{-5} mbar. Using temperature controller (Carbolite - 1200 ^{o}C Horizontal Split Tube), temperature is set up at desired level with a ramping speed of 25 °C per minutes. Once the temperature is getting to target under vacuum, sample holder is moved into heating zone (by load-lock arm) for 18 minutes. The temperature, then, starts to drop naturally with keeping the sample inside for 7 minutes. Finally, the sample holder is pulled off into quenching zone to prevent additional carbon precipitation.

Regardless of implantation energy, we find progressive structuring of dark fragments with an increasing of annealing temperature. The surface looks very homogeneous (almost single contrast appears), in case of (a)

for both, while dark fragments are clearly observed at 900 °C—annealed samples. The differences due to implantation energy (between Figure 5.13. and Figure 5.14.) are not detectable in this step.
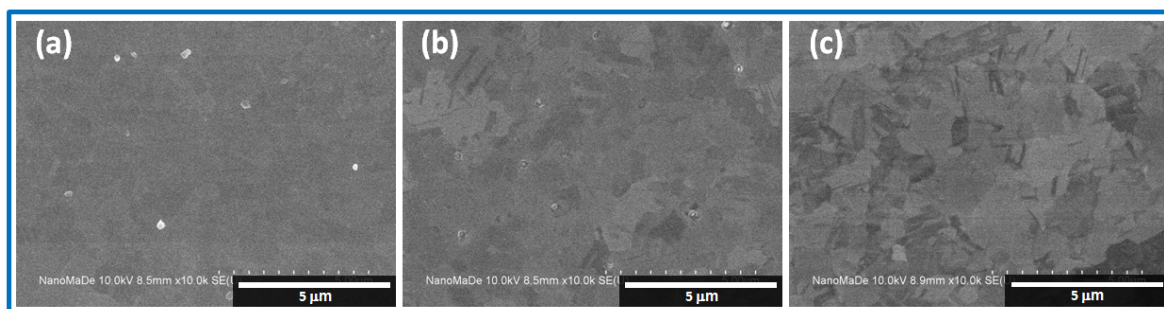
Figure 5.13. Effect of annealing after 120-keV implantation: Carbon ion implantation has been performed on Ni(200 nm)/SiO$_2$ (300 nm)/Si with 120 keV, 5 x 10^{15}/cm^2. Top-view SEM images of annealed samples at (a) 450 °C, (b) 750 °C, and (c) 900 °C, for 18 minutes under vacuum. In the cooling process, samples are quenched out to cool zone after 7 minutes of slow cooling.
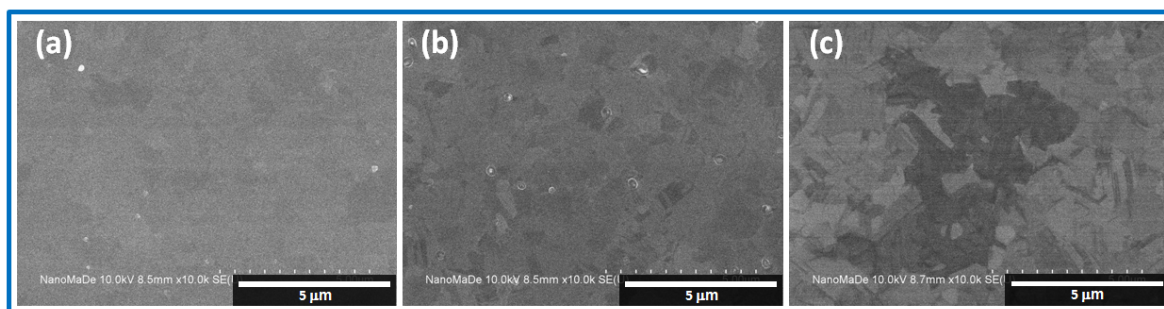
Figure 5.14. Effect of annealing after 20-keV implantation: Carbon ion implantation has been performed on Ni(200 nm)/SiO$_2$ (300 nm)/Si with 20 keV, 5 x 10^{15}/cm^2. Top-view SEM images of annealed samples at (a) 450 °C, (b) 750 °C, and (c) 900 °C, for 18 minutes under vacuum. In the cooling process, samples are quenched out to cool zone after 7 minutes of slow cooling.

The Raman spectra can deliver more detailed information on the evolution of graphene formation. From annealed samples at 450 °C, two wide and large contributions can be observed; one is D peak at 1370 cm^{-1} and the other is G peak at 1590 cm^{-1}. However, 2D peak (centered at around 2700 cm^{-1}) contribution is negligible. At higher temperature, 750 °C with green color in Figure 5.15., three peaks which are closely related to graphene appeared more clearly. Especially, in case of high implantation energy, the spectrum shows relatively narrow G peak (FWHM of G peak is around 62.0 cm^{-1}). Integrated intensity ratio of I$_D$/I$_G$=0.88, I$_G$/I$_{2D}$=1.70 is recorded. Purple color in Figure 5.15. shows annealed sample at 900 °C.

The most significant changes in spectra are that: (i) disappearance of D peak, (ii) sharpening of G peak, and (iii) redshift and desymmetrization of 2D peak. The I$_D$/I$_G$ for (a) 120 keV, and for (b) 20 keV is 0.09, 0.06,

respectively, while 1.47 and 1.02 of $I_G/2_D$ are recorded. Those values are fairly comparable to high-quality carbon materials. Especially, G_{FWHM} is 29.32cm^{-1}, 33.03 cm^{-1}, implying well-crystallized structure. The experimental G_{FWHM} was measured on a single crystal graphite as 13 cm^{-1},[67] and ~25 cm^{-1} is expected for CVD-grown single layer graphene[51]. It is worth to note that graphite-like structure is generated rather than desired graphene, because of 2D peak redshift and its desymmetrization[51]. Again, this is mostly due to the fact that carbon diffusion in Ni layer is not homogeneous. The way to guide uniform carbon movement toward catalyst surface should be developed, for example, Ni pre-annealing via high temperature can be useful in decreasing the grain boundary density. Grain boundaries of Ni have significantly high carbon diffusion rate compared to bulk diffusion, thus the preferential diffusion flux associated with GBs could be limited.
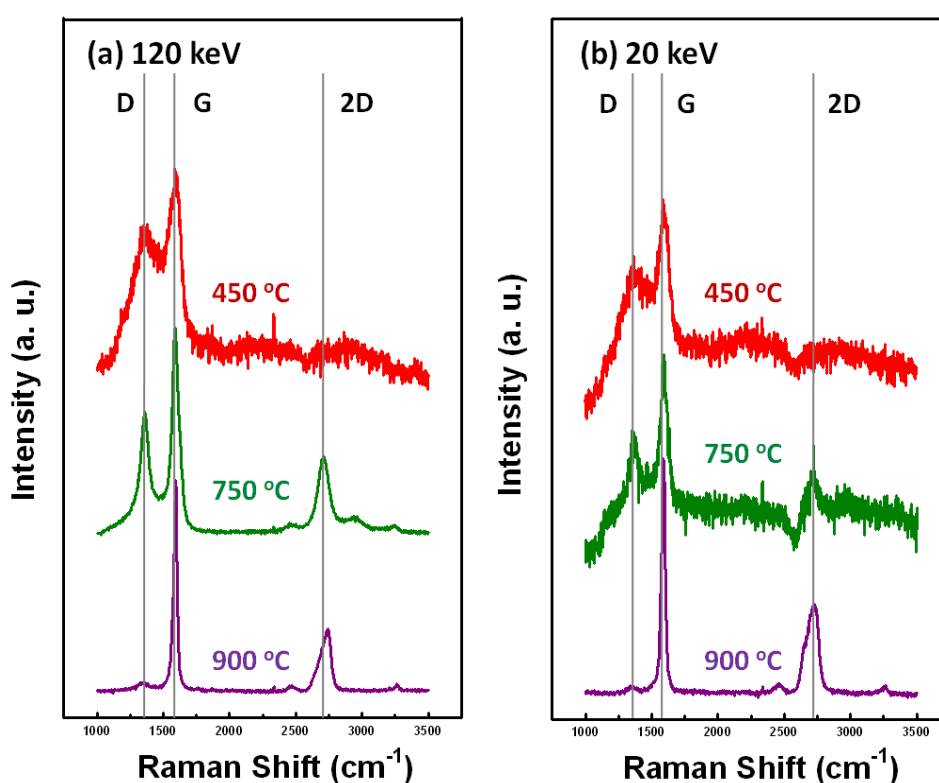
Figure 5.15. Raman spectra analysis (excited by 534 nm laser) from those samples in Figure 5.13. and Figure 5.14.

5.4.3. Investigation of Electrical Behavior

We have used the transfer length method (TLM)[68] to study the electrical properties of our few-layered graphene (FLG) films grown by ion implantation technique. Carbon implantation in those Ni films was performed at an energy of 80 keV using a dose of 16 x 10^{15} cm^{-2} which corresponds to the equivalent of ~4 graphene layers, followed by standard annealing process. For the transfer of FLG films onto Si/SiO$_2$ substrates, a 1.5 μm thick PMMA layer was first spin coated on top of the samples after annealing. The Ni layer was then

etched using a commercial etchant and the PMMA layer was dissolved once the film was deposited on the oxidized Si substrate [2, 3, 30]. The transferred FLG films were then masked and etched in an oxygen plasma and Pd electrodes were evaporated to a thickness of ~80 nm. A further annealing at 600 °C under vacuum was performed in order to improve contact resistances.

Figure 5.16. shows a SEM image of a typical TLM sample on oxidized Si. We have measured sheet resistances varying between 12 and 40 kΩ/sq. depending on the location on the host oxidized Si substrate. These high values tend to confirm that the films are not continuous.
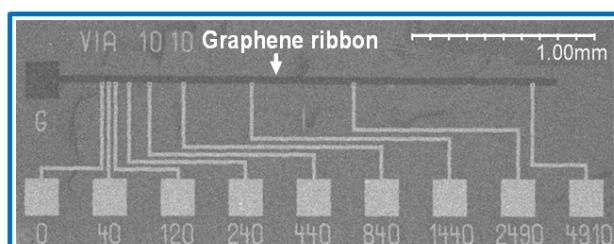
Figure 5.16. SEM image of a TLM device used for the measurement of the sheet resistance of few-layers graphene films transferred on Si/SiO$_2$

5.5. Conclusions

Recently, the CVD technique is the most-widely using technique for large-area, high-quality graphene synthesis. CVD is one of the essential tools in semiconductor industries, thus it has huge potentials toward industrialization/commercialization. However, the investigation of its growth process is hindered by complicated inter-related growth factors.

We introduced, for the first time, the ion implantation technique as an alternative way for graphene growth. As carbon dose and implantation energy can be precisely controlled in advance, we have more possibilities to understand the graphene growth mechanism. This, together with fundamental insights, could lead to better engineering of graphene growth process.

We have used the ion implantation of carbon into Ni thin films followed by high temperature annealing and quenching, in order to synthesize few-layer graphene (FLG).

     i.   Our observations indicate that the number of graphene layers in the FLG films is controlled by the graphene nucleation mechanism on Ni rather than by the amount of carbon available in the Ni film. Larger grains from Ni foils (instead of films) or pre-annealed Ni thin films would probably reduce the amount of nucleation centers and increase the overall uniformity of the

        graphene films.

ii.   Carbon diffusion in Ni is amazingly fast, thus strong re-distribution of carbon has occurred during annealing process. Thus, even we can control the implantation depth by energy, most of carbon atoms will be precipitated at surface, not at interface.

iii.   To obtain interfacial graphene by implantation technique, we believe that fast cooling process after low temperature annealing is required to freezing out carbon movement.

Implantation technique wouldn't be a suitable way for large-area graphene growth, like a CVD or PECVD technique. We believe, however, that new possibilities can be given by this way, especially in functional device architecture. For example, if we want to grow graphene layers on pre-defined area while device structure is already fabricated, ion implantation technique can be used with a sort of mask (either additional mask or device itself). This means that low temperature process is mandatory for avoid damage on the other components. Carbon implantation and precipitation at local places should be studied.

Reference

1.   Li, X., Cai, W., An, J., Kim, S., Nah, J., Yang, D., Piner, R., Velamakanni, A., Jung, I., Tutuc, E., Banerjee, S. K., Colombo, L. and Ruoff, R. S. Large-Area Synthesis of High-Quality and Uniform Graphene Films on Copper Foils. *Science* **324**, 1312-1314 (2009)

2.   Kim, K. S., Zhao, Y., Jang, H., Lee, S. Y., Kim, J. M., Kim, K. S., Ahn, J.-H., Kim, P., Choi, J.-Y. and Hong, B. H. Large-scale pattern growth of graphene films for stretchable transparent electrodes. *Nature* **457**, 706-710 (2009)

3.   Reina, A., Jia, X., Ho, J., Nezich, D., Son, H., Bulovic, V., Dresselhaus, M. S. and Kong, J. Large Area, Few-Layer Graphene Films on Arbitrary Substrates by Chemical Vapor Deposition. *Nano Letters* **9**, 30-35 (2008)

4.   Bae, S., Kim, H., Lee, Y., Xu, X., Park, J.-S., Zheng, Y., Balakrishnan, J., Lei, T., Ri Kim, H., Song, Y. I., Kim, Y.-J., Kim, K. S., Ozyilmaz, B., Ahn, J.-H., Hong, B. H. and Iijima, S. Roll-to-roll production of 30-inch graphene films for transparent electrodes. *Nat Nano* **5**, 574-578 (2010)

5.   Miyata, Y., Kamon, K., Ohashi, K., Kitaura, R., Yoshimura, M. and Shinohara, H. A simple alcohol-chemical vapor deposition synthesis of single-layer graphenes using flash cooling. *Applied Physics Letters* **96**, 263105-3 (2010)

6.   Guermoune, A., Chari, T., Popescu, F., Sabri, S. S., Guillemette, J., Skulason, H. S., Szkopek, T. and Siaj, M. Chemical vapor deposition synthesis of graphene on copper with methanol, ethanol, and propanol precursors. *Carbon* **49**, 4204-4210 (2011)

7.   Okano, M., Matsunaga, R., Matsuda, K., Masubuchi, S., Machida, T. and Kanemitsu, Y. Raman study on the interlayer interactions and the band structure of bilayer graphene synthesized by alcohol chemical vapor deposition. *Applied Physics Letters* **99**, 151916-3 (2011)

8.   Zhang, B., Lee, W. H., Piner, R., Kholmanov, I., Wu, Y., Li, H., Ji, H. and Ruoff, R. S. Low-Temperature Chemical Vapor Deposition Growth of Graphene from Toluene on Electropolished Copper Foils. *ACS Nano* **6**, 2471-2476 (2012)

9.   Liu, L., Zhou, H., Cheng, R., Chen, Y., Lin, Y.-C., Qu, Y., Bai, J., Ivanov, I. A., Liu, G., Huang, Y. and Duan, X. A systematic study of atmospheric pressure chemical vapor deposition growth of large-area monolayer graphene. *Journal of Materials Chemistry* **22**, 1498-1503 (2012)

10.   Wassei, J. K., Mecklenburg, M., Torres, J. A., Fowler, J. D., Regan, B. C., Kaner, R. B. and Weiller, B. H. Chemical Vapor Deposition of Graphene on Copper from Methane, Ethane and Propane: Evidence for Bilayer Selectivity. *Small*, n/a-n/a (2012)

11.   Li, X., Magnuson, C. W., Venugopal, A., An, J., Suk, J. W., Han, B., Borysiak, M., Cai, W., Velamakanni, A., Zhu, Y., Fu, L., Vogel, E. M., Voelkl, E., Colombo, L. and Ruoff, R. S. Graphene Films with Large Domain Size by a Two-Step Chemical Vapor Deposition Process. *Nano Letters* **10**, 4328-4334 (2010)

12.   Luo, Z., Lu, Y., Singer, D. W., Berck, M. E., Somers, L. A., Goldsmith, B. R. and Johnson, A. T. C. Effect of Substrate Roughness and Feedstock Concentration on Growth of Wafer-Scale Graphene at

Atmospheric Pressure. *Chemistry of Materials* **23**, 1441-1447 (2011)

13. Wood, J. D., Schmucker, S. W., Lyons, A. S., Pop, E. and Lyding, J. W. Effects of Polycrystalline Cu Substrate on Graphene Growth by Chemical Vapor Deposition. *Nano Letters* **11**, 4547-4554 (2011)

14. Baraton, L., Cojocaru, C. S. and Pribat, D. International Patent 0805769-2008, Process forcontrolled growth of graphene films (2008)

15. Large, L. N. Ion implantation :A new method of doping semiconductors - I. *Contemporary Physics* **10**, 277-298 (1969)

16. Fritzsche, C. Ion Implantation into Semiconductors. *Angewandte Chemie International Edition in English* **17**, 496-505 (1978)

17. Mun, J. H., Lim, S. K. and Cho, B. J. Local Growth of Graphene by Ion Implantation of Carbon in a Nickel Thin Film followed by Rapid Thermal Annealing. *Journal of The Electrochemical Society* **159**, G89-G92 (2012)

18. Baraton, L., He, Z., Lee, C. S., Maurice, J.-L., Cojocaru, C. S., Gourgues-Lorenzon, A.-F., Lee, Y. H. & Pribat, D. Synthesis of few-layered graphene by ion implantation of carbon in nickel thin films. *Nanotechnology* **22**, 085601 (2012)

19. Ziegler, J. F., Biersack, J. P. and Littmark, U. The Stopping and Range of Ions in Solids. Pergamon Press, New York (1985)

20. Schumm, M., Koerdel, M., Müller, S., Zutz, H., Ronning, C., Stehr, J., Hofmann, D. M. and Geurts, J. Structural impact of Mn implantation on ZnO. *New Journal of Physics* **10**, 043004 (2008)

21. Somani, P. R., Somani, S. P. and Umeno, M. Planer nano-graphenes from camphor by CVD. *Chemical Physics Letters* **430**, 56-59 (2006)

22. Baraton, L., He, Z., Lee, C. S., Cojocaru, C. S., Chatelet, M., Maurice, J.-L., Lee, Y. H. and Pribat, D. On the mechanisms of precipitation of graphene on nickel thin films. *EPL (Europhysics Letters)* **96**, 46003 (2011)

23. and D. Pribat, L. B. a. Z. B. H. a. C. S. L. a. C. S. C. a. M. C. a. J.-L. M. a. Y. H. L. On the mechanisms of precipitation of graphene on nickel thin films. *EPL (Europhysics Letters)* **96**, 46003 (2011)

24. Kim, E. S., Shin, H.-J., Yoon, S.-M., Han, G. H., Chae, S. J., Bae, J. J., Gunes, F., Choi, J.-Y. and Lee, Y. H. Low-temperature graphene growth using epochal catalyst of PdCo alloy. *Applied Physics Letters* **99**, 223102-3 (2011)

25. Kumar, S., McEvoy, N., Lutz, T., Keeley, G. P., Nicolosi, V., Murray, C. P., Blau, W. J. and Duesberg, G. S. Gas phase controlled deposition of high quality large-area graphene films. *Chemical Communications* **46**, 1422-1424 (2010)

26. Liu, W., Li, H., Xu, C., Khatami, Y. and Banerjee, K. Synthesis of high-quality monolayer and bilayer graphene on copper using chemical vapor deposition. *Carbon* **49**, 4122-4130 (2011)

27. Reina, A., Thiele, S., Jia, X., Bhaviripudi, S., Dresselhaus, M., Schaefer, J. and Kong, J. Growth of large-area single- and Bi-layer graphene by controlled carbon precipitation on polycrystalline Ni surfaces. *Nano Research* **2**, 509-516 (2009)

28.   Chen, S., Cai, W., Piner, R. D., Suk, J. W., Wu, Y., Ren, Y., Kang, J. and Ruoff, R. S. Synthesis and Characterization of Large-Area Graphene and Graphite Films on Commercial Cu-Ni Alloy Foils. *Nano Letters* **11**, 3519-3525 (2011)

29.   Chae, S. J., Güneş, F., Kim, K. K., Kim, E. S., Han, G. H., Kim, S. M., Shin, H.-J., Yoon, S.-M., Choi, J.-Y., Park, M. H., Yang, C. W., Pribat, D. and Lee, Y. H. Synthesis of Large-Area Graphene Layers on Poly-Nickel Substrate by Chemical Vapor Deposition: Wrinkle Formation. *Advanced Materials* **21**, 2328-2333 (2009)

30.   Yu, Q., Lian, J., Siriponglert, S., Li, H., Chen, Y. P. and Pei, S.-S. Graphene segregated on Ni surfaces and transferred to insulators. *Applied Physics Letters* **93**, 113103-3 (2008)

31.   Oshima, C. and Ayato, N. Ultra-thin epitaxial films of graphite and hexagonal boron nitride on solid surfaces. *Journal of Physics: Condensed Matter* **9**, 1 (1997)

32.   López, G. A. and Mittemeijer, E. J. The solubility of C in solid Cu. *Scripta Materialia* **51**, 1-5 (2004)

33.   Mattevi, C., Kim, H. and Chhowalla, M. A review of chemical vapour deposition of graphene on copper. *Journal of Materials Chemistry* **21**, 3324-3334 (2011)

34.   Li, X., Cai, W., Colombo, L. and Ruoff, R. S. Evolution of Graphene Growth on Ni and Cu by Carbon Isotope Labeling. *Nano Letters* **9**, 4268-4272 (2009)

35.   Earnshaw, A. and Harrington, T. J. The chemistry of the transition elements. Oxford University Press (1972)

36.   Sutter, P., Hybertsen, M. S., Sadowski, J. T. and Sutter, E. Electronic Structure of Few-Layer Epitaxial Graphene on Ru(0001). *Nano Letters* **9**, 2654-2660 (2009)

37.   L처pez, G. A. and Mittemeijer, E. J. The solubility of C in solid Cu. *Scripta Materialia* **51**, 1-5 (2004)

38.   Sun, Z., Hämäläinen, S. K., Sainio, J., Lahtinen, J., Vanmaekelbergh, D. and Liljeroth, P. Topographic and electronic contrast of the graphene moiré on Ir(111) probed by scanning tunneling microscopy and noncontact atomic force microscopy. *Physical Review B* **83**, 081415 (2011)

39.   Ding, Y., Gao, P. X. and Wang, Z. L. Catalyst-Nanostructure Interfacial Lattice Mismatch in Determining the Shape of VLS Grown Nanowires and Nanobelts: A Case of Sn/ZnO. *Journal of the American Chemical Society* **126**, 2066-2072 (2004)

40.   Reich, S., Maultzsch, J., Thomsen, C. and Ordej처n, P. Tight-binding description of graphene. *Physical Review B* **66**, 035412 (2002)

41.   Chang, T.-M. and Carter, E. A. Structures and Growth Mechanisms for Heteroepitaxial fcc(111) Thin Metal Films. *The Journal of Physical Chemistry* **99**, 7637-7648 (1995)

42.   Preobrajenski, A. B., Ng, M. L., Vinogradov, A. S. and Mårtensson, N. Controlling graphene corrugation on lattice-mismatched substrates. *Physical Review B* **78**, 073401 (2008)

43.   Pletikosić, I., Kralj, M., Pervan, P., Brako, R., Coraux, J., N'Diaye, A. T., Busse, C. and Michely, T. Dirac Cones and Minigaps for Graphene on Ir(111). *Physical Review Letters* **102**, 056808 (2009)

44.   Sutter, P., Sadowski, J. T. and Sutter, E. Graphene on Pt(111): Growth and substrate interaction.

Physical Review B **80**, 245411 (2009)

45.   Bao, W., Miao, F., Chen, Z., Zhang, H., Jang, W., Dames, C. and Lau, C. N. Controlled ripple texturing of suspended graphene and ultrathin graphite membranes. *Nat Nano* **4**, 562-566 (2009)

46.   Liu, N., Pan, Z., Fu, L., Zhang, C., Dai, B. and Liu, Z. The origin of wrinkles on transferred graphene. *Nano Research* **4**, 996-1004 (2011)

47.   http://www.ion-beam-services.com/

48.   Ziegler, J. F., Ziegler, M. D. and Biersack, J. P. SRIM – The stopping and range of ions in matter (2010). *Nuclear Instruments and Methods in Physics Research Section B: Beam Interactions with Materials and Atoms* **268**, 1818-1823 (2010)

49.   Lander, J. J., Kern, H. E. and Beach, A. L. Solubility and Diffusion Coefficient of Carbon in Nickel: Reaction Rates of Nickel-Carbon Alloys with Barium Oxide. *Journal of Applied Physics* **23**, 1305-1309 (1952)

50.   Bolotov, L., Vakar, Z., Gall', N., Makarenko, I., Rut'kov, E., Titkov, A., Tontegode, A. and Usufov, M. Topographic study by scanning-tunneling microscopy of a two-dimensional graphite film on Re(1010). *Physics of the Solid State* **40**, 1423-1426 (1998)

51.   Ferrari, A. C., Meyer, J. C., Scardaci, V., Casiraghi, C., Lazzeri, M., Mauri, F., Piscanec, S., Jiang, D., Novoselov, K. S., Roth, S. and Geim, A. K. Raman Spectrum of Graphene and Graphene Layers. *Physical Review Letters* **97**, 187401 (2006)

52.   Wang, W. X., Liang, S. H., Yu, T., Li, D. H., Li, Y. B. and Han, X. F. The study of interaction between graphene and metals by Raman spectroscopy. *Journal of Applied Physics* **109**, 07C501-3 (2011)

53.   Lin, M., Tan, J. P. Y., Boothroyd, C., Loh, K. P., Tok, E. S. and Foo, Y.-L. Dynamical Observation of Bamboo-like Carbon Nanotube Growth. *Nano Letters* **7**, 2234-2238 (2007)

54.   Helveg, S., Lopez-Cartes, C., Sehested, J., Hansen, P. L., Clausen, B. S., Rostrup-Nielsen, J. R., Abild-Pedersen, F. and Norskov, J. K. Atomic-scale imaging of carbon nanofibre growth. *Nature* **427**, 426-429 (2004)

55.   Abild-Pedersen, F., Nørskov, J. K., Rostrup-Nielsen, J. R., Sehested, J. and Helveg, S. Mechanisms for catalytic carbon nanofiber growth studied by ab initio density functional theory calculations. *Physical Review B* **73**, 115419 (2006)

56.   He, Z. B., Maurice, J. L., Lee, C. S., Gohier, A., Pribat, D., Legagneux, P. and Cojocaru, C. S. Etchant-induced shaping of nanoparticle catalysts during chemical vapour growth of carbon nanofibres. *Carbon* **49**, 435-444 (2011)

57.   Hofmann, S., Sharma, R., Ducati, C., Du, G., Mattevi, C., Cepek, C., Cantoro, M., Pisana, S., Parvez, A., Cervantes-Sodi, F., Ferrari, A. C., Dunin-Borkowski, R., Lizzit, S., Petaccia, L., Goldoni, A. and Robertson, J. In situ Observations of Catalyst Dynamics during Surface-Bound Carbon Nanotube Nucleation. *Nano Letters* **7**, 602-608 (2007)

58.   Marchini, S., Günther, S. and Wintterlin, J. Scanning tunneling microscopy of graphene on Ru(0001). *Physical Review B* **76**, 075429 (2007)

59. Zhu, H., Suenaga, K., Hashimoto, A., Urita, K., Hata, K. and Iijima, S. Atomic-Resolution Imaging of the Nucleation Points of Single-Walled Carbon Nanotubes. *Small* **1**, 1180-1183 (2005)

60. Rodríguez-Manzo, J. A., Janowska, I., Pham-Huu, C., Tolvanen, A., Krasheninnikov, A. V., Nordlund, K. and Banhart, F. Growth of Single-Walled Carbon Nanotubes from Sharp Metal Tips. *Small* **5**, 2710-2715 (2009)

61. He, Z., Maurice, J.-L., Gohier, A., Lee, C. S., Pribat, D. and Cojocaru, C. S. Iron Catalysts for the Growth of Carbon Nanofibers: Fe, Fe3C or Both? *Chemistry of Materials* **23**, 5379-5387 (2011)

62. Laurent Baraton and Zhanbing He and Chang Seok Lee and Jean-Luc Maurice and Costel Sorin Cojocaru and Anne-Fran챌oise Gourgues-Lorenzon and Young Hee Lee and Didier, P. Synthesis of few-layered graphene by ion implantation of carbon in nickel thin films. *Nanotechnology* **22**, 085601

63. Morgan, A. E. and Somorjai, G. A. Low energy electron diffraction studies of gas adsorption on the platinum (100) single crystal surface. *Surface Science* **12**, 405-425 (1968)

64. Eizenberg, M. and Blakely, J. M. Carbon monolayer phase condensation on Ni(111). *Surface Science* **82**, 228-236 (1979)

65. Shelton, J. C., Patil, H. R. and Blakely, J. M. Equilibrium segregation of carbon to a nickel (111) surface: A surface phase transition. *Surface Science* **43**, 493-520 (1974)

66. Eizenberg, M. and Blakely, J. M. Carbon interaction with nickel surfaces: Monolayer formation and structural stability. *The Journal of Chemical Physics* **71**, 3467-3477 (1979)

67. Piscanec, S., Lazzeri, M., Robertson, J., Ferrari, A. C. and Mauri, F. Optical phonons in carbon nanotubes: Kohn anomalies, Peierls distortions, and dynamic effects. *Physical Review B* **75**, 035427 (2007)

68. Berger, H. H. Models for contacts to planar devices. *Solid-State Electronics* **15**, 145-158 (1972)

Outline

Chapter VI. Conclusions and Perspectives 157

Chapter VI. Conclusions and Perspectives

6.1. Conclusions

Since the discovery of graphite, fullerene, carbon nanotube, and graphene, all the known forms of carbon allotropes have been intensively investigated. For such a long time, fundamental knowledge has been accumulated on graphene due to the fact that graphene is the basic building block for all others. However still, isolating or directly growing a single graphene sheet remains a challenge.

Theoretical physicists first succeeded in isolation of graphene, by the micromechanical exfoliation of HOPG (Highly Oriented Pyrolytic Graphite) [1]. This technique or other early preparation methods, such as chemical exfoliation of HOPG [2] or epitaxial growth by high-temperature annealing of SiC (0001) in UHV (ultra-high vacuum)[3], appeared to fall short in terms of reproducibility or scalability. In contrast, methods involving the catalytic crystallization of graphene on a metallic substrate, compatible with large-area fabrication, appeared well adapted to meet the requirements for industrial application.

Chemical vapor deposition (CVD) on a metallic substrate[4, 5] is now considered as a strong candidate for large-area and uniform graphene growth. Such a route, however, has two critical limitations: one is high-temperature processing (~ 1000 °C) – low-temperature is always preferable in an industrial perspective – and the other one is the necessity of transferring on an insulating (functional) substrate, which introduces not only an additional step in the process, but also structural defects and chemical contamination.

In the present thesis work, we investigated new graphene growth techniques with the idea to limit or suppress those drawbacks. We focused on two techniques differentiated by the way the carbon atoms are introduced into the metal catalyst film: (i) direct-current plasma-enhanced CVD (dc-PECVD) and (ii) carbon ion implantation.

(i) The plasma-assisted graphene growth process consists in the exposure of the metal film to a highly reactive plasma to introduce carbon atoms at and near the film surface. Performing this at elevated temperature makes the carbon atoms to diffuse throughout the film. Our team had developed a large experience of dc-PECVD in the growth of vertically aligned carbon nanotubes. Here, we have adapted this method to graphene growth: we were thus able to prepare graphene layers on Ni at 450 °C. Moreover, in addition to the top-surface layer, we obtained with this technique another graphene layer in-between Ni and the underlying insulating substrate (SiO$_2$ or glass)[32-34]. That second graphene layer placing itself directly on the insulating (functional) substrate, we developed a simple process for using it directly as a sensor without transfer[34]. This: direct growth of graphene on an insulating substrate and its direct use in a functioning device, can be considered as the main achievement of the present thesis work.

(ii) We were the first to propose carbon ion implantation for supplying carbon atoms to the Ni layer, prior to obtaining graphene upon annealing[35, 36]. By separating introduction and annealing, this technique allowed us to isolate important factors of a heat treatment. Thus, through precise control of carbon dose/implantation energy, we were able, by using this method, to get fundamental insight into the graphene growth mechanisms[37].

For most of the experiments, we employed nickel as catalyst, under the form of 200-nm thick films deposited by e-beam evaporation onto an insulating substrate. For PECVD, we used a high density and highly reactive plasma generated by the combination of CH_4 and H_2. We applied a procedure patented[35] by our team, which postulated that two graphene layers could be formed (at the surface and at the interface). We thus confirmed this postulate and preliminary experiments[38]. In such a process, the surface graphitic layer includes damages due to direct exposure to plasma. The underlying graphene on insulating substrate is protected from plasma exposure and requires no transfer for its use.

We have shown, with our implantation experiments[37], that carbon diffusion is very significant in redistributing carbon in Ni, especially through grain boundaries. In PECVD, grain boundaries would help driving C to the interface, but a complex mechanism related to plasma also has to be taken into account: we obtained interfacial graphene with PECVD while we did not get it with implantation. We now explain this absence of interface graphene after implantation by observing that carbon diffusion in Ni is quite fast[39], so that most of implanted carbon atoms will out-diffuse (within a few tens of seconds at 450 °C) rather than precipitate at interface. Thus the PECVD growth includes a complex – probably dynamic – mechanism that promotes precipitation at the interface.

Due to this fast diffusion, the final carbon distribution in a Ni film thus depends on the annealing treatment that is applied during or after carbon has been introduced. We showed in particular that two kinds of graphitic materials are obtained after a given treatment: one under the form of single crystals of few-layer graphene/graphite, grown during the high temperature plateau, and a second under the form of nanocrystalline few-layer graphene, grown during cooling.

Finally, on the graphene grown by PECVD directly on glass at low temperature, we thus developed a humidity sensor, by direct electrode printing. Beyond this proof of concept, we need to further investigate growth mechanisms and annealing conditions for the development of various transfer-free, low-temperature, graphene applications.

To conclude, we believe that the research carried out during this thesis work has brought a significant brick in the building and understanding of low-cost methods for making functional graphene devices.

6.2. Perspectives

Using a highly reactive plasma, we succeeded in growing nanocrystalline graphene directly on insulating substrate. As grain boundaries (GBs) would increase sensor properties, this would be a good approach to enhance the sensing performance of graphene-based devices[51-54]. However, those defects also diffuse charge carriers; this means that an optimization process between sensing capability and signal transport is required. Thus, engineering of graphene crystallinity from nanocrystalline to microcrystalline order will be a highly interesting research subject in the years to come, as it will bring a new understanding of these two effects of GBs. Various catalyst metals including alloy structure could be further studied with enlargement of grain size by pre-annealing process.

Ion implantation for graphene growth is definitely a novel technique that possibly can be used in functional way.

(i) In general, the conventional lithography process (photo-resist (PR) coating, UV exposure, PR develop, oxygen plasma etching, PR strip) on graphene is required for device applications. However, it is very difficult to get graphene having smooth edges, thus the performance of device is limited by edge effects. Using pre-patterned catalyst, several of graphene forms, such as graphene nanoribbons (GNRs), graphene quantum dots (GQDs), and graphene channels for transistors, can be grown with smooth edges. Source and drain electrodes could be simply deposited on patterned-graphene, thus allowing one to investigate the performance of graphene itself.

(ii) Furthermore, carbon ions can be implanted on a sort of mask; then, via annealing treatment, we can grow patterned graphene at desired local position. To make precise structures of graphene pattern, we can possibly use inversion-mask of one used for implantation, which aims to apply some chemical/physical treatment that could suppress the carbon precipitation. This will lead to the formation of "*precipitation-barrier*", thus patterned-graphene could be appeared with better resolution.

(iii) If we can find suitable insulating substrates where carbon could be implanted and then precipitate on it, ion implantation would be a strong technique for graphene applications. For example, carbon could be implanted on surfaces that correspond to electrodes and channel area, and then we could repeat ion implantation on channel for the formation of bilayer graphene. After annealing process, bilayer graphene would be connected to both electrodes (of single layer graphene). Thus, such a self-assembled graphene transistor would be expected to have the lowest contact resistance between electrode and channel.

To realize the full potential of the techniques we have used (dc-PECVD and implantation), however, perfect control of both carbon diffusion and precipitation in/on metal is a prerequisite condition. There is a lot of interconnected factors that can influence graphene growth, i.e. implantation or plasma energy, carbon dose, types of substrate, annealing conditions (temperature, increasing/decreasing speed, annealing time, surrounding atmosphere). Among those factors, we have found out in the present work that the cooling condition in annealing treatments tends to be the most critical parameter. Thus, cooling speed and surrounding atmosphere during cooling (vacuum, or nitrogen, argon, and hydrogen[55, 56]) should be extensively studied to understand more of the growth mechanisms associated with precipitation from a solid mixture or solution.

As the present work comes to its end, we are investigating these mechanisms by using a new technique, which we call "Sub-plantation", where the carbon atoms are implanted at low energy into the metallic film. Our team started this development in order to reproduce some of the dc-PECVD conditions in ultra-high vacuum and ultra-clean environment, after realizing that the carbon radicals had a significant kinetic energy in the dc-PECVD process (where the electric field reaches several hundreds of volts). The team thus designed an ultra-high vacuum (UHV) chamber jointly equipped with a carbon ion gun on the one hand and XPS, LEED and Auger analysis on the other hand: "FENIX" – Facility for Elaboration of Nanomaterials with In-situ analysis at EcolePolytechnique (X). In FENIX, we can keep carbon contamination to a minimum, which is mandatory to understand the formation of graphene on the catalytic layer.

With such a sub-plantation in a single-crystal metal film epitaxied on a single crystal insulating substrate, one should be able to (1) better understand the way a metal surface helps building up the graphene lattice and (2) develop high-quality low-temperature graphene films directly on a functional substrate.

Reference

1.   Novoselov, K. S., Geim, A. K., Morozov, S. V., Jiang, D., Zhang, Y., Dubonos, S. V., Grigorieva, I. V. and Firsov, A. A. Electric Field Effect in Atomically Thin Carbon Films. *Science* **306**, 666-669 (2004)

2.   Li, X., Wang, X., Zhang, L., Lee, S. and Dai, H. Chemically Derived, Ultrasmooth Graphene Nanoribbon Semiconductors. *Science* **319**, 1229-1232 (2008)

3.   Berger, C., Song, Z., Li, T., Li, X., Ogbazghi, A. Y., Feng, R., Dai, Z., Marchenkov, A. N., Conrad, E. H., First, P. N. and de Heer, W. A. Ultrathin Epitaxial Graphite: 2D Electron Gas Properties and a Route toward Graphene-based Nanoelectronics. *The Journal of Physical Chemistry B* **108**, 19912-19916 (2004)

4.   Reina, A., Jia, X., Ho, J., Nezich, D., Son, H., Bulovic, V., Dresselhaus, M. S. and Kong, J. Large Area, Few-Layer Graphene Films on Arbitrary Substrates by Chemical Vapor Deposition. *Nano Letters* **9**, 30-35 (2008)

5.   Li, X., Cai, W., An, J., Kim, S., Nah, J., Yang, D., Piner, R., Velamakanni, A., Jung, I., Tutuc, E., Banerjee, S. K., Colombo, L. and Ruoff, R. S. Large-Area Synthesis of High-Quality and Uniform Graphene Films on Copper Foils. *Science* **324**, 1312-1314 (2009)

6.   Obraztsov, A. N., Obraztsova, E. A., Tyurnina, A. V. and Zolotukhin, A. A. Chemical vapor deposition of thin graphite films of nanometer thickness. *Carbon* **45**, 2017-2021 (2007)

7.   Hojati-Talemi, P. and Simon, G. P. Field emission study of graphene nanowalls prepared by microwave-plasma method. *Carbon* **49**, 2875-2877 (2011)

8.   Yamada, T., Ishihara, M., Kim, J., Hasegawa, M. and Iijima, S. A roll-to-roll microwave plasma chemical vapor deposition process for the production of 294 mm width graphene films at low temperature. *Carbon* **50**, 2615-2619 (2012)

9.   Yuan, G. D., Zhang, W. J., Yang, Y., Tang, Y. B., Li, Y. Q., Wang, J. X., Meng, X. M., He, Z. B., Wu, C. M. L., Bello, I., Lee, C. S. and Lee, S. T. Graphene sheets via microwave chemical vapor deposition. *Chemical Physics Letters* **467**, 361-364 (2009)

10.   Vitchev, R., Malesevic, A., Roumen, H. P., Kemps, R., Mertens, M., Vanhulsel, A. and Haesendonck, C. V. Initial stages of few-layer graphene growth by microwave plasma-enhanced chemical vapour deposition. *Nanotechnology* **21**, 095602 (2010)

11.   Kalita, G., Wakita, K. and Umeno, M. Low temperature growth of graphene film by microwave assisted surface wave plasma CVD for transparent electrode application. *RSC Advances* **2**, 2815-2820 (2012)

12.   Kim, E. S., Shin, H.-J., Yoon, S.-M., Han, G. H., Chae, S. J., Bae, J. J., Gunes, F., Choi, J.-Y. and Lee, Y. H. Low-temperature graphene growth using epochal catalyst of PdCo alloy. *Applied Physics Letters* **99**, 223102-3 (2011)

13.   Kim, Y., Song, W., Lee, S. Y., Jeon, C., Jung, W., Kim, M. and Park, C. Y. Low-temperature synthesis of graphene on nickel foil by microwave plasma chemical vapor deposition. *Applied Physics Letters* **98**, 263106-3 (2011)

14.   Kumar, A., Voevodin, A. A., Zemlyanov, D., Zakharov, D. N. and Fisher, T. S. Rapid synthesis of few-layer graphene over Cu foil. *Carbon* **50**, 1546-1553 (2012)

15.   Dato, A., Radmilovic, V., Lee, Z., Phillips, J. and Frenklach, M. Substrate-Free Gas-Phase Synthesis of Graphene Sheets. *Nano Letters* **8**, 2012-2016 (2008)

16.   Dato, A. and Michael, F. Substrate-free microwave synthesis of graphene: experimental conditions and hydrocarbon precursors. *New Journal of Physics* **12**, 125013 (2010)

17.   Malesevic, A., Vitchev, R., Schouteden, K., Volodin, A., Zhang, L., Tendeloo, G. V., Vanhulsel, A. and Chris Van, H. Synthesis of few-layer graphene via microwave plasma-enhanced chemical vapour deposition. *Nanotechnology* **19**, 305604 (2008)

18.   Wang, S. M., Pei, Y. H., Wang, X., Wang, H., Meng, Q. N., Tian, H. W., Zheng, X. L., Zheng, W. T. and Liu, Y. C. Synthesis of graphene on a polycrystalline Co film by radio-frequency plasma-enhanced chemical vapour deposition. *Journal of Physics D: Applied Physics* **43**, 455402 (2010)

19.   Zhu, M., Wang, J., Holloway, B. C., Outlaw, R. A., Zhao, X., Hou, K., Shutthanandan, V. and Manos, D. M. A mechanism for carbon nanosheet formation. *Carbon* **45**, 2229-2234 (2007)

20.   Lee, B.-J., Yu, H.-Y. and Jeong, G.-H. Controlled Synthesis of Monolayer Graphene Toward Transparent Flexible Conductive Film Application. *Nanoscale Research Letters* **5**, 1768 - 1773 (2010)

21.   Kalita, G., Kayastha, M. S., Uchida, H., Wakita, K. and Umeno, M. Direct growth of nanographene films by surface wave plasma chemical vapor deposition and their application in photovoltaic devices. *RSC Advances* **2**, 3225-3230 (2012)

22.   Terasawa, T.-o. and Saiki, K. Growth of graphene on Cu by plasma enhanced chemical vapor deposition. *Carbon* **50**, 869-874 (2012)

23.   Kim, J., Tsugawa, K., Ishihara, M., Koga, Y. and Hasegawa, M. Large-area surface wave plasmas using microwave multi-slot antennas for nanocrystalline diamond film deposition. *Plasma Sources Science and Technology* **19**, 015003 (2010)

24.   Woo, Y., Kim, D.-C., Jeon, D.-Y., Chung, H.-J., Shin, S.-M., Li, X.-S., Kwon, Y.-N., Seo, D. H., Shin, J., Chung, U. I. and Seo, S. Large-grained and Highly-ordered Graphene Synthesized by Radio Frequency Plasma-enhanced Chemical Vapor Deposition. *ECS Transactions* **19**, 111-114 (2009)

25.   Kim, J., Ishihara, M., Koga, Y., Tsugawa, K., Hasegawa, M. and Iijima, S. Low-temperature synthesis of large-area graphene-based transparent conductive films using surface wave plasma chemical vapor deposition. *Applied Physics Letters* **98**, 091502-3 (2011)

26.   Lee, B.-J., Lee, T.-W., Park, S., Yu, H.-Y., Lee, J.-O., Lim, S.-H. and Jeong, G.-H. Low-temperature synthesis of thin graphite sheets using plasma-assisted thermal chemical vapor deposition system. *Materials Letters* **65**, 1127-1130 (2011)

27.   Kumar, S., Levchenko, I., Cheng, Q. J., Shieh, J. and Ostrikov, K. Plasma enables edge-to-center-oriented graphene nanoarrays on Si nanograss. *Applied Physics Letters* **100**, 053115-4 (2012)

28.   Qi, J. L., Zheng, W. T., Zheng, X. H., Wang, X. and Tian, H. W. Relatively low temperature synthesis of graphene by radio frequency plasma enhanced chemical vapor deposition. *Applied Surface Science*

257, 6531-6534 (2011)

29.   Lee, J.-K., Chung, H.-J., Heo, J., Seo, S., Cho, I. H., Kwon, H.-I. and Lee, J.-H. Reliability of bottom-gate graphene field-effect transistors prepared by using inductively coupled plasma-chemical vapor deposition. *Applied Physics Letters* **98**, 193504-3 (2011)

30.   Nandamuri, G., Roumimov, S. and Solanki, R. Remote plasma assisted growth of graphene films. *Applied Physics Letters* **96**, 154101-3 (2010)

31.   Jaeho, L., Hyun-Jong, C., Jaehong, L., Hyungcheol, S., Jinseong, H., Heejun, Y., Sung-Hoon, L., Sunae, S., Jaikwang, S., Chung, U. i., Inkyeong, Y. and Kinam, K. in Electron Devices Meeting (IEDM), 2010 IEEE International 23.5.1-23.5.4 (2010).

32.   Lee, C. S., Baraton, L., He, Z., Maurice, J.-L., Chaigneau, M., Pribat, D. and Cojocaru, C. S. in Carbon Nanotubes, Graphene, and Associated Devices III 77610P-7 (SPIE, San Diego, California, USA, 2010).

33.   Lee, C. S., Baraton, L., He, Z., Maurice, J.-L., Pribat, D. and Cojocaru, C. S. Graphene growth directly on functional substrate. HAL, hal-00525357 (2010)

34.   Lee, C. S., Cojocaru, C. S., Moujahid, W., Lebental, B., Chaigneau, M., Châtelet, M., Normand, F. L. and Jean-Luc, M. Synthesis of conducting transparent few-layer graphene directly on glass at 450 °C. *Nanotechnology* **23**, 265603 (2012)

35.   Baraton, L., Cojocaru, C. S. and Pribat, D. Process for controlled growth of graphene films. International Patent No. 0805769-2008 (2008)

36.   Baraton, L., He, Z., Lee, C. S., Maurice, J.-L., Cojocaru, C. S., Gourgues-Lorenzon, A.-F., Lee, Y. H. and Pribat, D. Synthesis of few-layered graphene by ion implantation of carbon in nickel thin films. *Nanotechnology* **22**, 085601 (2011)

37.   Baraton, L., He, Z. B., Lee, C. S., Cojocaru, C. S., Châtelet, M., Maurice, J.-L., Lee, Y. H. and Pribat, D. On the mechanisms of precipitation of graphene on nickel thin films. *EPL (Europhysics Letters)* **96**, 46003 (2011)

38.   Baraton, L., Gangloff, L., Xavier, S., Cojocaru, C. S., Huc, V., Legagneux, P., Lee, Y. H. and Pribat, D. in Carbon Nanotubes, Graphene, and Associated Devices II 73990T (SPIE, San Diego, California, USA, 2009).

39.   Lander, J. J., Kern, H. E. and Beach, A. L. Solubility and Diffusion Coefficient of Carbon in Nickel: Reaction Rates of Nickel-Carbon Alloys with Barium Oxide. *Journal of Applied Physics* **23**, 1305-1309 (1952)

40.   Zhang, L., Shi, Z., Wang, Y., Yang, R., Shi, D. and Zhang, G. Catalyst-free growth of nanographene films on various substrates. *Nano Research* **4**, 315-321 (2011)

41.   Yang, W., He, C., Zhang, L., Wang, Y., Shi, Z., Cheng, M., Xie, G., Wang, D., Yang, R., Shi, D. and Zhang, G. Growth, Characterization, and Properties of Nanographene. *Small* **8**, 1429-1435 (2012)

42.   Jerng, S. K., Yu, D. S., Kim, Y. S., Ryou, J., Hong, S., Kim, C., Yoon, S., Efetov, D. K., Kim, P. and Chun, S. H. Nanocrystalline Graphite Growth on Sapphire by Carbon Molecular Beam Epitaxy. *The Journal of Physical Chemistry C* **115**, 4491-4494 (2011)

43.   Lippert, G., Dabrowski, J., Lemme, M., Marcus, C., Seifarth, O. and Lupina, G. Direct graphene growth on insulator. *physica status solidi (b)* **248**, 2619-2622 (2011)

44.   Bi, H., Sun, S., Huang, F., Xie, X. and Jiang, M. Direct growth of few-layer graphene films on SiO2 substrates and their photovoltaic applications. *Journal of Materials Chemistry* **22**, 411-416 (2012)

45.   Jerng, S. K., Lee, J. H., Yu, D. S., Kim, Y. S., Ryou, J., Hong, S., Kim, C., Yoon, S. and Chun, S. H. Graphitic Carbon Growth on MgO(100) by Molecular Beam Epitaxy. *The Journal of Physical Chemistry C* **116**, 7380-7385 (2012)

46.   Sun, J., Lindvall, N., Cole, M. T., Teo, K. B. K. and Yurgens, A. Large-area uniform graphene-like thin films grown by chemical vapor deposition directly on silicon nitride. *Applied Physics Letters* **98**, 252107-3 (2011)

47.   Hong, G., Wu, Q.-H., Ren, J. and Lee, S.-T. Mechanism of non-metal catalytic growth of graphene on silicon. *Applied Physics Letters* **100**, 231604-5 (2012)

48.   Medina, H., Lin, Y.-C., Jin, C., Lu, C.-C., Yeh, C.-H., Huang, K.-P., Suenaga, K., Robertson, J. and Chiu, P.-W. Metal-Free Growth of Nanographene on Silicon Oxides for Transparent Conducting Applications. *Advanced Functional Materials* **22**, 2123-2128 (2012)

49.   Teng, P.-Y., Lu, C.-C., Akiyama-Hasegawa, K., Lin, Y.-C., Yeh, C.-H., Suenaga, K. and Chiu, P.-W. Remote Catalyzation for Direct Formation of Graphene Layers on Oxides. *Nano Letters* **12**, 1379-1384 (2012)

50.   Scott, A., Dianat, A., Borrnert, F., Bachmatiuk, A., Zhang, S., Warner, J. H., Borowiak-Palen, E., Knupfer, M., Buchner, B., Cuniberti, G. and Rummeli, M. H. The catalytic potential of high-kappa dielectrics for graphene formation. *Applied Physics Letters* **98**, 073110-3 (2011)

51.   Ohba, T. and Kanoh, H. Intensive Edge Effects of Nanographenes in Molecular Adsorptions. *The Journal of Physical Chemistry Letters* **3**, 511-516 (2012)

52.   Salehi-Khojin, A., Estrada, D., Lin, K. Y., Bae, M.-H., Xiong, F., Pop, E. and Masel, R. I. Polycrystalline Graphene Ribbons as Chemiresistors. *Advanced Materials* **24**, 53-57 (2012)

53.   Araujo, P. T., Terrones, M. and Dresselhaus, M. S. Defects and impurities in graphene-like materials. *Materials Today* **15**, 98-109 (2012)

54.   Terrones, H., Lv, R., Terrones, M. and Mildred, S. D. The role of defects and doping in 2D graphene sheets and 1D nanoribbons. *Reports on Progress in Physics* **75**, 062501 (2012)

55.   Gao, L., Ren, W., Zhao, J., Ma, L.-P., Chen, Z. and Cheng, H.-M. Efficient growth of high-quality graphene films on Cu foils by ambient pressure chemical vapor deposition. *Applied Physics Letters* **97**, 183109-3 (2010)

56.   Vlassiouk, I., Regmi, M., Fulvio, P., Dai, S., Datskos, P., Eres, G. and Smirnov, S. Role of Hydrogen in Chemical Vapor Deposition Growth of Large Single-Crystal Graphene. *ACS Nano* **5**, 6069-6076 (2011)

Chang Seok LEE

Tel. +82 (0)31 280 8227
Mob. +82 (0)10 8707 4584
cs0801.lee@samsung.com
cslee0801@gmail.com

Personal Information

Work Address	Graphene Center, **Samsung Advanced Institute of Technology (SAIT)** San 14-1, Nongseo-Dong, Giheung-Gu, Yongin, Gyeonggi-Do 446-712, Korea
Nationality	Rep. of Korea (South Korea)
Date of Birth	01 August 1984

Research Interest

Development of Low-dimensional Materials   **– Graphene, h-BN, MoS_2 (2-D)**

– CNTs/CNFs, Si NWs (1-D)

– Topological insulator

- Growth of High Quality Graphene/CNTs at Low Temperature
- Toward Transfer-free Graphene Applications
- Graphene/CNTs-based Multifunctional Sensing Platform
- Transparent, Conducting, Printable, Stretchable, Foldable Opto-electronics
- Carbon-based Nanostructure as an Electron Source in part of X-ray or Display

Education

10. Oct. 2012	PhD defense at Amphi. Carnot, Ecole Polytechnique
Oct.2009 ~ Sep.2012	**Ph.D. Candidate** LPICM-Ecole Polytechnique, France Supervisor: **Prof. Jean-Luc Maurice**
Feb.2008 ~ Sep.2009	**MSc** Ingénierie de I'Innovation Technologique and Laboratoire de Physique des Interfaces et Couches Minces (LPICM) Ecole Polytechnique, France Supervisor: **Prof. Didier Pribat**
Feb.2007 ~ Jan.2008	**MSc** Department of Information Display and Advanced Display Research Center (ADRC), Kyung Hee University, South Korea Supervisor: **Prof. Kyu Chang Park**
Mar.2003 ~ Feb.2007	**Dual degree Bachelor** of Physics, Information Display, Kyung Hee University, South Korea Supervisor: **Prof. Jin Jang**

Award or Scholarship

Oct.2011 ~ Sep.2012	ITA(Ingénieur Technicien Assistant), CNRS[*]
Oct.2009 ~ Sep.2010	5th Blaise Pascal Scholarship, Managing by France-Korea Government
Mar.2008 ~ Aug.2009	Scholarship by President of graduate school from KHU[**]
Mar.2007 ~ Feb.2008	Scholarship from MEST[***]
Sep.2006 ~ Dec.2006	Scholarship from MEST[***]
Sep.2003 ~ Jul.2005	Scholarship for Outstanding Students from KHU[**]

Work Experience

Nov.2012 ~	**SAIT[*], Graphene Research Center**, Senior Research Scientist
Aug.2011 ~ Sep.2012	**NNPC**(National Nanotechnology Policy Center), Korea
Aug.2010 ~ Present	GTB(Global Trends Briefing) Reporter operating by **KISTI[**]**
Jan.2009 ~ Dec.2011	**SAIT Europe**
Feb.2008 ~ Sep.2009	Internship at **LPICM, Ecole Polytechnique**
	High quality CNT/CNF Growth using water vapor chemistry
Aug.2008 ~ Jul.2009	Participation in Project (Directed by Prof. Park Hun-Kuk)
	"Nano-Technology based Novel Radiographic System Research Center", Supported by SDI[***]

Publications in Journal/Proceedings[*]

* referred to Web of Science

01. **Chang Seok Lee**, Costel Sorin Cojocaru, Waleed Moujahid, Bérengère Lebental, Marc Chaigneau, Marc Châtelet, François Le Normand and Jean-Luc Maurice
Synthesis of conducting transparent few-layer graphene directly on glass at 450 ^{o}C
Nanotechnology **23**, 265603 (2012)

02. Z. B. He, J.-L. Maurice, Aurélien Gohier, **Chang Seok Lee**, D. Pribat, and C. S. Cojocaru
Iron catalysts for the growth of carbon nanofibers: Fe or Fe_3C?
Chemistry of Materials **23**(24), 5379-5387 (2011)

03. L. Baraton, Z. B. He, **C. S. Lee**, J.-L. Maurice, C.-S. Cojocaru, Y. H. Lee, D. Pribat
On the Mechanisms of Precipitation of Graphene on Nickel
Europhys. Lett. **96**(4), 46003 (2011)

04. Z. B. He, **C. S. Lee**, J.-L. Maurice, D. Pribat, P. Haghi-Ashtiani, and C. S. Cojocaru
Vertically oriented nickel nanorods/carbon nanofibers core/shell structures synthesized by plasma-enhanced chemical vapor deposition
Carbon **49**(14), 4710-4718 (2011)

05. L. Baraton, Z. B. He, **C. S. Lee**, J.-L. Maurice, C.-S. Cojocaru, Y. H. Lee, D. Pribat
Synthesis of few-layers graphene by ion implantation of carbon in nickel thin films

Nanotechnology **22**, 085601 (2011)

06. Z. B. He, J.-L. Maurice, **C. S. Lee**, A. Gohier, D. Pribat, and C.-S. Cojocaru,
Etchant-induced shaping of nanoparticle catalysts during chemical vapor deposition of carbon nanofibres
Carbon **49**(2), 435-444 (2011)

07. **C. S. Lee**, L. Baraton, Z. B. He, J.-L. Maurice, M. Chaigneau, D. Pribat, and C. S. Cojocaru
Dual graphene films growth process based on plasma-assisted chemical vapor deposition
Proc. SPIE, **7761**, 77610P (2010)

08. Z. B. He, J.-L. Maurice, **C. S. Lee**, C. S. Cojocaru, A. Caillard, and D. Pribat
Nickel catalyst faceting in plasma-enhanced direct current chemical vapor deposition of carbon nanofibers
AJSE C-Theme Issues **35**(1C), 19 (2010)

09. Je Hwan Ryu, Ki Seo Kim, Yi Yin Yu, **Chang Seok Lee**, Yi Sang Lee, Jin Jang, and Kyu Chang Park
Enhanced Electron Emission of Carbon Nanotube Arrays Grown Using the Resist-Protection-assisted Positioning Technique
Journal of Information Display **9**(4), 30 (2008)

10. **Chang Seok Lee**, Je Hwang Ryu, Han Eol Lim, KyungWoo Min, Il Ok Jeong, S.   Manivannan, Jin Jang, KyuChang Park and Ki Seo Kim
Electron Emission from Robust CNTs Grown by Resist-Assisted Patterning
J. Korean Physical Society **53**, 2735 (2008)

11. S. Manivannan, Il Ok Jeongg, Je Hwang Ryu, **Chang Seok Lee**, Ki Seo Kim, Jin Jang and Kyu Chang Park
Purification and Preparation of Single-Walled Carbon Nanotube Films
J. Korean Physical Society **53**, 5 (2008)

12. Je Hwang Ryu, Ki Seo Kim, **Chang Seok Lee**, Jin Jang, and Kyu Chang Park
Effect of electrical aging on field emission from carbon nanotube field emitter arrays
J. Vac. Sci. Technol. B **26**, 856 (2008)

13. S. Manivannan, Il Ok Jeongg, Je Hwang Ryu, **Chang Seok Lee**, Ki Seo Kim, Jin Jang, Kyu Chang Park
Dispersion of single-walled carbon nanotubes in aqueous and organic solvents through a polymer wrapping functionalization
J. Mater. Sci.: Mater. In Electron. **20**(3), 223 (2009)

14. K. S. Kim, J. H. Ryu, **C. S. Lee**, H. E. Lim, J. S. Ahn, J. Jang and K. C. Park
Study on enhanced electron emission current of carbon nanotube by thermal and HF treatments
Journal of the Korean Vacuum Society **17**, 2 (2008)

15. Ki Seo Kim, Je Hwang Ryu, **Chang Seok Lee**, Jin Jang, Kyu Chang Park
Enhanced and stable electron emission of carbon nanotube emitter arrays by post-growth hydrofluoric acid treatment
J. Mater. Sci.: Mater. In Electron. **20**, 120 (2009)

16. S. Manivannan, J.H. Ryu, I.O. Jeong, **C.S. Lee**, K.S. Kim, J. Jang, and K.C. Park
Dispersion and preparation of transparent conductive carbon nanotube films
IDW '07, *Proc. 14*TH *International Display Workshops*, **1-3**, 605-608 (2007)

17. N.Y. Song, K.H. Kim, K.S. Kim, **C.S. Lee**, J.H. Ryu, B.K. Choo, K.C. Park, and J. Jang
Growth of regular CNT array using ink-stamping process
IDW '07, *Proc. 14*TH *International Display Workshops*, **1-3**, 1403-1406 (2007)

18. K.W. Min, J.H. Ryu, K.S. Kim, **C.S. Lee**, N.Y. Song, I.O. Jeong, S. Manivannan, J. Jang, and K.C. Park
Growth of carbon nanotubes on glass substrate for electronic devices
IDW '07, *Proc. 14*TH *International Display Workshops*, **1-3**, 2197-2200 (2007)

19. K.S. Kim, J.H. Ryu, **C.S. Lee**, S. Manivannan, J.S. Ahn, J. Jang, and K.C. Park
Enhanced electron emission properties of carbon nanotube by post growth treatment

IDW '07, *Proc. 14TH International Display Workshops*, **1-3**, 2201-2204 (2007)

20. K.S. Kim, J.H. Ryu, **C.S. Lee**, J.S. Ahn, J. Jang, and K.C. Park
    Enhanced electron emission current of carbon nanotubes emitter arrays after constant bias-aging
    IEEE 20TH IVNC, 169-170 (2007)

Book Chapter

01. L. Baraton, Z. B. He, **C. S. Lee**, J.-L. Maurice, C.-S. Cojocaru, Y. H. Lee, D. Pribat
    Study of Graphene Growth Mechanism on Nickel Thin Films
    Selected papers from the Workshop on Fundamentals and Applications of Graphene: *GRAPHITA 2011*, 1-7 (2012), DOI: 10.1007/978-3-642-20644-3_1
    Edited by L. Ottaviano and V. Morandi

Contributions to Conferences

01. **Chang Seok Lee**, Costel Sorin Cojocaru, Waleed Moujahid, Berengere Lebental, Marc Chaigneau, Marc Châtelet, François Le Normand, and Jean-Luc Maurice[*]
    Synthesis of conducting transparent graphene layers directly on insulator at 450 °C
    International Conference on Nanoscience + Technology 2012(ICN+T2012), 23-27, July, 2012 in Paris, France

02. B. Lebental[*], W. Moujahid, **C. S. Lee**, J.-L. Maurice, and C.S. Cojocaru
    Graphene-based resistive humidity sensor for *in-situ* monitoring of drying shrinkage and intrinsic permeability in concrete
    NICMO4: 4th International Symposium on Nanotechnology in Construction, 20-22, May, 2012 in Crete, Greece

03. F. Le Normand[*], **C. S. Lee**, J.-L.Maurice, C. S. Cojocaru, M. Châtelet, M. Chaigneau, D. Muller, C. Speisser
    Thin graphene layers (TGL) by carbon implantation into nickel films and thermal diffusion towards surface (Oral)
    E-MRS 2012 Spring Meeting, in Strasbourg, France, 14-18, May 2012
    SYMPOSIUM R: Science and technology of nanotubes, graphene and 2D layered materials

04. Eric Vinod Sandana, **Chang Seok Lee**, Costel Sorin Cojocaru, Waleed Moujahid, Berengere Lebental, Marc Chaigneau, Marc Châtelet, François Le Normand, and Jean-Luc Maurice
    Synthesis of conducting transparent few-layer graphene directly on glass at 450 °C (Poster)
    Graphene 2012, 10-13, April, 2012 in Brussels, Belgium

05. **C. S. Lee**, W. Moujahid, B. Lebental, M. Châtelet, F. Le Normand, J.-L. Maurice[*], and C. S. Cojocaru
    DEVELOPING LOW-COST GRAPHENE DEVICES
    GDR-I GNT, 23-27, Jan. 2012 in Lyon, France

06. **C. S. Lee**, J.-L. Maurice, C. S. Cojocaru, M. Châtelet, M. Chaigneau, D. Muller, C. Speisser, and F. Le Normand[*]
    Graphene films by carbon implantation and surface diffusion (Oral)
    ITFPC, 14-17, Nov. 2011 in Nancy, France

07. **C. S. Lee**, J.-L. Maurice, F. Le Normand[*], M. Châtelet[*], and C. S. Cojocaru,
    Low-temperature growth of microcrystalline graphene at the interface between Ni and functional insulating substrate by PECVD (Poster)

Lavoisier Discussions, Graphene on metals: CVD growth and exploitation, 26-27, Oct. 2011 in Sorèze, France

08. **Chang Seok Lee**, Jean-Luc Maurice[*], Zhanbing He, Didier Pribat, Marc Châtelet, François Le Normand, Claude Speisser, and Costel Sorin Cojocaru
Growth of graphene using a nickel thin film (Poster)
NanoteC'11, 31 Aug.-3 Sep. 2011 in Nantes, France

09. Zhanbing He[*], Jean-Luc Maurice, Aurélien Gohier, **Chang Seok Lee**, Didier Pribat, and Costel Sorin Cojocaru
Iron catalysts for the growth of carbon nanofibers: Fe, Fe_3C or both? (Poster)
NanoteC'11, 31 Aug.-3 Sep. 2011 in Nantes, France

10. L. Baraton[*], Z. He, **C. S. Lee**, J.-L. Maurice, C. S. Cojocaru, Y. H. Lee, and D. Pribat
HRTEM Study of Graphene Growth Mechanism on Nickel Thin Films (Oral)
GraphITA, 15-18, May 2011 in Assergi-L'Aquila, Italia

11. **C. S. Lee**, L. Baraton, Z. B. He, J.-L. Maurice[*], and C. S. Cojocaru
A STUDY OF PRECIPITATION OF GRAPHENE ON NICKEL (Oral)
Annual GDR-I GNT meeting, 7-11, Feb.2011 in Dourdan, France

12. A. Gohier[*], **C. S. Lee**, Z. He, J.-L. Maurice, C. Robert, G. Rose, E. Caristan, P. Legagneux, D. Pribat, C.S. Cojocaru
Water based PECVD process for the growth of oriented and patterned carbon nanotubes (Oral)
Annual GDR-I GNT meeting, 7-11, Feb.2011 in Dourdan, France

13. **C. S. Lee**[*], L. Baraton, Z. B. He, J.-L. Maurice, D. Pribata, and C. S. Cojocaru
VERSATILE SYNTHESIS OF GRAPHENE ON INSULATING SUBSTRATES USING PLASMA-ENHANCED CHEMICAL VAPOR DEPOSITION (Poster)
French Symposium on Emerging Technologies for micro-nanofabrication (JNTE'10), 24-26, Nov.2010 in Ecole Polytechnique, France

14. A.Gohier[*], **C. S. Lee**, C. Robert, G. Rose, P. Legagneux, D. Pribata, and C. S. Cojocaru
WATER-BASED PROCESS FOR THE GROWTH OF ORIENTED CARBON NANOTUBES
French Symposium on Emerging Technologies for micro-nanofabrication (JNTE'10), 24-26, Nov.2010 in Ecole Polytechnique, France

15. Z. B. He[*], **C. S. Lee**, J.-L. Maurice, D. Pribata, P. Haghi-Ashtiani, and C. S. Cojocaru
Vertically aligned cabon nanofibers filled with nickel nanorods by plasma-enhanced chemical vapor deposition
The 17th International Microscopy Congress (IMC17), 19-24, Sep.2010 in Rio de Janeiro (Brazil)

16. **C. S. Lee**[*], L. Baraton, Z. B. He, J.-L. Maurice, Marc Chaigneau, D. Pribata, and C. S. Cojocaru
Dual graphene growth behavior connected to inter-graphite pillars and its electrical characteristics (in oral)
SPIE NanoScience + Engineering, 1-5, Aug.2010 in San Diego (USA)

17. D. Pribat[*], L. Baraton, Z. B. He, **C. S. Lee**, J.-L. Maurice, and C. S. Cojocaru
Graphene synthesis by ion implantation of carbon in nickel thin films (in oral)
SPIE NanoScience + Engineering, 1-5, Aug.2010 in San Diego (USA)

18. A. Gohier[*], **C. S. Lee**, C. Robert, G. Rose, P. Legagneux, D. Pribat, and C. S. Cojocaru
WATER-BASED PROCESS FOR THE GROWTH OF ORIENTED CARBON NANOTUBES
11th International Conference on the Science and Application of Nanotubes (NT10), 27.Jun.-02, Jul.2010 in Montréal, Canada

19. **C. S. Lee**[*], Z. B. He, L. Baraton, J.-L. Maurice, P. Legagneux, and C. S. Cojocaru
On the use of water in the growth of carbon nanofibres (in poster)
E-MRS 2010 Spring Meeting, in Strasbourg, France, 8-10,Jun.2010
SYMPOSIUM P: Science and technology of nanotubes, nanowires and graphene

20. L. Baraton[*], **C. S. Lee**, Z. B. He, J.-L. Maurice, D. Pribata, and C. S. Cojocaru
    Graphene growth directly on functional substrate (in oral)
    E-MRS 2010 Spring Meeting, in Strasbourg, France, 8-10,Jun.2010
    SYMPOSIUM P: Science and technology of nanotubes, nanowires and graphene

21. Je Hwang Ryu[*], **Chang Seok Lee**, Na Young Song, Han Eol Lim, Il Ok Jeong, Jun Won Lim, Taek Byung Son, S. Manivannan, Jin Jang, Kyu Chang Park,"K-04 : Growth of the Carbon Nanotips with Resist-Assisted Patterning Process" 2008 Korean Physical Society, Spring Conference 17 Mar. 2008

22. J.H.Ryu[*], **C.S.Lee**, H.E.Lim, J.W.Lim, B.T.Son, J.Jang and K.C.Park, "Growth of the carbon nano-tip with resist assisted-patterning process", The 21st International Vacuum Nanoelectronics Conference (IVNC) 15 July 2008

23. Je Hwang Ryu[*], **Chang Seok Lee**, Han Eol Lim, Kyu Chang Park, Hae Young Choi, Jong Uk Kim, "PT-P26 : The Carbon nanotube-electron emitter for X-ray source"
    The 34th Korean Vacuum Society, Winter Conference, 14. Feb. 2008

24. Je Hwang Ryu[*], **Chang Seok Lee**, Ki Seo Kim, Han Eol Lim, Kyung Woo Min, Il Ok Jeong, S. Manivannan, Jin Jang and Kyu Chang Park, "Enhanced Electron Emission with Robust CNTs Grown by Resist-Assisted Patterning Process" Society for Information Display (SID'08), Los Angeles, California, USA, 18-23 May 2008

25. **Chang Seok Lee**, Je Hwang Ryu, Han Eol Im, Il Ok Jeongg, S. Manivannan, Jin Jang and Kyu Chang Park[*], "Electron Emission from Robust Carbon Nanotubes Grown by Resist-Assisted Patterning Process" International Conference on Advanced Materials (ICAM 2008), Kottayam, India, 18-21 Feb. 2008

26. S. Manivannan[*], Il Ok Jeongg, Je Hwang Ryu, **Chang Seok Lee**, Jin Jang and Kyu Chang Park,"Conducting and Transparent Electrodes from Single-Walled Carbon Nanotubes",International Conference on Advanced Materials (ICAM 2008), Kottayam, India, 18-21 Feb. 2008

27. S. Manivannan[*], J. H. Ryu, I. O. Jeong, **C. S. Lee**, K. S. Kim, J. Jang, K. C. Park, "FMCp-25 : Dispersion and Preparation of Transparent Conductive Carbon Nanotube Films",The 14th International Display Workshops (IDW 07), Sapporo, Japan, 5-7 Dec. 2007

28. Ki Seo Kim[*], Je Hwang Ryu, **Chang Seok Lee**, S. Manivannan, Jung Sun Ahn, Jin Jang and Kyu Chang Park,"FED3-4 : Enhanced electron emission properties of carbon nanotube by post growth treatment", The 14th International Display Workshops (IDW '07), Sapporo, Japan, 5-7 Dec. 2007

29. Kyung Woo Min, Je Hwang Ryu, Ki Seo Kim, **Chang Seok Lee**[*], Na Young Song, Il Ok Jeung, S. Manivannan, Jin Jang and Kyu Chang Park,"FED3-3 : Growth of carbon nanotubes on glass substrate for electronic devices",The 14th International Display Workshops (IDW '07), Sapporo, Japan, 5-7 Dec. 2007

30. Na Young Song[*], Ki Hwan Kim, Ki Seok Kim, **Chang Seok Lee**, Je Hwang Ryu, Byoung Kwon Choo, Kyu Chang Park and Jin Jang, "MEMS5-2 : Growth of regular CNT array using ink-stamping process",The 14th International Display Workshops (IDW '07), Sapporo, Japan, 5-7 Dec. 2007

31. Sellaperumal Manivannan[*], Il Ok Jeongg, Je Hwang Ryu, **Chang Seok Lee**, Ki Seo Kim, Jin Jang and Kyu Chang Park, "Fr2-NAN-11 : Purification and Preparation of Single-Wall Carbon Nanotube Films",The 5th International Conference on Advanced Materials and Devices (ICAMD 2007), Jeju, Korea, 12-14 Dec. 2007

32. **Chang Seok Lee**[*], Je Hwang Ryu, Ki Seo Kim, Kyung Woo Min, Il Ok Jeongg, S. Manivannan, Jin Jang and Kyu Chang Park,"Fr2-NAN-26 : Electron emission from robust CNT grown by resist-assisted patterning process",The 5th International Conference on Advanced Materials and Devices (ICAMD 2007), Jeju, Korea, 12-14 Dec. 2007

33. Je Hwang Ryu[*], Ki Seo Kim, **Chang Seok Lee**, Kyung Woo Min, Il Ok Jeong, Manivannans, Jin Jang, Kyu Chang Park,"K-15 : Enhanced Electron Emission Current of as grown CNT by Post-Treatments",2007 Korean Physical Society, Fall conference, 18 Oct. 2007

34. **Chang Seok Lee**[*], Je Hwang Ryu, Ki Seo Kim, Il Ok Jeongg, S. Manivannan, Jin Jang and Kyu Chang Park,"P2-105 : Growth of Carbon Nanotubes on Metal Substrate for Electronic Devices", The 7th International Meeting on Information Display (IMID 2007), EXCO, Daegu, Korea, 27-31 Aug. 2007 (Poster)

35. Ki Seo Kim[*], Je Hwang Ryu, **Chang Seok Lee**, S. Manivannan, Jong Hyun Moon, Jung Sun Ahn, Jin Jang and Kyu Chang Park, "P1-79 : Effect of Current-Aging on Field Emission from Carbon Nanotube Field Emitter Arrays", The 7th International Meeting on Information Display (IMID 2007), EXCO, Daegu, Korea, 27-31 Aug. 2007

36. S. Manivannan[*], Je Hwang Ryu, Il Ok Jeongg, **Chang Seok Lee**, Ki Seo Kim, Jin Jang and Kyu Chang Park,"P2-103 : Dispersion of Single-Walled Carbon Nanotubes for Display Applications", The 7th International Meeting on Information Display (IMID 2007), EXCO, Daegu, Korea, 27-31 Aug. 2007

37. Ki Seo Kim[*], Je Hwang Ryu, **Chang Seok Lee**, Kyung Woo Min, Il Ok Jeongg, S. Manivannan, Jin Jang and Kyu Chang Park, "Stable electron emission of carbon nanotubes grown by RAP process",The 10th Field Emission Workshop (FEW 07) 9-11 Aug. 2007

38. Je Hwang Ryu[*], Ki Seo Kim, Kyung Woo Min, **Chang Seok Lee**, Il Ok Jeongg, S. Manivannan, Jong Hyun Moon, Jin Jang and Kyu Chang Park, "Aa-P.011 : Growth of Carbon Nanotubes on Substrate with RAP Process for Flat Lamp", The 10th Asia Pacific Physics Conference (APPC) 2007 (Poster)

39. Je Hwang Ryu[*], Kyung Woo Min, Ki Seo Kim, **Chang Seok Lee**, Il Ok Jeongg, Jong Hyun Moon, Jin Jang and Kyu Chang Park,"KP-066 : Growth of Carbon Nanotubes on Glass Substrate with a-Si",2007 Korean Physical Society, Spring Conference

Résumé

Cette thèse présente de nouveaux modes de croissance du graphène, basés sur le dépôt PECVD d'une part et l'implantation ionique d'autre part. En séparant la phase de recuit de la phase d'introduction, l'implantation ionique – que nous fûmes les premiers à employer – nous a permis d'isoler des facteurs importants du traitement thermique. Nous avons ainsi pu obtenir une compréhension profonde de certains des mécanismes de croissance : du fait d'une diffusion très rapide, la distribution finale du carbone dans un film de Ni dépend du détail du traitement thermique qui est appliqué pendant ou après l'introduction de carbone. Nous montrons en particulier que deux espèces de matériaux graphitiques sont obtenues après un traitement donné : constituées de fins monocristaux de graphite d'une part, qui se développentvraisemblablement durant le plateau haute température, et de "few-layer graphene" nanocristallin d'autre part qui apparaît très certainement durant le refroidissement. Le dépôt PECVD soumet un film métallique à un plasma hautement réactif, introduisant des atomes de carbone dans le voisinage de sa surface.Effectuer cette opération à haute température provoque la diffusion des atomes de carbone à travers le film. Cette technique a délivré notamment des nanotubes de carbone d'excellente qualité. Ici, nous l'avons adaptéeà la croissance de graphèneet en avons obtenu des films de graphène sur Ni, à des températures aussi basses que 450 °C. De plus, cette technique s'est avérée délivrer un deuxième film de graphène, à l'interfaceentre le Ni et son substrat isolant (SiO_2ou verre). Ce second film se plaçant directement sur un substrat fonctionnel, nous avons développé un procédé simple pour l'utiliser directement dans undispositif, sans transfert. Nous avons ainsi développé un capteur d'humidité, par simple impression d'électrodes. Au-delà de cette preuve de concept, nous devons maintenant explorer plus avant les mécanismes de croissance et les conditions de recuit pour le développement d'applications de ce graphène sans-transfert et basse-température.

Mots-Clés: graphène : croissance catalytique,croissance directement sur isolant, croissance basse température, solubilité/diffusivité de C dans Ni, PECVD, implantation ionique

Abstract

In this thesis work, we developed a new paradigm in the field of graphene growth, based on PECVD and Ion Implantation techniques. Exposure of the metal film to highly reactive plasma introduces carbon atoms at and near the film surface; performing this at elevated temperature makes the carbon atoms to diffuse throughout the film.After adapting this method to graphene growth, it delivered graphene layers on Ni at 450 °C. Moreover, in addition to the top-surface layer, we obtained with this technique another graphene layer in-between Ni and the underlying insulating substrate (SiO_2 or glass). That second graphene layer placing itself directly on the insulating (functional) substrate, we developed a simple process for using it directly as a sensor without transfer. We were the first to propose carbon ion implantation for supplying carbon atoms to the Ni layer, prior to obtaining graphene upon annealing. By separating introduction and annealing, this technique allowed us to isolate important factors of a heat treatment. We were thus able, by using this method, to get fundamental insight into the graphene growth mechanisms. Due to fast diffusion, the final carbon distribution in a Ni film depends on the details of the annealing treatment that is applied during or after carbon has been introduced. We show in particular that two kinds of graphitic materials are obtained after a given treatment: one under the form of single crystals of few-layer graphene/graphite, grown during the high temperature plateau, and a second under the form of nanocrystalline few-layer graphene, grown during cooling.Finally, on the graphene grown by PECVD directly on glass at low temperature, we thus developed a humidity sensor, by direct electrode printing. Beyond this proof of concept, we need to further investigate growth mechanisms and annealing conditions for the development of various transfer-free, low-temperature, graphene applications.

Keywords: graphene: catalyzed growth, direct growth on insulator, low-temperature growth, transfer-free, carbon solubility/diffusivity in Ni, PECVD, ion implantation

Résumé

Cette thèse présente de nouveaux modes de croissance du graphène, basés sur le dépôt PECVD d'une part et l'implantation ionique d'autre part. En séparant la phase de recuit de la phase d'introduction, l'implantation ionique – que nous fûmes les premiers à employer – nous a permis d'isoler des facteurs importants du traitement thermique. Nous avons ainsi pu obtenir une compréhension profonde de certains des mécanismes de croissance : du fait d'une diffusion très rapide, la distribution finale du carbone dans un film de Ni dépend du détail du traitement thermique qui est appliqué pendant ou après l'introduction de carbone. Nous montrons en particulier que deux espèces de matériaux graphitiques sont obtenues après un traitement donné : constituées de fins monocristaux de graphite d'une part, qui se développentvraisemblablement durant le plateau haute température, et de "few-layer graphene" nanocristallin d'autre part qui apparaît très certainement durant le refroidissement. Le dépôt PECVD soumet un film métallique à un plasma hautement réactif, introduisant des atomes de carbone dans le voisinage de sa surface.Effectuer cette opération à haute température provoque la diffusion des atomes de carbone à travers le film. Cette technique a délivré notamment des nanotubes de carbone d'excellente qualité. Ici, nous l'avons adaptéeà la croissance de graphèneet en avons obtenu des films de graphène sur Ni, à des températures aussi basses que 450 °C. De plus, cette technique s'est avérée délivrer un deuxième film de graphène, à l'interfaceentre le Ni et son substrat isolant (SiO_2ou verre). Ce second film se plaçant directement sur un substrat fonctionnel, nous avons développé un procédé simple pour l'utiliser directement dans undispositif, sans transfert. Nous avons ainsi développé un capteur d'humidité, par simple impression d'électrodes. Au-delà de cette preuve de concept, nous devons maintenant explorer plus avant les mécanismes de croissance et les conditions de recuit pour le développement d'applications de ce graphène sans-transfert et basse-température.

Mots-Clés: graphène : croissance catalytique,croissance directement sur isolant, croissance basse température, solubilité/diffusivité de C dans Ni, PECVD, implantation ionique

Abstract

In this thesis work, we developed a new paradigm in the field of graphene growth, based on PECVD and Ion Implantation techniques. Exposure of the metal film to highly reactive plasma introduces carbon atoms at and near the film surface; performing this at elevated temperature makes the carbon atoms to diffuse throughout the film.After adapting this method to graphene growth, it delivered graphene layers on Ni at 450 °C. Moreover, in addition to the top-surface layer, we obtained with this technique another graphene layer in-between Ni and the underlying insulating substrate (SiO_2 or glass). That second graphene layer placing itself directly on the insulating (functional) substrate, we developed a simple process for using it directly as a sensor without transfer. We were the first to propose carbon ion implantation for supplying carbon atoms to the Ni layer, prior to obtaining graphene upon annealing. By separating introduction and annealing, this technique allowed us to isolate important factors of a heat treatment. We were thus able, by using this method, to get fundamental insight into the graphene growth mechanisms. Due to fast diffusion, the final carbon distribution in a Ni film depends on the details of the annealing treatment that is applied during or after carbon has been introduced. We show in particular that two kinds of graphitic materials are obtained after a given treatment: one under the form of single crystals of few-layer graphene/graphite, grown during the high temperature plateau, and a second under the form of nanocrystalline few-layer graphene, grown during cooling.Finally, on the graphene grown by PECVD directly on glass at low temperature, we thus developed a humidity sensor, by direct electrode printing. Beyond this proof of concept, we need to further investigate growth mechanisms and annealing conditions for the development of various transfer-free, low-temperature, graphene applications.

Keywords: graphene: catalyzed growth, direct growth on insulator, low-temperature growth, transfer-free, carbon solubility/diffusivity in Ni, PECVD, ion implantation